UNIVERSITY OF CAPE TOWN
IYUNIVESITHI YASEKAPA • UNIVERSITEIT VAN KAAPSTAD

FACULTY OF ENGINEERING AND THE BUILT ENVIRONMENT

Department of Civil Engineering

A Critical Evaluation of the Use of Crack Width Requirements in the Durability Design of Marine Reinforced Concrete Structures

Submitted in partial fulfilment of the requirements for the degree of

Master of Science in Engineering, specialising in Structural Engineering

By

Nicholas Elias

Supervisor: Professor Hans Beushausen

January 2023

Declaration

I know the meaning of plagiarism and declare that all the work in this document, save for that which is properly acknowledged, is my own. This dissertation has been submitted to the Turnitin module (or equivalent similarity and originality checking software) and I confirm that my supervisor has seen my report and any concerns revealed by such have been resolved with my supervisor.

This dissertation makes use of the UCT Author-date referencing system.

Signed:

Signed by candidate

Nicholas Norman Elias

23/01/2023

Dedication

This dissertation is dedicated to my parents, Norman and Roma Elias, for all their support and encouragement throughout my education. None of this would have been possible without you.

Abstract

Crack width requirements (CWRs), which aim to limit cracks in reinforced concrete (RC) to maximum prescribed values, play a major – and often dominant – role in the design of marine RC structures. However, there are several issues with the current CWRs, chief among which is the fact that, despite decades of research, no clear relationship between crack width and steel reinforcement corrosion rate in concrete has been found. Instead, there exist two opposing schools of thought in the literature – one which says that there is a relationship between crack width and reinforcement corrosion rate, and one which argues that no such relationship exists – with good evidence to support both schools of thought.

Recent research has shown that even small cracks, with widths below the required values, may lead to extensive corrosion. It is therefore uncertain whether designing for the CWRs actually improves durability and extends the service life of marine RC structures. Furthermore, the use of the CWRs, which frequently results in large increases in the required amount of reinforcing steel, may lead to significant increases in the cost and environmental impact of marine RC structures. Yet, to date, these impacts have not been quantified.

In order to address these issues, this study was aimed at evaluating the effect of designing to meet the current CWRs on the durability, cost, and environmental sustainability of marine RC structures. This was done by designing two sets – one with, and one without the CWRs – of typical marine RC structural elements. Based on real industry projects, two different types of elements were designed – a crane rail beam for a coal export jetty in Matola, Mozambique, and a precast crown wall unit for a breakwater in Rupert's Bay, St. Helena Island. The designs were carried out using a combination of *BS 6349* and *EN 1992-1-1:2004*, as these are the codes of practice typically used in the South African coastal engineering industry. The effects of designing for the current CWRs on durability, cost, and environmental sustainability were then quantified by carrying out service life modelling, life cycle cost assessments (LCCAs) and estimating embodied carbon (EC) values for the designed members.

The results of the service life modelling show that, for the range of crack widths likely to occur in practice, the use of the current CWRs does not improve durability, and may even reduce service life, as they encourage the use of more, smaller diameter reinforcement bars, which has the effect of increasing corrosion rate and reducing the time taken for a critical amount of the reinforcement to be lost due to corrosion. Furthermore, the results of the LCCA and EC estimates imply that the current CWRs are not the most cost-effective method for durability design and may result in significant increases in cost and environmental impact. Taken together, these results suggest that, even if a relationship is assumed to exist between crack width and corrosion rate, the current CWRs are neither the most effective, nor efficient way of addressing the effects of cracking on the durability of marine RC structures.

It is therefore recommended that the current crack width requirements should be removed from the durability design codes of practice and replaced with either a limitation on steel stress, a more lenient crack width requirement (for example, of 0.5 mm rather than 0.3 mm), or a performance-based crack width requirement, which takes better account of the complexity of cracking and its effect on durability. It is also recommended that engineers be given the option to use other methods of providing durability, such as the use of crack-sealing and waterproofing admixtures, or hydrophobic treatments, instead of the current CWRs.

However, before any of these recommendations can be implemented, the results of this study need to be confirmed with further research. Owing to the limitations of both service life modelling and accelerated laboratory corrosion, it is recommended that this further research should take the form of an extensive evaluation of the durability performance of existing marine RC structures.

Acknowledgements

I would like to thank the following people and institutions for their assistance throughout this research:

My supervisor, Professor Hans Beushausen, for his invaluable advice and guidance, which has played an immense role in shaping this research into something I am very proud of. I will miss working with you Prof.

Phil Smith and Marco Talotti from PRDW Consulting Port and Coastal Engineers, for providing me with this research topic and assisting me with the design of the beams and wall units.

Charl Coetzee, Alwyn Carstens, and Precillian Ngandu from Concrete Units, for developing construction cost estimates for the beams and wall units.

My Iranian friends, Reza Homayoonmehr and Mahdi Mirabrishami, for both their friendship and their help with modelling the corrosion initiation period in cracked RC – the method used in this study was based on their advice.

The Harry Crossley Foundation, for their generous funding of my master's degree, without which this research would not have been possible.

All the staff and students in the Concrete Materials and Structural Integrity Research Unit (CoMSIRU) at UCT, which I am honoured to have been a part of. The feedback and discussions during the monthly CoMSIRU seminars played a vital role in the development of this research.

My family – Roma, Norman, and Melissa Elias – for their love and support throughout both my degrees.

My girlfriend, Dana Chiles, for her love and support – and for putting up with me babbling on about concrete all the time.

My friends on the sixth floor of the New Engineering Building – Alex, Aaron, Areej, Josh, Meghan, Nadiya, Sean, and Tais – for all the great memories over the last two years.

Table of Contents

Declaration i
Dedication ii
Abstract iii
Acknowledgements iv
Table of Contents v
List of Figures x
List of Tables xiii
Definition of Terms and Symbols xv
Acronyms xv
1. Introduction 1
1.1 Background to the Study 1
1.2 Problem Statement 1
1.3 Objectives of the Study 2
1.4 Scope and Limitations of the Study 3
1.5 Structure of the Dissertation 4
2. Literature Review 5
2.1 Introduction 5
2.2 Reinforced Concrete Marine Structures 6
2.2.1 Port Structures 6
2.2.2 Coastal Structures 8
2.3 Durability and Service Life of Reinforced Concrete Marine Structures 8
2.3.1 Factors Influencing Durability and Service Life 8
2.3.2 The Concrete System 9
2.3.3 An Overview of Chloride-Induced Reinforcement Corrosion 12
2.3.4 Mechanisms of Chloride Transport into Marine Concrete 12
2.3.5 The Corrosion Process 15
2.3.6 Stages of Service Life for Marine Reinforced Concrete Structures 16
2.4 Cracking of Reinforced Concrete 17
2.4.1 Description and Quantification of Cracking 17
2.4.2 Shrinkage Cracking 18
2.4.3 Thermal Cracking due to Hydration Heat 20

2.4.4 Thermal Cracking due to Ambient Temperature Fluctuations 21
2.4.5 Flexural Cracking 22
2.5 The Effect of Cracks on the Durability of Marine Reinforced Concrete Structures 22
2.5.1 The Effect of Cracks on Transport Mechanisms and Corrosion Initiation 23
2.5.2 Mechanisms of Corrosion in Cracked Reinforced Concrete 24
2.5.3 The Effect of Cracks on Corrosion Propagation 25
2.5.4 The Relationship Between Crack Width and Corrosion Propagation 28
2.5.5 Implications for Crack Width Design 31
2.6 Durability Design of Reinforced Concrete Marine Structures 32
2.6.1 BS 6349 and the Eurocodes 32
2.6.2 American Standards 34
2.6.3 Australian Standards 34
2.6.4 Japanese Guidelines 35
2.6.5 South African Standards 35
2.7 Crack Width Design 35
2.7.1 Code Requirements for Crack Width Design 36
2.7.2 Crack Width Formulas 39
2.7.3 Critique of the Current Crack Width Requirements 41
2.7.4 Developments in Crack Width Design 42
2.8 Service Life Modelling of Cracked Reinforced Concrete 43
2.8.1 Existing Models for the Corrosion Initiation Period 43
2.8.2 Modelling the Corrosion Initiation Period in Cracked Reinforced Concrete 45
2.8.3 Models for Determining Corrosion Rate 47
2.8.4 Modelling the Corrosion Propagation Period 48
2.8.5 Conclusion on Service Life Modelling of Cracked Reinforced Concrete 49
2.9 Methods for Determining Cost Implications 50
2.10 Methods for Determining Impacts on Environmental Sustainability 51
3. Methodology 53
4. Member Design 54
4.1 Matola Jetty Beam 54
4.1.1 Overview of Member 55
4.1.2 Calculation of Design Loads 56
4.1.3 Member Analysis 57

4.1.4 ULS and SLS Design 58
4.1.5 Crack Width Design 59
4.1.6 Summary of the Matola Jetty Beam Design 59
4.2 St. Helena Breakwater Crown Wall 61
4.2.1 Overview of Member 61
4.2.2 Calculation of Design Loads 62
4.2.3 Member Analysis 63
4.2.4 ULS and SLS Design 64
4.2.5 Crack Width Design 65
4.2.6 Summary of the St. Helena Breakwater Crown Wall Design 66
5. Service Life Modelling 67
5.1 Selection of Input Parameters 67
5.2 Determination of Effective Cover Depth 68
5.3 Calculation of the Corrosion Initiation Period 70
5.4 Determination of Representative Corrosion Rates 70
5.4.1 Determination of α Factors 71
5.4.2 Determination of β Factors 72
5.4.3 Calculation of Base Corrosion Rates 74
5.4.4 Final Values of Representative Corrosion Rates 75
5.5 Calculation of the Corrosion Propagation Period 75
5.6 Calculation of Total Service Life 77
6. Quantification of Material Amounts 78
7. Determination of Member Costs 79
7.1 Determination of Construction Costs 79
7.2 Determination of Maintenance Costs 81
7.3 Determination of Repair Costs 82
7.4 Determination of Escalation and Discount Rates 82
7.5 Calculation of LCC for Strategy A 82
7.6 Calculation of LCC for Strategy B 83
7.7 Calculation of LCC for Strategy C 83
7.8 Calculation of LCC for Strategy D 84
7.9 Summary of LCCA Results 84
8. Embodied Carbon Estimates 86

8.1 Estimation of Member EC Values 86
8.2 Estimation of Total EC Values 87
8.3 Determination of EC Values for Typical Marine Structures 88
9. Discussion of Results 89
9.1 The Effect of the Crack Width Requirements on Durability 89
9.1.1 The Effect of the Crack Width Requirements on Corrosion Initiation 89
9.1.2 The Effect of the Crack Width Requirements on Corrosion Propagation and Service Life 89
9.2 The Effect of the Crack Width Requirements on Life Cycle Cost 90
9.2.1 Life Cycle Cost Analysis of the Beams 91
9.2.2 Life Cycle Cost Analysis of the Wall Units 91
9.2.3 The Effect of Reapplication Time on the Life Cycle Cost of Hydrophobic Coatings 92
9.2.4 The Cost-Effectiveness of the Crack Width Requirements 93
9.3 The Effect of the Crack Width Requirements on Environmental Sustainability 95
9.4 Limitations of the Study 96
9.5 Final Evaluation of the Effectiveness and Role of the Crack Width Requirements .. 97
9.6 The Way Forward 98
10. Conclusion 100
10.1 The Effect of the Crack Width Requirements on Durability 100
10.2 The Effect of the Crack Width Requirements on Life Cycle Cost 101
10.3 The Effect of the Crack Width Requirements on Environmental Sustainability . 102
10.4 Overall Evaluation of the Effectiveness and Role of the Crack Width Requirements 102
11. Recommendations for Further Work 104
Reference List 105
Appendix A: Matola Jetty Beam Design Calculation Sheets 113
Appendix B: St. Helena Breakwater Crown Wall Design Calculation Sheets 114
Appendix C: Matola Jetty Beam Drawings 115
Appendix D: St. Helena Breakwater Crown Wall Drawings 116
Appendix E: Service Life Modelling Calculations 117
Appendix F: Life Cycle Cost Analysis Calculations 118
F.1 Construction Costs: Concrete Units Quotation 118
F.2 Construction Cost Calculations 120

F.3 Full Life Cycle Cost Calculations 122
F.3.1 Matola Jetty Beams 122
F.3.2 St. Helena Breakwater Crown Wall Units 124
F.3.3 Coating Time Sensitivity Analysis 128
F.4 Calculation of Increases in LCC 132
F.4.1 Matola Jetty Beams 132
F.4.2 St. Helena Island Crown Wall Units 132
Appendix G: Embodied Carbon Estimates 133
Appendix H: Signed Ethics Approval 134

List of Figures

Figure 2-1: Two caisson units under construction in the Port of Cape Town (Smith, 2016b:23). 7
Figure 2-2: Precast counterfort wall units under construction in Saldanha Bay, South Africa (Paul & Zietman, 1999:11)..... 7
Figure 2-3: A jetty in Simon's Town, South Africa (left) and a wharf in Mossel Bay, South Africa (right) (Smith, 2016b:36). 7
Figure 2-4: A diagram of the factors which influence the durability of marine RC structures (adapted from Ballim, Alexander & Beushausen, 2009:156). 9
Figure 2-5: A diagrammatic representation of a concrete sample, showing how the ITZ phases may interlink to produce pathways for the ingress of aggressive agents (adapted from Ballim, Alexander & Beushausen, 2009:159)..... 11
Figure 2-6: A diagrammatic representation of the transport mechanisms which typically occur in marine RC structures, shown here for a seawall (adapted from Santhanam & Otieno, 2016:138). 14
Figure 2-7: A diagrammatic representation of a corrosion cell (adapted from Raupach, 1996:330). 15
Figure 2-8: Diagrammatic representations of typical micro- and macrocells (adapted from Raupach, 1996:331). 16
Figure 2-9: A graphical representation of the service life of a marine reinforced concrete structure (adapted from Alexander & Beushausen, 2019:25). 16
Figure 2-10: An example of a crack comparator (left, ACI Committee 224, 1993:9) and a crack width gauge in use (right)..... 18
Figure 2-11: Typical plastic and drying shrinkage cracking patterns on slab panels (adapted from Day & Clarke, 2003:4). 19
Figure 2-12: Typical vertical cracking in a concrete wall due to hydration heat development and subsequent restrained contraction (adapted from Day & Clarke, 2003:4). 21
Figure 2-13: A diagram showing the typical locations of flexural cracks for simply supported and continuous beams and slabs (adapted from Day & Clarke, 2003:4). 22
Figure 2-14: An illustration of the ingress paths of chlorides in uncracked and cracked concrete (adapted from Ma, Zhao and Gong, 2019:1569). 24
Figure 2-15: A diagram showing microcell corrosion occurring at a coincident crack, as described by Otieno (2014:29). 25
Figure 2-16: A diagram showing macrocell corrosion in which a series of intersecting cracks has led to the formation of anodes in the vicinity of the cracks (adapted from Bezuidenhout & van Zijl, 2019:2184). Note that the location and shape of the anodes is based on the visual observations of Bezuidenhout and van Zyl (2019) and the corrosion mapping of cracked beams carried out by Zhang, François and Yu (2020) and Geiker et al. (2021). 25
Figure 2-17: A diagram of the type of macrocell corrosion described by Arya and Myrzakulova (2019:4), in which both anodes and cathodes form in the vicinity of cracks. 25
Figure 2-18: A diagrammatic representation of the four-stage corrosion development process at intersecting cracks (adapted from Chen et al., 2020:18). 26

Figure 2-19: The box and whisker plot produced by Lapi, Orlando and Spinelli (2018), showing w_{th}/w_{exp} ratios for a variety of existing crack width formulas. Note the performance of the *EN 1992-1-1:2004* formula, circled in red, and the Model Code 2010 formula, circled in green. 40
Figure 2-20: A simplified illustration showing how cracking does not necessarily lead to instant initiation of corrosion (adapted from Ramezanianpour et al., 2018:1467). 45
Figure 2-21: An illustration showing the effective cover depth concept for cracked concrete (adapted from Ramezanianpour et al., 2018:1467). 46
Figure 2-22: A framework showing the costs expected for each of the life cycle stages for a typical marine RC structure (adapted from Younis, Ebead and Judd (2018:155)). 51
Figure 3-1: A research framework showing the seven stages of the methodology used in the study. 53
Figure 4-1: A typical RC coal export jetty in Dalrymple Bay, Australia (adapted from Dalrymple Bay Coal Terminal, n.d.). Note the shiploader crane, conveyor systems, and crane rail beams. 54
Figure 4-2: A diagrammatic representation of Beam B402, showing its dimensions (in mm). 55
Figure 4-3: A flowchart showing the steps of the design process for Beam B402. 56
Figure 4-4: A summary of the design of the B402 beams, showing 3-D and section views of the beams designed with and without the crack width requirements ("CWRs"). 60
Figure 4-5: An aerial photograph of the completed breakwater in Rupert's Bay, St. Helena Island (PRDW, n.d.). 61
Figure 4-6: A simplified cross-sectional diagram of the St. Helena breakwater crown wall. . 61
Figure 4-7: A diagrammatic representation of a typical F01 wall unit, showing its dimensions (in mm). Note that protruding reinforcement for the purposes of connecting the wall units to the cast-in-situ base and capping is not shown. 62
Figure 4-8: An illustration of the distribution of lateral wave pressures on the F01 wall units, adapted from the wave loading information provided by PRDW. 63
Figure 4-9: A diagram of the analysis model for the St. Helena crown wall. 64
Figure 4-10: A summary of the design of the F01 wall units, showing 3-D views of the wall units designed with and without the crack width requirements ("CWRs"). 66
Figure 5-1: A diagrammatic representation of the five-step method for determining the service lives of cracked marine RC structures. 67
Figure 5-2: A diagrammatic representation of a typical triangular-shaped crack. 69
Figure 5-3: A plot of reinforcing bar diameter vs. corrosion rate, showing the exponential relationship fitted to the plot. 72
Figure 5-4: A plot of increase in A_{Sprov} vs. β values, showing the linear relationship fitted to the plot. 73
Figure 9-1: A bar graph showing the service lives of the members designed in this study. 90
Figure 9-2: A summary of the LCCA results for the beams. Note that the two left-most bars have the same value as, for the members designed without the CWRs, the total LCC is simply equal to the construction cost. 91
Figure 9-3: A summary of the LCCA results for the wall units. 92
Figure 9-4: A bar graph showing the effect of varying the hydrophobic coating reapplication time on the LCC of the beams for Strategy D. 93

Figure 9-5: A bar graph showing the effect of varying the hydrophobic coating reapplication time on the LCC of the wall units for Strategy D. 93
Figure 9-6: A bar graph showing the percentage change in LCC, relative to the members designed without the CWRs, for all the other design strategies. 94
Figure 9-7: A summary of the A1-A3 EC values estimated for the members designed in this study. 96
Figure 9-8: A flow chart showing how the results of this study suggest that it does not make sense to design for the CWRs. 98

List of Tables

Table 2-1: A table summarising the conclusions of a number of studies conducted on the influence of cracking on corrosion. Note that the list of studies is not exhaustive (adapted from Käthler et al., 2020a:146-147)..... 29
Table 2-2: Design service life categories and requirements, according to *BS 6349-1-1:2013* (adapted from The British Standards Institution, 2013b:51)..... 33
Table 2-3: Definition of exposure conditions according to *BS 6349-1-4:2013* (adapted from The British Standards Institution, 2013a:8)..... 34
Table 2-4: A summary of the crack width requirements of typical codes of practice for the durability design of marine reinforced concrete structures (adapted from Otieno, Beushausen & Alexander, 2012:28; Balázs et al., 2013:101; Smith, 2016a:86)..... 36
Table 2-5: A summary of three of the most widespread existing SLMs (adapted from Pillai & Annapareddy, 2013:565). 43
Table 2-6: A summary of some of the corrosion propagation models available in the literature. 48
Table 4-1: Load combinations which were used in the design of the B402 beams, for both ULS and SLS. 57
Table 4-2: A summary of the maximum bending moments (M_u), shear forces (V_u), torsional moments (T_u) and deflections (δ_{max}) for the B402 beams. 58
Table 4-3: A summary of the reinforcement provided in the B402 beams to meet the ULS and SLS requirements of *EN 1992-1-1*. 58
Table 4-4: A summary of the reinforcement provided in the B402 beams to meet the crack width requirements of *EN 1992-1-1* and *CIRIA C660*. Note that this reinforcement was curtailed. . 59
Table 4-5: The load factors which were used in the analysis of the F01 wall units (The British Standards Institution, 2010). 63
Table 4-6: A summary of the Prokon analysis results, showing the ultimate bending moments and shear forces per metre width of wall unit. 64
Table 4-7: A summary of the reinforcement provided in the F01 wall units to meet the ULS and SLS requirements of *EN 1992-1-1*. 65
Table 5-1: Input parameters used for the service life modelling calculations. 68
Table 5-2: A summary of the effective depth calculations for the study. 70
Table 5-3: A summary of the α values determined for the members in this study. 72
Table 5-4: A summary of the β values determined for the members in this study. 74
Table 5-5: A summary of the i_{base} values determined for the members in this study. 75
Table 5-6: A summary of the representative corrosion rates for the members in this study. .. 75
Table 5-7: A summary of the propagation period (t_p) values determined for the members in this study. 77
Table 6-1: A summary of the volume of materials used in each of the designed members. ... 78
Table 7-1: A summary of the construction costs for the members designed in this study..... 80
Table 7-2: A summary of the costs of various admixtures. 81
Table 7-3: A summary of the coating reapplication sensitivity analysis. 84
Table 7-4: A summary of the results of the LCCA. 85
Table 8-1: A1-A3 EC values for each of the members in the study. 87

Table 8-2: Total, structure-wide, A1-A3 EC values for each of the members designed in the study. 87
Table 8-3: A1-A3 EC values for typical marine structures and the Matola jetty. 88
Table 9-1: Increases in total project LCC for each of the design strategies, relative to the cheapest option (full calculations shown in Appendix F.4). 94

Definition of Terms and Symbols

Acronyms

CPAP	Contract price adjustment provisions
CWD	Crack width design
CWR	Crack width requirement
EC	Embodied carbon
FA	Fly ash
GGBS	Ground granulated blastfurnace slag
GWP	Global warming potential
LCC	Life cycle cost
LCCA	Life cycle cost analysis
PV	Present value
NPV	Net present value
RC	Reinforced concrete
SCM	Supplementary cementitious material
SF	Silica fume
SLM	Service life model

1. Introduction

1.1 Background to the Study

Marine structures, such as quays, jetties, piers, seawalls, and breakwaters, provide vital infrastructure for trade and development and play a crucial role in protecting human settlements from the effects of coastal erosion and sea level rise. Regardless of their specific use, these structures are almost always made from, or at least partially make use of, reinforced concrete (RC). This is as RC is generally considered to be the most suitable material for use in the marine environment, owing to its inherent strength, durability, versatility and cost-effectiveness (Alexander & Nganga, 2016:2-3).

However, the durability of marine RC structures may be significantly reduced by corrosion of the reinforcing steel, which is the primary deterioration mechanism for RC structures in the marine environment (Alexander & Nganga, 2016:4). Such structures are exposed to chloride ions, which are present in seawater (Smith, 2016a:65), and which penetrate into the concrete (Owens, 2013:119). Once the chloride ions penetrate to the level of the reinforcing steel in sufficient concentration, they may cause the reinforcing steel to corrode (Owens, 2013:126), which reduces the cross-sectional area of the steel and can result in cracking, delamination and spalling of the concrete. This damage is unsightly, costly to repair, and may lead to failure of the structure if sufficiently severe.

Reinforcement corrosion thus poses a significant threat to marine RC structures. In order to mitigate this threat, the design of marine RC structures tends to include designing for durability (Smith, 2016a:65). Such durability design is generally aimed at limiting the ingress of chloride ions into the concrete, through the provision of low-penetrability cover concrete over the reinforcement. Currently, this is mostly still done according to prescriptive approaches (Alexander & Beushausen, 2019:19), in which limiting values for various design parameters – such as concrete compressive strength, w/c ratio, binder type, cover depth and cement content – are specified.

One of the most significant specifications of the current prescriptive durability design approaches are crack width requirements. Concrete may crack for a variety of reasons – including shrinkage, thermal movements, or applied loads. These cracks are a normal, expected property of concrete structures, and generally do not pose a threat to their safety. However, cracks may reduce the durability of marine RC structures by providing paths through which chloride ions, moisture and oxygen can easily reach the reinforcing steel and promote corrosion (Otieno, Beushausen & Alexander, 2016:373).

To reduce the effect of cracking on the durability of RC structures, crack width requirements typically involve limiting crack widths to certain maximum values, through the provision of adequate reinforcing steel (which provides tensile restraint to the concrete and therefore prevents or limits cracking and crack opening). Design codes such as the *Eurocodes*, *BS 6349* and the Australian and American standards all provide "crack width" formulas, which can be used to determine the amount and layout of reinforcing steel required (Smith, 2016a:84). Crack width requirements thus play an important role in the design of marine RC structures, and often dominate the design, resulting in significant increases in the amount of reinforcing steel used (Basteskår et al., 2019a:8).

1.2 Problem Statement

Despite the widespread use and importance of crack width requirements, most of the current requirements are based on an outdated understanding of the influence of cracking on durability. This is primarily due to the fact that most of the requirements have not been updated since they were first introduced in the 1980s (Basteskår et al., 2019a:3). While some of the existing crack width formulas

have been updated (Basteskår et al., 2019a:3), the overall concepts have not changed, and are therefore still based on outdated research, conducted before or during the 1980s.

In contrast to this, research on the influence of cracks on durability, which has been ongoing for decades (Arya & Myrzakulova, 2019:2), has led to an understanding of the influence of crack width on durability which differs significantly from that provided by the current crack width requirements. While the current requirements emphasize the importance of crack width, many studies have shown that other crack properties, such as crack orientation and frequency, may be equally important (Arya & Myrzakulova, 2019:2-3). Furthermore, the influence of crack width on durability has been found to depend, to some extent, on other concrete properties, such as cover depth, cover quality, and resistivity of the concrete (Otieno, Beushausen & Alexander, 2016:377). Some of these properties, such as concrete quality and resistivity, are not directly designed for in current durability design approaches. This all suggests that the current crack width requirements do not accurately account for the behaviour of cracked concrete in real structures.

While recent research (Otieno, Beushausen & Alexander, 2012; Otieno, Beushausen & Alexander, 2016; Van Hung, Hung & Viet, 2018) has also investigated the effects of crack width on corrosion rates and structural service life, the overall effectiveness of the current crack width requirements, as applied in the design of real structures, has not yet been evaluated or quantified. It is clear, from recent studies, that greater crack widths do generally result in shorter service lives (Otieno, Beushausen & Alexander, 2012:1806; Van Hung, Hung & Viet, 2018:12). However, Otieno, Beushausen and Alexander (2016:381) also found that even small cracks, with widths below those of the current crack width requirements, may lead to rapid corrosion initiation and the development of significant corrosion rates. The extent to which the current crack width requirements result in more durable structures is thus uncertain – particularly as the requirements frequently call for the use of additional reinforcing steel, which may simply cause more, faster corrosion damage if the limited crack widths are not successful in preventing the ingress of chloride ions and do not adequately reduce corrosion rates.

In addition to the effectiveness of the current crack width requirements at providing durability, the effects of the requirements on the costs and environmental sustainability of marine RC structures are also uncertain. The use of additional reinforcing steel, frequently associated with the crack width requirements, is likely to significantly affect the construction costs of marine RC structures, as well as their sustainability (as reinforcing steel is a finite, manufactured material). Furthermore, the effectiveness of the current crack width requirements at providing durability also influences costs and sustainability, through the need for maintenance and repairs. Despite this, it appears that no studies which specifically determine the cost and environmental sustainability implications of the current crack width requirements have been undertaken.

There is thus a great need to evaluate the durability, cost, and environmental sustainability implications of using the current crack width requirements. It is clear that the current requirements may be outdated. However, the extent to which this is the case is not certain. The requirements may still be adequate if they produce durable structures, with negligible economic and environmental impacts, or, they may be inadequate if the implications of their use are significantly negative. An evaluation of the durability, cost, and environmental sustainability implications of the current crack width requirements was therefore necessary to determine the adequacy of the requirements, in order to help inform decisions about whether updates or changes to the current durability design provisions are needed.

1.3 Objectives of the Study

The general objective of the study was to evaluate the implications of using the current crack width design requirements on the durability, cost, and environmental sustainability of marine RC structures.

The specific objectives and research questions that were considered to meet this general objective were as follows:

I. Determine and evaluate the effects of using the crack width requirements on the durability of marine RC structures
    - How can the effectiveness of the crack width requirements for providing durability be quantified?
    - Does designing for crack width requirements result in longer service lives (i.e., better durability)?

II. Evaluate the costs associated with using the crack width requirements for the durability design of marine RC structures
    - What are the types of costs which may be associated with the use of the crack width formulas?
    - How can these costs be quantified?
    - What are the costs of using the crack width requirements, and are these significantly higher than those of not using the crack width requirements?
    - How do the costs of using the crack width requirements compare to the costs of other methods of providing durability, such as the use of hydrophobic coatings? Are the crack width requirements the most cost-effective way of providing durability?

III. Evaluate the impacts of using the crack width requirements on the environmental sustainability of marine RC structures
    - How can the environmental sustainability of marine RC structures be quantified? Are there existing methods available to do this?
    - What are the impacts of using the crack width requirements on the environmental sustainability of marine RC structures, in quantitative terms?
    - Does designing for the crack width requirements result in larger environmental impacts? And if so, how significant are the impacts?

1.4 Scope and Limitations of the Study

The study focused on determining the implications of the current crack width design requirements on the durability, cost, and environmental sustainability of marine RC structures. As such, crack width requirements for flexural cracks and restrained drying shrinkage and thermal cracks were considered in the study. The study did not consider:

- Investigating the accuracy of the crack width formulas, or comparisons between the requirements specified in different design codes. Previous studies, such as those carried out by Lapi, Orlando, and Spinelli (2018) and McLeod and Viljoen (2019), have been conducted on these topics and it is known that the crack width formulas are often inaccurate (Alexander, Beushausen & Otieno, 2012:28)
- Crack width requirements for purposes other than providing durability, such as for preventing leaking in water-retaining structures
- The effects of other crack-related properties, such as frequency or orientation, on the durability of marine RC structures – only the influence of crack width on durability was investigated

- The secondary effects of durability on environmental sustainability – although poor durability will result in additional environmental impacts, for example through repairs or reconstruction, these effects were not quantified in this study.

1.5 Structure of the Dissertation

The dissertation begins with an introduction, during which a background to the study is provided, along with a description of the research problem and the objectives, scope, and limitations of the study. This is followed by a literature review in Chapter 2, which provides additional background information on marine reinforced concrete structures, their durability, and the processes which cause cracking in concrete. The literature review also discusses the influence of cracking on durability, and how crack width requirements are used within durability design. A brief outline of the methodology used for the study is then provided in Chapter 3, before the methodology for each stage of the study is described in Chapters 4 (Member Design), 5 (Service Life Modelling), 6 (Quantification of Material Amounts), 7 (Determination of Member Costs) and 8 (Member Embodied Carbon Estimations). The results of the study are then discussed in Chapter 9, from which conclusions and recommendations for future research are made in Chapters 10 and 11, respectively.

2. Literature Review

2.1 Introduction

This chapter aims to develop an understanding of the role of the current crack width design requirements in the durability design of marine RC structures, as well as to highlight existing methods, available in the literature, which can be used to evaluate their implications. As such, the chapter is split into three sections, as follows:

- **Section A**: *The Effects of Cracks on the Durability of Marine Reinforced Concrete Structures*
- **Section B**: *Crack Width Design – Current State of the Art*
- **Section C**: *Methods for Quantifying the Implications of the Current Crack Width Design Requirements*

Section A begins with an overview of the different types of marine RC structures, in order to place the study in context and provide an understanding of the types of structural elements used in marine RC structures. A discussion of the durability and service lives of marine RC structures is then provided, with specific reference to chloride-induced reinforcement corrosion, including mechanisms of chloride transport into concrete and the reinforcement corrosion process. Mechanisms of concrete cracking relevant to the crack width design of marine RC structures – namely shrinkage, thermal, and flexural cracking - are then discussed. With all the necessary background information thus provided, Section A is concluded with an evaluation of the effects of cracks on the durability of marine RC structures.

Section B aims to explain the current crack width design requirements and place them in context within the durability design of marine RC structures. This is done in two parts. The first part provides a broad outline of the durability design of marine RC structures, with a focus on the standards and codes of practice available in the UK, USA, Australia, Japan, and South Africa. The second part focuses specifically on the code requirements used for crack width design in South Africa, before providing a theoretical background to the crack width formulas used in the crack width design process. A critique of the current crack width requirements is then provided, along with a discussion of recent developments and possible solutions.

Section C focuses on providing background information for the methods used in this study to quantify the effects of designing for crack width on the durability, cost, and environmental sustainability of marine RC structures. As such, Section C is split into three parts, on service life modelling, life cycle cost analysis, and the calculation of embodied carbon.

SECTION A: *The Effects of Cracks on the Durability of Marine Reinforced Concrete Structures*

2.2 Reinforced Concrete Marine Structures

Marine structures can be generally defined as structures which are in contact with, or near to, the sea (Alexander & Nganga, 2016:2). These structures may be located either on the seashore, or partially or fully submerged in the sea (Alexander & Nganga, 2016:4). There are two main types of marine structures – port structures, which are used for berthing, loading, and unloading of ships and boats (Smith, 2016b:17), and coastal structures, which are located on or near to the coast and may be subjected to waves, currents, and sea splash and spray (Smith, 2016b:46).

Concrete is widely used in both port and coastal structures due to its versatility (which means it can be cast in almost any shape), cost-effectiveness, strength and durability (Alexander & Nganga, 2016:2-3). However, concrete is relatively weak when subjected to tensile forces, and is thus often reinforced with steel bars or rods (Owens, 2013:157). The resulting material, referred to as reinforced concrete (RC), is strong in both tension and compression, and can therefore be used for almost any type of structure. As such, RC is used in many different types of marine structures – the most significant of which are discussed in the following sections.

2.2.1 Port Structures

There are three main types of port structures which use significant amounts of RC – quay walls, jetties and wharves, and dry docks and ship lifts. Each of these types of port structure is discussed below.

Quay walls have two primary functions – firstly, they provide a place for vessels to berth, and secondly, they retain land which allows space for cargo to be stored (Smith, 2016b:17-18). A wide variety of quay wall types are available, but the most used are (Smith, 2016b:17-27):

- Blockwork walls, in which unreinforced, precast concrete blocks are stacked to form the quay wall, which is then finished with a cast-in-situ RC capping beam
- Caisson walls, which are constructed using large, RC "box" units that are floated into place and then filled with sand or other material to sink them into position. Figure 2-1 shows how the caisson units are essentially formed by concrete walls which are joined to make boxes
- Cantilever walls, which are made of precast RC wall units, generally consisting of both a wall and a base for stability
- Counterfort walls, which are similar to cantilever walls, except that they include counterforts for additional strength and stiffness, as shown in Figure 2-2

Jetties are typically used for berthing vessels which do not require large amounts of space to store cargo – such as fishing and recreational vessels (Smith, 2016b:33). Jetties may also be used for restaurants and shops, or as outlook platforms (Burcharth & Hughes, 2006:VI-2-6), and typically run perpendicular to shore (Gaythwaite, 2016:313). In contrast to this, wharves are built parallel to, and against, the shoreline (Gaythwaite, 2016:314). Figure 2-3 shows examples of a wharf and jetty.

Jetties and wharves are typically constructed as "deck on pile" systems, in which a RC deck slab is supported by RC piles (Smith, 2016b:33-34), although in some cases the deck slab may be supported on beams, which are in turn supported by piles. "Skeletal" jetties, which are composed only of beams and piles, may also be constructed in situations where deck slabs are not needed – such as for the offloading of iron ore and coal by conveyor systems (Smith, 2016b:37).

Dry docks and ship lifts are used for the construction and repair of marine vessels, and make use of many of the same structural systems as those used in the construction of quay walls and jetties – such as cantilever walls and caissons (Smith, 2016b:42).

Figure 2-1: Two caisson units under construction in the Port of Cape Town (Smith, 2016b:23).

Figure 2-2: Precast counterfort wall units under construction in Saldanha Bay, South Africa (Paul & Zietman, 1999:11).

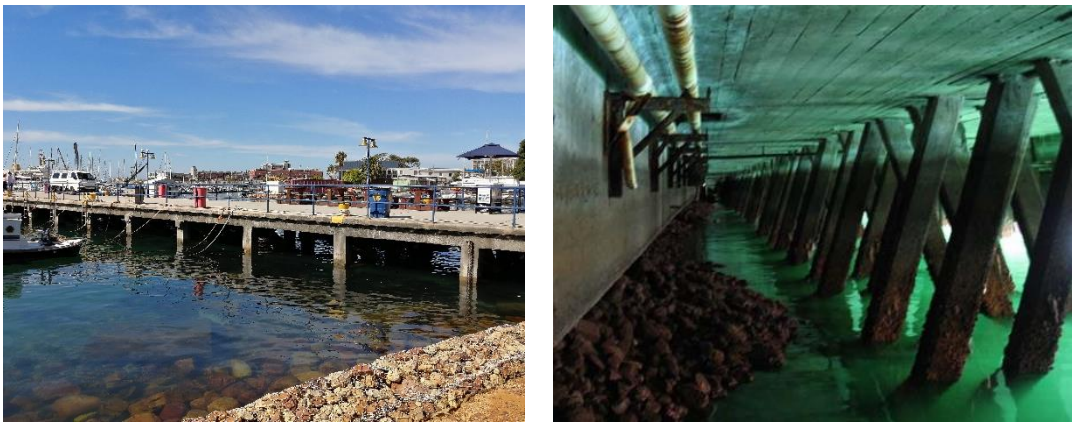

Figure 2-3: A jetty in Simon's Town, South Africa (left) and a wharf in Mossel Bay, South Africa (right) (Smith, 2016b:36).

2.2.2 Coastal Structures

While the term "coastal structures" encompasses a wide variety of structures, from seawalls to coastal buildings (Smith, 2016b:46), only four types of coastal structures – seawalls, breakwaters, coastal jetties, and coastal bridges – consistently use sufficient quantities of RC to be relevant to this study. Each of these types of coastal structures is discussed below.

Seawalls protect coastal land from flooding due to storm surges and waves (Burcharth & Hughes, 2006:VI-2-1), and are typically built using RC cantilever walls (Smith, 2016b:46). Breakwater structures are primarily built to protect harbour basins from waves and storm surges, such that calm conditions are available for marine vessels to safely berth and transfer cargo (Burcharth & Hughes, 2006:VI-2-5). These structures may either be of the "sloping front", rubble mound type, or the "vertical front" type, which can be constructed from caissons or blockwork walls (Burcharth & Hughes, 2006:VI-2-5). Rubble mound breakwaters may use precast concrete armour units, such as dolosse, but these are typically made without any steel reinforcement (Smith, 2016b:48).

Coastal jetties are very similar to port jetties, except that they are built in unprotected water, and are thus subject to wave and current forces, and may be used for a wider variety of functions (Smith, 2016b:52). Some of these functions include loading and offloading cargo, serving as beach groynes, or housing sand bypass facilities, seawater intakes and effluent outfalls (Smith, 2016b:52). Despite the differences in expected loads and functions, coastal jetties are typically built using the same structural systems as port jetties – that is, RC deck slabs supported on RC beams and/or piles.

Bridges located in coastal regions are typically designed as marine structures, as they are exposed to the same corrosive environmental actions as marine structures (Smith, 2016b:53). These bridges, much like jetties, are also typically constructed using RC piles, columns, beams, and deck slabs.

2.3 Durability and Service Life of Reinforced Concrete Marine Structures

The durability of a structure can be defined as its ability to resist deterioration for the duration of its design life, without losing its functionality or requiring significant rehabilitation (Ballim, Alexander & Beushausen, 2009:155). The concept of durability is thus inherently linked to the concept of service life – which is defined as the length of time during which the structure is functional, without requiring major repairs or rehabilitation (Nilsson, 2019:123-124). In fact, service life can be seen simply as a quantitative measurement of durability (Nilsson, 2019:123).

2.3.1 Factors Influencing Durability and Service Life

Figure 2-4 shows how the durability of marine RC structures is influenced by interactions between many factors, which can be divided into two groups – factors that relate to the concrete itself, and external factors that relate to the loads and actions to which the RC is exposed (Ballim, Alexander & Beushausen, 2009:156). Together, the factors which relate to the properties of the concrete itself form the "concrete system" (Ballim, Alexander & Beushausen, 2009:156). Within the concrete system, the most important factors are the binder type, water/binder (w/b) ratio, curing conditions, compaction and initial temperature development of the concrete (Ballim, Alexander & Beushausen, 2009:156). The influence of each of these factors on the deterioration resistance of the concrete system are discussed in Section 2.3.2.

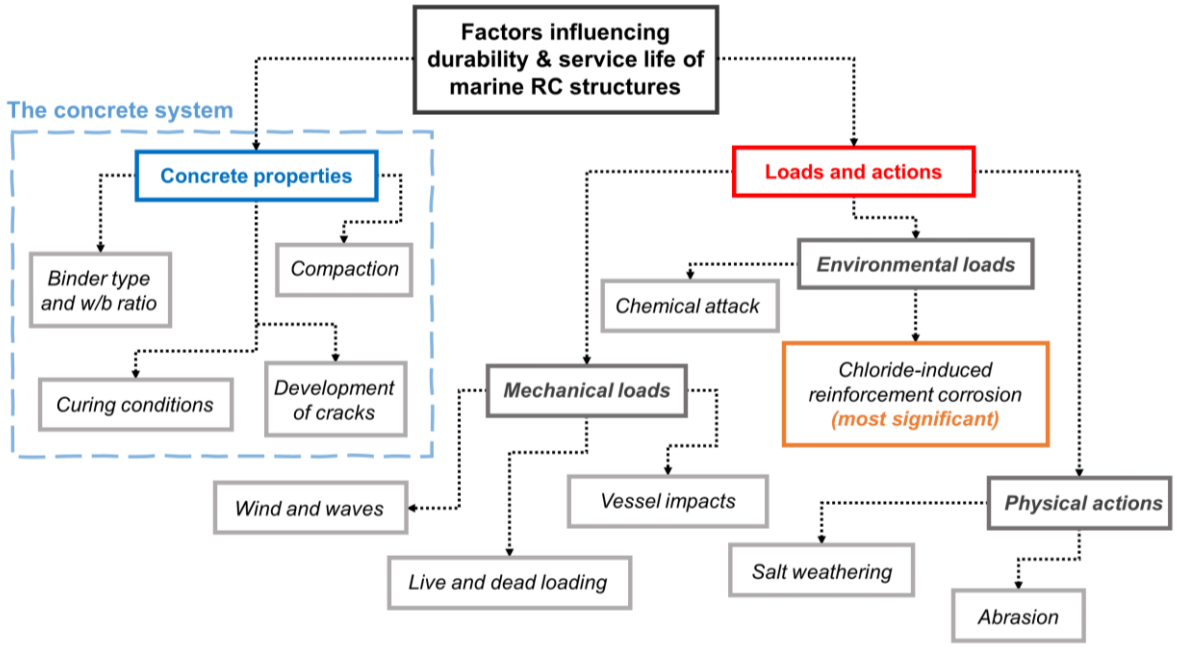

Figure 2-4: A diagram of the factors which influence the durability of marine RC structures (adapted from Ballim, Alexander & Beushausen, 2009:156).

There are three different types of loads and actions which affect RC durability in marine environments – mechanical loads, physical actions and environmental loads (Alexander & Nganga, 2016:4). Mechanical loads may come from wind, waves, vessel impacts and dead and live loading of the structure, while physical actions include abrasion and salt weathering (Alexander & Nganga, 2016:4; Santhanam & Otieno, 2016:144). Environmental loads may include chemical attack on the concrete, or corrosion of the reinforcement – which in marine environments tends to be caused by the ingress of chlorides into the concrete (Alexander & Nganga, 2016:4). However, despite the variety of loads and actions that may affect durability, it is widely acknowledged that chloride-induced reinforcement corrosion is the most significant deterioration mechanism, which plays the largest role in determining the durability and service life of marine RC structures (Rahimi et al., 2014:1; Santhanam & Otieno, 2016:144; Nilsson, 2019:124). Chloride-induced reinforcement corrosion, and the transport mechanisms through which it is initiated, is discussed in detail in Sections 2.3.3 to 2.3.5.

2.3.2 The Concrete System

Concrete is a complex, heterogenous material, made from a mixture of cementitious material or "binder", admixtures, aggregates, and water (Sousa-Coutinho, 2009:153). When this mixture sets, it produces a solid material which consists of three distinct phases (Li & Liang, 2011:153):

- **Aggregates**, which are classified as either "coarse" or "fine", depending on their size, and which typically make up approximately 75% of the volume of concrete (Li & Liang, 2011:23-24)
- **Hardened cement paste (HCP)**, primarily composed of calcium silicate hydrate ($C_3S_2H_8$, or "C-S-H") and calcium hydroxide ($Ca(OH)_2$), which make up about 50-60% and 25% of the HCP phase, respectively (Sousa-Coutinho, 2009:159; Li & Liang, 2011:38). The significant portion of $Ca(OH)_2$ in the HCP results in the formation of a highly alkaline environment, with concrete pH values typically being greater than 12 (Li & Liang, 2011:38)
- **An interfacial transition zone (ITZ)**, which is an area of hardened cement paste between the HCP and aggregate phases, which differs significantly in structure and properties from the HCP

phase as a result of the boundary provided by the aggregate phase (Ballim, Alexander & Beushausen, 2009:159). The ITZ phase is typically only about 10-50 μm thick, but has a significant influence on concrete properties (Li & Liang, 2011:153)

The properties of the concrete system are ultimately determined by these three phases, and the interactions between them. Where durability is concerned, the most important concrete property is penetrability – which can be defined as the ease with which aggressive species can travel into the concrete (Ballim, Alexander & Beushausen, 2009:156). This is because deterioration of concrete structures almost always occurs due to the ingress of aggressive species, such as chlorides, carbon dioxide, oxygen and moisture (Richardson, 2002:38). The concrete system thus resists deterioration through a combination of chemical and physical resistance, which serves to reduce the penetrability of the concrete (Schiessl & Lay, 2005:91; Thomas, 2016:154).

For marine RC structures, which deteriorate primarily because of chloride-induced reinforcement corrosion, the chemical resistance of the concrete system is largely a function of its chloride-binding capacity and the high alkalinity of the concrete (Ballim, Alexander & Beushausen, 2009:160). Chloride binding occurs due to chemical reactions between components of the HCP (particularly tricalcium aluminate, C_3A, and calcium aluminoferrite, C_4AF) and chlorides which have penetrated into the concrete (Ballim, Alexander & Beushausen, 2009:160). These reactions result in the formation of Friedel's salt, such that the chlorides are bound in the salt, and cannot travel further into the concrete (Nilsson, 2003:18). However, the mechanism of chloride binding is currently not completely understood, and also includes a physical binding component (Nilsson, 2003:18). Despite this, it is clear that chloride binding is influenced by a wide variety of factors (Nilsson, 2003:18), and can be improved significantly by the use of supplementary cementitious materials (SCMs) such as fly ash (FA) and ground granulated blastfurnace slag (GGBS) in the binder, which result in higher alumina concentrations (Thomas, 2016:154).

The physical resistance of the concrete system is largely a function of the structure and complexity of the concrete's pore system (Schiessl & Lay, 2005:91). This is as concrete penetrability is lower for small, disconnected pores than for systems of large, interconnected pores (Richardson, 2002:38). There are ultimately three significant types of pores in concrete, either in the HCP or ITZ phases (Sousa-Coutinho, 2009:159-160):

- Gel pores, which are voids between hydrated cement particles
- Capillary pores, i.e., voids which were originally occupied by water, and have not been occupied by hydrated cement particles
- Macropores, which are entrapped air voids which were not removed when the concrete was compacted

However, only capillary pores tend to contribute significantly to concrete penetrability, as gel pores and macropores are typically not interconnected (Sousa-Coutinho, 2009:160). It is also widely acknowledged that the ITZ is significantly more porous than the HCP (Ballim, Alexander & Beushausen, 2009:159; Li & Liang, 2011:154; Alexander, Bentur & Mindess, 2017:27). This is as the aggregates create a "wall" effect, such that the binder particles cannot efficiently fit together against the aggregate, and bleeding in the concrete leads to water being trapped on aggregate surfaces, particularly on the aggregate undersides (Alexander, Bentur & Mindess, 2017:27).

The greater porosity of the ITZ, combined with an increase in microcracking in the ITZ (Alexander, Bentur & Mindess, 2017:11), means that the ITZ tends to be significantly more penetrable than the HCP, such that aggressive agents often travel primarily through the ITZ (Ballim, Alexander & Beushausen,

2009:159). Figure 2-5 shows how ITZs frequently interlink, creating pathways for the ingress of aggressive agents (Ballim, Alexander & Beushausen, 2009:159).

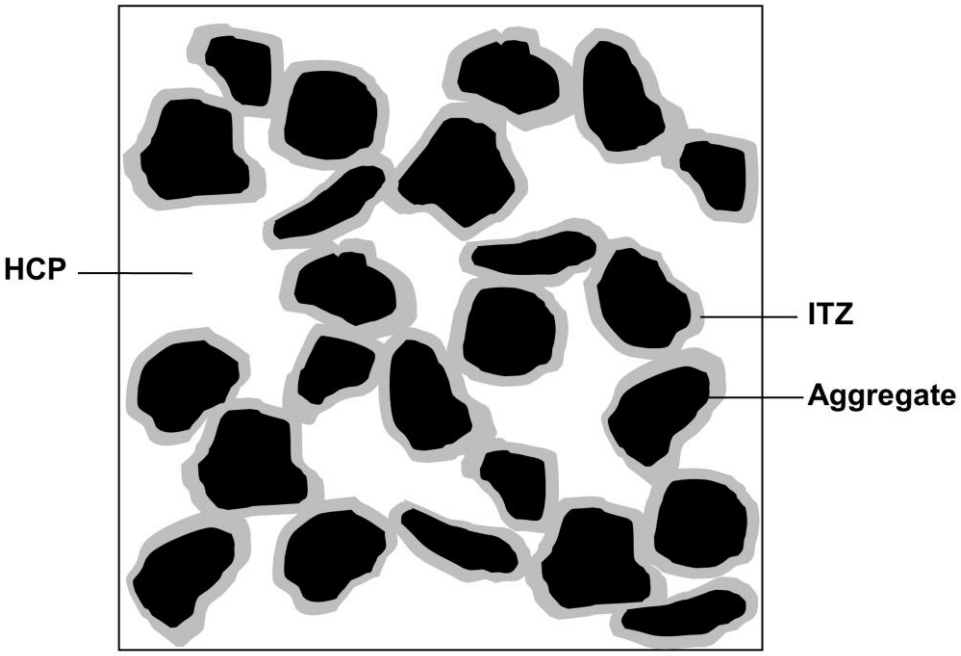

Figure 2-5: A diagrammatic representation of a concrete sample, showing how the ITZ phases may interlink to produce pathways for the ingress of aggressive agents (adapted from Ballim, Alexander & Beushausen, 2009:159).

The number, size, and structure of concrete pores, and thus the penetrability of a given concrete, depends on a variety of factors – such as binder type, w/b ratio, curing conditions, initial temperature development, and compaction (Ballim, Alexander & Beushausen, 2009:156). The use of SCMs in the binder is known to reduce penetrability in two ways. Firstly, SCM particles tend to be significantly smaller than cement particles, allowing a much denser microstructure to be achieved in both the HCP and the ITZ, as the SCM particles fill up the spaces between hydrated cement particles (Li & Liang, 2011:158). Secondly, many SCMs, such as FA and GGBS, are pozzolanic – meaning that they react with the $Ca(OH)_2$ produced in the hydration reactions of the ordinary Portland cement (PC) to form additional C-S-H (Li & Liang, 2011:159; Alexander, Bentur & Mindess, 2017:49) – thereby further densifying the concrete microstructure.

The w/b ratio has perhaps the biggest influence on concrete penetrability, with larger w/b ratios producing more penetrable concrete (Richardson, 2002:40; Basheer, 2009:57; Thomas, 2016:154). This is as larger w/b ratios are associated with larger spaces between binder particles, such that not all of the space is ultimately filled with hydration products – thereby resulting in more capillary pores (Alexander, Bentur & Mindess, 2017:18). The spaces between binder particles also depend upon the extent of hydration of the concrete – hydrated binder particles are larger than un-hydrated particles, such that the more hydration reactions occur, the smaller the spaces, and thus pores, will be (Alexander, Bentur & Mindess, 2017:18). Curing, which ensures that concrete moisture and temperature conditions are kept at suitable levels for the maximum number of hydration reactions to occur, and the initial temperature development of the concrete with hydration, thus also play a significant part in determining concrete penetrability (Alexander, Bentur & Mindess, 2017:18). Finally, the degree of compaction also influences porosity, by reducing the number of macropores. However, as stated before, the influence of macropores on concrete penetrability tends not to be significant, due to their isolated nature (Sousa-Coutinho, 2009:160).

2.3.3 An Overview of Chloride-Induced Reinforcement Corrosion

Reinforcing steel, by itself, will corrode if left exposed in the presence of water and oxygen (Ballim, Alexander & Beushausen, 2009:163; Nilsson, 2019:115). However, this corrosion is prevented in RC, even if water and oxygen are present, by a layer of iron oxides which forms around the reinforcing steel. This layer, known as the "passive layer", forms due to the high alkalinity of concrete (Nilsson, 2019:115), which, as discussed in Section 2.3.2, occurs because of the large amounts of $Ca(OH)_2$ present in the HCP (Li & Liang, 2011:38). For corrosion of the reinforcement to occur, the passive layer thus has to be destroyed. There are two mechanisms which may destroy the passive layer – carbonation, or chloride ingress – although only chloride ingress is generally significant in the marine environment (Smith, 2016a:65).

The transport mechanisms which are responsible for the ingress of chlorides into concrete are discussed in detail in Section 2.3.4. As a result of these mechanisms, more and more chloride ions penetrate into the concrete with time, at increasing depths. Eventually, the concentration of chlorides at the reinforcing steel will reach a critical concentration, known as the chloride threshold (Nilsson, 2019:115) – beyond which depassivation of the steel occurs. The chloride threshold is most commonly presented as a ratio of the total mass of chlorides to the total mass of cement, and is typically about 0.4% (Santhanam & Otieno, 2016:144).

Once depassivation of the steel has occurred, the steel will begin to corrode (if enough oxygen and water is available) – leading to the formation of corrosion products such as rust. These corrosion products have a greater volume than the uncorroded steel (Nilsson, 2019:115), and therefore cause expansive stresses to develop in the concrete – resulting in cracking, delamination and eventually spalling of the concrete covering the reinforcement.

The cracking, delamination and spalling which occur because of chloride-induced reinforcement corrosion significantly affects the appearance and functionality of reinforced concrete structures. The corrosion of the reinforcement also reduces the effective area of reinforcement provided to the concrete, which may reduce the safety and stability of the structure considerably (Alexander & Beushausen, 2019:17). This, combined with the fact that corrosion of the reinforcement may occur rapidly once initiated (Rahimi et al., 2014:1), makes chloride-induced reinforcement corrosion a significant problem and the biggest threat to the durability of marine RC structures.

2.3.4 Mechanisms of Chloride Transport into Marine Concrete

There are four distinct mechanisms by which aggressive agents (such as chlorides, carbon dioxide, oxygen and water) may travel into concrete – permeation, diffusion, sorption and migration (Ballim, Alexander & Beushausen, 2009:156-157). Each of these mechanisms, and the ways in which they contribute to chloride ingress and the deterioration of marine RC structures, are discussed in this section.

Permeation refers to the movement of a fluid (i.e., a liquid or gas) through the concrete pore structure, from an area of higher pressure to an area of lower pressure (Ballim, Alexander & Beushausen, 2009:157), while the pore structure is saturated with the fluid (Alexander, Bentur & Mindess, 2017:56). As such, the rate of permeation depends on both the penetrability, and the moisture state of the concrete (Ballim, Alexander & Beushausen, 2009:157). It is also worth noting that ionic species, such as chlorides, which are soluble in fluids such as water, may also be transported into concrete with permeation of the fluid (Santhanam & Otieno, 2016:139).

Diffusion is the movement of a fluid or ionic species from a region of higher concentration, to a region of lower concentration, through the pore structure of the concrete (Thomas, 2016:153), and occurs only in partially or fully saturated concrete (Ballim, Alexander & Beushausen, 2009:157). Diffusion is

particularly relevant for marine RC structures, and other concrete structures exposed to salts, as these structures tend to develop high surface concentrations of salts, which then diffuse inwards (Alexander, Bentur & Mindess, 2017:57). In addition to chlorides and other salts, diffusion is also the primary transport mechanism for oxygen into concrete, without which reinforcement corrosion could not occur (Ballim, Alexander & Beushausen, 2009:158).

The rate of diffusion depends on temperature, the type of fluid or ionic species under consideration, and the penetrability and moisture condition of the concrete (Ballim, Alexander & Beushausen, 2009:157). However, the process of diffusion is relatively complex, and is also influenced by the presence of damage (such as cracks and voids) in the concrete, electrochemical processes associated with reinforcement corrosion (Ballim, Alexander & Beushausen, 2009:157), and the mechanism of chloride binding discussed in Section 2.3.2 (Alexander, Bentur & Mindess, 2017:58).

Absorption (also referred to as "convection") describes the movement of a liquid (typically water) into concrete by the action of capillary forces (Alexander, Bentur & Mindess, 2017:57). Absorption is heavily influenced by the pore structure and moisture state of the concrete (Ballim, Alexander & Beushausen, 2009:157), and is most significant in concrete which is exposed to cyclic wetting and drying (Alexander, Bentur & Mindess, 2017:57). As such, absorption plays a significant role in the transport of chlorides (which are dissolved in seawater) into marine RC structures, resulting in the accumulation of chlorides at the concrete surface (Alexander, Bentur & Mindess, 2017:57). However, beyond the surface and relatively shallow depths, the capillary forces become too weak to transport significant amounts of liquid and chlorides into the concrete (Ballim, Alexander & Beushausen, 2009:157).

Migration (also referred to as accelerated diffusion) occurs when ions, in a solution, move under an electrical field, towards a positive charge (Ballim, Alexander & Beushausen, 2009:158; Thomas, 2016:154). However, migration does not typically occur in concrete structures (Santhanam & Otieno, 2016:139), and is instead most commonly used to simulate the diffusion of chlorides in accelerated chloride laboratory tests (Ballim, Alexander & Beushausen, 2009:158).

It can thus be seen that the aggressive agents (namely chlorides, oxygen, and water) primarily responsible for the deterioration of marine RC structures may penetrate into the RC by several different mechanisms. However, in practice, these transport mechanisms seldom operate alone, and in fact generally work in conjunction with one another to promote the ingress of aggressive species into the concrete (Ballim, Alexander & Beushausen, 2009:158). This is particularly true for the ingress of chlorides. Figure 2-6 shows the various combinations of transport mechanisms which are typically responsible for the ingress of chlorides in marine RC structures.

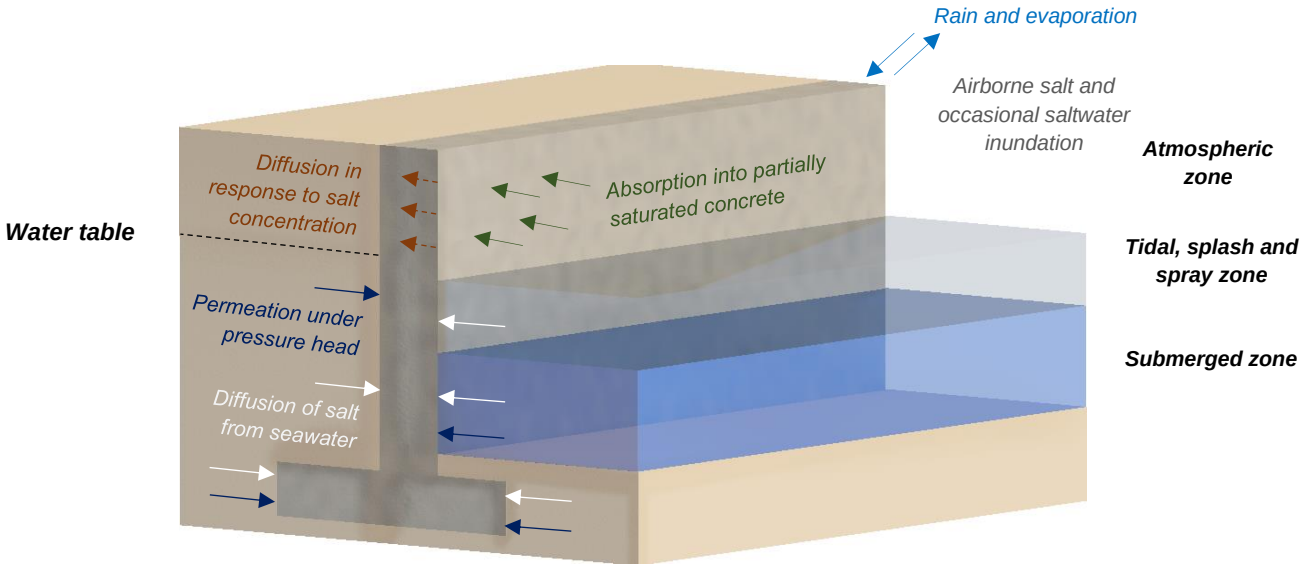

Figure 2-6: A diagrammatic representation of the transport mechanisms which typically occur in marine RC structures, shown here for a seawall (adapted from Santhanam & Otieno, 2016:138).

Note how the presence of the various transport mechanisms depends upon the area of the structure under consideration. Three such areas are typically considered in the design of marine RC structures (Santhanam & Otieno, 2016:140):

- The atmospheric zone, in which the RC is exposed to both airborne chlorides and wetting and drying because of rain – leading to both absorption (typically in the first few millimetres of the concrete) and diffusion playing a role in the ingress of chlorides
- The tidal, splash and spray zone, where the RC is exposed to cyclic wetting and drying by seawater, such that absorption, permeation, and diffusion all occur. Absorption occurs within the first few millimetres of the concrete where the concrete is exposed to seawater splash and spray, resulting in high chloride concentrations which then diffuse deeper into the RC (Thomas, 2016:154). Lower down in the tidal zone, the RC typically does not dry out, and is thus almost constantly saturated – and therefore exposed primarily to permeation and diffusion
- The submerged zone, in which both permeation and diffusion occur, as the RC is exposed to both high pressures (due to the hydrostatic forces exerted by the seawater) and high concentrations of chlorides (in the seawater)

However, in order to model the ingress of chlorides into marine RC structures, for the purposes of service life modelling and durability design, diffusion is assumed to be the dominant chloride transport mechanism (Ballim, Alexander & Beushausen, 2009:178). This is a valid assumption for the submerged zone, and the lower parts of the tidal, splash and spray zone, where diffusion does indeed tend to dominate (Ballim, Alexander & Beushausen, 2009:158). However, it is not strictly accurate for the atmospheric and tidal, splash and spray zones – where the presence of both absorption and diffusion in the first few millimetres of the concrete (referred to as the convection zone) makes the overall process of chloride ingress complex and unclear (Ballim, Alexander & Beushausen, 2009:158). This complexity is typically solved by effectively ignoring the convection zone in service life models, as beyond the convection zone, the effect of absorption is negligible and diffusion does indeed dominate (Ballim, Alexander & Beushausen, 2009:158).

2.3.5 The Corrosion Process

Once sufficient chloride ingress has occurred to destroy the passive layer, corrosion of the reinforcing steel takes place in a two-stage process (Raupach, 1996:330), involving the formation of a corrosion cell, made up of anodes and cathodes on the reinforcing steel (Ballim, Alexander & Beushausen, 2009:168). Figure 2-7 shows how, within the corrosion cell, iron is converted to iron(II) (thereby releasing electrons) at the anode, while the released electrons travel to the cathode and react with oxygen and water to form hydroxide ions (Ballim, Alexander & Beushausen, 2009:168). The conversion of iron to iron(II) results in the formation of rust and deterioration of the steel (Raupach, 1996:330). Note how the corrosion process is dependent upon the availability of oxygen and water, as well as the ability of the electrons released at the anode to travel through the concrete to the cathode.

The corrosion process also depends upon the type of corrosion cell formed. Corrosion cells may either form as microcells, in which the anodes and cathodes are of similar, small, size, or as macrocells, with relatively small anodes and large cathodes, that may be next to the anodes or up to a few metres away from them (Raupach, 1996:331). The two types of corrosion cells are illustrated in Figure 2-8. Microcells generally produce relatively uniform corrosion along the length of the reinforcing steel, while macrocells cause large, localised losses of steel at the anodes, in a process known as pitting corrosion (Raupach, 1996:331).

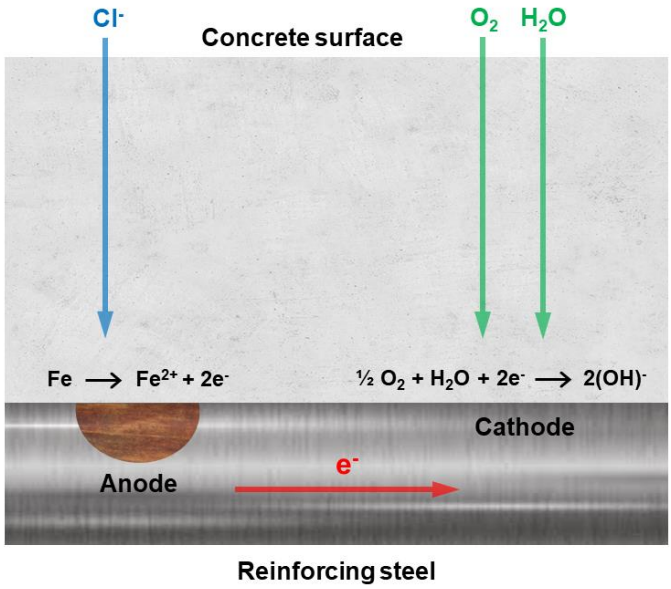

Figure 2-7: A diagrammatic representation of a corrosion cell (adapted from Raupach, 1996:330).

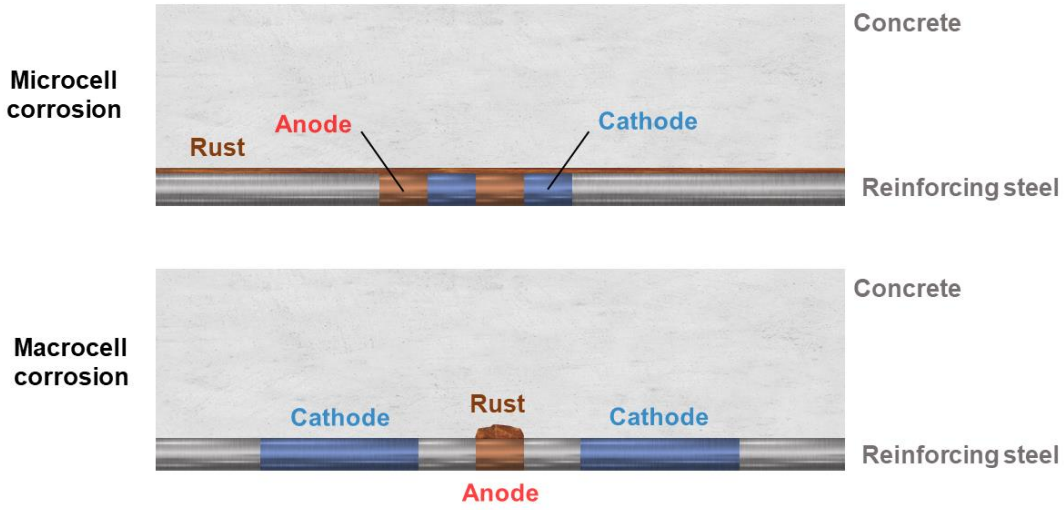

Figure 2-8: Diagrammatic representations of typical micro- and macrocells (adapted from Raupach, 1996:331).

2.3.6 Stages of Service Life for Marine Reinforced Concrete Structures

The service lives of marine RC structures are typically split into two stages (Tuutti, 1982:18) with reference to the chloride-induced reinforcement corrosion process. These stages are represented graphically in Figure 2-9. The first stage, the corrosion initiation phase, is the time period from the construction of the structure, until the chloride threshold is reached at the level of the reinforcing steel (Alexander & Beushausen, 2019:24). It thus follows that the second stage, the propagation phase, is the stage in which corrosion of the steel and subsequent damage (cracking, delamination and spalling) occurs (Alexander & Beushausen, 2019:24). The propagation phase can thus be defined as the time period from the initiation of reinforcement corrosion, until the corrosion damage becomes unacceptable (Alexander, Beushausen & Otieno, 2012:31), and the service life of the structure is deemed to be over.

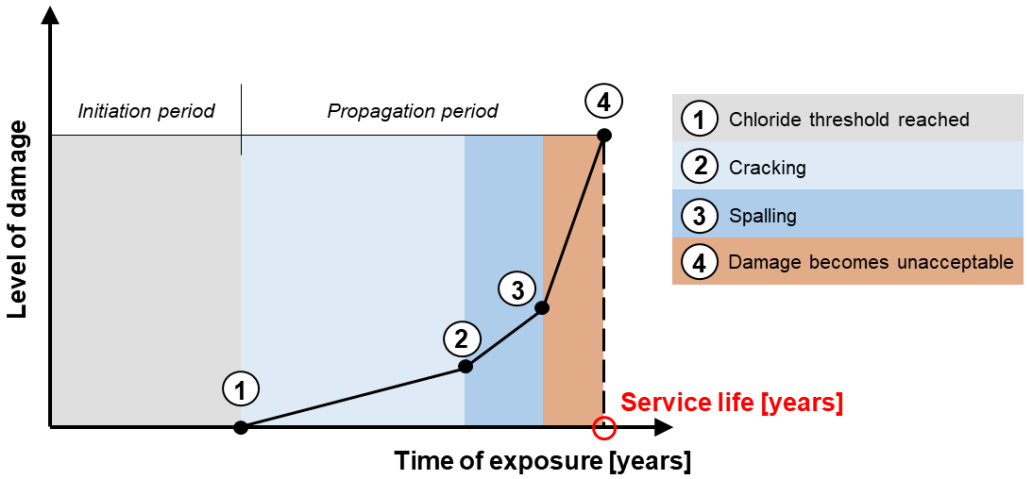

Figure 2-9: A graphical representation of the service life of a marine reinforced concrete structure (adapted from Alexander & Beushausen, 2019:25).

2.4 Cracking of Reinforced Concrete

Cracking is a common feature of concrete, with the vast majority of RC structures experiencing some form of cracking during their service lives (Alexander, Bentur & Mindess, 2017:62). Concrete cracks when it is subjected to tensile stresses which are greater than its tensile strength, which is known to be very low (Mihashi & Leite, 2004:141). There are many different sources of tensile stresses in concrete and consequently, there are many different causes of cracking. The American Concrete Institute (ACI Committee 224, 1993:2-9) provides a comprehensive list of 11 different causes of cracking, which includes, amongst others, cracking due to shrinkage, thermal stresses, chemical reactions, reinforcement corrosion and applied loads. However, only three cracking mechanisms – shrinkage cracking, thermal cracking (due to both hydration heat development and ambient temperature fluctuations) and flexural (or tensile) cracking – are relevant to the durability design of marine RC structures (Smith, 2016a:84).

It is also worth noting that cracks in concrete may vary significantly in scale, from "microcracks", which are less than 30 μm in width, to "macrocracks", which are typically 100 μm to several mm wide, and are generally visible (Alexander, Bentur & Mindess, 2017:63). All of these cracks, regardless of scale, are likely to influence the properties of concrete, such as strength and penetrability (ACI Committee 224, 1993:2). However, in practice, it is very difficult to design for the prevention of microcracking, the effects of which may be variable and insignificant, depending on the microcrack width (Alexander, Bentur & Mindess, 2017:63). The crack width design of marine RC structures therefore focuses on macrocracking, and as such, only macrocracking will be discussed in this section of the literature review, with the term "cracking" referring only to macrocracking.

2.4.1 Description and Quantification of Cracking

Before the various types of cracking relevant to the durability design of marine RC structures can be discussed, it is necessary to define the crack properties which are used to describe and quantify cracking. This is as these properties vary depending on the type of cracking under consideration, and as such, they play an important role in classifying the types of cracking (ACI Committee 224, 1993:9; Richardson, 2002:209; Basheer & Barbhuiya, 2009:177). Where the durability design of marine RC structures is concerned, understanding the properties of cracks, and the ease with which they may be measured, also goes some way to explaining the focus on crack widths, as opposed to other crack properties, in durability design.

A variety of crack properties may be used to describe cracks, and of these, the most significant are (Richardson, 2002:209):

- Crack width, which is typically measured as the width of the crack opening at the concrete surface
- Crack depth, i.e., the distance from the opening of the crack, at the concrete surface, to its tip within the concrete
- Crack length, from beginning to end
- Taper of the crack, i.e., the extent to which the crack narrows from its opening to its tip
- Crack orientation, which is typically specified relative to the reinforcing steel, and may be either "coincident", if the crack runs along the reinforcement, or "intersecting" if the crack runs across the reinforcement (Arya & Myrzakulova, 2019:3)
- Crack spacing, typically quantified in terms of crack frequency, which may be seen as the number of cracks in a given length (Shaikh, 2018:2)

- Crack pattern, with some types of cracking, such as shrinkage cracking, producing cracks in regular or irregular patterns

However, it should be noted that, of the properties which may be used to describe cracks, only four (width, orientation, spacing, and pattern) may be easily measured or determined in practice. Measurement of crack depth and taper is made difficult by the inaccessible nature of cracks for physical tools such as rulers and tape measures, and by the presence of debris in cracks which may significantly reduce the accuracy of electronic methods such as the ultrasonic pulse velocity test. Determining crack length is complicated by the fact that many cracks are not linear, and follow twisting, winding paths which make quick measurements with rulers or tape measures very difficult.

In contrast to this, crack width may be measured relatively easily with a crack comparator, which is essentially a small-scale, portable microscope with scaled measurements on the lens (ACI Committee 224, 1993:9), or with a crack width gauge, as shown in Figure 2-10. Crack spacing may be measured simply with a tape measure, while crack orientation and pattern can be determined visually, with knowledge of the layout of reinforcement in the structure.

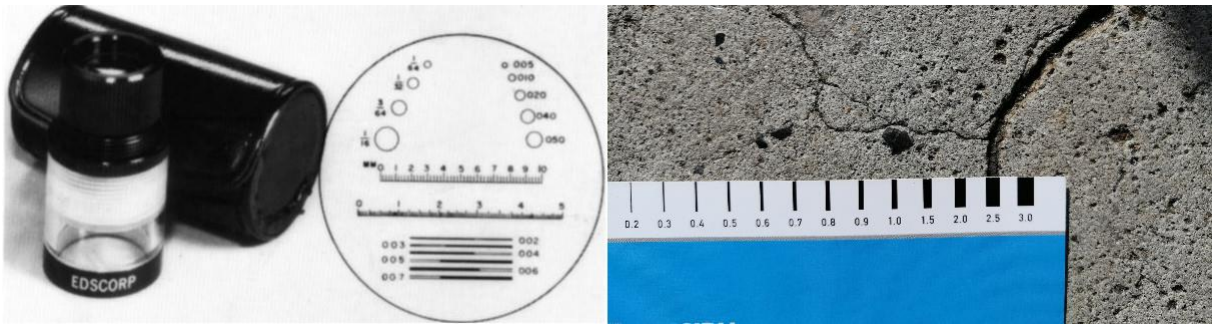

Figure 2-10: An example of a crack comparator (left, ACI Committee 224, 1993:9) and a crack width gauge in use (right).

It can thus be seen that, while cracks may be described by several properties, only crack width and spacing may be used practically to quantify cracks (as crack orientation and pattern, by definition, are not quantitative). It is because of this that discussions of concrete cracking in the literature tend to focus on crack width when describing cracks (ACI Committee 224, 2001; Day & Clarke, 2003; Alexander, Bentur & Mindess, 2017), and the durability design of marine RC structures aims to limit crack widths – the success of the design at limiting other crack properties, such as taper or depth, cannot easily be verified in practice.

2.4.2 Shrinkage Cracking

Shrinkage cracking occurs when moisture is lost from concrete (Alexander & Beushausen, 2009:131), which results in a decrease in concrete volume. If this decrease in volume is restrained, and cannot freely occur, then the concrete will be placed under strain, leading to the development of tensile stresses and cracking (Safiuddin et al., 2018:4). Most concrete is restrained, with the restraint either being provided internally, by aggregates, reinforcement and uneven drying of the concrete, or externally, such as when concrete is cast onto older concrete which has already hardened (Alexander & Beushausen, 2009:132-133).

Shrinkage cracking may occur in a variety of patterns (Day & Clarke, 2003:4), and may be significant in width and density (Alexander & Beushausen, 2009:132). There are four main types of shrinkage which may produce cracking in concrete:

- Plastic shrinkage, which occurs due to the evaporation of water in freshly cast concrete, when the concrete's tensile strength is at its lowest (Holt & Leivo, 2004:521). Plastic shrinkage cracking typically occurs in diagonal or "map" patterns (Boshoff & Combrinck, 2013:34), as shown in Figure 2-11, and may also occur in approximately parallel lines over reinforcement. These cracks may be up to 3 mm wide, and are generally between 20 and 50 mm deep, with lengths of about 50 mm to 3 m (Day & Clarke, 2003:10) – although in some cases plastic shrinkage cracks may reach significant depths (Moelich, Kruger & Combrinck, 2020:2). The spacing of diagonal plastic shrinkage cracks varies, but may be as much as 1 to 2 m (Day & Clarke, 2003:10)
- Drying shrinkage, caused by a loss of water to evaporation when the concrete is in a hardened state (Mihashi & Leite, 2004:142). Drying shrinkage cracks may form in many different types of patterns, although they often develop perpendicular to the direction with the greatest restraint (Day & Clarke, 2003:16). Figure 2-11 shows an example of such a case, where cracking occurs in a relatively straight line, perpendicular to the longer side of the slab – which provides the greatest restraint (Day & Clarke, 2003:16). The widths of drying shrinkage cracks also vary significantly, depending on the magnitude of shrinkage and the degree of restraint (Day & Clarke, 2003:16)
- Autogenous shrinkage, which results from water being used up in the hydration of cement particles (Mihashi & Leite, 2004:142)
- Carbonation shrinkage, a long-term type of shrinkage that occurs due to reactions between the hardened cement paste and atmospheric carbon dioxide (Holt & Leivo, 2004:522)

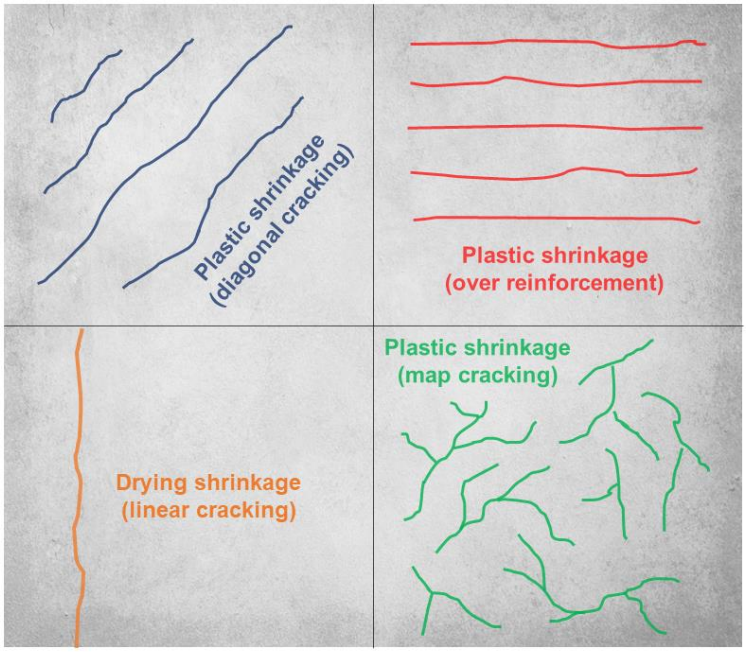

Figure 2-11: Typical plastic and drying shrinkage cracking patterns on slab panels (adapted from Day & Clarke, 2003:4).

However, plastic shrinkage is typically only relevant for surfaces exposed to drying – such as slab and floor surfaces, which have not been cast against formwork – and the effects of carbonation shrinkage are generally assumed to be insignificant. Thus, for most concrete, only drying shrinkage is significant

– although high strength concrete may experience considerable autogenous shrinkage (Alexander & Beushausen, 2009:131).

2.4.3 Thermal Cracking due to Hydration Heat

Thermal cracking occurs in a similar manner to shrinkage cracking and is in fact often classified as a type of shrinkage cracking (Holt & Leivo, 2004:522). Like shrinkage cracking, thermal cracking occurs due to volume changes in the concrete, which impose strains, and thus tensile stresses, on restrained concrete. However, unlike shrinkage cracking, the volume changes which cause thermal cracking are the result of changes in internal and external concrete temperatures (Mihashi & Leite, 2004:143), which lead to expansion and contraction of the concrete. These temperature changes may be caused either by the hydration of binder as the concrete hardens, or by fluctuations in ambient temperature conditions (ACI Committee 224, 1993:4; Barre, 2016:143; El-Reedy, 2019:188). Thermal cracking due to binder hydration is discussed in this section, while thermal cracking due to changes in ambient temperature conditions is covered in Section 2.4.4.

The hydration of binder, which occurs in exothermic reactions, leads to heat development within the concrete (Mihashi & Leite, 2004:143). This heat development causes the concrete to expand, and if this expansion is restrained, compressive stresses will develop (Day & Clarke, 2003:12). However, these compressive stresses are low, as the majority of the heat development occurs within 12 to 18 hours after placement of the concrete, when the concrete's modulus of elasticity is still relatively small (Day & Clarke, 2003:12). Furthermore, as concrete is strong in compression, the compressive stresses produced by the development of heat do not result in the concrete cracking.

Instead, cracking occurs when the concrete begins to cool down and contract (El-Reedy, 2019:188). This is as the exterior concrete, which is cooled by exposure to the environment, contracts before the interior concrete, which is insulated and thus retains more heat (ACI Committee 224, 1993:4). Consequently, the contraction of the exterior concrete is restrained by the interior concrete, leading to the development of tensile stresses in the exterior concrete. Additional restraint may also be provided externally, by other members or surfaces onto which the concrete may be joined or placed upon (Emborg & Bernander, 1994:2893). The resultant tensile stresses will be relatively large, as the concrete has a higher modulus of elasticity during cooling, as it begins to harden and gain strength, than during the development of hydration heat (Day & Clarke, 2003:12).

The development and loss of hydration heat, and thus the tensile stresses which cause cracking, is influenced by several factors, including (Day & Clarke, 2003:12):

- The type and amount of binder used
- Weather conditions at the time of concrete placing and hardening
- The type of formwork used
- The geometry of the member

As heat develops due to the hydration of the binder, the amount of binder used will significantly influence the amount of heat generated. The use of SCMs such as FA and GGBS in the binder also has a large influence on the amount and rate of heat generated, as FA and GGBS tend to slow down the rate of hydration (Emborg & Bernander, 1994:2894). Higher ambient temperatures will of course result in higher concrete temperatures, and also increase the rate of hydration reactions, while the use of certain types of formwork, such as formwork made from timber, provides greater insulation and thus results in higher concrete temperatures (Day & Clarke, 2003:12).

The geometry of a concrete member ultimately has a large effect on its susceptibility to thermal cracking due to hydration heat development. This is as larger, thicker members provide good insulation to the interior concrete, while any heat developed in thinner members will be lost to the outside environment before it can build up within the member. Consequently, thermal cracking due to hydration heat development tends to be most significant for large concrete members, such as bridge piers, deep beams, footings, and thick walls and columns (ACI Committee 224, 1993:4).

Thermal cracking due to hydration heat may occur in similar patterns to drying and plastic shrinkage, with map cracking being particularly common. Where walls are concerned, vertical cracks often appear, starting from the bottom, with the foundations providing significant restraint to any thermal contraction (Day & Clarke, 2003:14). An example of such vertical cracking is shown in Figure 2-12. Regardless of the crack pattern, cracks which form due to the development and subsequent cooling of hydration heat may exhibit a variety of widths and spacings, depending on the amount of reinforcing steel provided (Day & Clarke, 2003:14). Crack width design, which determines this amount, thus has a large influence on the development of thermal cracks due to hydration heat.

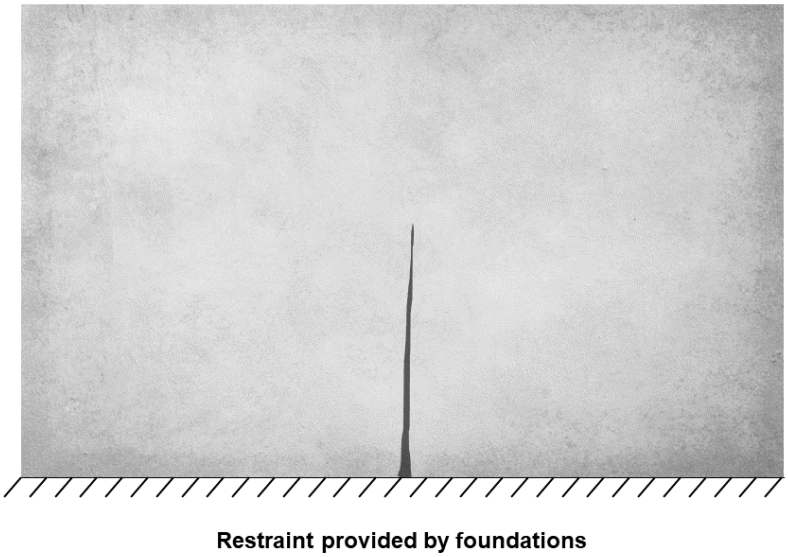

Figure 2-12: Typical vertical cracking in a concrete wall due to hydration heat development and subsequent restrained contraction (adapted from Day & Clarke, 2003:4).

2.4.4 Thermal Cracking due to Ambient Temperature Fluctuations

All marine RC structures are exposed to temperature and moisture fluctuations, over both daily and seasonal cycles (Richardson, 2002:225). These fluctuations result in volume changes in the concrete. During the day, when temperatures are higher, the concrete will heat up and expand, before cooling down and contracting again overnight (Richardson, 2002:228). Combined with this, the concrete will also cool down and contract during the autumn and winter months, and heat up and expand during spring and summer (Richardson, 2002:228).

Wherever such movements are restrained, tensile stresses will develop in the concrete, potentially leading to cracking (Richardson, 2002:225). However, particularly vulnerable are structures and members which are only partially exposed to the external environment (ACI Committee 224, 1993:4) – such as beams and piles in jetties, which are exposed to sunlight and rain on the sides of the jetty, and sheltered underneath the deck. This is as expansion and contraction will not occur uniformly over such members, with the result that the expansion and contraction of the exposed portion is restrained by the sheltered portion (ACI Committee 224, 1993:4). In such conditions, decreases in temperature will cause

restrained contraction, and thus cracking, in the exposed portion, while temperature increases will cause tensile stresses and cracking in the sheltered portion, as it tries to restrain the expansion of the exposed portion (ACI Committee 224, 1993:4).

Ambient temperature fluctuations and their associated movements may produce new cracks, or they may result in the opening, closing, and widening of existing cracks in the long term (Richardson, 2002:213). Where new cracks are produced, they may vary significantly in pattern, width, and spacing, depending on a variety of factors – such as the magnitude of the temperature changes, the coefficient of thermal expansion and modulus of elasticity of the concrete, and the degree to which the concrete is restrained (ACI Committee 224, 1993:4).

2.4.5 Flexural Cracking

Unlike shrinkage and thermal cracking, the tensile stresses that lead to flexural cracking are the result of applied loads (ACI Committee 224, 1993:8). While concrete is not typically used for members experiencing direct tension, concrete is frequently used for beams, slabs, and columns, which are subjected to tensile stresses through bending. Flexural cracks therefore often develop in the tension zones of reinforced concrete beams, slabs, and columns. Figure 2-13 shows examples of how such cracks typically occur in common types of beams and slabs. These cracks occur in relatively linear patterns, and develop primarily as a function of the amount of stress in the reinforcing steel – with higher steel stresses producing wider cracks (ACI Committee 224, 1993:8).

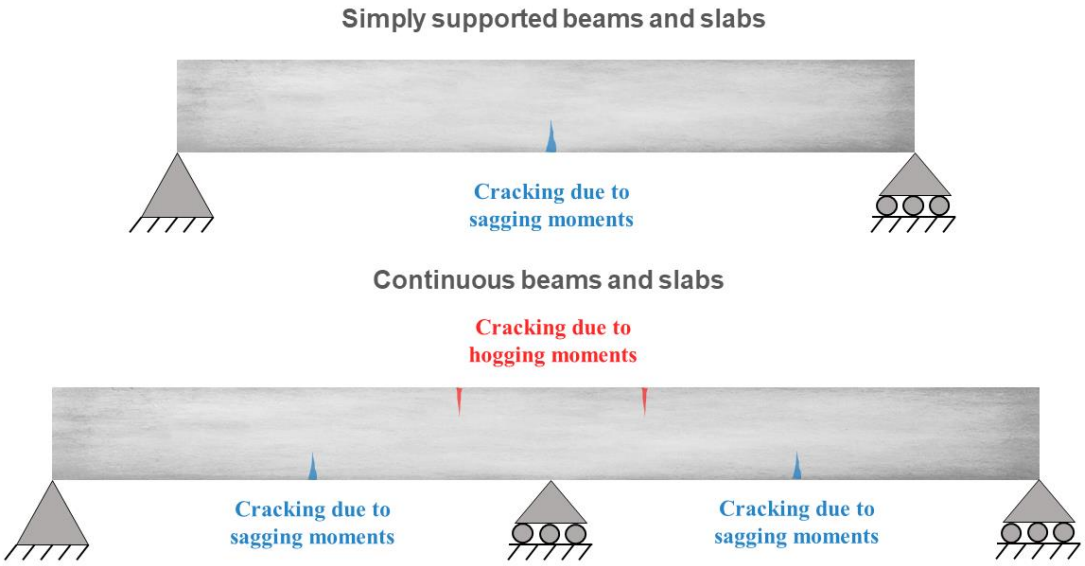

Figure 2-13: A diagram showing the typical locations of flexural cracks for simply supported and continuous beams and slabs (adapted from Day & Clarke, 2003:4).

2.5 The Effect of Cracks on the Durability of Marine Reinforced Concrete Structures

A significant amount of research has been carried out on the effects of cracks on the durability of marine RC structures (Arya & Myrzakulova, 2019:2), with the earliest study reportedly being carried out in the 1930s (Li & Li, 2019:1). Many of these studies have focussed on the use of crack width limitations in durability design, which has been debated, without conclusion, since the 1970s (Käthler et al., 2020a:145).

The research, which has been carried out in a variety of countries (Arya & Myrzakulova, 2019:1), using both accelerated laboratory corrosion, and natural corrosion in field conditions, has led to two opposing schools of thought on the influence of crack width on corrosion (Richardson, 2002:229). The first of these believes that wider cracks result in faster corrosion initiation, but crack width has no influence on corrosion propagation. In contrast to this, the second school of thought maintains that wider cracks result in both faster corrosion initiation and propagation. It can thus be seen that the influence of cracks on corrosion initiation and propagation are different issues, with much of the debate focussing on the influence of crack width on corrosion propagation. As such, the influence of cracks on corrosion initiation and propagation are discussed here separately. The effect of cracks on corrosion initiation is discussed in Section 2.5.1, while, due to the complexity of the topic, the influence of cracks on corrosion propagation is dealt with in three sections (Sections 2.5.2 to 2.5.4).

2.5.1 The Effect of Cracks on Transport Mechanisms and Corrosion Initiation

Cracks significantly alter the transport properties and prevailing transport mechanisms of concrete (Otieno, 2014:30), although the extent to which this is the case is not fully understood at present (Santhanam & Otieno, 2016:405). Whereas diffusion is the dominant chloride transport mechanism in uncracked marine RC, permeation and absorption have been found to also play a significant role in the transport of chlorides and other aggressive species in cracked marine RC (Otieno, 2014:31).

This is as cracks significantly increase concrete permeability, sorptivity and diffusivity (Ghasemzadeh & Pour-Ghaz, 2015:10; Lu, Li & Liu, 2017:453-454; Zhang et al., 2019:1; Principigallo, 2020:163). For example, Wang et al. (1997:391) found that an increase in crack width from about 0.05 mm to 0.5 mm resulted in a permeability coefficient increase of six orders of magnitude. Cracks increase absorption by acting as capillary tubes and linking existing capillary pores, while in the case of permeation and diffusion, they provide new paths which allow for permeation and diffusion to occur not just away from the exterior concrete surface, as is the case for uncracked concrete, but also outwards from the crack (Li & Li, 2019:1; Ma, Zhao & Gong, 2019:1568). This effect is illustrated in Figure 2-14.

The increases in permeability, sorptivity and diffusivity associated with cracks have been found to increase as crack width increases (Wang & Zhang, 2016:10; Lu, Li & Liu, 2017:454; Shaikh, 2018:7-8) – although absorption will only increase up to a certain point, before beginning to decrease, as wider cracks serve to reduce the capillary forces responsible for absorption (Torrijos, Giaccio & Zerbino, 2010:114-115). However, the transport mechanisms present in cracked concrete are relatively complicated. In addition to crack width, other crack properties, such as crack type, frequency, depth, and shape, also have a significant influence on concrete transport properties (Otieno, 2014:35). Torrijos, Giaccio and Zerbino (2010:120) found that both absorption and permeability increases as crack frequency increases, while Otieno (2014:35) observed that chlorides penetrate deeper where cracks are deeper. Li and Li (2019:10) also found that the influence of cracks on concrete transport properties differs for single and multiple cracks, as crack interconnectivity plays a significant role when multiple cracks or crack “networks” are present.

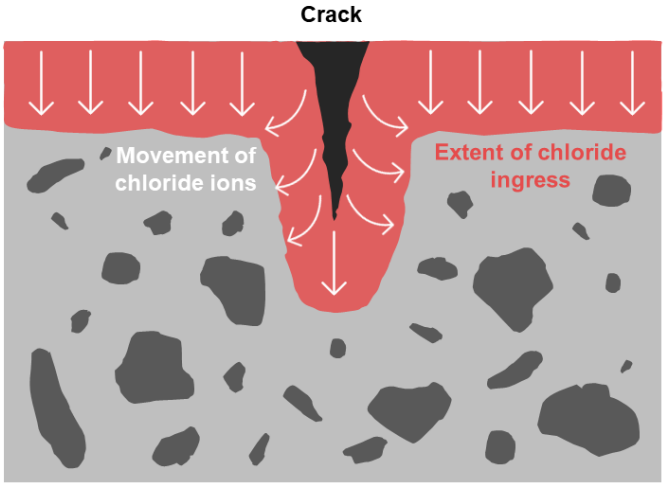

Figure 2-14: An illustration of the ingress paths of chlorides in uncracked and cracked concrete (adapted from Ma, Zhao and Gong, 2019:1569).

It is thus clear that, while crack width does influence the ingress of chlorides and other aggressive agents into marine RC, this influence cannot be viewed in isolation from other other crack properties. Yet, while the exact influence of cracks on the transport of aggressive agents into concrete is unclear, and depends on multiple crack properties, it has been shown conclusively that cracks allow chlorides, oxygen and moisture to rapidly penetrate to the level of the reinforcing steel (Otieno, Beushausen & Alexander, 2016:373; Van Hung, Hung & Viet, 2018:1; Li & Li, 2019:1). This is significant, as it means that the presence of cracks will cause faster (often instant) initiation of corrosion, with the result that the length of the corrosion initiation period is often taken as zero in cracked concrete (Miyagawa, 1985:58; Otieno, Alexander & Beushausen, 2010:394; Bhaskar et al., 2011:247). This effectively reduces the structure's service life to the propagation period only (Otieno, Beushausen & Alexander, 2012:1806).

2.5.2 Mechanisms of Corrosion in Cracked Reinforced Concrete

The reason that cracks cause instant initiation of corrosion in marine RC structures is that, by allowing for the rapid transport of chlorides to the level of the reinforcing steel, they cause depassivation of the steel in the area around the cracks. This leads to the formation of corrosion cells in the vicinity of the cracks (Beeby, 1978:78). Although the exact process behind the formation of these cells is not fully understood (Otieno, 2014:29), there are three potential types of corrosion cells which may form as a result of cracking:

- Microcells, in which both the anode(s) and cathode(s) are located in the crack (Otieno, 2014:29), as shown in Figure 2-15. These types of cells typically occur in coincident cracks, as coincident cracks expose large amounts of reinforcing steel to chlorides, oxygen, and moisture, such that both anodic and cathodic reactions can be sustained in the cracked region (Otieno, 2014:29)
- Macrocells, with only the anodes being located at the crack (Miyagawa, 1985:58). These macrocells generally only form in concrete with intersecting cracks, such that the anodes are located at the cracks, and the cathodes form in the uncracked regions between the cracks (Otieno, 2014:54), as shown in Figure 2-16. In order for corrosion to occur, oxygen thus has to travel through the uncracked concrete to reach the cathodes (Otieno, 2014:29)
- Macrocells, with both anodes and cathodes located at the cracks, as shown in Figure 2-17. Arya and Myrzakulova (2019:3-5) describe these types of cells as occurring in concrete with high

crack frequencies, such that not all cracked regions become anodes, and the oxygen required for the cathodic reactions is supplied through the cracks

However, it must be noted that much of the research has focussed on the effect of single, or relatively few cracks, on single reinforcing steel bars. In actual marine RC structures, which typically have multiple layers of reinforcement, in two directions, and many cracks, the formation and distribution of anodes and cathodes will be complex (Bezuidenhout & van Zijl, 2019:2184), and potentially different to those described above. Nonetheless, the above, theoretical, corrosion mechanisms provide an adequate basis to describe the development of corrosion in real, cracked marine RC structures.

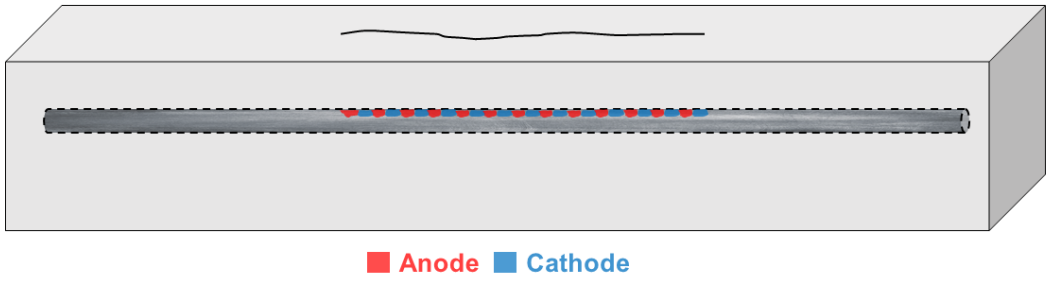

Figure 2-15: A diagram showing microcell corrosion occurring at a coincident crack, as described by Otieno (2014:29).

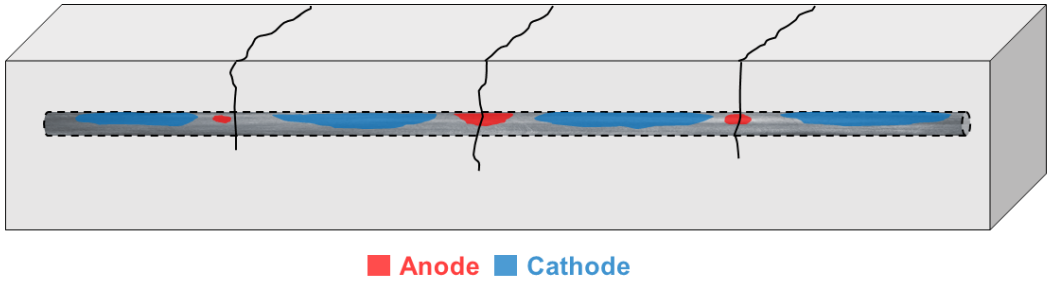

Figure 2-16: A diagram showing macrocell corrosion in which a series of intersecting cracks has led to the formation of anodes in the vicinity of the cracks (adapted from Bezuidenhout & van Zijl, 2019:2184). Note that the location and shape of the anodes is based on the visual observations of Bezuidenhout and van Zyl (2019) and the corrosion mapping of cracked beams carried out by Zhang, François and Yu (2020) and Geiker et al. (2021).

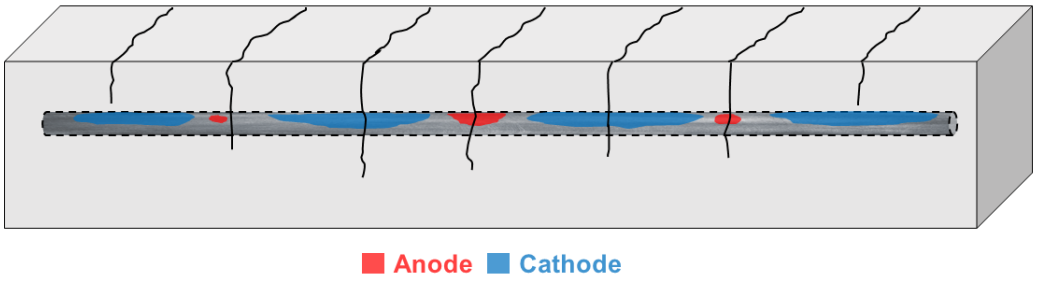

Figure 2-17: A diagram of the type of macrocell corrosion described by Arya and Myrzakulova (2019:4), in which both anodes and cathodes form in the vicinity of cracks.

2.5.3 The Effect of Cracks on Corrosion Propagation

The effect of cracks on the development of corrosion can be significant. Coincident cracks are known to often result in high corrosion rates, and hence rapid deterioration (Beeby, 1978:80; Otieno, Alexander & Beushausen, 2010:394), while intersecting cracks can lead to equally significant deterioration, as they

may result in localised ("pitting") corrosion which encourages the formation of coincident cracks. Based on observation of real RC structures in the marine environment, Chen et al. (2020:17-19) found that this tends to occur in a four-stage process, illustrated in Figure 2-18, in which each stage of the process sees an increase in the penetrability of the concrete, and hence in corrosion rate.

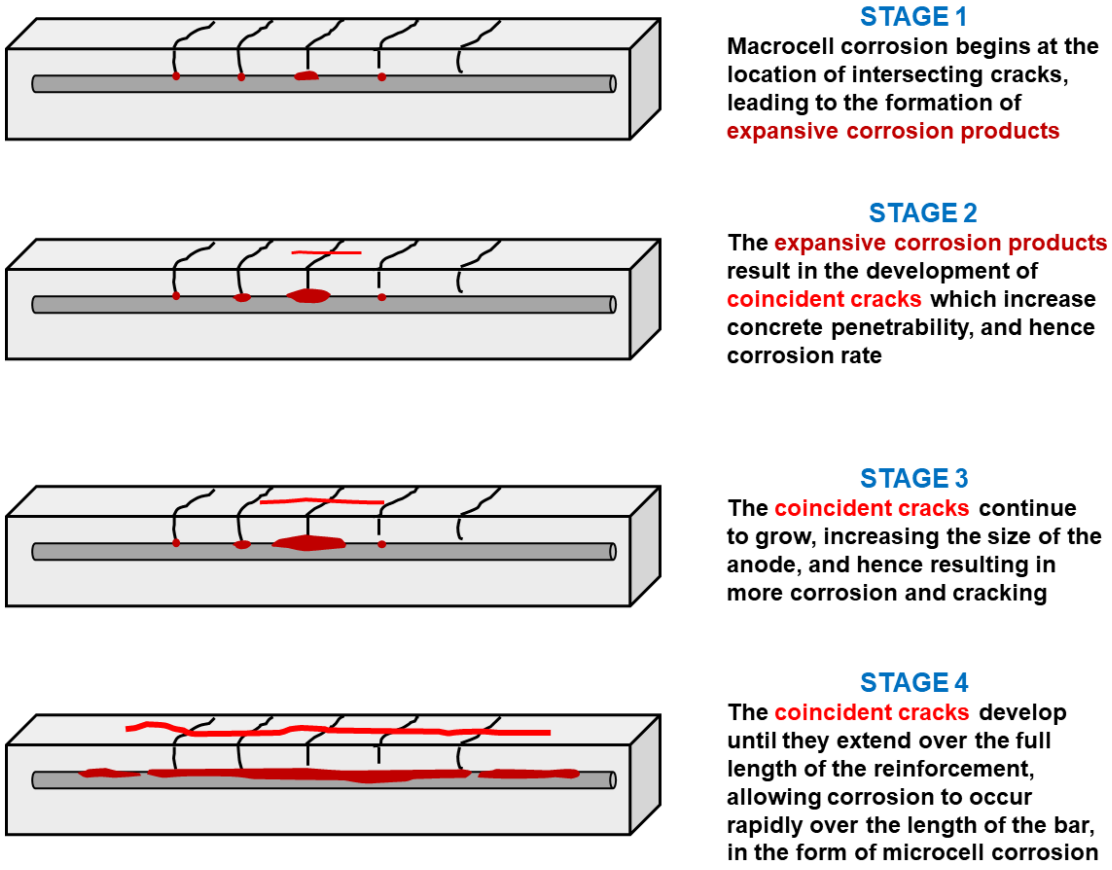

Figure 2-18: A diagrammatic representation of the four-stage corrosion development process at intersecting cracks (adapted from Chen et al., 2020:18).

However, while it is clear and undisputed that cracks lead to instant initiation of corrosion, the effects of cracking on corrosion propagation are very complex, and are not completely understood (Otieno, Alexander & Beushausen, 2010:394). Once corrosion is initiated, it may not necessarily continue, and if it does, the rate at which it does may be subject to several factors, such as crack width, orientation and frequency, cover depth, activity or dormancy of the crack, and concrete properties (Otieno, Beushausen & Alexander, 2016:373; Shaikh, 2018:1; Arya & Myrzakulova, 2019:2-3). This complexity has led to much debate about whether cracks have a significant influence on the propagation of corrosion (Scott & Alexander, 2007:497), during which two opposing schools of thought have developed (Otieno, Alexander & Beushausen, 2010:394).

The first school of thought, led by researchers such as Beeby (1978), believes that the presence of cracking has no influence on the subsequent rate of corrosion (Otieno, Alexander & Beushausen, 2010:394). Their argument is based on the principles of corrosion described in Section 2.3.5; namely, that the anodic and cathodic reactions responsible for corrosion rely on the presence of oxygen and water at the cathode, and the ability of electrons to travel from the anode to the cathode. As the availability of oxygen and water at the cathode is determined by the penetrability of the concrete at the cathode (which is a function of concrete quality), and the mobility of electrons depends on the resistivity of the concrete,

and not the presence of cracks, it follows that the existence of cracks should not influence the corrosion process (Beeby, 1978:79; Miyagawa, 1985:58; Raupach, 1996:329).

This view is supported by some experimental and observational evidence. For example, Li and Li (2019:8) reference a study by François et al. (2018), which found that, after 26 years of exposure to the marine environment, the influence of cracks on corrosion rate was insignificant. When reviewing a number of studies, conducted in both laboratory and field conditions, Beeby (1978:80) found that corrosion caused by intersecting cracks tended to be very localised, and did not generally lead to spalling or other forms of significant damage. Even Chen et al. (2020:8), who argued that intersecting cracks can lead to considerable damage (as shown in Figure 2-18), found that not all intersecting cracks resulted in corrosion.

In contrast to the first school of thought, other researchers, such as Otieno, Alexander and Beushausen (2010), Scott and Alexander (2007), and Raupach (1996), maintain that cracks have a significant effect on the propagation of corrosion. They base this primarily on recent experimental evidence, and on the complex nature of cracking, which results in scenarios where the arguments put forth by researchers such as Beeby (1978) do not necessarily hold true.

In a series of experiments, carried out using both accelerated laboratory corrosion and exposure to the marine environment, Otieno, Beushausen and Alexander (2016:385) found that the presence of cracks resulted in significant increases in corrosion rates – although the extent to which this was the case was found to depend on concrete cover depth, quality and resistivity (Otieno, Beushausen & Alexander, 2016:377). Other researchers, such as Scott and Alexander (2007), Chen et al. (2020) and Lai et al. (2020) reported similar results. Even as far back as 1985, Miyagawa (1985:67) found that cracks wider than 0.1 mm led to the formation of macrocells and subsequent corrosion.

This experimental evidence directly contradicts, and seems to disprove, the argument that corrosion rate is determined only by the availability of oxygen and water at the cathode, and the resistivity of the concrete. The most likely explanation for this is that the influence of cracking is significantly more complex than was originally expected. Käthler et al. (2020a) conducted a review of 27 different studies on the influence of crack width on corrosion propagation (including many of those mentioned above), and drew three key conclusions (Käthler et al., 2020a:153):

- The effect of cracks on corrosion rate does not remain constant and appears to diminish as the duration of the exposure to the marine environment increases. This can potentially be explained by the fact that, as time goes on, the cracks may be filled with corrosion products and debris, reducing their impact on concrete penetrability (Li & Li, 2019:9)
- Cracks seem to have a greater effect on corrosion propagation when the test members are exposed to near-saturated or cyclic wetting and drying conditions, such as would occur in accelerated laboratory corrosion and the tidal, splash and spray zone in the marine environment. One potential explanation for this is that, in cyclic wetting and drying conditions, any corrosion products or debris which may accumulate in cracks are continually washed away, ensuring that the effect of cracking does not diminish with time (Li & Li, 2019:9)
- Cracks have a definite influence on corrosion propagation in concrete with w/b ratio less than 0.4. Above this ratio, no such clear influence exists. This makes sense, as low-quality concrete (i.e., concrete with high w/b ratio) will be very penetrable, and will have low resistivity, such that corrosion will propagate rapidly irrespective of the presence of cracks. In contrast to this, cracks will have a significant influence on the penetrability of high-quality concrete, which otherwise wouldn't be conducive to the propagation of corrosion

It thus appears that cracks have no clearly defined influence on corrosion propagation, and may result in a wide range of effects, depending on the time period under consideration, exposure conditions, and concrete quality and mix design. Furthermore, crack frequency and orientation may play a significant role in determining the extent to which cracks influence corrosion. High frequency cracks may result in the formation of both anodes and cathodes in the vicinity of the cracks (see Figure 2-17), in which case oxygen and water will be readily available at the cathodes, such that corrosion will propagate as a direct result of the presence of cracking.

While intersecting cracks have been found to sometimes, but not always, lead to corrosion propagation (Chen et al., 2020:1), even Beeby (1978:80) concedes that coincident cracks can often result in significant spalling and damage. This makes sense, as microcell corrosion, which typically occurs at coincident cracks, is not limited by the presence of oxygen and water at the cathode, or the resistivity of the concrete, as both the anodes and cathodes are equally exposed by the presence of cracking. As intersecting cracks may potentially produce coincident cracks (Chen et al., 2020:18), and, in real marine RC structures, which typically have reinforcement in both directions, any crack may be a coincident crack (Arya & Myrzakulova, 2019:3-4), the first school of thought, led by researchers such as Beeby (1978), may not always be applicable in practice.

Ultimately, it follows that, while there may be no clear relationship between cracking and corrosion propagation, the presence of cracking represents a significant threat to the durability of marine RC structures. This implies that it is necessary to control, and reduce, the presence of cracking. However, in the context of the uncertainty surrounding the influence of cracking on corrosion propagation, this is difficult to achieve in practice. Despite the wide variety of factors which have been shown to influence the effect of cracking on corrosion propagation, to date, only one crack property – crack width – is used in durability design to control cracking. In order to evaluate the effectiveness of doing so, it is first necessary to understand whether there is any relationship between crack width itself and corrosion propagation.

2.5.4 The Relationship Between Crack Width and Corrosion Propagation

Despite the fact that the issue of crack width control has been debated since the 1970s, no clear answer about the relationship between crack width and corrosion propagation has yet been found (Käthler et al., 2020a:145). In many ways, the ‘two schools of thought’ which are evident in the debate about the influence of cracking on corrosion propagation in general, extend to the influence of crack width in particular. Table 2-1 shows how many of the studies which have been conducted to date are split between either concluding that there is no relationship between crack width and corrosion rate (shown in orange), or that wider cracks result in higher corrosion rates (shown in green).

Of the studies which found that there is no relationship between crack width and corrosion rate, the most significant and oft quoted in the literature is that carried out by Beeby (1978). Based on several exposure tests carried out in the marine environment in the 1960s and 70s, Beeby (1978:77) argued that, although crack width has a significant influence on corrosion rate in the short-term (two years), there is no long-term relationship between crack width and corrosion rate (after a period of ten years). Furthermore, he argued that the apparent relationship between crack width and corrosion rate in the short-term is a statistical illusion, caused by the fact that wider cracks will result in faster corrosion initiation (Beeby, 1978:78). This means that, when corrosion rates are measured in the short-term (for example, after two years), corrosion at the wider cracks will have been ongoing for a longer period, leading to a higher measured corrosion rate. In the long-term, when corrosion had been ongoing for approximately equal lengths of time in both the narrower and wider cracks, the measured corrosion rates were found to be very similar, regardless of crack width (Beeby, 1978:78).

Table 2-1: A table summarising the conclusions of a number of studies conducted on the influence of cracking on corrosion. Note that the list of studies is not exhaustive (adapted from Käthler et al., 2020a:146-147).

Reference	Year	Exposure duration [years]	Conclusion: "Is there a relationship between crack width and corrosion rate?"
Tremper	1947	10	No
Rehm and Moll	1964	1.2	Yes
Atimtay and Ferguson	1973	1.6, 2	No
Beeby	1978	10	No
Makita et al.	1980	2.7	Yes
O'Neil	1980	25	Yes
Okada and Miyagawa	1980	0.25	Unclear
Suzuki et al.	1990	0.5	No
Misra and Uomoto	1991	1.2	Yes
Ohta	1991	10, 20	No
Lorentz and French	1995	0.77	Yes
Arya and Ofori-Darko	1996	2	Not investigated
Schiessl and Raupach	1997	2	Yes, but to an extent that decreases as exposure time increases
Francois and Arliguie	1999	12 (27)	No
Mohammed et al.	2001	0.25, 1.33	Yes, but to an extent that decreases as exposure time increases
Mohammed et al.	2001	15	Yes, but only for cracks > 0.5 mm wide
Marcotte and Hansson	2003	4	Not investigated
Bi and Subramanian	2006	1.33	Not investigated
Scott and Alexander	2007	1.5	Yes
Jaffer and Hansson	2008	1.5	Not investigated
Otieno et al., Otieno	2009	0.6	Yes
Paradis	2009	1.4	Yes
Jimenez-Quero et al.	2010	5	Yes, but to an extent that depends on w/b ratio
Sangoju et al.	2011	0.06	Yes
Otieno et al.	2012	0.6	Yes
Ahmadi et al.	2014	0.01, 0.2, 0.7, 1.2	Yes
Li et al.	2017	0.2, 0.3, 0.4, 0.5	Yes

The argument put forth by Beeby (1978) about the general influence of cracks on corrosion propagation – that is, that corrosion rate is governed by concrete resistivity and the availability of oxygen and water at the cathode – also applies here. As neither concrete resistivity nor the availability of oxygen and water at the cathode is a function of crack width, it follows that corrosion rate should not be a function of crack width. This view is supported by Miyagawa (1985:88), who found that corrosion rate depends more on

the ratio of the cathodic to anodic area, than on crack width. More recently, other researchers, such as Yu et al. (2015:257) and Chen et al. (2020:14) have also found that there is no relationship between crack width and corrosion rate, with the maximum amounts of corrosion damage not necessarily occurring at the widest cracks.

However, most of the recent research has shown that there is likely to be a relationship between corrosion rate and crack width, even if this relationship is heavily influenced by other factors, such as cover depth and concrete quality and resistivity (Otieno, Beushausen & Alexander, 2016:377). Scott and Alexander (2007:501) found that an increase in crack width from 0.2 to 0.7 mm resulted in an increase in corrosion rate of 11-75%, depending on binder type, while Otieno, Beushausen and Alexander (2016:377) found that corrosion rate increased as crack widths increased from "incipient", to 0.4, and then 0.7 mm. These findings were attributed to the fact that increasing crack widths result in larger concentrations of chlorides at the reinforcing steel, larger areas of exposed steel (and thus larger anodes), and prevent the cracks from healing autogenously or being sealed by debris or corrosion products (Scott & Alexander, 2007:501).

Furthermore, both Otieno, Alexander and Beushausen (2010:399) and Scott and Alexander (2007:501) found that even relatively narrow cracks, with widths less than those specified in crack width requirements, resulted in significant, non-zero corrosion rates. Particularly, Alexander, Beushausen and Otieno (2012:51) reported that very narrow, "incipient" cracks still increased corrosion rates by at least 40%, depending on binder type. However, it should be noted that both the studies conducted by Scott and Alexander (2007) and Otieno, Beushausen and Alexander (2016) were conducted in the short-term, over periods of 1.5 and 2.25 years, respectively. Although this would seem to limit the relevance of their findings, as a result of the issues associated with short-term studies identified by Beeby (1978:78), they both utilised accelerated laboratory corrosion (at least in part), such that they can be said to have simulated long-term exposure conditions.

Richardson (2002:230) also observed that the conclusions drawn by Beeby (1978) are only true for isolated intersecting cracks – for coincident cracks, or series of intersecting cracks, the availability of oxygen at the cathode, and hence corrosion rate, may depend on crack width. Evidence for this is provided by Chen et al. (2020:20), who found that corrosion rate increased as coincident crack width increased. As reinforcement is frequently placed in both directions and used as shear links in 'real' marine RC structures, these findings imply that the influence of crack width on corrosion rate may be significant in practice.

There are thus valid arguments for both schools of thought. This introduces an apparent contradiction, as they cannot both be true. However, due to the complexity of cracking and its influence on corrosion propagation, it may be that both schools of thought could be true for a given situation, depending on the crack and concrete properties – particularly crack orientation and self-healing ability (Richardson, 2002:229). Other researchers have also highlighted the influences of wetting and drying conditions (Käthler et al., 2020b) and construction defects (Yu et al., 2015; Zhang, François & Yu, 2020), which may have a significant effect on corrosion propagation.

The situation is further complicated by the shortcomings of many of the existing studies. In their review of 27 studies on the influence of cracking on corrosion, Käthler et al. (2020a:153) found that only 7 of the studies were sufficiently robust in their methodologies. The others were all either too short, didn't accurately represent the conditions experienced by real marine RC structures, or used inaccurate methods of measuring corrosion (Käthler et al., 2020a:153). This means that there is simply not enough experimental evidence to truly evaluate the effects of crack width on corrosion rate, at least for the present time.

Ultimately, the relationship between crack width and corrosion rate is unclear, owing both to the complexity of the problem, and to a lack of adequate studies on the subject. Despite this, it can be concluded that, in certain circumstances, wider cracks can lead to greater corrosion, even if this is not always the case. Examples of such circumstances include when cracks are coincident or are located in the splash and spray zone (where constant washing of the crack will prevent crack healing or sealing), or when construction defects (such as bleeding, segregation and plastic settlement) increase concrete penetrability to such an extent that oxygen and water are freely available at the cathodes.

2.5.5 Implications for Crack Width Design

The lack of clarity on the relationship between crack width and corrosion rate has led some authors, such as Beeby (1978:80), to argue that crack width limitations are misguided, and ultimately unlikely to ensure durability. However, as the experimental evidence suggests that wider cracks may be associated with greater corrosion, at least in certain circumstances, there may be cases in which designing to limit crack width is beneficial and improves durability. But the extent to which this is the case is not clear, particularly as it appears that no existing studies have translated the corrosion rates determined in previous studies into service life predictions. Furthermore, as even relatively narrow cracks were found to increase corrosion rates, it is not clear whether designing for crack width will provide adequate service life – even if doing so may result in lower corrosion rates than if crack widths were not limited.

There is thus considerable need to evaluate the effects of designing for crack width limitations on the service life of marine RC structures. However, before this can be done, it is necessary to understand how crack width design is carried out, and what "adequate" service life means in the context of marine RC structures. Both of these topics are discussed in the following section (*Section B: Crack Width Design: Current State of the Art*) of the literature review.

SECTION B: *Crack Width Design – Current State of the Art*

2.6 Durability Design of Reinforced Concrete Marine Structures

The design of marine RC structures is dominated by durability design (Smith, 2016a:65), which is relatively unique (Smith, 2016a:68-69), due to the harsh nature of the marine environment. As discussed in Section 2.3, the biggest threat to the durability of marine RC structures is chloride-induced reinforcement corrosion. The primary aim of the durability design of marine RC structures is therefore to provide adequate service life through the selection of materials, construction methods and structural details (Ballim, Alexander & Beushausen, 2009:156) which will limit or prevent the ingress of chloride ions into the concrete.

There are currently two main methods which may be used for the durability design of RC structures – prescriptive design methods, and performance-based approaches (Nilsson, 2019:124). Prescriptive design methods specify limiting values for various concrete properties, such as binder content, water/binder ratio and compressive strength (Alexander & Beushausen, 2019:19). However, many of the specified concrete properties, such as compressive strength, have no direct link to concrete durability (Alexander & Beushausen, 2019:19). As a result of this, and many other issues, prescriptive design methods are widely regarded as outdated, and limited in their effectiveness (Alexander & Beushausen, 2019:20).

The second method of durability design, performance-based design, aims to address the shortcomings of the prescriptive methods. This is done by designing the concrete mix and layout of reinforcement directly to limit or prevent chloride ingress (Smith, 2016a:69). Service life modelling (Nilsson, 2019:125) and testing of properties which directly relate to durability (Alexander & Beushausen, 2019:20) is then carried out to verify the adequacy of both the design and the as-built structure. Consequently, performance-based approaches are much more likely to provide durable RC structures.

The durability design of marine RC structures, like any other type of structure, is based on codes of practice and national standards (Smith, 2016a:66). Many codes and standards are available for marine RC structures, of which the most important, and most commonly used in the South African marine structures industry, are (Smith, 2016a:71-73):

- BS 6349 (used in conjunction with the Eurocodes)
- American standards
- Australian standards
- Japanese guidelines
- South African standards

Each of these codes and standards are discussed in detail in the following sections, in order to provide a comprehensive understanding of the different approaches to durability design which are currently available, and the role of crack width requirements within these approaches.

2.6.1 BS 6349 and the Eurocodes

Of all the codes and standards used in the design of marine RC structures, BS 6349 is generally considered to be the best and most comprehensive (Smith, 2016a:69). The name “BS 6349” refers to a “family” of different codes, which each deal with different parts of the design of marine structures. Of these, *BS 6349-1-4:2013*, which gives guidance on durability design (Smith, 2016a:71), is the most relevant to this discussion, along with *BS 6349-1-1:2013*.

BS 6349-1-1:2013 provides guidance on the design service life to be used for various types of marine structures, as shown in Table 2-2. *BS 6349-1-4:2013* also defines various exposure conditions, as shown in Table 2-3. Exposure conditions play a vital role in the durability design of reinforced concrete marine structures, as the chlorides, water and oxygen required for reinforcement corrosion are present in different quantities, depending on the area of the structure under consideration. This means that different parts of marine RC structures deteriorate at different rates, with the worst deterioration typically being observed in the "tidal" (XS2/3) and "splash and spray" (XS3) zones (Santhanam & Otieno, 2016:145). Consequently, durability design requirements differ depending on exposure conditions.

When it comes to durability design itself, *BS 6349-1-4:2013* is largely prescriptive, and includes specifications and limiting values for the following properties, based on the selected design service life and exposure class (Smith, 2016a:71):

- Binder type
- Binder content
- Water/binder ratio
- Concrete cover
- Concrete crack width

However, the requirements of *BS 6349-1-4:2013* take a wide range of materials – such as the supplementary cementitious binders fly ash (FA) and ground granulated blastfurnace slag (GGBS) – into account (The British Standards Institution, 2013a:11). *BS 6349-1-4:2013* is thus considered to be particularly comprehensive (Smith, 2016a:71), moreso than other prescriptive design requirements. Furthermore, *BS 6349-1-4:2013* does allow for performance-based design methods to be used, although it does not give much guidance on how to do so (Smith, 2016a:71).

Table 2-2: Design service life categories and requirements, according to *BS 6349-1-1:2013* (adapted from The British Standards Institution, 2013b:51).

Design working life category	Indicative design working life (years)	Examples
1	10	Temporary structures, which are not to be reused
2	10 to 25	Structural parts designed to be replaceable within a structure or facility of longer design working life
3	15 to 30	Structures dedicated to non-renewable natural resources, petrochemicals or similar industrial or commercial applications (such as open-piled jetties, mooring and berthing dolphins, Ro-Ro linkspans)
4	50	Common port infrastructure for commercial and industrial ports including reclamation, shore protection, breakwaters, quay walls
5	100	Common port infrastructure including breakwaters for ports of nationally significant strategic or economic value. Infrastructure for regional flood defence or coastal management infrastructure

Table 2-3: Definition of exposure conditions according to *BS 6349-1-4:2013* (adapted from The British Standards Institution, 2013a:8).

Exposure class	Description
XS1	Exposed to airborne salt but not in direct contact with seawater
XS2	Permanently submerged
XS2/3	Frequently wetted (e.g., mid and lower tidal zone and backfilled)
XS3	Infrequently wetted (e.g., upper tidal, splash/spray, "dry" internal faces of submerged structures)

2.6.2 American Standards

There is no single American equivalent to the BS 6349 suite of codes. Instead, the American Concrete Institute (ACI), U.S Army Corps of Engineers and Naval Facilities Engineering Command have all produced guidelines for the durability design of marine structures (Smith, 2016a:72). The most significant of these guidelines are the ACI's *Building Code Requirements for Structural Concrete (ACI 318-05)* and *Guide for the Design and Construction of Fixed Offshore Concrete Structures (ACI 357R-84)*. These provide prescriptive durability design requirements, based on exposure conditions, for properties such as cement content, water/cement ratio, concrete compressive strength and cover depth (ACI Committee 357, 1997:4-5).

ACI 357R-84 (ACI Committee 357, 1997:9) also specifies limiting tensile stress values and minimum steel requirements, in order to limit cracking. There are thus no direct crack width requirements in the American standards. Furthermore, the American standards are limited by the fact that they don't allow for the use of cement extenders such as FA or GGBS, and only consider plain, Portland cement in their design requirements (Smith, 2016a:88).

2.6.3 Australian Standards

Australian durability design is governed by three standards – *Guidelines for the Design of Maritime Structures (AS 4997)*, *Concrete Structures (AS 3600)* and *Specification and Supply of Concrete (AS 1379)* (Smith, 2016a:72). These standards are based on providing a 25 year service life only (Smith, 2016a:89), which significantly limits their usefulness. Nonetheless, *AS 4997* (Standards Australia, 2005:33-34) is relatively comprehensive, and provides general, prescriptive, requirements for the following parameters:

- Concrete compressive strength
- Binder content
- Water/binder ratio
- Curing requirements

Furthermore, *AS 4997* (Standards Australia, 2005:34-38) specifies the following additional prescriptive requirements, based on exposure conditions:

- Maximum drying shrinkage values
- Minimum concrete cover depth
- Maximum reinforcing steel stresses under normal (serviceability) conditions

Thus, like the American standards, the Australian standards don't directly specify crack control requirements, and instead aim to control cracking through drying shrinkage and reinforcing steel stress requirements. However, unlike the American standards, the Australian standards do allow for the use of cement extenders, such as FA and GGBS (Standards Australia, 2005:34).

2.6.4 Japanese Guidelines

Two guidelines are used in the durability design of marine RC structures in Japan – the Japan Society of Civil Engineers (JSCE) *Guidelines for Concrete No. 15 (Design)* and *Guidelines for Concrete No. 16 (Materials and Construction)* (Smith, 2016a:72). Asides from a few prescriptive requirements, the JSCE guidelines follow a performance-based approach (Smith, 2016a:89). The prescriptive requirements are given in the *Guidelines for Concrete No. 16* (Japan Society of Civil Engineers, 2010a:400), and include minimum cement content and maximum water/binder ratio values.

Guidelines for Concrete No. 15 provides the performance-based approach, which involves extensive calculations in order to verify that the chloride concentration at the reinforcement does not exceed the threshold value within the structure's service life (Smith, 2016a:90-91). While a full discussion of the performance-based calculations is beyond the scope of this literature review, it is noteworthy that both crack width and crack spacing must be calculated, and serve as input parameters to the performance-based design calculations (Smith, 2016a:91).

Furthermore, the calculated crack width values are not allowed to exceed specified maximum values, which are a function of the exposure conditions, type of reinforcement used and concrete cover depth (Japan Society of Civil Engineers, 2010b:132). However, these maximum crack width values are not prescriptive in nature, as they alone are not presented as a guarantee of durability – checking that the design crack width values are less than the maximum values is merely a step in the overall, performance-based design process.

2.6.5 South African Standards

There are two main sets of South African standards which may be used for the durability design of marine RC structures (Smith, 2016a:73):

- The South African National Standards (SANS) standards, *SANS 10100-1 (The Structural Use of Concrete, Part 1: Design)* and *SANS 10100-2 (The Structural Use of Concrete, Part 2: Materials and Execution of Work)*
- The South African National Roads Agency SOC Limited (SANRAL) *Table 6000/1*

SANS 10100-2 (South African National Standards, 2014:28) provides limited prescriptive design requirements for concrete compressive strength and cover depth, based on exposure conditions. In contrast to this, the SANRAL *Table 6000/1* specifies a combination of prescriptive (minimum cover depth) and performance-based (binder types, minimum Chloride Conductivity Index) requirements (Smith, 2016a:95). However, neither of the SANS or SANRAL standards specify crack width requirements.

2.7 Crack Width Design

In Section 2.6 it was shown that crack width requirements form part of many of the durability design codes of practice for marine RC structures, such as *BS 6349-1-4:2013* and the Japanese Guidelines. These requirements are the main, if not only, way in which codes of practice deal with the effect of cracking on durability (Li & Li, 2019:9). The design process which must be carried out to meet the specified crack width requirements is referred to as "crack width design", and primarily focuses on the

provision and detailing of steel reinforcement to resist tensile stresses, thereby limiting crack widths to the specified values (Smith, 2016a:84). It is assumed that, if crack widths are limited in such a way, the influence of the cracks on chloride ingress won't be significant, and corrosion will occur almost as if the concrete is uncracked (Alexander, Beushausen & Otieno, 2012:1806).

Both the current crack width requirements, and the methodologies used in crack width design to meet these requirements, are discussed in this section of the literature review. Section 2.7.1 provides a general overview of the code requirements and methodologies used for crack width design, while Section 2.7.2 discusses one particular, critical, aspect of crack width design – the use of crack width formulas to predict maximum crack widths. Based on issues raised in the literature, a critique of the current requirements and methodologies used in the crack width design process is then made in Section 2.7.3, while potential developments, which could be used to address these issues, are presented in Section 2.7.4.

2.7.1 Code Requirements for Crack Width Design

Crack width requirements are typically specified in design codes as limiting crack width values, which cannot be exceeded. These limiting values are generally based on experimental data or practical experience (Li & Li, 2019:9), and are summarised in Table 2-4 for several codes of practice. It is worth noting that, while the crack width requirements are typically specified as a function of exposure environment, the requirements for the marine environment do not differentiate between the submerged, tidal, splash and spray, and atmospheric zones – even though the severity of reinforcement corrosion has been shown to vary considerably between these zones (see Section 2.6.1).

Table 2-4: A summary of the crack width requirements of typical codes of practice for the durability design of marine reinforced concrete structures (adapted from Otieno, Beushausen & Alexander, 2012:28; Balázs et al., 2013:101; Smith, 2016a:86).

Code of Practice	Specified Limiting Crack Width [mm]
***ACI Committee 224* (2001)**	0.15
***JSCE* (1986)**	0.15
EN 1992-1-1:2004	0.3
BS EN 1992-2:2005	0.3
fib Model Code 2010	0.2

Asides from specifying limiting crack width values, the various design codes also provide methods for crack width design, to ensure that the limiting values are met. Two distinct types of cracking are considered in the design codes – flexural cracking, and shrinkage cracking (which includes the effects of both thermal and drying shrinkage) (Beeby & Narayanan, 2005:150). These two types of cracking are designed for separately, as shrinkage and flexural cracks tend not to occur at the same locations on RC members – meaning that the effects of flexural and shrinkage crack widths do not need to be superimposed when determining crack widths (Smith, 2016a:87).

In the South African marine structures industry, flexural crack width design is generally based on the requirements of *EN 1992-1-1:2004* or *BS EN 1992-2:2005*, while shrinkage crack width design is typically carried out according to the requirements provided in *BS EN 1992-3:2006* and *CIRIA C660* (Smith, 2016a:86). This research, and the remainder of this section of the literature review, will therefore focus on these design codes. Regardless of the design code used, however, standard industry practice is to design first for flexural cracking, and then to check that the resultant reinforcement is adequate to

control/limit shrinkage cracking, in both the short- and long-term (Bamforth, 2007:35). Summaries of the code requirements for flexural, and then thermal/shrinkage crack width design are thus presented below. Detailed descriptions of the code requirements can be found in the relevant codes.

2.7.1.1 Crack Width Design for Flexural Cracking

Crack width design for flexural cracking involves satisfying two criteria, both of which are provided in *EN 1992-1-1:2004* (Beeby & Narayanan, 2005):

1. **Provision of a minimum area of reinforcing steel**, such that the steel does not yield and remains elastic
2. **Ensuring that the design crack width is less than the relevant limiting crack width value**

The first criterion is necessary to ensure that the crack width formulas, used to satisfy the second criterion, are valid, as they assume that cracking does not cause yielding of the steel. If the steel yields when the concrete first cracks, then only one, wide, crack will form (Beeby & Narayanan, 2005:150), and this would likely also be disadvantageous where durability is concerned. However, if the minimum reinforcement requirements are met, then cracking will occur in a controlled manner, in accordance with the predictions of the crack width formulas (Beeby & Narayanan, 2005:150). In order to satisfy the first criterion, *EN 1992-1-1:2004* (European Committe for Standardisation (CEN), 2004:120) provides a formula, shown in Equation 2-1, which can be used to calculate the minimum area of reinforcing steel required to prevent yielding of the steel.

$$A_{s,min}\sigma_s = k_c k f_{ct,eff} A_{ct} \qquad \textbf{Equation 2-1}$$

Where: $A_{s,min}$ is the minimum area of reinforcing steel to be provided in the tensile zone

: σ_s is the maximum permissible stress in the reinforcement, immediately after cracking occurs (commonly taken as the yield strength of the steel)

: k_c is a coefficient which accounts for the form of loading applied to the member. Formulas for the calculation of k_c are provided in *EN 1992-1-1:2004*

: k is a coefficient which accounts for non-uniform stress distributions

: $f_{ct,eff}$ is the tensile strength of the concrete at the time when cracking first occurs

: A_{ct} is the area of concrete which is in the tensile zone for the section

The second criterion can be satisfied by one of two methods – either without calculations, by simply reading maximum bar diameter and spacings from tables provided in *EN 1992-1-1:2004*, or by direct calculation of maximum crack width (Beeby & Narayanan, 2005:157-158). However, the tables provided in *EN 1992-1-1:2004* are based on several assumptions – for example, it is assumed that the cover depth to the reinforcement is 25 mm, and that the tensile strength of the concrete at the time of cracking is 2.9 MPa (CEN, 2004:123). As such, the first method cannot always be used, whereas the second method is more robust. If the second method is used, *EN 1992-1-1:2004* provides a formula for the calculation of maximum flexural crack width, w_k, as shown in Equation 2-2 (CEN, 2004:124):

$$w_k = S_{r,max}(\varepsilon_{sm} - \varepsilon_{cm})$$ **Equation 2-2**

Where: $S_{r,max}$ is the maximum crack spacing. Formulas for the calculation of $S_{r,max}$ are provided in *EN 1992-1-1:2004*

: ε_{sm} is the mean strain in the reinforcing steel, under the action of service (i.e., not ultimate) load, considering the effects of imposed deformations and tension stiffening

: ε_{cm} is the mean strain in the uncracked concrete between the cracks. A formula for the calculation of the term (ε_{sm} - ε_{cm}) is provided in *EN 1992-1-1:2004*

From Equation 2-2, and the formulas for calculation of $S_{r,max}$ and (ε_{sm} - ε_{cm}) given in *EN 1992-1-1:2004*, it can be seen that there are four possible methods which may be used in flexural crack width design to limit crack widths (Mosley, Bungey & Hulse, 2007:152):

- Limit the stress in the steel, by increasing the amount of reinforcement provided
- Use smaller reinforcing bars, such that the bar spacing, and thus crack spacing, will be reduced
- Increase the effective reinforcement ratio, by reducing the effective tension area – this can be achieved by reducing the cover depth
- Use deformed (high bond) reinforcing bars, rather than plain (mild) steel bars

However, the third and fourth options are often not practical, as the cover depth cannot be reduced below the minimum needed to meet durability requirements, and deformed bars are typically already used for tension reinforcement, such that there generally is not an option to switch from plain to deformed bars to limit crack widths. This means that, in practice, the flexural crack width requirements are often met through the provision of additional reinforcing steel, and/or the use of smaller diameter reinforcing bars, spaced closely together (Basteskår et al., 2019a:7).

2.7.1.2 Crack Width Design for Shrinkage Cracking

The shrinkage crack width design process is not as simple as that for flexural crack width design, and involves practical considerations, such as assumptions about construction details and development of hydration heat, to a much greater degree (Smith, 2016a:85). As such, the requirements for shrinkage crack width design are provided separately, in *CIRIA C660*, which gives guidance on cracking due to heat of hydration, long-term ambient temperature fluctuations, and drying shrinkage (Bamforth, 2007:3). However, the approach provided in *CIRIA C660* is still based upon the requirements of *EN 1992-1-1:2004*, which have simply been modified to apply to shrinkage cracking (Bamforth, 2007:20).

CIRIA C660 provides two possible shrinkage crack width design methods – a full method, and a simplified method – depending on the amount of information available at the time of design (Bamforth, 2007:20). Regardless of which method is chosen, the design process has four steps (Bamforth, 2007:20):

1. Selection of the design crack width, based upon the design situation and environment (the marine environment in the case of this research)
2. Estimation of the restrained strain, which allows the risk of cracking to be established
3. Estimation of the crack-inducing strain
4. Determination of the reinforcement required to control crack spacing and width

Detailed guidance on each of the four steps is provided in *CIRIA C660* (Bamforth, 2007). However, it is worth noting that step two should consider strains produced both in the short-term (by heat of

hydration and autogenous shrinkage), and in the long-term (by ambient temperature fluctuations and drying shrinkage) (Bamforth, 2007:30-31). Furthermore, as alluded to above, step four follows the same two-step process as for flexural cracking – it is first checked that the area of reinforcing steel provided is greater than the minimum, after which the amount and layout of reinforcement required to limit crack widths to the required value is determined (Bamforth, 2007:21). The formulas for minimum reinforcement area and crack width are also the same as those specified for flexural cracking in *EN 1992-1-1:2004* (Bamforth, 2007:31).

2.7.2 Crack Width Formulas

There are four different types of models which may be used to develop crack width formulas (Lapi, Orlando & Spinelli, 2018:1483):

- Analytical models, which are based on theories of stress and strain, and steel-concrete bond slip
- Semi-analytical models, where simplications have been made to the analytical models
- Empirical models, which are based on relationships in experimental data
- Numerical models, such as finite element or damage models

However, the complexity of cracking makes the development of analytical models difficult, such that most current crack width formulas are based on semi-analytical or empirical models (Lapi, Orlando & Spinelli, 2018:1485). The crack width formula provided in *EN 1992-1-1:2004* makes use of a semi-analytical model (Lapi, Orlando & Spinelli, 2018:1485), in which crack width is calculated as a function of crack spacing and steel strain (see Equation 2-2), with the derivation of this formula being discussed in detail by Beeby and Narayanan (2009) and Mosley, Bungey and Hulse (2007). The model was first developed by Borges (1966) (Lapi, Orlando & Spinelli, 2018:1487), and was then included in the *CEB-FIP* Model Code 1978 and Model Code 1990, before ultimately being adopted, with some minor changes, by *EN 1992-1-1:2004* (Lapi, Orlando & Spinelli, 2018:1491-1493).

Likewise, the crack width formula used in the *fib* Model Code 2010 – which is likely to guide the development and implementation of crack width formulas in future codes of practice – is also based on a semi-analytical model in which crack width is calculated as a function of crack spacing and steel strain (Balázs et al., 2013:105). In fact, the Model Code 2010 follows a very similar approach to that used in *EN 1992-1-1:2004*, with only relatively minor differences in the formulas used to calculate crack spacing, while both codes use the same formula for steel strain, based on the Model Code 1990 (Lapi, Orlando & Spinelli, 2018:1494). This is an important finding, as it means that the method currently used for crack width design in *EN 1992-1-1:2004* is unlikely to change significantly with the introduction of future, updated codes of practice.

It is also important to note that cracking is essentially a random phenomenon, with both crack width and spacing exhibiting considerable scattering (i.e., crack width and spacing will vary considerably, even if all other variables are kept constant) (Lapi, Orlando & Spinelli, 2018:1485). This variability means that a probabilistic approach is needed to develop models for crack width, with most design codes using the 95^{th} percentile as the characteristic crack width (i.e., only 5% of crack width values are expected to exceed the calculated crack width value) (Lapi, Orlando & Spinelli, 2018:1485).

The highly variably nature of cracking is also reflected in the performance of the existing crack width formulas, which show significant scattering between different models. Lapi, Orlando and Spinelli (2018) compared calculated crack widths, for a variety of crack width formulas, with experimental results from four different studies, representing 380 data points. Each of the four studies, carried out between 1956

and 1996 (Lapi, Orlando & Spinelli, 2018:1496), directly determined crack widths, using optical micrometers, for a range of variables including steel stress, cover depth, reinforcement diameter and effective reinforcement ratio (Lapi, Orlando & Spinelli, 2018:1496-1498). Based on their comparisons, Lapi, Orlando and Spinelli (2018:1496) found that the coefficient of variability between the results of the existing crack width formulas ranges from 30 – 50%, depending on variables such as concrete tensile strength. In practice, this means that the calculated crack width value, and thus the amount and layout of reinforcement used, is very sensitive to the designer's choice of crack width formula (Lapi, Orlando & Spinelli, 2018:1496).

In order to illustrate the comparison between the results of the crack width formulas and the experimentally determined crack widths, Lapi, Orlando and Spinelli (2018:1498-1500) determined values of the ratio w_{th}/w_{exp}, where w_{th} is the predicted crack width, and w_{exp} is the experimentally measured crack width, for a variety of input parameters and for each of the four studies considered. These w_{th}/w_{exp} values were then used to produce a box and whisker plot, shown in Figure 2-19, for each of the existing crack width formulas studied by Lapi, Orlando and Spinelli (2018).

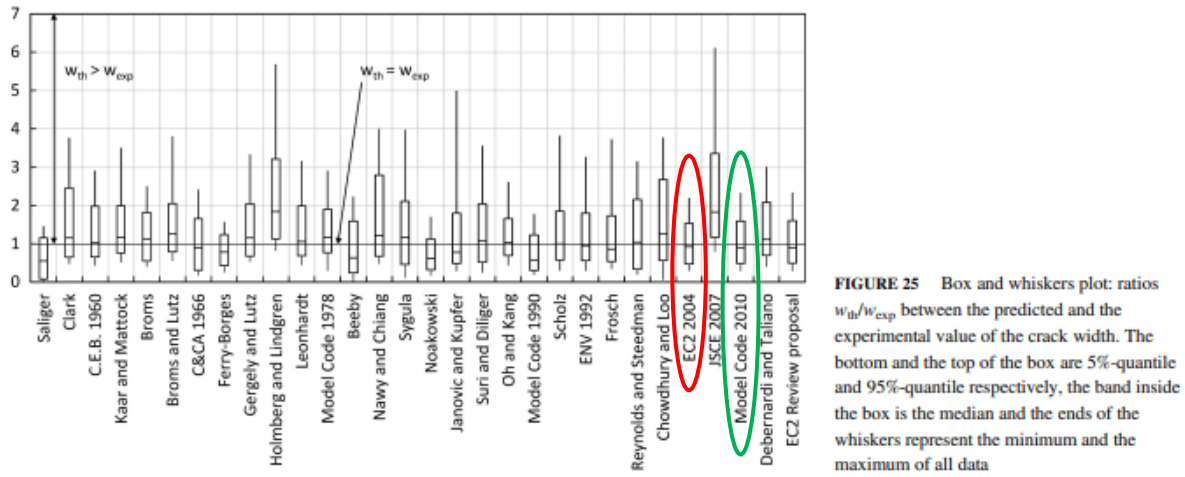

FIGURE 25 Box and whiskers plot: ratios w_{th}/w_{exp} between the predicted and the experimental value of the crack width. The bottom and the top of the box are 5%-quantile and 95%-quantile respectively, the band inside the box is the median and the ends of the whiskers represent the minimum and the maximum of all data

Figure 2-19: The box and whisker plot produced by Lapi, Orlando and Spinelli (2018), showing w_{th}/w_{exp} ratios for a variety of existing crack width formulas. Note the performance of the *EN 1992-1-1:2004* formula, circled in red, and the Model Code 2010 formula, circled in green.

From Figure 2-19, it appears that the crack width formula used in *EN 1992-1-1:2004* provides reasonably accurate results, which tend to be in better agreement with experimental data than many other crack width formulas. This is as the formula used in *EN 1992-1-1:2004* has a median w_{th}/w_{exp} value very close to one, and a relatively small range in w_{th}/w_{exp} values. It can therefore be seen that the crack width formula provided in *EN 1992-1-1:2004* is a reasonably accurate engineering approximation of a highly complex, variable phenomenon.

Figure 2-19 also shows that the crack width formula used in the Model Code 2010 produces very similar results to the formula provided in *EN 1992-1-1:2004*. This is to be expected, given the similarities between the two formulas highlighted above. It is therefore unlikely that there will be a major difference between the results of crack width design carried out according to *EN 1992-1-1:2004* and the Model Code 2010 (although the Model Code 2010 has a stricter crack width requirement than *EN 1992-1-1:2004* (0.2 mm vs. 0.3 mm), the effects of which are discussed further in Section 9). This is an important finding, as it suggests that the conclusions of this study, which investigates crack width design according to *EN 1992-1-1:2004*, are likely to also apply to the Model Code 2010 and therefore to crack width design in future codes of practice.

2.7.3 Critique of the Current Crack Width Requirements

In Section 2.5 it was found that there is no clear relationship between crack width and the propagation of corrosion. This is the primary criticism of the current crack width requirements, made by authors such as Beeby (1978) and Basteskår et al. (2019b:685), who observed that there have been no durability problems for Norwegian infrastructure as a result of cracking, even though some of the infrastructure was not designed for crack width requirements. However, this is not the only criticism of the current crack width requirements which may be found in the literature. There are several issues with the requirements themselves, and with their use in engineering practice.

Even if there was a clear link between crack width and corrosion rate, authors such as Raupach (1996) and Basteskår et al. (2019b) argued that the current crack width requirements, which tend to result in the use of closely spaced, small diameter bars, with small cover depths (Basteskår et al., 2019b:685), may actually reduce durability. Raupach (1996:335) found that the use of twelve 8 mm diameter bars, as opposed to two 20 mm bars (both with nearly the same total cross-sectional area) will result in a 4.5 times greater corrosion rate. This is as the total exposed surface area of steel increases as bar size decreases – meaning that the use of smaller diameter bars will expose more steel, ultimately resulting in faster corrosion and therefore reduced service life (Raupach, 1996:335). This would imply that the current crack width requirements are not effective at providing durability. However, as most of the existing experimental research has focused on the effects of cracking on the corrosion of single bars, more experimental research focusing on multiple bars is needed to confirm these findings.

There are also several technical deficiencies with the current crack width requirements – the crack width formulas underestimate crack widths of two way spanning slabs, as they were developed for beams (ACI Committee 224, 2001:20), and overestimate crack widths for very large or deep members (Fredericks, 2019:iv). The current crack width formulas are also known to not be very accurate (Alexander, Beushausen & Otieno, 2012:28), although, as discussed above, the complexity of cracking makes it unlikely that any perfectly accurate formulas will ever be developed.

It is also apparent that there is a lack of nuance in the current crack width requirements, with a single requirement being specified for all marine RC members, even though the extent and severity of corrosion has been shown to vary considerably between the submerged, tidal, splash and spray, and atmospheric zones. It is because of this, and the influence of other factors such as cover depth, concrete quality, and crack characteristics, that Otieno, Beushausen and Alexander (2012:1806) believe that having a single crack width for all cases is flawed, and unlikely to be effective or efficient in providing durability.

In Section 2.5, it was found that even small cracks, with widths below the current crack width requirements, may result in faster corrosion initiation and propagation. This directly contradicts the fundamental philosophy of crack width design – that, if crack widths are limited to the required values, corrosion will proceed as if for uncracked concrete, and service life can be calculated based on the corrosion initiation period only (Otieno, Beushausen & Alexander, 2012:1806). If even small cracks, with widths below the current crack width requirements, result in significant reductions in service life, then this philosophy will be invalid, and the crack width requirements will not be effective at providing durability.

Authors such as Basteskår et al. (2019a:1-2) also note that there is considerable ambiguity in codes such as *EN 1992-1-1:2004* – particularly with determination of the strain redistribution parameter, k_2, and with which situations require direct calculation of crack width. The current thermal crack width requirements are also often not properly understood by design engineers, and may not accurately account for advances in concrete technology (Angelucci, 2018:1). This ambiguity, lack of understanding and outdatedness may result in overconservative designs in which excessive amounts of reinforcing steel

(up to several hundred percent greater than the amount needed for ULS requirements) are provided to control cracking (Basteskår et al., 2019a:8). It is likely that this use of large amounts of additional reinforcing steel will have notable cost and environmental implications.

It can thus be seen that there are several significant issues with the current crack width requirements. These issues range from fundamental (the fact that there is no clear relationship between crack width and corrosion rate, and that even very small cracks may lead to propagation of corrosion) to technical (deficiencies with the crack width formulas themselves). These issues all have the potential to limit or reduce the effectiveness of the current crack width requirements at providing durability. It is therefore vital that these issues be studied further, to determine the extent to which they limit durability, and whether the current requirements are acceptable. It is within this context that this study investigated the implications of two of the issues on the effectiveness of crack width design – the influence of small cracks on the propagation of corrosion, and the use of large additional quantities of reinforcing steel to meet the requirements.

2.7.4 Developments in Crack Width Design

In response to the issues with the current crack width requirements raised above, several possible improvements to the crack width design process have been proposed in the literature:

- To combat the lack of nuance in the current crack width requirements, Otieno, Beushausen and Alexander (2012) argue for the adoption of performance-based crack width requirements. These performance-based requirements would entail the use of a nomograph to convert the required service life into a crack width limit, as a function of concrete quality, cover depth, crack characteristics and exposure conditions (Otieno, Beushausen & Alexander, 2012:1805). However, further, long-term research would still be required to develop this nomograph (Otieno, Beushausen and Alexander, 2012:1814)
- Because current crack width formulas overestimate crack widths for large/deep members, Fredericks (2019:iv) recommends the use of numerical modelling, rather than the analytical formulas specified in design codes, to determine crack widths for large RC members
- As a result of the inaccuracies of the current crack width formulas, and because there is no clear relationship between crack width and corrosion rate, Basteskår et al. (2019b:685-686) recommend that crack width requirements should not be used, and instead steel stress should be limited in order to minimise cracking and its effects. This is already partially accounted for in the Model Code 2010, which gives the engineer a choice between either designing directly for crack width, or indirectly controlling cracking by limiting steel stress (Balázs et al., 2013:103).
- Arya and Myrzakulova (2019:10) found that cover depth had a greater influence on corrosion than crack width. However, the use of larger covers will lead to larger surface crack widths, such that excessive amounts of reinforcing steel would be required to meet the crack width requirements (Arya & Myrzakulova, 2019:10). As such, they propose an alternative approach to crack width design, in which larger covers are used, but with reinforcement which cannot corrode, such as glass fibre reinforced plastic, placed at shallow depths to control cracking (Arya & Myrzakulova, 2019:10)

It can thus be seen that potential improvements or changes to the current crack width requirements and design process are available, should the existing requirements be found to be ineffective or inefficient.

SECTION C: *Methods for Quantifying the Implications of the Current Crack Width Design Requirements*

2.8 Service Life Modelling of Cracked Reinforced Concrete

In the service life modelling of RC structures, the service life of the structure, t_s, is typically defined as the sum of the corrosion initiation and propagation periods (t_i and t_p, respectively), as shown in Equation 2-3.

$$t_s = t_i + t_p \qquad \textbf{Equation 2-3}$$

In theory, service life modelling of RC structures therefore involves separately determining the lengths of the initiation and propagation periods, and summing them to find the total service life of the structure (Otieno, Beushausen & Alexander, 2011:241). However, in practice, most existing service life models (SLMs) consider the service life to be equal to the initiation period only (Andrade, 2020:283), even though the length of the propagation period may be significant (Gulikers, 2005:71). Furthermore, the existing SLMs were developed considering uncracked concrete, and therefore do not account for the effects of cracking on the length of the initiation period (Ramezanianpour et al., 2018:1461). This makes it difficult to use the existing SLMs to estimate the service lives of real, cracked RC structures.

However, significant advances in the field of service life modelling, considering both the initiation period in cracked RC, and the propagation period, have been made in recent years. Ultimately, these advances can be combined with the existing SLMs to develop an approach for estimating the service lives of cracked RC structures, which considers both the initiation and propagation periods. The focus of this section of the literature review is thus on explaining how such an approach can be developed for use in this study.

2.8.1 Existing Models for the Corrosion Initiation Period

A wide variety of models for the corrosion initiation period are currently available, with most having been developed in the 1990s and early 2000s. Of these, some of the most significant and widespread, in both the literature and in industry, are the *Life-365*, *Duracrete* and *ClinConc* models. Each of these models are summarised in Table 2-5 and discussed in detail below.

Table 2-5: A summary of three of the most widespread existing SLMs (adapted from Pillai & Annapareddy, 2013:565).

Model	Modelling Approach	Computational Approach	Development Date
Life-365	Empirical	Deterministic & Probabilistic	2000
Duracrete	Empirical	Probabilistic	1996-1999
ClinConc	Physical	Deterministic	Mid-1990s

All three models are based on solving Fick's Second Law (Pillai & Annapareddy, 2013:563), although they differ in the way they choose to solve it, the input variables they consider when doing so, and their modelling and computational approaches. Fick's Second Law, shown in Equation 2-4, is a partial differential equation which describes the diffusion of chloride ions into concrete as a function of both time and distance (Pillai & Annapareddy, 2013:563). By solving this equation, it is possible to find the

time when the concentration of chlorides at the level of the reinforcing steel reaches the threshold concentration and active corrosion begins. This time then provides the length of the corrosion initiation period, t_i.

$$\frac{\partial C(x,t)}{\partial t} = D\frac{\partial^2 C(x,t)}{\partial x^2} \qquad \textbf{Equation 2-4}$$

Where: C is the concentration of chlorides
: D is the chloride diffusion coefficient
: x is the chloride penetration depth
: t is the exposure time for the structure

The first of the models, the *Life-365* model, was first released by the American Concrete Institute (ACI) in 2000 (Tang, Utgenannt & Boubitsas, 2015:1410), although it has undergone significant development and verification since then (Life-365, n.d.). The model uses an iterative, finite difference approach to solve Fick's Second Law over a series of time steps, with the diffusion coefficient, D, being modelled as a function of both time and temperature (Pillai & Annapareddy, 2013:565). The model also considers the w/b ratio and the amount of extenders (such as FA and GGBS) used in the mix design, as well as the type, exposure zone and geographic location of the structure (Oslakovic, Bjegovic & Mikulic, 2010:1404). This ultimately makes the *Life-365* model relatively comprehensive, and suitable for use for a wide variety of marine structures.

The *Duracrete* model was developed in Europe, as a result of a European Union (EU) research project on performance-based durability design of concrete structures, which ran from 1996 to 1999 (European Commission, n.d.). In contrast to the other two models, *Duracrete* uses a purely probabilistic approach, in which the probability of service life failure during service life T, $P_f(T)$, is kept to an acceptably low value (Oslakovic, Bjegovic & Mikulic, 2010:1398). The length of the initiation period can thus be determined by setting the probability of failure, $P_f(T)$, as equal to the acceptable failure probability for the structure and working backwards to find t_i (Pillai & Annapareddy, 2013:567). However, other than the use of a probabilistic approach, the *Duracrete* model is similar to the other two models, as it is still based on Fick's Second Law, and uses many of the same variables.

The *ClinConc* model was developed in the mid-1990s, although it has been recently updated (Tang, Utgenannt & Boubitsas, 2015:1411). It is widely considered to be one of the most sophisticated models for the corrosion initiation period (Athibaranan, Karthikeyan & Rawat, 2022:5), particularly as it takes account of chloride binding, unlike the other two models. It is also a physical model, based on the principles of mass balance and chloride binding, in contrast to the *Life-365* and *Duracrete* models, which are purely empirical (Tang, Utgenannt & Boubitsas, 2015:1411). However, like the *Life-365* model, the *ClinConc* model also uses a finite difference approach to solve an equation based on Fick's Second Law (Pillai & Annapareddy, 2013:566). Despite its advantages, there is unfortunately one significant limitation with the *ClinConc* model – it was developed for the submerged zone, and needs extensive modification for use in the atmospheric or tidal, splash and spray zones (Athibaranan, Karthikeyan & Rawat, 2022:5).

Several studies have evaluated the performance of the existing models at predicting the length of the corrosion initiation period. Oslakovic, Bjegovic and Mikulic (2010:1404-1408) found that predictions made using the *Life-365* model were in close agreement with values measured for a real marine RC bridge in Croatia, while for the same structure, the *Duracrete* model significantly overestimated the length of the corrosion initiation period. This was explained by the fact that the *Duracrete* model

overestimates the reduction in diffusion coefficient with time for concretes using extenders such as FA and GGBS (Oslakovic, Bjegovic & Mikulic, 2010:1408).

The results of Tang, Utgenannt and Boubitsas (2015:1414) seem to corroborate this, as they found that the *Duracrete* model underestimates chloride ingress. Pillai and Annapareddy (2013:577) also note that the *Duracrete* model is highly sensitive to the selection of input parameters and should therefore only be used when these parameters are known or can be modelled with a high degree of confidence. Finally, both Tang, Utgenannt and Boubitsas (2015:1414) and Pillai and Annapareddy (2013:577) found that the *ClinConc* model produces accurate results, which are generally comparable to those of *Life-365*.

It can thus be seen that the *Life-365* model, which produces relatively accurate results, is most suited for use in this study, as the *Duracrete* model overestimates the length of the corrosion initiation period, and the *ClinConc* model was developed for the submerged zone only. However, the *Life-365* model, like all of the existing models for the initiation period, was developed assuming that the concrete is uncracked (Ehlen, Thomas & Bentz, 2009:42). This means that it cannot be used, at least without modification, to estimate the length of the initiation period in cracked concrete.

2.8.2 Modelling the Corrosion Initiation Period in Cracked Reinforced Concrete

In Section 2.5.1 it was noted that cracks cause faster corrosion initiation, such that the length of the corrosion initiation period is often taken as zero in cracked concrete. However, this may be overly conservative, as depending on the depth of the crack, cracking does not always result in instant initiation of corrosion, as shown in Figure 2-20. This is particularly relevant for RC structures with large cover depths, such as marine RC structures, for which crack depth may be less than cover depth (Ramezanianpour et al., 2018:1466). It is thus still worthwhile to consider the length of the initiation phase in the service life modelling of cracked RC (Otieno, 2014:187).

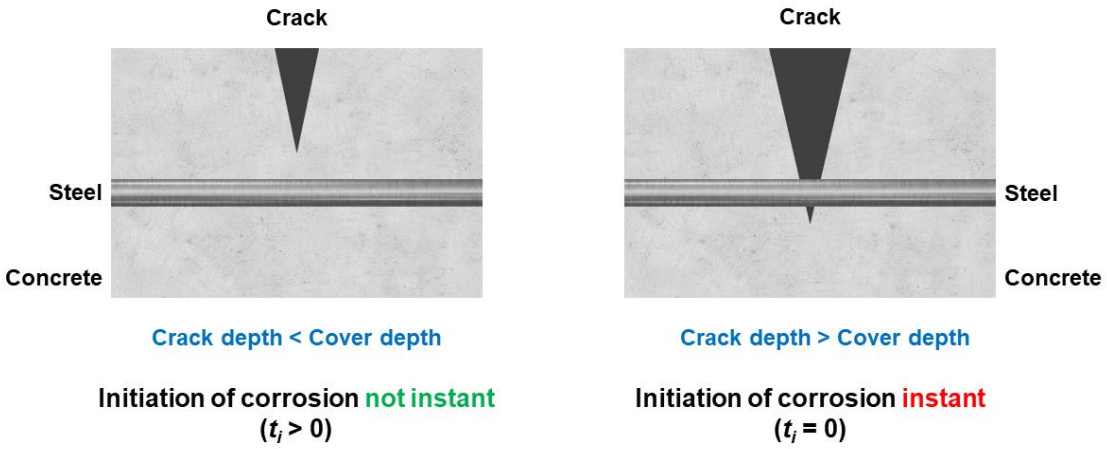

Figure 2-20: A simplified illustration showing how cracking does not necessarily lead to instant initiation of corrosion (adapted from Ramezanianpour et al., 2018:1467).

At present, there are not many methods available in the literature for determining the length of the corrosion initiation period in cracked concrete (Otieno, 2014:188). In fact, only one such method, developed by Ramezanianpour et al. (2018), was found during this literature review. Ramezanianpour et al. (2018:1467) developed a formula for flexural cracks, which allows crack depth to be estimated as a function of crack width. At the same time, based on beam samples exposed to the tidal zone for 48 months, Ramezanianpour et al. (2018:1466-1467) also found that cracks with widths less than 0.1 mm do not result in increased penetrability and faster corrosion initiation.

This is contradicted by the work done by Otieno, Beushausen and Alexander (2016:381), who found that, after approximately 27 months of exposure in the tidal zone, corrosion was initiated much sooner in beam samples with incipient (i.e., very small) cracks than in uncracked beam samples. This led to the samples with incipient cracks exhibiting higher corrosion rates than the uncracked samples, which had yet to begin active corrosion. However, for samples made using GGBS and having w/b ratios of 0.4, i.e., the same mix design as the members considered in this study, the increase in corrosion rate from uncracked to incipient-cracked specimens was found to be relatively minor, at only 8% (Otieno, Beushausen & Alexander, 2016:381). Furthermore, it was observed that, after 31 weeks (approximately 8 months) of exposure, active corrosion had not yet been initiated in the incipient-cracked samples made using GGBS and with w/b ratios of 0.4 (Otieno, Alexander & Beushausen, 2010:398) – in other words, initiation of corrosion was not instant. It was therefore assumed for the purposes of this study that the effect of very small (i.e., 0.1 mm) cracks on the initiation of corrosion is negligible, such that the findings of Ramezanianpour et al. (2018) could be used for modelling of the corrosion initiation period.

Based on their findings, Ramezanianpour et al. (2018:1468) proposed that, by assuming that flexural cracks are wedge-shaped, their formula for crack depth can be used to determine the depth at which the width of a crack is equal to 0.1 mm and corrosion initiation occurs as if the concrete were uncracked. This depth can then be used to determine the effective cover depth, i.e., the cover depth for which the concrete is effectively uncracked, as shown in Figure 2-21. Once the effective cover depth is known, it can be used in traditional SLMs, such as those described in Section 2.8.1 above, to find the length of the corrosion initiation period in cracked concrete. Of course, if the depth of the crack is such that it is wider than 0.1 mm even at the level of the reinforcing steel, then the length of the corrosion initiation period is taken as zero (Ramezanianpour et al., 2018:1467).

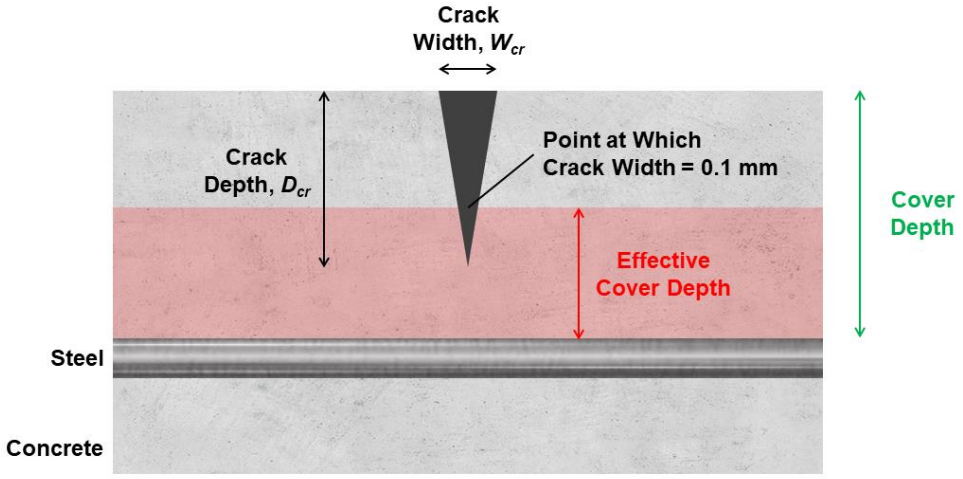

Figure 2-21: An illustration showing the effective cover depth concept for cracked concrete (adapted from Ramezanianpour et al., 2018:1467).

There are, however, some limitations with this method – the formula relating crack width and depth was developed for flexural cracks only, and only considers concrete which is either made from pure Portland cement, or Portland cement with 7.5% silica fume (SF) replacement (Ramezanianpour et al., 2018:1468). Nevertheless, it is likely that the method will still provide reasonable estimates of effective cover depth even for other types of cracks and concretes with other extenders, such as FA and GGBS. The method developed by Ramezanianpour et al. (2018) can thus be seen as a simple, effective method for modifying traditional SLMs, such as *Life-365*, *Duracrete* or *ClinConc*, to account for the effects of cracking.

2.8.3 Models for Determining Corrosion Rate

Once corrosion has been initiated, the length of the propagation period is primarily governed by the corrosion rate of the reinforcing steel (Otieno, Beushausen & Alexander, 2011:241). As such, corrosion rate is a key variable in corrosion propagation modelling, and thus needs to be discussed before the propagation period models themselves. It is important to note that the corrosion rate, defined as the amount of steel lost over a given time, is not necessarily constant, and may vary due to changes in the availability of oxygen and moisture (Andrade, 2020:284). However, to simplify the prediction of the propagation period, most models for the propagation period make the conservative assumption that the corrosion rate remains constant throughout the propagation period (Otieno, 2014:191). This constant corrosion rate, referred to as the "representative" corrosion rate (Otieno, 2014:191), is what corrosion rate models ultimately aim to determine.

There are many existing models for determining corrosion rates, which can be broadly divided into two categories – either empirical models, or electrochemical models (Gulikers, 2005:76). Gulikers (2005:76-83) describes several of these existing corrosion rate models, such as the Morinaga model, the concrete resistivity model, and various electrochemical models. However, none of these models account for the effects of cracking, at least not directly.

Only one corrosion rate model, developed by Otieno (2014), directly accounts for the effects of cracking, and is comprehensive and robust enough for use in this study. The model is empirical in nature and allows for the prediction of corrosion rate as a function of cover depth, concrete quality (represented by the 90-day chloride diffusion coefficient, D_{90}) and crack width. There are several limitations with Otieno's model (2014), which would need to be accounted for in order for it to predict accurate results for real marine RC structures:

- The model was developed based on beam samples which were exposed to either accelerated laboratory corrosion, or natural corrosion in the marine tidal zone, for a period of approximately 2 years and 3 months (Otieno, 2014:167). It is assumed that the stable corrosion rates observed at the end of this period will remain sufficiently constant to be used as the representative corrosion rate, although this is unlikely to be the case in reality (Otieno, 2014:189)
- The beam samples used to develop the model each contained a single 10 mm diameter reinforcing bar (Otieno, 2014:187). As such, the model does not account for the fact that corrosion rate varies with changes in the number of reinforcing bars (Bezuidenhout & van Zijl, 2019:2188) and bar diameter (Raupach, 1996:335)
- The model was developed considering single flexural cracks only (Otieno, 2014:187). The effects of multiple cracks, as are typically found in real flexural members, or other types of cracks, such as thermal and shrinkage cracks, were not considered

Unfortunately, in the absence of long-term corrosion rate results, or data considering other types of cracking, there is no way of addressing the first and third limitations; the model simply must be used assuming that the corrosion rate remains stable and that the effect of multiple cracks is not significant. This is likely to reduce the accuracy of the model, but even so, it is still the best model available. The second limitation can, however, be addressed by using the findings of Bezuidenhout and van Zijl (2019) and Raupach (1996) to modify the model to account for differences in the size and number of reinforcing bars used. Such modifications are discussed further in Section 5.

2.8.4 Modelling the Corrosion Propagation Period

The corrosion propagation period was defined in Section 2.3.6 as the length of time from corrosion initiation until the corrosion-induced damage becomes unacceptable. As such, determination of the length of the corrosion propagation phase depends on how "unacceptable" damage is defined (Alexander, Beushausen & Otieno, 2012:31). Andrade and Izquierdo (2020:1725) note that there are four definitions of "unacceptable damage" or "limit states" which may be used to mark the end of the propagation phase:

- A decrease in the cross-sectional area of the reinforcing steel, typically in the range of 5 to 25% (Alexander, Beushausen & Otieno, 2012:32)
- Cracking of the concrete cover due to the expansion of corrosion products
- Deterioration of the bond between the steel and concrete
- Loss of load-bearing capacity

Any of these four limit states can be used to develop models for the propagation period, although decrease in cross-sectional area and corrosion-induced cover cracking are the most frequently used (Alexander, Beushausen & Otieno, 2012:31-32).

A large number of propagation period models have been developed (Cui & Alipour, 2018:653), and are all either empirical, numerical or analytical in nature (Jamali et al., 2013:227-229). Empirical models are based on experimental results, while numerical models are developed using finite element modelling and analytical models are based on the principles of electrochemistry and solid mechanics (Otieno, Beushausen & Alexander, 2011:241-242). A selection of the existing models for the propagation period are shown in Table 2-6.

Table 2-6: A summary of some of the corrosion propagation models available in the literature.

Authors/Reference	Model Type	Limit State	Error Range [% Below / Above Experimental Results]
El Maaddawy and Soudki (2007)	Analytical	Cover cracking	-23.3 / 24.0
Lu, Liu and Jin (2010)	Analytical	Cover cracking	-12.1 / 18.9
Otieno (2014)	Analytical	Decrease in steel area	Not calculated
Xi and Yang (2017)	Analytical	Cover cracking	Not calculated
Bezuidenhout and van Zijl (2019)	Analytical	Decrease in steel area	Not calculated
Andrade (2020)	Analytical	Decrease in steel area	Not calculated
Lun et al. (2021)	Analytical	Cover cracking	-9.40 / 11.0

The models presented by Otieno (2014), Bezuidenhout and van Zijl (2019), and Andrade (2020) are very similar, as they are all based on Faraday's law, which describes the mass of steel lost as a function of time and the corrosion rate (Bezuidenhout & van Zijl, 2019:2189). All three models are therefore

relatively simple models, which allow the length of the propagation period to be calculated as a function of representative corrosion rate and initial bar diameter. While no error ranges were calculated for the models, and their accuracy thus cannot be compared, it is likely that all three models will yield very similar (if not the same) results.

In contrast to the models which use decrease in steel area as a limit state, the cover cracking models are relatively complex, and consider many variables, such as the representative corrosion rate, initial bar diameter, cover depth, w/c ratio, chloride content, temperature, relative humidity, and concrete resistivity (Lun et al., 2021:8). As a result of this complexity, the cover cracking models are able to produce relatively accurate results (as shown in Table 2-6), particularly in the case of the model produced by Lun et al. (2021), which was developed specifically for real RC structures in the natural marine environment (Lun et al., 2021:2).

However, it should be noted that more complex models do not necessarily yield more accurate results (Alexander & Beushausen, 2019:24), particularly as many of the variables used in the cover cracking models cannot be reliably determined, and therefore often need to be selected based on conservative assumptions (Otieno, Beushausen & Alexander, 2011:243). In the case of this study, many of the variables considered by Lun et al. (2021), such as temperature, relative humidity, and concrete resistivity are not known with any certainty.

It can thus be seen that there are a wide range of propagation period models available, with two types being applicable to this study – those based on predicting time until a certain percentage of the reinforcing steel cross-section is lost, and those which calculate the time until corrosion-induced cracking of the cover concrete. As the accuracy of the first type was not assessed in the literature, and the accuracy of the second type may be reduced by the need to make conservative assumptions for many of the input variables, it is not possible to choose a propagation period model for use in this study based on accuracy. Instead, the choice of model for the study was based on the relative importance of the limit states (either loss in steel cross-section or cover cracking) for the members under consideration; this is discussed further in Section 5.

2.8.5 Conclusion on Service Life Modelling of Cracked Reinforced Concrete

While the existing SLMs such as *Life-365*, *Duracrete* and *ClinConc* do not account for the effects of cracking, it has been shown in this section of the literature review that it is possible to predict the service life of cracked marine RC structures. This can be done in five steps, by:

- Using the crack depth model developed by Ramezanianpour et al. (2018) to determine the effective cover depth of the cracked RC
- Inputting the effective cover depth into one of the existing SLMs to determine the length of the initiation period, t_i
- Using the corrosion rate model developed by Otieno (2014) to determine the representative corrosion rate
- Inputting the representative corrosion rate into one of the existing propagation period models to determine the length of the propagation period, t_p
- Summing the initiation and propagation periods to find the total service life of the structure, t_s

This five-step method is applied to this study, and discussed further, in Section 5.

2.9 Methods for Determining Cost Implications

Although a wide variety of methods for determining cost implications are available, the most used method, in both the literature and the industry, is the life cycle cost analysis (LCCA) method (Yang, Li & Pang, 2013:161; Fregonara, Ferrando & Pattono, 2018:1; Van Cauteren et al., 2022:2). This method involves the determination of the total cost, referred to as the life cycle cost (LCC), over the entire service life of a structure or structural element (Kubba, 2010:327). In a structural engineering context, the LCCA method is often used to compare the cost implications of different design options (e.g., the use of carbon steel reinforcement vs. the use of stainless steel reinforcement), in a way that accounts for the fact that the different options will incur different costs over their service lives (Val & Stewart, 2003:344).

The LCC of a structure (or structural element), which is ultimately a measurement of the entire cost of the structure, from design to demolition (Dwaikat & Ali, 2018:304), is determined by summing up all the individual costs associated with the structure, over its entire service life (De Gijt & Vinks, 2011:135). However, doing so is not necessarily straightforward, as inflation and other macroeconomic effects will cause the value of the currency used to measure costs to decrease over the service life of the structure. This means that costs incurred in the future, such as maintenance costs, will be higher than they would be in the present (Val & Stewart, 2003:345). To account for this, and allow for a single cost to be determined upfront, the net present value (NPV) method is used to convert (or "discount") future costs into equivalent values at the present time, assuming a constant discount rate (De Gijt & Vinks, 2011:135). It can thus be seen that there are three steps to determining the LCC of any structure:

- Step 1: Determine the absolute value of each of the costs associated with the structure, in future terms where applicable (e.g., for maintenance costs)
- Step 2: Convert the absolute cost values to present values (PVs) using the NPV method
- Step 3: Sum up the individual PVs

The individual costs considered in Step 1 will vary from structure to structure, but are typically broken down into the costs associated with each stage of the structure's service life (Stevens, 1978:6). For marine structures, which do not typically have significant operating costs, life cycle costs can generally be broken down into the following five stages (De Gijt & Vinks, 2011:136):

- Planning, design, and engineering (PDE) costs
- Construction (C) costs
- Maintenance (M) costs
- Repair (R) costs
- Demolition (D) costs

The costs incurred during each of these stages will vary depending on the type of marine structure. Figure 2-22 shows a breakdown of some of the costs which would typically be considered during each of the stages for marine RC structures, based on findings in the literature (Kubba, 2010:269; De Gijt & Vinks, 2011:136; Younis, Ebead & Judd, 2018:155).

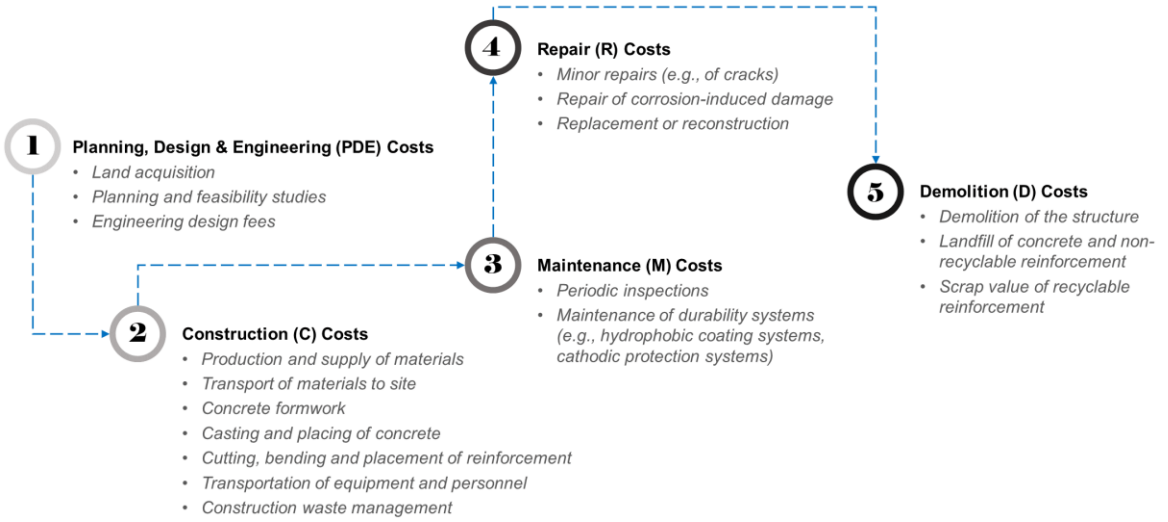

Figure 2-22: A framework showing the costs expected for each of the life cycle stages for a typical marine RC structure (adapted from Younis, Ebead and Judd (2018:155)).

2.10 Methods for Determining Impacts on Environmental Sustainability

The construction industry plays a major role in the production of greenhouse gasses (GHGs) and the anthropogenic use of material and energy (Hart, D'Amico & Pomponi, 2021:403). RC is the single-most used material in the construction industry, with an estimated global consumption of 21 to 31 billion tons per year (Knoeri, Sanyé-Mengual & Althaus, 2013:909), while the production of cement and steel alone accounts for about one-sixth of the world's carbon dioxide (CO_2) emissions (Bras & Faustino, 2019:87). The production and use of RC therefore results in significant impacts on environmental sustainability.

In order to select materials and design methods which reduce the environmental impact of RC, it is first necessary to quantify these environmental impacts, so that the different materials and design methods can be compared. To this end, several methods to assess environmental impact have been developed, including cumulative energy demand (CED), global warming potential (GWP), ozone depletion potential (ODP), acidification potential (AP), nutrification potential (NP), and photochemical ozone creation potential (POCP) (Müller, Haist & Vogel, 2014:322). Of these, the most reported in the literature and most frequently used in the construction industry are CED and GWP. This study thus focuses on GWP as an indicator of environmental sustainability, although CED would have been equally applicable.

GWP is a measure of a material's contribution to global warming, considering the amount of carbon dioxide (CO_2), nitrogen oxides (NO_x) and methane (CH_4) released in its production and use (Voo et al., 2014:4). It is measured in kilograms of equivalent CO_2 emissions ($kgCO_2e$) and is hence typically referred to as embodied carbon (EC) in the construction industry (The Institution of Structural Engineers, 2020:1). EC values for structural components are calculated considering the entire lifecycle of the component, which is split into four stages (The Institution of Structural Engineers, 2020:1):

- The product stage, covering the extraction, transport, and manufacture of raw materials into the finished component

- The construction stage, which includes emissions from transport of the component to site, and its installation on site
- The use stage, which covers emissions from any maintenance and repair work which may be required during the component's service life
- The end-of-life stage, which accounts for the GHGs released during deconstruction and disposal of the component after its service life has ended

Detailed descriptions of the calculation process for each of the stages, as well as the data required for the calculations, are provided in the *How to Calculate Embodied Carbon* (2020) guide produced by the Institution of Structural Engineers (IStructE).

3. Methodology

In Section 2, it was concluded that there are a variety of issues with the current crack width design process, two of which were chosen to be investigated by this study:

- The influence of small cracks, with widths equal to or below the required values, on the effectiveness of the crack width requirements at providing durability
- The potential cost and environmental sustainability impacts of using additional reinforcing steel to meet the crack width requirements

To investigate these two issues, a seven-stage methodology was adopted for the study, as shown in Figure 3-1.

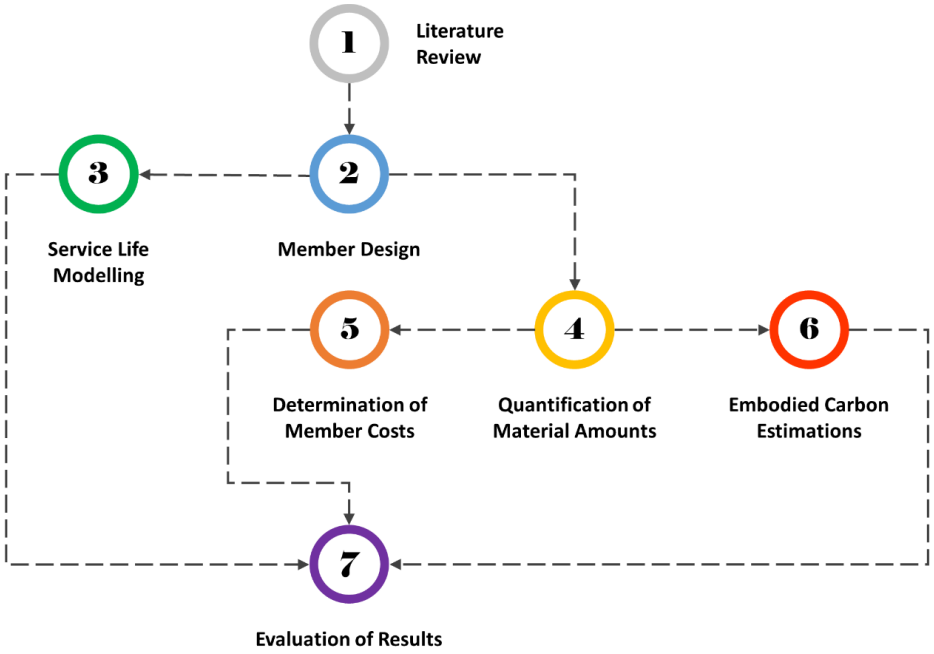

Figure 3-1: A research framework showing the seven stages of the methodology used in the study.

Stage 1, the literature review, has already been presented in Section 2. The key aspect of this methodology is the second stage, "Member Design", in which two sets of "typical" marine RC members, as would be found in common marine structures, were designed. One set of members was designed to meet the crack width requirements, while the other set was not, thus allowing for direct comparisons between designing for crack width, and not designing for crack width, to be made. This meant that when the service lives (Stage 3) and cost and environmental impacts (Stages 4 to 6) of the designed members were determined, comparing the differences between the results for the two sets of members allowed for conclusions to be drawn about:

- Whether designing to meet crack width requirements is effective at providing longer service lives (i.e., better durability)
- Whether designing to meet crack width requirements results in significantly greater costs and environmental impacts

In this way, the study was able to investigate two important issues with the current crack width design process.

4. Member Design

In Section 2.2 it was shown that most marine RC structures are typically composed of beams, piles, slabs, and walls. However, piles, which are generally only exposed to axial load, are not typically designed for crack width requirements – and when they are, they are designed as beams. Furthermore, the design process is very similar for marine RC slabs and walls, with walls typically being designed as slabs (Mosley, Bungey & Hulse, 2007:309). As such, only two different types of members – beams and walls – were designed in this study.

The selection of beams and walls to design was carried out with the assistance of PRDW Consulting Port and Coastal Engineers, who provided design information from past projects. As such, two members – one beam, and one precast wall unit – were selected to be designed:

- A crane rail beam for a jetty in Matola, Mozambique
- A precast wall unit for a breakwater crown wall in St. Helena Island

An overview of the design of these members is provided in this section of the report, while detailed design calculations can be found in Appendices A and B. Drawings of the designed members are shown in Appendices C and D.

The design of both members was carried out in accordance with the requirements of *EN 1992-1-1* and *BS 6349*, with the advice and assistance of PRDW Consulting Port and Coastal Engineers (henceforth referred to as "PRDW").

4.1 Matola Jetty Beam

The Matola jetty was originally designed by PRDW in 2015 as a coal export jetty for the port city of Matola in Mozambique. However, due to a drop in the price of coal, it was never built. The jetty was to be composed of RC beams supported on RC piles, with one-way spanning precast RC deck slabs resting on the beams. To facilitate loading and unloading of ships berthed at the jetty, both shiploader cranes and a conveyor system were designed to operate along the length of the jetty. If built, the Matola jetty would have looked much like the Dalrymple Bay coal terminal shown in Figure 4-1.

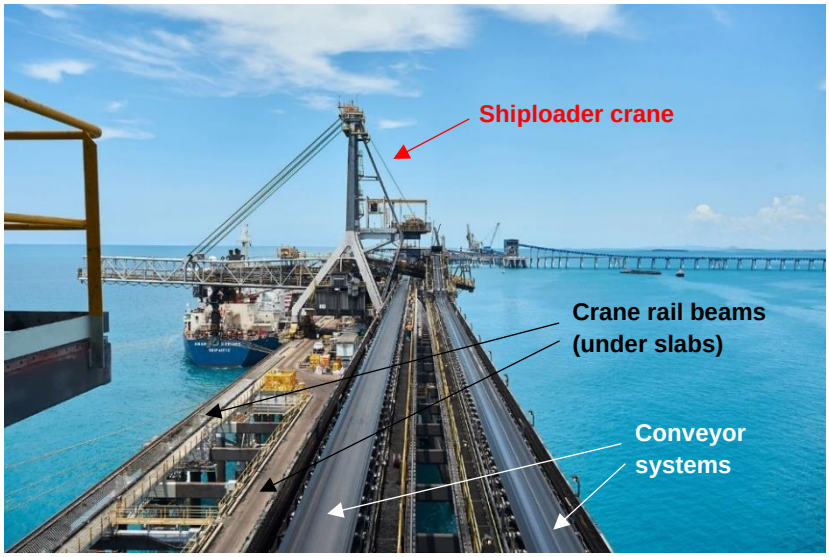

Figure 4-1: A typical RC coal export jetty in Dalrymple Bay, Australia (adapted from Dalrymple Bay Coal Terminal, n.d.). Note the shiploader crane, conveyor systems, and crane rail beams.

As the jetty was to be a common port structure, for commercial and industrial use, it was designed for a 50 year service life (The British Standards Institution, 2013b:51).

4.1.1 Overview of Member

The Matola jetty made use of three different types of beams:

- Crane rail beams, which supported the shiploader crane rails and the deck slabs
- Conveyor beams, supporting the conveyor systems only
- Deck slab beams, which supported the deck slabs only

However, of the three types of beams, only the crane rail and conveyor beams were subjected to large, sustained flexural loading – meaning that crack width design was likely to only be a critical design consideration for the crane rail and conveyor beams. Of the crane rail and conveyor beams, either could have been designed in this study, with similar results, as both were subjected to relatively similar loading conditions. It was therefore decided to design one of the crane rail beams – designated Beam B402 – simply as the crane rail beams represented the majority of the beams in the jetty and were therefore more representative of the Matola jetty beams as a whole. The crane rail beams were also subjected to a more complex arrangement of loads, thereby making for a more interesting and challenging design.

When the B402 beams were originally designed by PRDW, they were designed to be constructed in two stages, to reduce transport weight and costs – the outer segments of the beams were to be first precast in "U" shapes, before being transported to site and filled with in-situ concrete to produce the complete, rectangular, shape of the beams. However, designing the beams in this way would add unnecessary complexity, and no additional value, to this research. As such, it was decided to simply design the beams as monolithic precast beams, with rectangular cross-sections. The dimensions of the B402 beams are therefore as shown diagrammatically in Figure 4-2, where the design length of the beam is taken as the distance between centres of supports (15 m).

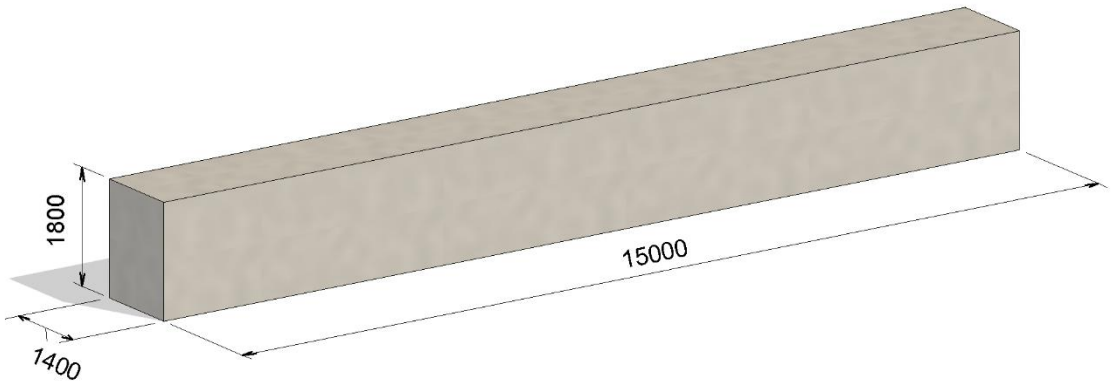

Figure 4-2: A diagrammatic representation of Beam B402, showing its dimensions (in mm).

The design process which was followed for Beam B402 is shown diagrammatically in Figure 4-3, with each step being explained in the following subsections. Note that, as discussed in Section 3, two separate designs were carried out – one with, and one without, considering the crack width requirements.

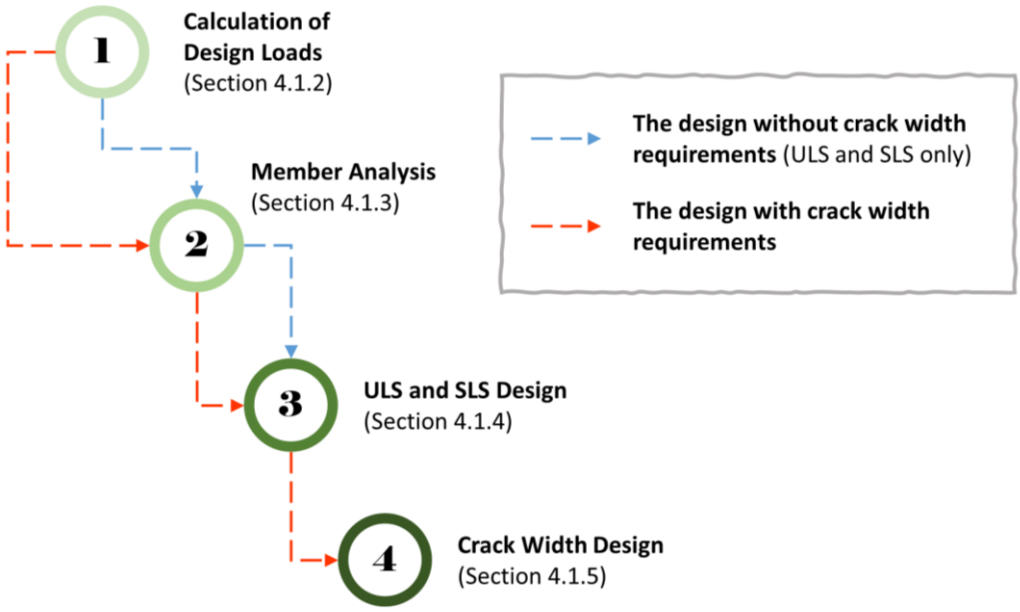

Figure 4-3: A flowchart showing the steps of the design process for Beam B402.

4.1.2 Calculation of Design Loads

The B402 beams were subjected to several different types of loads, of which the following were included in their design:

- The self-weight of the beams, jetty deck slabs, and vehicle barrier on the seaward side of the jetty deck
- Vehicle loads, applied on the deck slabs
- Live loads, applied on the walkways and access platforms
- Shiploader crane loads (both vertical and horizontal), for the two types of shiploaders (*ELB* and *Sandvik*) expected to operate on the jetty. These loads were applied with the shiploaders placed in various critical positions on the beams

Values for these loads were determined using the loading information provided by PRDW from their original design of the Matola jetty. The following loads were not considered in the analysis of the beams:

- Temperature loads, as they were unlikely to have a significant effect on the beams, and would have added unnecessary complexity to the research
- Mooring and berthing loads, as they would not have been applied to the beams, and are only necessary to consider for the global stability of the jetty structure
- Conveyor and tripper car loads, as these loads are only applied at conveyor gallery support plinths, which are not positioned over the B402 beams
- Wind loads, since these loads were unlikely to have a significant effect, when compared with the vertical forces acting on the beams
- Loads which were ignored in the original design carried out by PRDW, such as water sump loads, self-weight of services and wave and current loads

The load combinations which were used for the four different types of loads acting on the B402 beams are shown in Table 4-1. Load and combination factors for the various combinations were determined in accordance with *BS 6349-2*, as was the case for the original design produced by PRDW.

Table 4-1: Load combinations which were used in the design of the B402 beams, for both ULS and SLS.

Load Combination	Combination Definition	Leading Load
A	D + L + V + E	E
B*	D + L + V + S	S
C-1	D + L + V	L
C-2	D + L + V	V
Definition of Loads		
D	Self-weight of the beam and other structural components	
V	Vehicle load	
L	Live load	
E	ELB shiploader loads	
S	Sandvik shiploader loads	

*Note that Load Combination B is to be used for ULS only, as the Sandvik shiploader will only be operational when the ELB shiploader is being serviced.

4.1.3 Member Analysis

The loads applied to the beams resulted in the development of bending moments, shear forces and torsional moments (due to the eccentricities of some of the applied forces) within the beams. In order to determine the magnitude of these moments and forces, the beams were analysed using the analysis software *Prokon*, for each of the load combinations discussed in Section 4.1.2 above. Separate analyses were carried out for the ultimate and serviceability limit states (ULS and SLS, respectively), as well as for crack width design, which requires that the member be analysed for sustained service loading only.

The beams were analysed for three separate support conditions:

- Simply supported at both ends
- As a continuous beam, with the shiploaders placed on an interior span
- As a continuous beam, with the shiploaders placed on an end span

However, it was decided not to consider the results of the analyses with the beams simply supported at both ends, and instead to design the beams purely as continuous beams. This was done to avoid an overly conservative design, as the beams will only be simply supported during construction. In service (when the ultimate loads will be applied), the beams will be continuous, as in-situ concrete plugs will be used to connect the precast beam elements.

The maximum bending moments, shear forces, torsional moments, and deflections for each of the analysed limit states (ULS, SLS and crack width design, or “CWD”) are shown in Table 4-2. These values were then used in the design of the beams.

Table 4-2: A summary of the maximum bending moments (M_u), shear forces (V_u), torsional moments (T_u) and deflections (δ_{max}) for the B402 beams.

Limit State	M_u[a] [kNm]	V_u [kN]	T_u [kNm]	δ_{max} [mm]
ULS	8815/-10973	4108	442.0	17.61
SLS	4878/-6626	2252	135.9	10.64
CWD	4463/-6065	2066	-	9.72

a. Note that positive moments indicate sagging, whereas negative moments indicate hogging.

4.1.4 ULS and SLS Design

The ULS and SLS design of the B402 beams involved the following design checks, all of which were carried out in accordance with the specifications of *EN 1992-1-1* and *BS 6349-1-4:2013*:

- Bending strength, in both sagging and hogging (ULS)
- Shear strength (ULS)
- Torsional strength (ULS)
- Deflection (SLS)
- Maximum and minimum amounts of reinforcement, and other detailing checks not related to crack width limitation (SLS)
- Durability, i.e., cover depth and mix design selection (SLS)

As a result of the above checks, the B402 beams were designed to have a cover depth of 75 mm, and to use class C35/45 concrete, with 50% GGBS, a minimum binder content of 380 kg/m^3, and a maximum w/b ratio of 0.4. The maximum provision of reinforcement (i.e., not considering curtailment of the reinforcement) to meet the ULS and SLS checks listed above is shown in Table 4-3. Note that curtailment of the sagging and hogging longitudinal reinforcement was carried out, such that the reinforcement areas specified in Table 4-3 were not provided throughout the entire length of the beams.

Table 4-3: A summary of the reinforcement provided in the B402 beams to meet the ULS and SLS requirements of *EN 1992-1-1*.

Type of Reinforcement	Reinforcement Provided	Area of Reinforcement Provided
Sagging (longitudinal reinforcement)	One layer of 11 Y40 bars	13823 mm^2
Hogging (longitudinal reinforcement)	One layer of 13 Y40 bars	16336 mm^2
Shear and torsion links	Y16 links, with four links (i.e., eight legs) provided every 400 mm	4.021 mm^2/mm
Torsion (longitudinal reinforcement)	6 Y32 bars, with four bars placed in the corners, and two in the side faces of the beams	4825 mm^2

4.1.5 Crack Width Design

The crack width design of the B402 beams considered both flexural and thermal/shrinkage cracking. The beams were first designed for flexural cracking, for the sagging and hogging moments present in the beams under sustained loads. Only the self-weight of the beams and other structural components, and the serviceability loads of the *ELB* shiploader were considered as sustained loads. The *ELB* shiploader loads were treated as sustained, as the *ELB* shiploader will frequently be parked along the jetty for long periods of time, such that cracks caused by the *ELB* shiploader loads will contribute to corrosion of the reinforcing steel.

The design of the B402 beams for flexural cracking resulted in the provision of additional reinforcement, for both the sagging and hogging moments, as shown in Table 4-4. This is as the amount of reinforcement provided for the ULS and SLS requirements discussed in Section 4.1.4 above was not adequate to limit flexural cracking to below the 0.3 mm requirements of *EN 1992-1-1*. For the sagging moments, the size of the reinforcement was decreased from Y40 to Y32 bars, to aid in reducing crack spacing, and therefore crack width. However, this was not possible for the hogging moments, as too many Y32 bars would have been required, such that the bars would not have fit into the beams with adequate spacing.

In order to meet the thermal and shrinkage crack width requirements, two types of thermal and shrinkage cracking are typically checked – early-age thermal cracking due to heat of hydration when the precast beam elements are cast, and long-term cracking due to shrinkage and variations in ambient temperature. However, in the case of the B402 beams, long-term thermal and shrinkage movements of the beams won't be restrained, as the beams will sit on bearings which allow longitudinal movement. As such, only early-age thermal cracking was checked, and was found not to be significant, such that no additional reinforcement was required to limit thermal and shrinkage cracking.

As the B402 beams are deeper than 1 metre, *EN 1992-1-1* specifies that additional reinforcement should be provided in the side faces, up to the height of the neutral axis, to control and limit cracking in the side faces (Mosley, Bungey & Hulse, 2007:133). The side face reinforcement required to meet these requirements is shown in Table 4-4, and was provided in both the sagging and hogging zones of the beams.

Table 4-4: A summary of the reinforcement provided in the B402 beams to meet the crack width requirements of *EN 1992-1-1* and *CIRIA C660*. Note that this reinforcement was curtailed.

Type of Reinforcement	Reinforcement Provided	Area of Reinforcement Provided
Sagging (longitudinal reinforcement)	One layer of 19 Y32 bars	15281 mm^2
Hogging (longitudinal reinforcement)	One layer of 15 Y40 bars	18850 mm^2
Side face reinforcement	One layer of 7 Y32 bars	5630 mm^2

4.1.6 Summary of the Matola Jetty Beam Design

A summary of the design of the B402 beams, highlighting the changes in reinforcement needed to meet the crack width requirements, is shown in Figure 4-4. Note that, in reality, the longitudinal

reinforcement shown in the 3-D views of Figure 4-4 would be extended past the end of the beams to allow for in-situ connection of the precast elements; however, for simplicity, this is not shown in Figure 4-4.

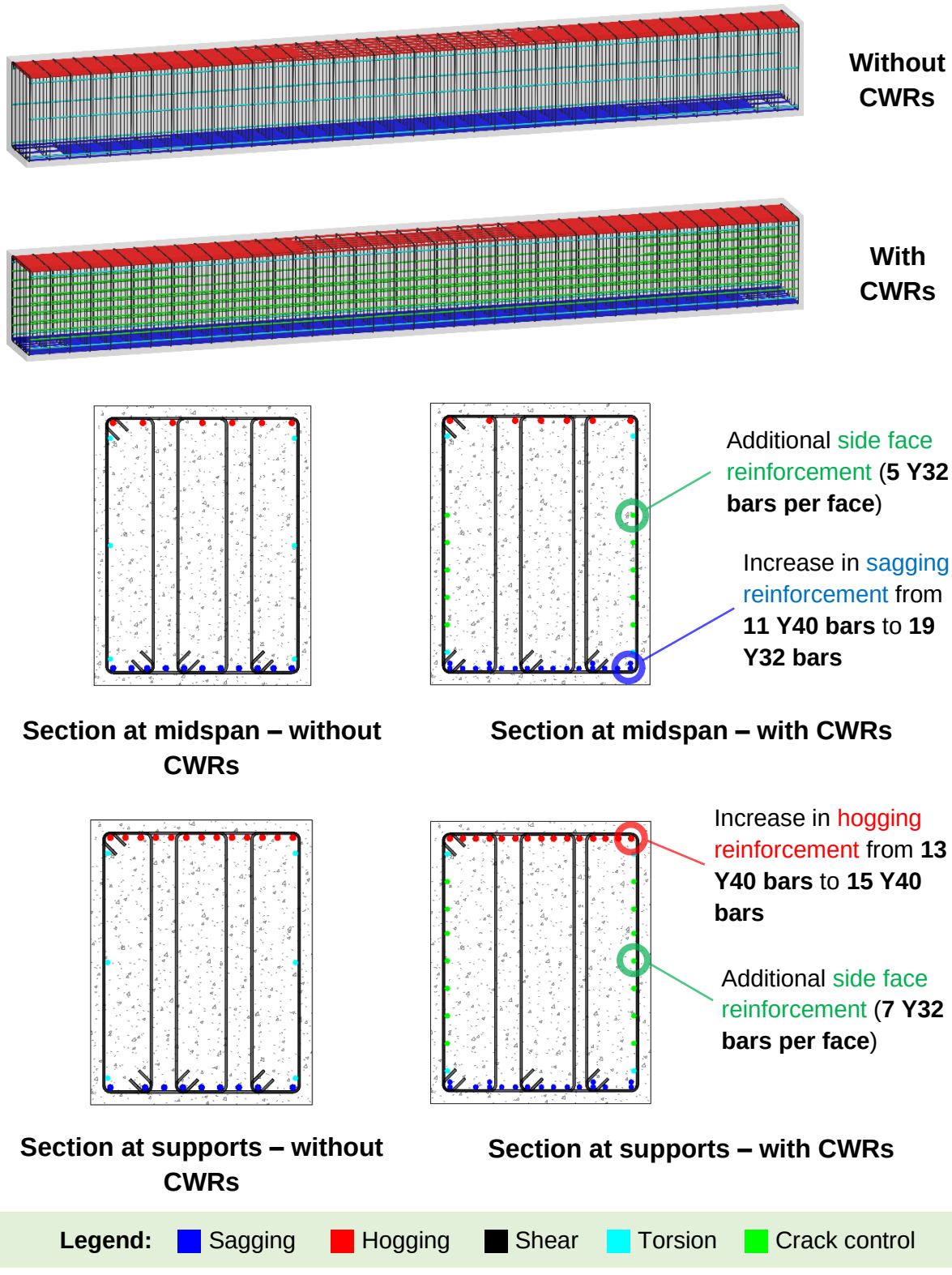

Figure 4-4: A summary of the design of the B402 beams, showing 3-D and section views of the beams designed with and without the crack width requirements ("CWRs").

4.2 St. Helena Breakwater Crown Wall

The St. Helena breakwater was designed by PRDW between 2011 and 2016 to provide protection for a cargo wharf in Rupert's Bay, St. Helena Island. The breakwater, shown in Figure 4-5, was designed as a horizontal composite breakwater, with an armoured rubble mound protecting a concrete blockwork wharf. To prevent wave overtopping, the design of the breakwater includes a reinforced concrete crown wall, the location of which is shown with red arrows in Figure 4-5. As the Rupert's Bay wharf is the only cargo wharf in St. Helena Island, the breakwater was deemed to be a port structure of national significance, and as such, was designed for a 100 year service life (The British Standards Institution, 2013b:51).

Figure 4-5: An aerial photograph of the completed breakwater in Rupert's Bay, St. Helena Island (PRDW, n.d.).

4.2.1 Overview of Member

The St. Helena breakwater crown wall was constructed from a series of precast reinforced concrete wall units, joined together by a cast-in-situ crown wall base and capping, as shown in Figure 4-6. Two types of wall units were used in the crown wall, known as wall units F01 and F02. The F01 units were much more common, making up much of the crown wall, and as such were chosen to be designed in this study. A typical F01 wall unit has a height of 3900 mm, a width of 2680 mm, and a thickness of 1000 mm, as shown in Figure 4-7.

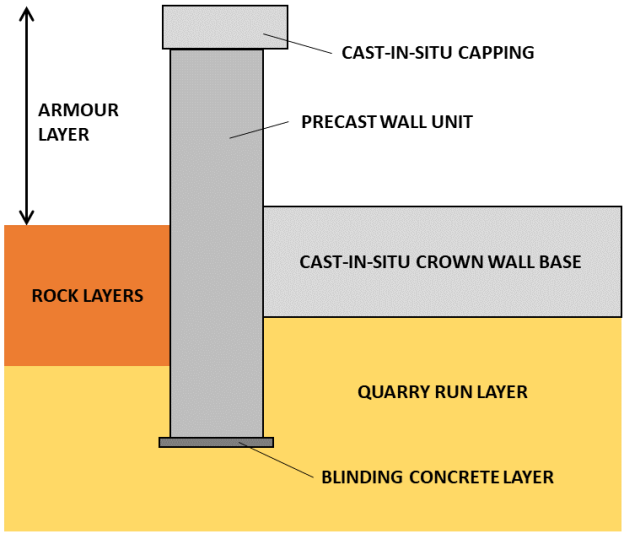

Figure 4-6: A simplified cross-sectional diagram of the St. Helena breakwater crown wall.

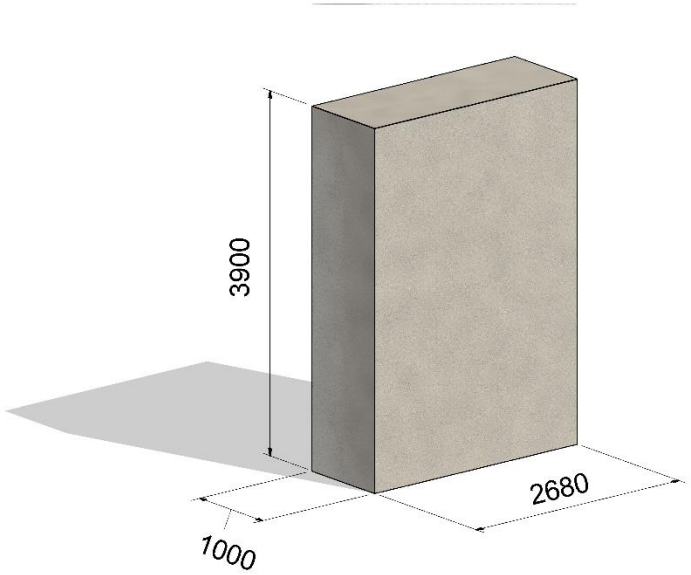

Figure 4-7: A diagrammatic representation of a typical F01 wall unit, showing its dimensions (in mm). Note that protruding reinforcement for the purposes of connecting the wall units to the cast-in-situ base and capping is not shown.

The design process for the F01 wall units was the same as that for the B402 beams shown in Figure 4-3; namely, the design started with determination of the design loads, before the wall units were analysed and designed, with two separate designs being carried out – one with, and one without, considering the crack width requirements.

4.2.2 Calculation of Design Loads

Due to the nature of the member, wave loading was considered to be the primary design load acting on the crown wall. It was decided not to consider the lateral pressure exerted on the crown wall by the quarry run layer, as this layer is approximately evenly distributed on both sides of the crown wall – meaning that the net force it exerts on the crown wall is approximately zero. As such, the design of the F01 wall units only considered the effects of wave loading. Furthermore, the uplift forces caused by wave loading were not considered, as they were only relevant for the stability design of the crown wall, and not for the detailed design of the F01 wall units. This meant that the design of the F01 wall units was based only on the lateral pressures caused by wave loading.

Wave loading information for the crown wall, in the form of lateral wave pressures, was provided by PRDW, for wave return periods of 1, 10, 100 and 1000 years. Due to the influence of the various layers of the rubble mound breakwater, the lateral wave pressures were split into upper and lower wave pressure components ($P_{H,U}$ and $P_{H,L}$, respectively) as shown in Figure 4-8.

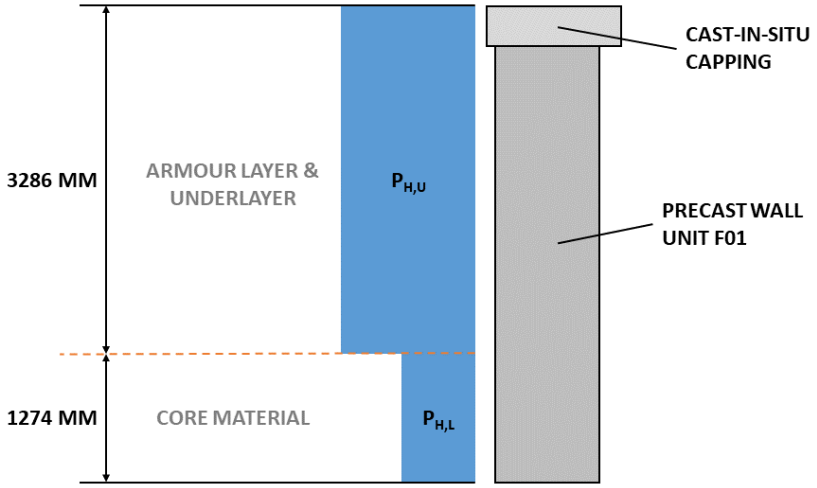

Figure 4-8: An illustration of the distribution of lateral wave pressures on the F01 wall units, adapted from the wave loading information provided by PRDW.

The 100- and 1000-year wave return period pressures (which represent the maximum pressures for normal and extreme operating conditions, respectively) were used in the ULS analysis of the F01 wall units. The 1-year wave return period pressures were used to conservatively represent the sustained service loads acting on the F01 wall units for flexural crack width design. The load factors which were used for these wave pressures were determined using *BS6349-2* and are shown in Table 4-5. Note that the 1000-year (extreme) case was taken as an accidental load due to its low probability of occurrence.

Table 4-5: The load factors which were used in the analysis of the F01 wall units (The British Standards Institution, 2010).

Load Case	Wave Return Period [Years]	Load Factor
Crack Width Design	1 (Service Case)	1.0
ULS	100 (Operating Case)	1.4
	1000 (Extreme Case)	1.0

4.2.3 Member Analysis

The F01 wall units were analysed as beams with unit width, as shown in Figure 4-9, based on the following assumptions:

- The cast-in-situ crown wall base, which is tied to reinforcement protruding from the F01 wall units, will act as a fixed support for the wall units
- The rock and quarry run layers, at the foot of the crown wall, do not provide adequate restraint to rotation, such that the F01 wall units were assumed to be pin supported at the foot of the wall
- For the purposes of the analysis, the F01 wall units and cast-in-situ capping were assumed to act as one rigid member (i.e., one beam)

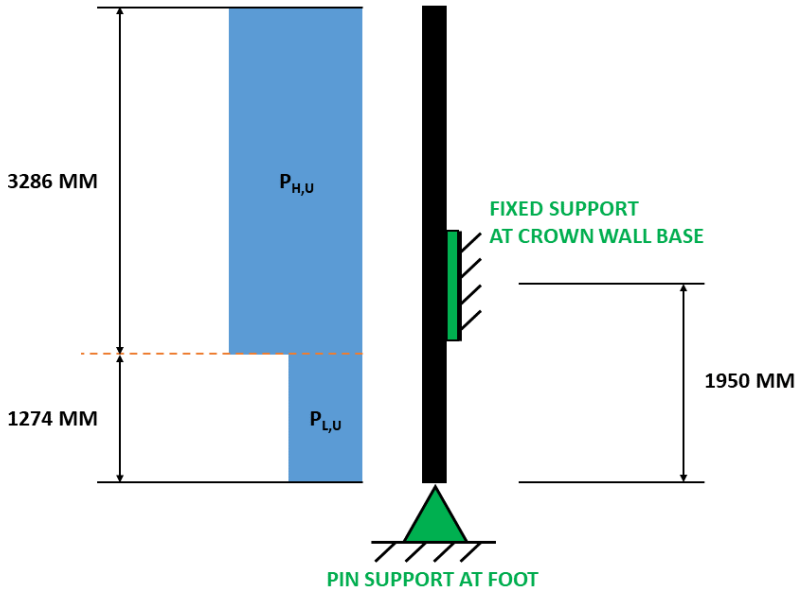

Figure 4-9: A diagram of the analysis model for the St. Helena crown wall.

Analysis of the F01 wall units was carried out using the analysis software *Prokon*, for both the ULS and crack width design (CWD) limit states. Due to the nature of the crown wall, deflection was not considered to be a critical limit state, and as such, no SLS analysis was carried out. The results of the analysis are shown in Table 4-6. These values were then used in the design of the F01 wall units, with the 100-year wave return period values being critical for the ULS case.

Table 4-6: A summary of the Prokon analysis results, showing the ultimate bending moments and shear forces per metre width of wall unit.

Limit State	Wave Return Period [Years]	Maximum Bending Moment[a] [kNm/m]	Maximum Shear Force [kN/m]
Crack Width Design	1	6.107/-140.7	107.8
ULS	100	15.53/-359.0	275.1
	1000	13.61/-314.4	240.9

a. Note that positive moments indicate sagging, whereas negative moments indicate hogging.

4.2.4 ULS and SLS Design

The ULS and SLS design of the F01 wall units involved the following design checks, all of which were carried out according to the specifications of *EN 1992-1-1* and *BS 6349-1-4:2013*:

- Bending strength, in both sagging and hogging (ULS)
- Shear strength (ULS)
- Maximum and minimum amounts of reinforcement, and other detailing checks not related to crack width limitation (SLS)
- Durability, i.e., cover depth and mix design selection (SLS)

As a result of the durability checks, the wall units were designed to have a cover depth of 75 mm, and to use class C35/45 concrete, with 50% GGBS, a minimum binder content of 380 kg/m^3, and a maximum w/b ratio of 0.4. Due to the relatively low bending moments and shear forces produced in the F01 wall units, and the large thickness of the wall units (1000 mm), the ULS and SLS design was governed by the minimum reinforcement requirements. As such, both the horizontal and vertical reinforcing steel provided for the wall units, shown in Table 4-7, was provided to meet the minimum reinforcement requirements, and was therefore not curtailed. It was also found that shear links were not necessary for the wall units, although clips were provided to hold the reinforcement cages together, as shown in Table 4-7.

Table 4-7: A summary of the reinforcement provided in the F01 wall units to meet the ULS and SLS requirements of *EN 1992-1-1*.

Type of Reinforcement	Reinforcement Provided	Area of Reinforcement Provided
Vertical Reinforcement	5 Y20 bars per metre of crown wall, in each face	1571 mm^2/m
Horizontal Reinforcement	5 Y20 bars per metre of crown wall, in each face	1571 mm^2/m
Clips	Y12 Shape Code 85 clips, at a maximum vertical and horizontal spacing of 1000 mm	-

4.2.5 Crack Width Design

The crack width design of the F01 wall units considered both flexural and thermal and shrinkage cracking, as was the case for the B402 beams. However, unlike the B402 beams, flexural cracking was relatively insignificant for the F01 wall units and did not result in the provision of additional reinforcement. As such, the crack width design of the F01 wall units was governed by thermal and shrinkage cracking, with both early-age and long-term thermal and shrinkage cracking being checked.

However, early-age thermal and shrinkage cracking was also found not to be significant. In contrast to this, long-term thermal and shrinkage cracking, due to the restraint provided by the crown wall base, was found to result in relatively large crack widths. To limit these crack widths to below the required value of 0.3 mm, the horizontal reinforcement was changed from 5 Y20 bars per metre of wall unit, to 8 Y16 bars per metre of wall unit. This resulted in a slight increase in the amount of steel used, from 1571 mm^2/m to 1608 mm^2/m.

It should also be noted that Y16 bars were only provided in the vicinity of the crown wall base (where restraint to the wall is at a maximum), and up to a height of 0.5 metres above the base. This is as cracking is expected to start within the first 0.5 metres above the base (i.e., about halfway between the base and top of the wall) and propagate down and upwards. The amount of restraint provided by the base is expected to decrease as the distance from the base increases. The restraint and resultant crack width beyond a height of 0.5 metres above the base was thus calculated and found not to be critical, as shown in Appendix B. Y16 bars were therefore only provided up to a height of 0.5 metres from the base.

Y16 bars were also not provided below the crown wall base, as the portion of the wall units below the base is embedded in rock and quarry run layers, and as such was not expected to be exposed to long-term ambient temperature changes and drying shrinkage.

4.2.6 Summary of the St. Helena Breakwater Crown Wall Design

A summary of the design of the F01 wall units, and the changes in reinforcement needed to meet the crack width requirements, is shown graphically in Figure 4-10. It should be noted that lapped bent bars were used for the vertical reinforcement in order to allow for adjustment of the reinforcement to ensure provision of adequate cover depth. Furthermore, for simplicity, the protruding reinforcement required for in-situ connections between the F01 wall units, and the crown wall base and capping, is not shown in Figure 4-10.

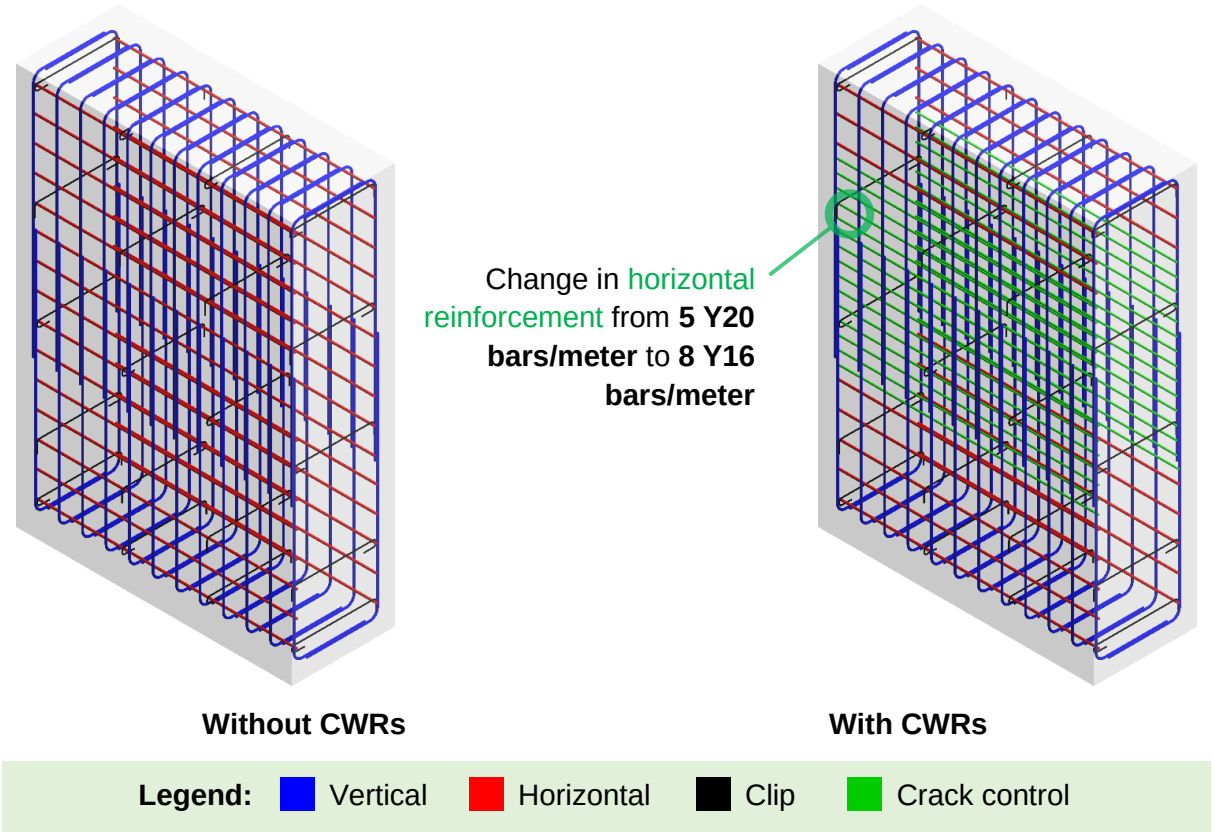

Figure 4-10: A summary of the design of the F01 wall units, showing 3-D views of the wall units designed with and without the crack width requirements ("CWRs").

5. Service Life Modelling

In order to quantify the effects of designing to meet the crack width requirements on the durability of marine RC structures, it was necessary to calculate the service lives of the members designed in Section 4. This was done by applying the five-step method developed for cracked RC structures in Section 2.8. The method is shown graphically in Figure 5-1, with an overview of each step being given in the following subsections. Detailed service life modelling calculations can be found in Appendix E.

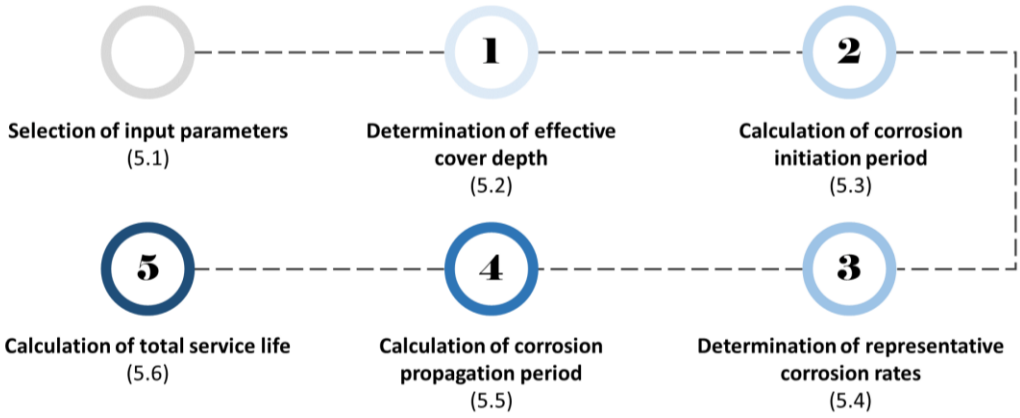

Figure 5-1: A diagrammatic representation of the five-step method for determining the service lives of cracked marine RC structures.

5.1 Selection of Input Parameters

Before the service life calculations could begin, it was necessary to select the required input parameters for each of the members designed with, and without, the crack width requirements (henceforth referred to as "CWRs"). These parameters were selected based on the following considerations:

- It was assumed that the 15 mm reinforcement placing tolerance included in the design cover depth of 75 mm (Smith, 2016a:82) will not always be met, such that the actual, in-situ cover depth, *C*, will be 60 mm
- Where a member had multiple sizes of longitudinal reinforcement, the smallest reinforcement diameter was selected as the critical reinforcement diameter, *D*, as corrosion rate increases as reinforcement diameter decreases (Raupach, 1996:335)
- The choice of critical reinforcement diameter, *D*, was based only on the longitudinal reinforcement – corrosion of shear or clip reinforcement was not considered to be critical. This was as, for the beams, the portions of the shear links exposed to corrosion by cracking (i.e., the top and bottom portions) contribute relatively little to the shear resistance of the member, while for the wall units, the clip reinforcement does not serve a structural function and was only necessary to hold the reinforcement cage together during construction
- The maximum in-service crack width, w_{cr}, was assumed to be equal to the limiting requirement of 0.3 mm for members designed with the CWRs. For the members designed without the CWRs, the crack widths calculated for the members before the provision of crack width reinforcement (see Appendices A and B) were used, rounded up to the nearest 0.05 mm

The input parameters for each of the members are thus as shown in Table 5-1 below.

Table 5-1: Input parameters used for the service life modelling calculations.

Member Type	**Matola Jetty Beams**		**St. Helena Breakwater Crown Wall Units**	
Design Type	**Designed without CWRs**	**Designed with CWRs**	**Designed without CWRs**	**Designed with CWRs**
Concrete Class [-]	C35/45	C35/45	C35/45	C35/45
Binder Type [-]	50% PC, 50% GGBS	50% PC, 50% GGBS	50% PC, 50% GGBS	50% PC, 50% GGBS
Water/Binder Ratio, *w/b* [-]	0.4	0.4	0.4	0.4
In-Situ Cover Depth, *C* [mm]	60	60	60	60
Critical Reinforcement Diameter, *D* [mm]	40	32	20	16
Maximum Crack Width, w_{cr} [mm]	0.45	0.30	0.35	0.30

5.2 Determination of Effective Cover Depth

The effective cover depth (i.e., the cover depth for which the concrete behaves as if uncracked), C_{eff}, of a typical cracked RC member is shown graphically in Figure 5-2, assuming a triangular-shaped crack. From Figure 5-2, C_{eff} can be determined by the following equation:

$$C_{eff} = C - d_{0.1} \; (for \; d_{0.1} < C)$$

$$(If \; d_{0.1} \geq C, then \; C_{eff} = 0 \; mm) \qquad \textbf{Equation 5-1}$$

Where: C is the in-situ cover depth of the member
: $d_{0.1}$ is the depth at which the width of the crack is equal to 0.1 mm

The depth at which the width of the crack is equal to 0.1 mm, $d_{0.1}$, can then be determined using the properties of similar triangles (see Figure 5-2), resulting in the following equation:

$$d_{0.1} = d_{cr} - 0.1\left(\frac{d_{cr}}{w_{cr}}\right) \qquad \textbf{Equation 5-2}$$

Where: d_{cr} is the crack depth
: w_{cr} is the crack width

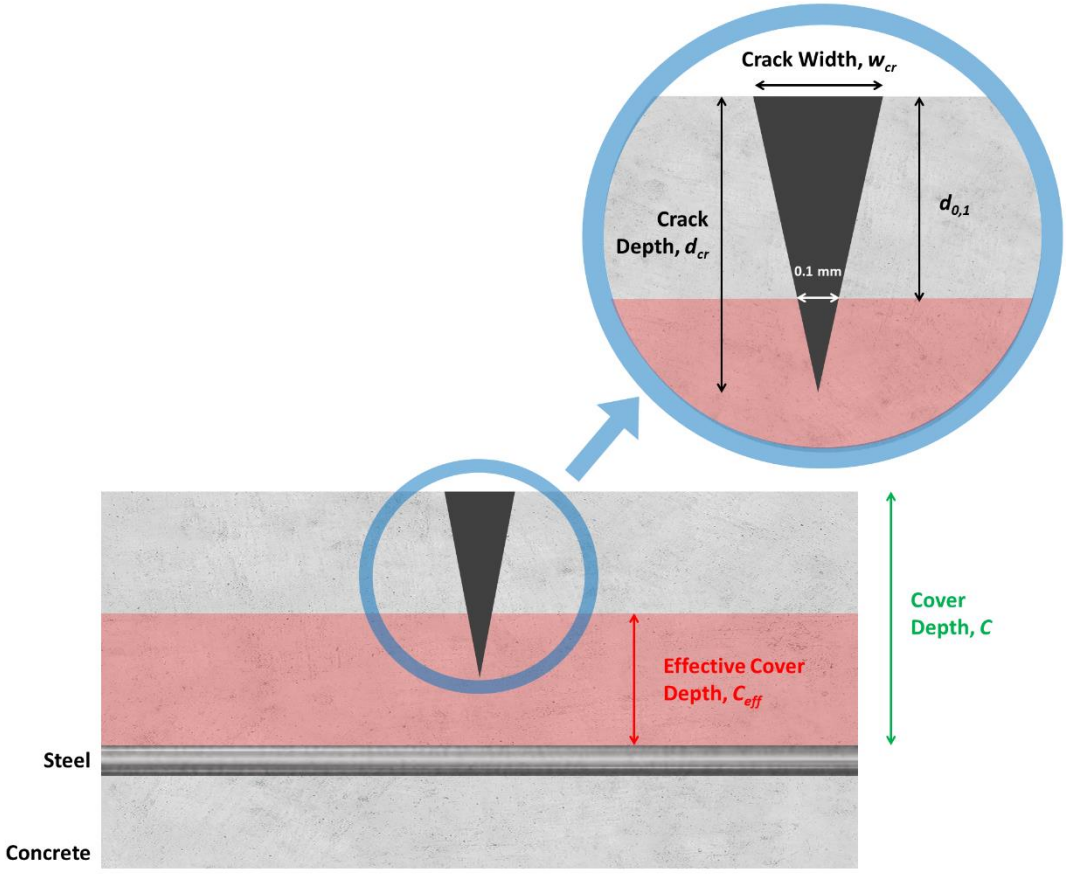

Figure 5-2: A diagrammatic representation of a typical triangular-shaped crack.

The crack depth, d_{cr}, can in turn be estimated from the crack width, w_{cr}, using the equations developed by Ramezanianpour et al. (2018). Ramezanianpour et al. (2018) developed two equations, for either plain Portland cement (PC) concrete (Equation 5-3) or concrete with 7.5% silica fume (SF) replacement (Equation 5-4).

$$For\ plain\ PC\ concrete: d_{cr} = 1.67 + \sqrt{(416 \times w_{cr}) - 0.63}\ [cm] \qquad \textbf{Equation 5-3}$$

$$For\ concrete\ with\ 7.5\%\ SF: d_{cr} = 0.2 + \sqrt{(375 \times w_{cr}) - 4.53}\ [cm] \qquad \textbf{Equation 5-4}$$

Ramezanianpour et al. (2018: 1467) noted that the concrete with 7.5% SF replacement had a finer concrete microstructure, resulting in reduced crack depth in the 7.5% SF samples, such that Equation 5-4 will predict lower crack depth values than Equation 5-3. As the members in this study used 50% GGBS replacement, which will also result in a finer microstructure (Li & Liang, 2011:158), it was decided to use Equation 5-4 to calculate crack depth in this study.

Equations 5-1, 5-2, and 5-4 were thus used to determine the effective cover depth for each of the members designed in this study, with the results being summarised in Table 5-2. From these results, it can be concluded that the effective cover depth is zero for all four members designed in this study.

Table 5-2: A summary of the effective depth calculations for the study.

Member Type	Matola Jetty Beams		St. Helena Breakwater Crown Wall Units	
Design Type	Without CWRs	With CWRs	Without CWRs	With CWRs
Cover Depth, C [mm]	60	60	60	60
Crack Depth, d_{cr} [mm]	130.1	105.9	114.6	105.9
Depth for 0.1 mm Crack Width, $d_{0.1}$ [mm]	101.2	70.6	81.9	70.6
Is $d_{0.1} > C$?	Yes	Yes	Yes	Yes
Effective Cover Depth, C_{eff} [mm]	0	0	0	0

5.3 Calculation of the Corrosion Initiation Period

As the effective cover depth is zero for all the members designed in this study, corrosion will be initiated instantly in all members. The length of the corrosion initiation period is therefore zero for all four members designed in this study, and no further initiation period calculations are required.

5.4 Determination of Representative Corrosion Rates

Representative corrosion rates for the members were determined using the corrosion rate model developed by Otieno (2014). However, Otieno's (2014) model does not account for different layouts and sizes of reinforcement, as the size and number of reinforcing bars are not variables in the model. It was therefore necessary to modify the model to account for the fact that different amounts and sizes of reinforcing bars were used for the members designed with, and without, the crack width requirements. This was done by multiplying the corrosion rates determined from Otieno's (2014) model by two factors, α and β, as shown in Equation 5-5.

$$i_{corr} = \alpha \times \beta \times i_{base} \qquad \textbf{Equation 5-5}$$

Where: i_{corr} is the representative corrosion rate used in this study
: α is a factor which accounts for differences in reinforcement diameter
: β is a factor which accounts for differences in the number of reinforcing bars used
: i_{base} is the base corrosion rate, determined using Otieno's (2014) model

It is important to note that the α and β factors were only used to account for differences in reinforcement size and layout between the members designed with and without the crack width requirements. The α and β factors were not used to directly convert the corrosion rates determined using Otieno's (2014) model (which was developed based on beam samples which only contained a single 10 mm diameter bar) to corrosion rates for members with multiple, larger diameter reinforcing bars. This is as there is not enough data in the literature to justify modifying Otieno's (2014) model in this way. Directly converting the corrosion rates determined using Otieno's (2014) model to corrosion rates for the

members designed in this study (using the same methodology used to estimate the α and β factors) would have resulted in very large changes in corrosion rate from those predicted by Otieno's (2014) model, and there is not sufficient evidence in the literature to support such changes.

It was therefore assumed that the base corrosion rates determined from Otieno's (2014) model are sufficiently representative of general corrosion rates for real marine RC structures, while the α and β factors account for the differences in corrosion rate expected because of the differences in reinforcement size and layout used in the members designed in this study. This is likely to limit the accuracy of the service lives determined in this study, as there may be significant differences in corrosion rate between the beam samples used by Otieno (2014) and real marine RC structures. However, given the lack of available corrosion rate data for real marine RC structures, the corrosion rates found in this study can be seen as reasonable estimates, which account for the effect on durability of changing the size and layout of the reinforcement to meet the crack width requirements.

5.4.1 Determination of α Factors

Raupach (1996:335) found that corrosion rate, i, increases with decreases in bar diameter, D, assuming the same total area of steel is used, as providing more, smaller diameter bars increases the surface area of the steel in the cathodic region. This effect is accounted for in this study by introducing the factor α, defined as follows:

$$\alpha = \frac{i_{smaller\ D}}{i_{larger\ D}} \qquad \textbf{Equation 5-6}$$

Schießl and Raupach (1997:61) found that, in general, the value of α ranges from about 1 to 3. However, they did not provide a general method to calculate α, and only calculated corrosion rates as a function of bar diameter for 8- and 20-mm diameter bars (Schießl & Raupach, 1997:61). The following steps were thus taken to estimate α for the members in this study:

- The corrosion rates calculated by Schießl and Raupach (1997:61) for the 8- and 20-mm diameter bars were placed on a plot of bar diameter vs. corrosion rate, as shown in Figure 5-3
- An exponential relationship was then fitted to the two points on the plot (note that a logarithmic relationship could also have been used, and would have yielded very similar results) and extrapolated to a bar diameter of 40 mm (the largest bar diameter used in this study)
- The equation for the exponential relationship, determined using *Microsoft Excel*, was used to estimate corrosion rates for a variety of bar diameters
- The estimated corrosion rates were then used to calculate α, in accordance with Equation 5-6

The resultant α values for the members in this study are thus shown in Table 5-3. An exponential relationship was chosen to account for the fact that the decrease in corrosion rate with increasing bar diameter will not continue infinitely and will instead be asymptotic. If this was not the case, and the relationship between corrosion rate and bar diameter was assumed to be linear, then the decreases in corrosion rate with increases in bar diameter would eventually result in negative corrosion rates (at a bar diameter of about 35 mm in the case of Figure 5-3), which is clearly not realistic. In practical terms, the use of the asymptotic, exponential relationship makes sense, as it is likely that, after a certain point, other factors, such as the availability of oxygen and moisture in the cathodic region, would have a larger impact on corrosion rate than further decreases in the exposed surface area of the reinforcement caused by increases in bar diameter.

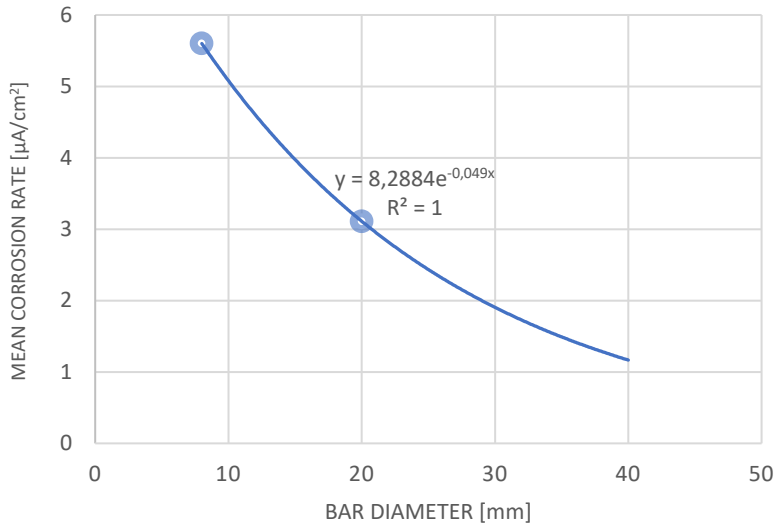

Figure 5-3: A plot of reinforcing bar diameter vs. corrosion rate, showing the exponential relationship fitted to the plot.

Table 5-3: A summary of the *α* values determined for the members in this study.

Member Type	**Matola Jetty Beams**		**St. Helena Breakwater Crown Wall Units**	
Design Type	**Without CWRs**	**With CWRs**	**Without CWRs**	**With CWRs**
Change in Bar Diameter due to CWRs[a]	-	Y40 to Y32	-	Y20 to Y16
α [-]	1.00	1.48	1.00	1.22

a. Note that the *α* values were calculated relative to the members designed without the crack width requirements, as these members had the larger reinforcement diameters.

It should be noted that the relationship shown in Figure 5-3, which was generated using only two data points, is unlikely to be accurate. However, given the lack of available data, it is sufficient for providing rough, engineering estimates of *α* – particularly as the resultant α values, which range between 1.00 and 1.48, are not dissimilar to the range of 1 to 3 reported by Schießl and Raupach (1997:61).

5.4.2 Determination of β Factors

Bezuidenhout and van Zijl (2019:2189) found that corrosion rate decreases as the number of bars (i.e., area of steel provided, As_{prov}) increases. They attributed this finding to a decrease in the cathodic area per bar, as assuming that the oxygen and moisture available in the cathodic region is shared approximately equally between the bars, less oxygen and moisture will be available at each bar as the number of bars increases, such that the size of the cathodic region of each bar decreases (Bezuidenhout & van Zijl, 2019:2188). To account for this effect, the factor *β*, a ratio expressing the corrosion rate of a member with more reinforcement, relative to another member with less, was introduced:

$$\beta = \frac{1}{1 + \left(\frac{\Delta_i}{100}\right)}$$ **Equation 5-7**

Where Δ_i is the percentage decrease in corrosion rate associated with a given increase in As_{prov}.

β was calculated as follows:

- Bezuidenhout and van Zijl (2019:2189) determined corrosion rates for beam samples with either 1,2 or 3 Y10 reinforcing bars.
- Percentage increase in As_{prov} and percentage decrease in corrosion rate values were calculated for each beam reinforcement amount (either 1,2 or 3 reinforcing bars), relative to the "original" case of 1 Y10 bar
- β values were then calculated for each of the beams and used to produce a plot of percentage increase in As_{prov} vs. β, as shown in Figure 5-4
- A linear relationship was fitted to the plot, with a very good fit (R^2 = 0.9918), using *Microsoft Excel*
- The equation for the linear relationship was then used to estimate β

The resultant β values for each of the members in the study are thus shown in Table 5-4.

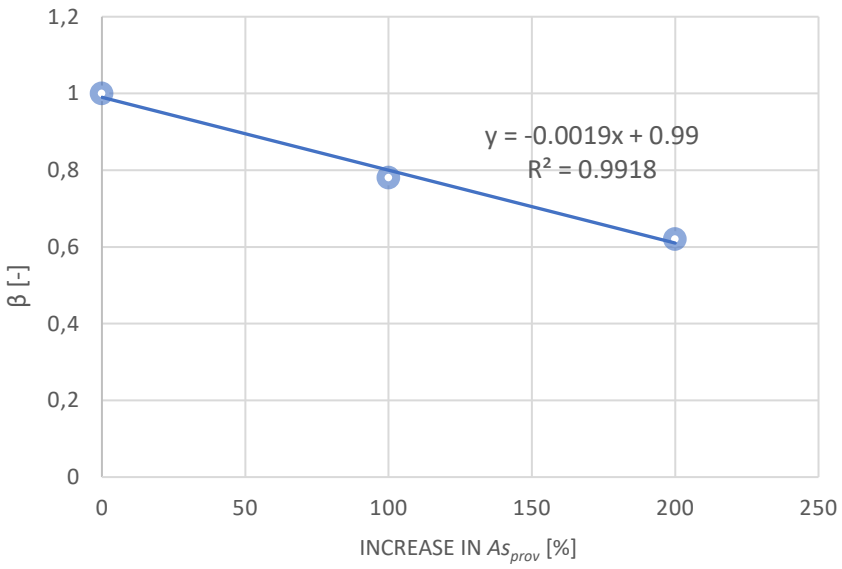

Figure 5-4: A plot of increase in A_{Sprov} vs. β values, showing the linear relationship fitted to the plot.

Table 5-4: A summary of the β values determined for the members in this study.

Member Type	Matola Jetty Beams		St. Helena Breakwater Crown Wall Units	
Design Type	**Without CWRs**	**With CWRs**	**Without CWRs**	**With CWRs**
Increase in As_{prov}[a] [%]	-	15.4	-	2.36
β [-]	1.00	0.96	1.00	0.99

a. Note that the β values were calculated relative to the members designed without the crack width requirements, as these members had smaller As_{prov} values, i.e., designing for the crack width requirements resulted in an increase in As_{prov}.

In practical terms, these β values mean that the corrosion rate for members designed to meet the crack width requirements will be lower than for the members designed without the requirements. However, as the β values are close to 1, this effect will be relatively minor.

5.4.3 Calculation of Base Corrosion Rates

The base corrosion rate, i_{base}, was calculated for each member using the corrosion rate model developed by Otieno (2014). Based on samples exposed to either laboratory or field conditions for approximately 2 years and 3 months (2.25 years), Otieno (2014) developed two separate formulas for corrosion rate in cracked marine RC, in either the laboratory or field environment. However, Otieno (2014:192) recommends using the model for laboratory conditions, as the data for field conditions was too variable at the end of the 2.25-year study period, such that no stable corrosion rate could be determined without further, long-term, research. The formula for laboratory conditions (shown in Equation 5-8) was thus chosen for use in this study.

The variables C and w_{cr} were already known, as input parameters for each of the members (see Table 5-1), while D_{90} was determined from the method provided by Otieno (2014:239) to estimate D_{90} using chloride conductivity index (*CCI*) values. As each of the members designed in this study used the same concrete mix design (50/50 PC/GGBS, with a *w/b* ratio of 0.40), the same *CCI* value was used for all members. This value, the mean *CCI* value measured by Otieno (2014:214) for 50/50 PC/GGBS concrete with a *w/b* ratio of 0.40, resulted in a D_{90} value of 7.05 x 10^{10} cm^2/s.

$$i_{base} = 5.18 \times e^{0.01(D_{90} \times 10^{10})} \times \left(\frac{C}{w_{cr}}\right)^{-a} [\mu A/cm^2] \qquad \textbf{Equation 5-8}$$

Where: D_{90} is the 90-day chloride diffusion coefficient
: C is the in-situ cover depth
: w_{cr} is the crack width
: $a = 0.96 \times (D_{90} \times 10^{10})^{-0.35}$

The values of i_{base}, calculated using Equation 5-8, are shown in Table 5-5.

Table 5-5: A summary of the i_{base} values determined for the members in this study.

Member Type	Matola Jetty Beams		St. Helena Breakwater Crown Wall Units	
Design Type	**Without CWRs**	**With CWRs**	**Without CWRs**	**With CWRs**
Base Corrosion Rate, i_{base} [µA/cm^2]	0.518	0.426	0.459	0.426

5.4.4 Final Values of Representative Corrosion Rates

With the values of α, β and i_{base} all being known, the representative corrosion rate, i_{corr}, was determined for each member using Equation 5-5 ($i_{corr} = \alpha \times \beta \times i_{base}$). The resultant representative corrosion rates for the members in this study are thus shown in Table 5-6.

Table 5-6: A summary of the representative corrosion rates for the members in this study.

Member Type	Matola Jetty Beams		St. Helena Breakwater Crown Wall Units	
Design Type	**Without CWRs**	**With CWRs**	**Without CWRs**	**With CWRs**
α	1.00	1.48	1.00	1.22
β	1.00	0.96	1.00	0.99
i_{base} [µA/cm^2]	0.518	0.426	0.459	0.426
i_{corr} [µA/cm^2]	**0.518**	**0.605**	**0.459**	**0.515**

From Table 5-6 it is clear that, for the members designed in this study, using more, smaller diameter bars to meet the crack width requirements has a negative overall effect, resulting in higher corrosion rates than if the crack width requirements had not been considered.

5.5 Calculation of the Corrosion Propagation Period

It was shown in Section 2.8.4 that there are two types of propagation period models readily available in the literature, depending on the limit state used to define the end of the propagation period:

- Models which calculate the time until a certain percentage of the reinforcement cross-section is lost
- Models which predict the time until corrosion-induced cracking of the cover concrete

Both limit states have significant practical consequences – loss in reinforcement cross-section has a direct effect on structural safety and stability, while cover cracking reduces aesthetic value and accelerates corrosion, resulting in increased maintenance requirements (Cui & Alipour, 2018:652). However, for the purposes of this study, structural safety was deemed to be more important, as aesthetic value is generally not a significant requirement for marine structures.

Furthermore, as discussed in Section 2.8.4, the models based on cover cracking are generally complex, and require many input variables, some of which are not always known and must be selected based on conservative assumptions. In contrast to this, the models based on loss of reinforcement cross-section are relatively simple and easy to use. It was thus decided to use a model based on loss of reinforcement cross-section in this study.

Three models based on loss of reinforcement cross-section were found in the literature, developed by Otieno (2014), Bezuidenhout and van Zijl (2019) and Andrade (2020). However, as each of the models was developed using Faraday's law, they are all very similar, and are likely to produce comparable results. The model developed by Bezuidenhout and van Zijl (2019), shown in Equation 5-9, was chosen for use in this study, as it was the most clearly presented and straightforward to use.

$$t_p = \frac{LS}{100 - \left[\left(D - \left(0.0116 \times i \times \alpha_{pit}\right)\right)^2 \times \frac{1}{D^2}\right] \times 100} \qquad \textbf{Equation 5-9}$$

Where: t_p is the length of the corrosion propagation period, in years

: *LS* is the limit state, i.e., the percentage loss in steel cross-section which defines the end of service life

: *D* is the initial reinforcement diameter

: *i* is the corrosion rate for the member

: α_{pit} is the pitting factor, used to account for the fact that the corrosion rate at a macrocell "pit" will be higher than the representative corrosion rate, which was determined for the reinforcement bar as a whole

An *LS* value of 15% was selected for the propagation period calculations. This is the median value of the 5 – 25% range for loss of cross-section which can safely be accommodated by typical design material safety factors, before ULS failure of the member occurs (Otieno, 2014:188). In particular, *EN 1992-1-1:2004* uses a material partial factor of 1.15 for reinforcing steel (European Committee for Standardisation (CEN), 2004:24), such that a member designed to *EN 1992-1-1:2004* will have 15% more reinforcement than what is required to prevent ULS failure. A 15% loss in steel cross-section would leave the member with only just enough steel to resist collapse under ULS and is therefore considered critical. Any further loss in cross-section would render the member potentially unsafe, thereby ending its usable service life.

An α_{pit} value of 10 was chosen based on the literature, as there is general agreement that highly localised macrocell corrosion, as would typically occur at the locations of cracks in marine RC members, is best represented by an α_{pit} value of 10 (Bezuidenhout & van Zijl, 2019:2192; Andrade, 2020:285; Chen et al., 2020:32).

The propagation period (t_p) values calculated using Equation 5-9, for each of the members in the study, are shown in Table 5-7. Note that t_p values were calculated using both the base and representative (i.e., modified) corrosion rates, such that there are two t_p values for each member. This was done so that the effect of modifying the corrosion rates could be evaluated.

Table 5-7: A summary of the propagation period (t_p) values determined for the members in this study.

Member Type	**Matola Jetty Beams**		**St. Helena Breakwater Crown Wall Units**	
Design Type	**Without CWRs**	**With CWRs**	**Without CWRs**	**With CWRs**
t_p, using base corrosion rates	50	49	28	24
t_p, using representative corrosion rates	50	34	28	20

However, it should be noted that the accuracy of the results shown in Table 5-7 is limited by the accuracy of the model developed by Bezuidenhout and van Zijl (2019), which has not been verified with laboratory or field results. Furthermore, it was assumed that the corrosion rate remains constant. This is unlikely to be the case, particularly if the cover concrete cracks before the 15% loss of cross-section limit state is reached. Nevertheless, despite these shortcomings, the results are valid engineering estimates, which can be reliably used for the comparisons made in this study.

5.6 Calculation of Total Service Life

The total service life of each member was calculated as the sum of the initiation and propagation periods. However, as the length of the initiation period was found to be zero for all members in the study, the total service life of each member is simply equal to the length of the propagation period. The propagation period values shown in Table 5-7 thus also represent the total service life of each member in the study.

6. Quantification of Material Amounts

The determination of the cost and environmental impact of each of the designed members depended on the amount of material (i.e., reinforcing steel and concrete) used in the member. As such, it was necessary to determine the total amount (represented by volume) of reinforcing steel and concrete used in each member. This was done according to the following steps:

- The total volume of each rebar type used in the members was automatically calculated during production of the rebar schedules (see Appendices C and D), using *Autodesk Revit*
- These total rebar volumes were summed up for each member, giving the total volume of reinforcing steel in each member
- The volume of each member was calculated simply as the product of its length, breadth, and height, as each member is rectangular
- The total volume of concrete in each member was thus found by subtracting the total volume of reinforcing steel from the volume of the member

The resultant volumes of reinforcing steel and concrete used in each member can be seen in Table 6-1.

Table 6-1: A summary of the volume of materials used in each of the designed members.

Matola Jetty Beams		
Design Type	Steel Volume [m^3]	Concrete Volume [m^3]
Without CWRs[a]	0.604	37.2
With CWRs[a]	0.773	37.0
St. Helena Breakwater Crown Wall Units		
Design Type	Steel Volume [m^3]	Concrete Volume [m^3]
Without CWRs[a]	0.072	10.4
With CWRs[a]	0.076	10.4

a. Note that “CWRs” refers to the crack width requirements

7. Determination of Member Costs

In Section 2.9 it was shown that the life cycle cost analysis (LCCA) method is very useful for comparing the total costs of different design choices. A LCCA was therefore carried out to determine the cost-effectiveness of designing to meet the crack width requirements when compared with alternative methods of providing durability (namely, crack-sealing admixtures and hydrophobic coatings). Life cycle costs (LCCs) were thus calculated for the following design strategies:

- Strategy A: without crack width design (CWD)
- Strategy B: with CWD
- Strategy C: without CWD, but with a crack-sealing admixture
- Strategy D: without CWD, but with a hydrophobic coating

According to Section 2.9, the LCC of a marine RC structure (or structural element) is typically defined as the sum of the planning, design, and operation (PDE), construction (C), maintenance (M), repair (R), and demolition (D) costs associated with the structure. However, it was assumed that the PDE and D costs for the members designed in this study would be the same for each of the design strategies – such that including the PDE and D costs would not have added any value to the study. The total LCC for each member and strategy was therefore calculated as shown in Equation 7-1; meaning that the resultant LCC values are "comparative", rather than "true", LCC values, as they do not include the PDE and D costs.

$$LCC_i(t) = C_{C,i} + C_{M,i}(t) + C_{R,i}(t) \qquad \textbf{Equation 7-1}$$

Where: $LCC_i(t)$ is the life cycle cost of design strategy i, at time t

: t is taken as the design life of the member (50 years for the beams and 100 years for the wall units)

: $C_{C,i}$ is the present value (PV) construction cost of design strategy i

: $C_{M,i}(t)$ is the total PV maintenance cost of design strategy i, at time t

: $C_{R,i}(t)$ is the total PV repair cost of design strategy i, at time t

An overview of the construction, maintenance, and repair costs for each of the design strategies, as well as an overview of the strategies themselves, is given in the following subsections, before the results of the LCCA are presented in subsection 7.9. Full calculations for the LCCA may be found in Appendix F.

7.1 Determination of Construction Costs

Construction costs were determined for each of the members with the help of Concrete Units (a local precast manufacturer), who provided cost estimates for each of the members, designed with and without the crack width requirements. The estimates were based on the cost of:

- The production and supply of the materials (concrete and reinforcement) used in each member
- The formwork (moulds) used to cast the members
- The labour associated with placing and casting the concrete used in the members
- The labour associated with bending and fixing of the reinforcement used in each member

Transport and construction waste management costs were not considered in the construction cost estimates for the members, both because such costs would have been difficult to quantify, and because they would have been unlikely to differ significantly between the members designed with and without the crack width requirements. The cost estimates provided by Concrete Units are therefore "ex yard", i.e., they are the costs associated with the precast yard only.

The estimated construction costs of the members are thus summarised in Table 7-1. The full quotation from Concrete Units, and the calculations carried out to derive the information in Table 7-1 from the quotation, are shown in Appendix F. It must also be noted that the cost estimates provided by Concrete Units are highly sensitive to changes in the price of steel and diesel, schedule requirements, and escalations due to inflation. The estimates are therefore based on the following conditions and limitations:

- The prices of steel (R 15.86/kg) and diesel (R 21.56/L) used for the estimates were reflective of the industry-standard prices as of May 2022
- A casting schedule of 5 jetty beams and 20 precast wall units per week was assumed, in addition to an 8-10 week set up period before casting could begin. This means that it would take approximately 23-28 weeks to produce the beams, and 20-22 weeks to produce the wall units. A faster casting schedule could be arranged, but would result in higher costs, primarily due to the cost of making more moulds

Finally, it is also important to note that the costs associated with the concrete used in each member (i.e., material, formwork, and casting costs) were approximately the same, regardless of whether the member was designed for the crack width requirements or not. The increase in cost due to crack width design is therefore solely due to increases in reinforcement material and fixing costs, as shown in Table 7-1.

Table 7-1: A summary of the construction costs for the members designed in this study.

Member Type	**Matola Jetty Beams**		**St. Helena Breakwater Crown Wall Units**	
Design Type	Without CWRs[a]	With CWRs[a]	Without CWRs[a]	With CWRs[a]
Construction Cost per Unit[b]	R 234 665.00	R 254 130.00	R 54 040.00	R 54 780.00
Increase in Reinforcement Material Cost per Unit[b]	-	R 13 576.16	-	R 507.52
Increase in Reinforcement Fixing Cost per Unit[b]	-	R 5 888.84	-	R 232.48
Total Construction Cost Increase per Unit[b]	**-**	**R 19 465.00**	**-**	**R 740.00**

a. Note that "CWRs" refers to the crack width requirements.
b. Note that the quoted costs exclude VAT.

The construction costs shown in Table 7-1 were thus used in the LCC calculations, with the addition of 15% VAT. These costs were treated as already being PV values, i.e., the escalation between the design of the members and their construction was not considered in the LCCA.

Cost estimates for the use of various crystalline crack-sealing and waterproofing admixtures were also provided by Concrete Units. These cost estimates are summarised in Table 7-2, and were also used, with the addition of 15% VAT, as PV values in the LCC calculations. The full quotation and associated calculations are available in Appendix F.

Table 7-2: A summary of the costs of various admixtures.

Admixture	Admixture Function	Admixture Cost per Unit[a]	
		Matola Jetty Beams	St. Helena Breakwater Crown Wall Units
Sika WT-200 P	Crack-sealing and waterproofing	R 10 416.00	R 2 912.00
PENETRON Admix	Crack-sealing and waterproofing	R 16 368.00	R 4 576.00
XYPEX ADMIX C-Series	Crack-sealing and waterproofing	R 15 810.00	R 4 420.00

a. Note that the quoted costs exclude VAT.

7.2 Determination of Maintenance Costs

Maintenance costs due to inspections and other routine maintenance requirements were assumed to be approximately the same for all four design strategies and were therefore not included in the LCCA. This is unlikely to be strictly true, as members with poorer durability (and thus more visible deterioration) are likely to elicit more frequent inspections. However, as the amount of routine maintenance and number of inspections carried out for a given structure varies considerably, depending on a variety of factors (such as the budget of the client and the future economic climate), it was decided not to account for inspection and maintenance costs in the LCCA. This means that the LCC values calculated for Strategies A and B, which resulted in lower service lives, may be underestimates. Nevertheless, for the purposes of this study, the calculated LCC values provided adequate estimates.

The only maintenance costs included in the LCCA were thus the costs of reapplying hydrophobic coatings for Strategy D. Hydrophobic coatings are a type of surface treatment, applied to RC to improve durability by making the surface of the concrete waterproof, thereby preventing moisture from reaching the reinforcing steel and causing corrosion. For the purposes of this study, it was decided to reapply the hydrophobic coatings every 25 years for strategy D. The selection of the 25-year reapplication interval was based upon the personal experience of the supervisor of this research (Professor Hans Beushausen) and is corroborated by the findings of Christodoulou et al. (2013:708) and Selander (2010:30), which indicate that hydrophobic coatings may remain effective more than 20 and 36 years after application, respectively.

A wide variety of hydrophobic coatings are available in the industry. However, Jappie (2019:74) notes that pure silane coatings are required for use in marine structures, due to the severity of the marine environment. A pure silane cream, Sikagard-706 Thixo, was therefore selected for use in this study. A rough estimate of the cost of Sikagard-706 Thixo was provided as R95/m^2 (in 2019 prices, assumed to include VAT) by Jappie (2019:xvii). It should be noted that the cost of accessing the members for the hydrophobic coatings (e.g., due to scaffolding) was not considered in the LCCA, as this cost would have been difficult to estimate.

7.3 Determination of Repair Costs

Based on consultation with the supervisor of this research (Professor Hans Beushausen) it was decided that a realistic repair strategy for the members would entail the use of the following:

- Good quality patch repairs, involving the removal of delaminated cover concrete, cleaning and treatment of the corroded reinforcement, and application of new concrete or mortar over the treated reinforcement (Strohmeier, 1994:25). It was expected that approximately 12.5% of the exposed surface area of the members would require repair in this way
- A hydrophobic coating, applied over the entire exposed surface area of the members, to prevent the formation of new anodes in the unrepaired RC adjacent to the patch repairs

Based on his personal experience, Professor Beushausen estimated that the service life of this repair strategy would be 20 years, after which additional repairs, using the same strategy, would be required. This is in general agreement with a case study discussed by Jappie (2019:xii), in which a patch repair and hydrophobic coating repair strategy was estimated to have a 20-year service life.

The repair costs for the members were therefore estimated as the sum of the patch repair and hydrophobic coating costs. The patch repair costs were estimated as R280/m^2 (in 2001 prices, assumed to include VAT), based on good quality patch repairs, according to Mackechnie and Alexander (2001:30). As was the case for the maintenance costs, Sikagard-706 Thixo was chosen for the hydrophobic coatings, at a cost of R95/m^2 (assumed to include VAT) in 2019 prices (Jappie, 2019:xvii). It should be noted that the cost of accessing the members for the repairs (e.g., due to scaffolding) was not considered in the LCCA, as this cost would have been difficult to estimate.

7.4 Determination of Escalation and Discount Rates

An escalation (inflation) rate was calculated as an average between June 2021 and June 2022, using the Contract Price Adjustment Provisions (CPAP) indices published for June 2022. This resulted in an escalation rate of 9.2%. It was assumed that this rate will remain constant throughout the design lives of the members.

The traditional South African discount rate of 8% (du Preez, 2004:466) was used for the LCCA. It was also assumed that this rate will remain unchanged throughout the member's design lives.

7.5 Calculation of LCC for Strategy A

In Strategy A, the members were designed without crack width requirements. This resulted in expected service lives of 50 years for the beams, and 28 years for the wall units, as presented in Section 5. This meant that no repairs were required for the beams (which had a 50-year design life), while the wall units required repairs every 20 years, from 28 years until the end of the wall units' design life (100 years). As there are no maintenance costs associated with Strategy A, the LCC of the beams was therefore determined simply as the value of the construction cost, while the LCC of the wall units was calculated as the sum of the construction cost and the cost of the required repairs.

7.6 Calculation of LCC for Strategy B

As the members in Strategy B were designed with the crack width requirements, two separate service lives were calculated for each member – one which was modified to account for the effect on corrosion rate of providing more, smaller bars to meet the crack width requirements, and one which was not. Two separate LCC values were therefore calculated for each of the members, as follows:

- For the beams, the unmodified service life of 49-years was sufficiently close to the design life of 50-years that it was determined that no repairs were required, and the LCC was simply the construction cost. For the modified service life of 34-years, however, repairs were required at 34-years; meaning that the LCC was the sum of the costs of construction and the repairs
- For the wall units, repairs were required every 20 years from the end of the calculated service lives (24 years for the unmodified corrosion rate, and 20 years for the modified corrosion rate) until the end of the wall units' design life of 100-years. LCC values for the wall units were therefore also determined as the sum of the costs of construction and the required repairs

7.7 Calculation of LCC for Strategy C

Strategy C was based on the addition of a crystalline waterproofing and crack-sealing admixture to the members designed without the crack width requirements. While any of the admixtures priced by Concrete Units could have been used for this purpose, the XYPEX ADMIX C-Series admixture was selected, as more data regarding its expected service life was available than for the other admixtures.

Crystalline admixtures, also known as permeability reducing admixtures, contain various chemicals which react with the water and hydration products in concrete to form crystalline precipitates (Gojević et al., 2021:2). In principle, these precipitates then block pores and agglomerate in cracks in the concrete, thereby reducing the penetrability of the concrete and sealing cracks. However, there is some debate in the literature about the effectiveness of crystalline admixtures. Some authors, such as Dao et al. (2010) found that the use of crystalline admixtures had very little effect on crack-sealing and durability, while others, such as Cuenca et al. (2021) and Kheaw-on, Khomwan and Sujjavanich (2021), found the opposite. The claims made by XYPEX, that their C-Series admixtures can provide service lives greater than 100 years in the marine environment (Xypex, 2022), should therefore be viewed with some scepticism.

Nevertheless, there is some evidence in the literature that the use of crystalline admixtures can result in service lives of approximately 100 years. The claims made by XYPEX are based on an investigation carried out on a real RC wharf in Victoria, Australia, which was constructed using the XYPEX C-Series admixture and with concrete properties comparable to those of the members designed in this study. After 19 years of exposure to the marine environment, the average time to corrosion initiation for the wharf was predicted to be approximately 164 years (Australasian Corrosion Consultants, 2014). Other studies, carried out independently, by Van Belleghem et al. (2017) and Sideris et al. (2019), estimated that test samples constructed using crack-sealing admixtures could have service lives greater than 90 years, depending on the mix design of the concrete.

For the purposes of this study, it was therefore assumed that corrosion will only be initiated after approximately 100 years for Strategy C. This meant that no repair or maintenance costs were required. The total LCC for Strategy C was thus simply the sum of the construction costs associated with designing the members without the crack width requirements and the use of the XYPEX C-Series admixture.

7.8 Calculation of LCC for Strategy D

In Strategy D, the members were not designed for the crack width requirements but were treated with Sikagard-706 Thixo hydrophobic coatings at the time of construction, and every 25 years thereafter. According to Sohawon (2018), who investigated the effect of hydrophobic coatings on the service lives of cracked marine RC structures, the use of a pure silane coating, such as Sikagard-706 Thixo, can result in service lives greater than 100 years. This was found to be the case even in concrete with 0.6 mm cracks – implying that hydrophobic coatings are effective even for cracked RC. Based on this evidence, it was decided that no repairs would be required for Strategy D. The Strategy D LCC values were therefore calculated as the sum of the construction and maintenance costs, considering that the hydrophobic coatings were reapplied every 25 years. For both the beams and wall units, it was assumed that the coatings were only applied to the exposed areas of the members, i.e., the soffits and side faces of the beams, and the portions of the wall units above the crown wall base and rock layers.

However, as it was expected that the calculated LCC values would be very sensitive to the time between coating reapplications, a sensitivity analysis was conducted, considering reapplication times of 10, 15, 20, 25, and 50 years. The results of this sensitivity analysis are shown in Table 7-3 and discussed further in Section 9.2.3.

Table 7-3: A summary of the coating reapplication sensitivity analysis.

Time Between Coatings	Life Cycle Cost [ZAR]	
	Beams	Wall Units
10 years	R 328 436.63	R 77 616.09
15 years	R 318 272.59	R 73 023.59
20 years	R 305 150.01	R 69 454.12
25 years	R 291 372.67	R 67 826.70
50 years	R 279 142.72	R 64 596.51

7.9 Summary of LCCA Results

A summary of the results of the LCCA, for all four strategies, is shown in Table 7-4. These results are discussed in detail in Section 9.

Table 7-4: A summary of the results of the LCCA.

Matola Jetty Beams (LCC per Beam)				
	Strategy A (No CWD[a])	Strategy B (CWD[a])	Strategy C (No CWD[a] + Waterproofing Admixture)	Strategy D (No CWD[a] + Hydrophobic Coating)
Construction Cost [ZAR]	R 269 864.75	R 292 249.50	R 288 046.25	R 269 864.75
Repair Cost [ZAR]	R 0.00	R 0.00[b] / R 37 772.98[c]	R 0.00	R 0.00
Maintenance Cost [ZAR]	R 0.00	R 0.00	R 0.00	R 21 507.92
Total Cost [ZAR]	**R 269 864.75**	**R 292 249.50[b] / R 330 022.48[c]**	**R 288 046.25**	**R 291 372.67**
St. Helena Breakwater Crown Wall Units (LCC per Wall Unit)				
	Strategy A (No CWD[a])	Strategy B (CWD[a])	Strategy C (No CWD[a] + Waterproofing Admixture)	Strategy D (No CWD[a] + Hydrophobic Coating)
Construction Cost [ZAR]	R 62 146.00	R 62 997.00	R 67 229.00	R 62 146.00
Repair Cost [ZAR]	R 19 589.25	R 18 742.28[b] / R 17 931.92[c]	R 0.00	R 0.00
Maintenance Cost [ZAR]	R 0.00	R 0.00	R 0.00	R 5 680.70
Total Cost [ZAR]	**R 81 735.25**	**R 81 739.28[b] / R 80 928.92[c]**	**R 67 229.00**	**R 67 826.70**

a. Note that "CWD" refers to crack width design.
b. Cost for Strategy B, using the base corrosion rate for the members designed with crack width design.
c. Cost for Strategy B, using the modified corrosion rate for the members designed with crack width design.

8. Embodied Carbon Estimates

The environmental impact associated with each of the members designed in the study was quantified by calculating embodied carbon (EC), which serves as an indicator of environmental impact. The main reason for the choice of EC, over other indicators such as cumulative energy demand (CED), was simply the fact that more resources for calculating EC are available in the literature.

As the members designed in the study were not actually produced, data about their installation on site, use and end-of-life treatment was not available. EC values were therefore only determined for the product stage (referred to as A1-A3 emissions), which is likely to account for the majority of the emissions produced by the members (The Institution of Structural Engineers, 2020:9). The estimation of A1-A3 EC values for the study was split into three stages:

- Estimation of A1-A3 emissions for each of the designed members (Section 8.1)
- Estimation of total, structure-wide A1-A3 emissions, for all the beams and wall units in the Matola jetty and St. Helena breakwater, respectively (Section 8.2)
- Determination of A1-A3 EC values for typical marine structures (Section 8.3), to place the results from the second stage in context

The calculations associated with each of these three stages are explained below, along with summaries of their results. Full calculations for each of the stages can be seen in Appendix G.

8.1 Estimation of Member EC Values

A1-A3 EC values were estimated for each member using the approach given in the *How to Calculate Embodied Carbon* (2020) guide produced by the Institution of Structural Engineers (IStructE). According to this approach, the A1-A3 EC value for each member is the sum of the A1-A3 EC values for the concrete and reinforcing steel in the member, as shown in Equation 8-1 (The Institution of Structural Engineers, 2020:30):

$$EC_{Total} = EC_{Concrete} + EC_{Reinforcement} \qquad \textbf{Equation 8-1}$$

The A1-A3 EC values for the concrete and reinforcing steel were calculated using Equation 8-2 (The Institution of Structural Engineers, 2020:4):

$$EC_i = Q_i \times ECF_i \qquad \textbf{Equation 8-2}$$

Where: EC_i is the A1-A3 EC value for material i (either concrete or reinforcement)
: Q_i is the quantity of material i, measured in kilograms
: ECF_i is the A1-A3 Embodied Carbon Factor for material i, determined from the data provided in the IStructE (2020) guide

The quantity of each material, Q, was determined by converting the material amounts for each member, presented as volumes in Section 6, into masses using the mass densities of concrete and reinforcing steel. *ECF* values for each material were then found using the *ECF* values presented in the IStructE guide (The Institution of Structural Engineers, 2020:11-12). Resultant A1-A3 values for each member, determined according to Equation 8-1 and Equation 8-2, are therefore shown in Table 8-1.

Table 8-1: A1-A3 EC values for each of the members in the study.

Member Type	**Matola Jetty Beams**		**St. Helena Breakwater Crown Wall Units**	
Design Type	Without CWRs[a]	With CWRs[a]	Without CWRs[a]	With CWRs[a]
Concrete EC [$kgCO_2e$]	8 214	8 170	2 296	2 296
Reinforcement EC [$kgCO_2e$]	9 375	11 998	1 118	1 180
Total A1-A3 EC [$kgCO_2e$]	**17 600**	**20 200**	**3 410**	**3 480**

a. Note that "CWRs" refers to the crack width requirements

8.2 Estimation of Total EC Values

Total, structure-wide A1-A3 EC values were estimated by multiplying the values for the individual beams and wall units found in Section 8.1 by the total number of beams in the Matola jetty, and the total number of wall units in the St. Helena Island breakwater, respectively. The total number of beams and wall units were determined based on the following assumptions:

- From the original drawings of the Matola jetty provided by PRDW, there were found to be approximately 144 beams in the jetty
- However, only about half of the beams had similar dimensions and loading conditions to the B401 beams designed in this study. The total number of B401-like beams (i.e., beams for which crack width design was critical) in the Matola jetty was therefore estimated to be 72
- According to the original drawings of the St. Helena Island Breakwater provided by PRDW, the breakwater crown wall is about 600 m long
- As each F01 precast crown wall unit is 2.7 m wide, there are thus approximately 225 F01 crown wall units in the breakwater

Total A1-A3 EC values, determined by multiplying the individual values for the beams and wall units by 72 and 225, respectively, are therefore shown in Table 8-2.

Table 8-2: Total, structure-wide, A1-A3 EC values for each of the members designed in the study.

Member Type	**Matola Jetty Beams**		**St. Helena Breakwater Crown Wall Units**	
Design Type	Without CWRs	With CWRs	Without CWRs	With CWRs
Total A1-A3 EC Over Entire Structure [$kgCO_2e$]	1 270 000	1 450 000	767 000	783 000

8.3 Determination of EC Values for Typical Marine Structures

A1-A3 EC values for typical breakwaters and quay walls were found in the literature and are shown in Table 8-3. However, no EC values could be found for jetties. An A1-A3 EC value for the Matola jetty was therefore estimated, using the same process as was used for the individual members in Section 8.1. Instead of calculating separate EC values for all the different members used in the jetty, EC values were calculated considering the total number and "average" characteristics of each of the different types of members, approximated as follows:

- 120 piles, with an average length of 22 m and an average diameter of 1.35 m
- 120 pile caps, with average dimensions of 2.5 x 2.5 x 1.5 m
- 144 beams, with average dimensions of 1.4 x 1.5 x 12 m
- 216 slabs, with average dimensions of 2.8 x 0.25 x 6.1 m

Each of the members used in the jetty was assumed to have 2% reinforcement by volume of concrete; this is a typical value for heavily loaded (and therefore heavily reinforced) members (South African National Standards, 2010:24) and is comparable to the reinforcement percentage of the B401 beams which were designed in this study. The resultant estimate for the A1-A3 EC of the Matola jetty is therefore shown in Table 8-3. This estimate, although rough, is in line with the values found in the literature, as the Matola jetty uses more material than the quay walls, but significantly less than the breakwaters.

Table 8-3: A1-A3 EC values for typical marine structures and the Matola jetty.

Structure Type	Construction	Length [m]	A1-A3 EC [$kgCO_2e$]	Source
Breakwater	Rubble mound	1 400	62 300 000	Broekens et al. (2012)
	Caisson		97 000 000	
Quay Wall	Steel sheet pile	200	919 000	ArcelorMittal (n.d.)
	RC diaphragm		1 700 000	
Matola Jetty	RC deck on piles	350	5 020 000	-

9. Discussion of Results

This section discusses the results presented in Sections 4 to 8, in order to evaluate the effects of designing to meet the crack width requirements ("CWRs") on the durability, costs, and environmental sustainability of marine RC structures. The limitations of the methodology used in this study, and the effects of these limitations on the results, are also discussed, after which a final evaluation of the overall effectiveness and use of the CWRs is made. This evaluation is then followed with a brief discussion on the future use of the CWRs and changes which could be made to better address the effects of cracking on the durability of marine RC structures.

9.1 The Effect of the Crack Width Requirements on Durability

The effect of the CWRs on durability was quantified using the five-step service life modelling method developed in Section 2.8. This method, which allowed for the determination of the lengths of both the corrosion initiation and propagation periods, is a significant finding by itself, as most existing service life models do not consider the propagation period and were not developed for cracked RC. As such, the method developed in this study, while relatively basic, represents an advancement in the service life modelling of real, cracked marine RC structures, which, with further development, could be used in future research and durability design.

The effect of the CWRs on the corrosion initiation period was found to be very different from the effect on the corrosion propagation period. The effect of the CWRs on the corrosion initiation and propagation periods are therefore discussed separately below, in Sections 9.1.1 and 9.1.2, respectively.

9.1.1 The Effect of the Crack Width Requirements on Corrosion Initiation

The effect of the CWRs on the length of the corrosion initiation period was found to be negligible – for all members, the length of the initiation period was determined to be zero, regardless of whether the member was designed with or without the CWRs. This supports the prevailing opinion in the literature, that for cracked RC, the length of the initiation period is negligible (Miyagawa, 1985:58; Otieno, Alexander & Beushausen, 2010:394; Bhaskar et al., 2011:247).

9.1.2 The Effect of the Crack Width Requirements on Corrosion Propagation and Service Life

As the length of the corrosion initiation period was found to be zero for all members, the service life of each member was defined simply as the length of the propagation period for that member. The service life results for each of the members designed in this study are thus shown graphically in Figure 9-1.

From Figure 9-1 it can be seen that, even in the best case, when using the base corrosion rates, the use of the CWRs resulted in service lives which were approximately equal to, or slightly lower than, those for the members designed without the CWRs. In the worst case, when considering the modified corrosion rates, the use of the CWRs resulted in significant decreases in service life, of 32% for the beams and 29% for the wall units. These findings are generally supported by the work of Basteskår et al. (2019b:685), who found no difference in the service lives of Norwegian marine RC structures designed with and without the CWRs, and by the experiments carried out by Francois and Arliguie (1999), which showed no difference in the degree of corrosion between beams with 0.2 and 0.5 mm cracks.

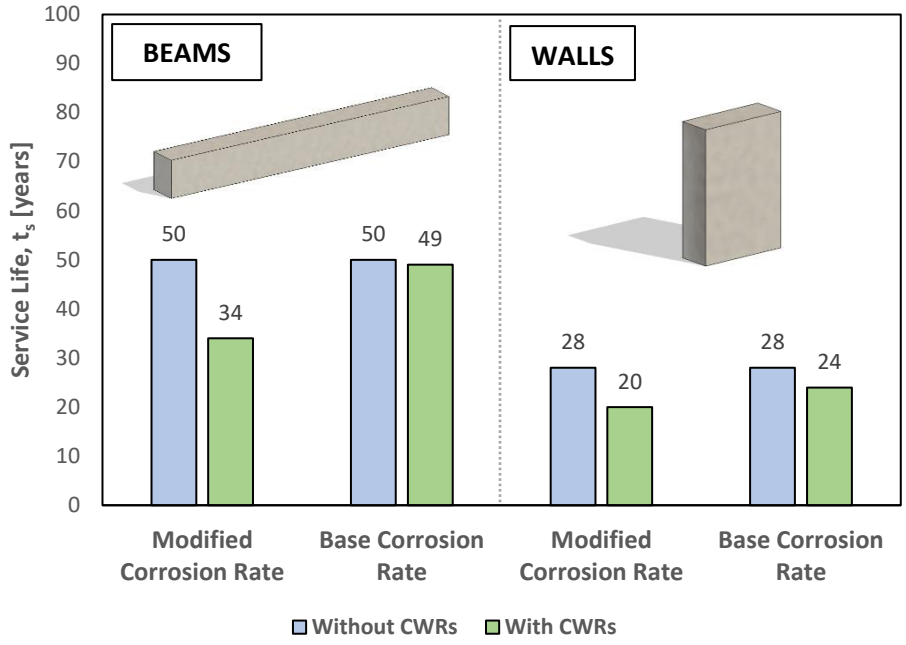

Figure 9-1: A bar graph showing the service lives of the members designed in this study.

These results, which seem to contradict the entire philosophy of the CWRs, can be explained by the fact that, while the CWRs result in smaller crack widths, the effect of these smaller crack widths on reducing the corrosion rate is relatively minor, as even relatively small cracks have been found to still induce significant corrosion (Otieno, Alexander & Beushausen, 2010). In the case of this study, the biggest decrease in crack width due to the use of the CWRs was found for the beams, for which the CWRs resulted in a decrease in crack width from 0.45 to 0.30 mm. Yet, this only resulted in a decrease in corrosion rate from 0.518 to 0.426 $\mu A/cm^2$, or about 18%.

This relatively minor decrease in corrosion rate was then counteracted by the use of smaller diameter bars to meet the CWRs, which has the effect of reducing the time taken to reach the limit state of a 15% loss in reinforcement cross-section, as cross-sectional area is a function of the square of the reinforcement diameter. In other words, a larger amount of steel needs to be corroded away for larger bars to reach the same percentage loss in cross-section as smaller bars – so it intuitively makes sense that members with larger diameter reinforcement will have longer service lives. Furthermore, when considering the modified corrosion rates, the decrease in corrosion rate caused by the reduction in crack width was additionally counteracted by the increase in corrosion rate caused by the use of more, smaller diameter bars, which increases the surface area of the reinforcement exposed by the crack. This effect is well attested-to in the literature, for example by Raupach (1996) and The Concrete Society (2015).

It can thus be seen that the use of the CWRs does not improve the durability of marine RC structures, and may even reduce it, as the effects of using more, smaller diameter bars to meet the requirements outweighs the relatively minor reductions in corrosion rate achieved by reducing crack widths.

9.2 The Effect of the Crack Width Requirements on Life Cycle Cost

To quantify the effects of the CWRs on the costs of marine RC structures, and evaluate the overall cost-effectiveness of the CWRs, a life cycle cost analysis (LCCA) was conducted on the members designed in this study, for the following design strategies:

- Strategy A: No crack width design ("CWD"), i.e., the members were designed without the CWRs
- Strategy B: With CWD, and considering the base and modified corrosion rates as two separate sub-strategies
- Strategy C: No CWD, but making use of a waterproofing and crack-sealing admixture
- Strategy D: No CWD, but with a hydrophobic coating applied

The results of this LCCA are presented and discussed for the beams and wall units in Sections 9.2.1 and 9.2.2, respectively, after which the effect on the results of the chosen reapplication time for the hydrophobic coatings is briefly discussed in Section 9.2.3. The overall cost-effectiveness of the CWRs, particularly when compared to the alternate methods of providing durability used in Strategies C and D, is then evaluated in Section 9.2.4.

9.2.1 Life Cycle Cost Analysis of the Beams

The results of the LCCA carried out for the beams are shown graphically in Figure 9-2. From these results, it can clearly be seen that the LCC of using the CWRs is significantly higher than for the members with no CWD. This is primarily due to the costs of using additional reinforcing steel, in a more congested layout, to meet the CWRs, and the costs of repairs when considering the modified corrosion rate, which only had a service life of 34 years, i.e., less than the 50-year design life of the beams.

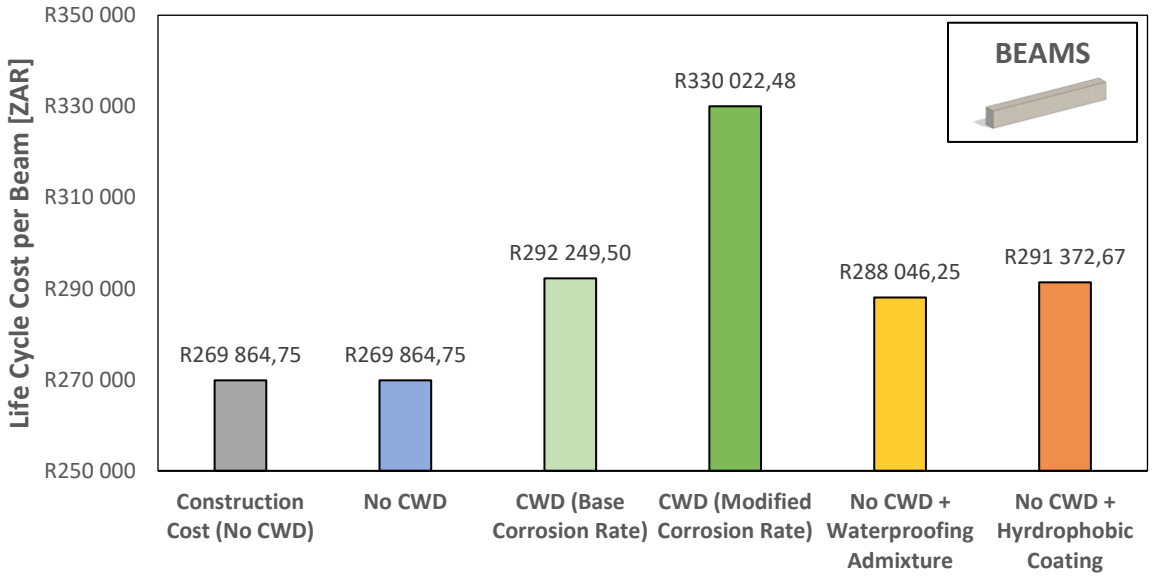

Figure 9-2: A summary of the LCCA results for the beams. Note that the two left-most bars have the same value as, for the members designed without the CWRs, the total LCC is simply equal to the construction cost.

Furthermore, it is also clear that the use of alternate methods of providing durability, such as waterproofing admixtures and hydrophobic coatings, is more cost-effective than the use of the CWRs. This is particularly true when considering the use of the CWRs with the modified corrosion rate, which resulted in a significantly higher LCC than for any of the other design strategies.

9.2.2 Life Cycle Cost Analysis of the Wall Units

Figure 9-3 shows the results of the LCCA carried out for the wall units. Due to the relatively minor amounts of additional reinforcing steel needed to meet the CWRs for the wall units, the LCCs of the

members designed with and without the CWRs are approximately the same. In fact, it is slightly more expensive to not use the CWRs – but this is just a discrepancy caused by the fact that the wall units designed without the CWRs required repairs at a later date, and as the discount rate used in the LCCA was lower than the escalation rate, these repairs were slightly more expensive in present value terms.

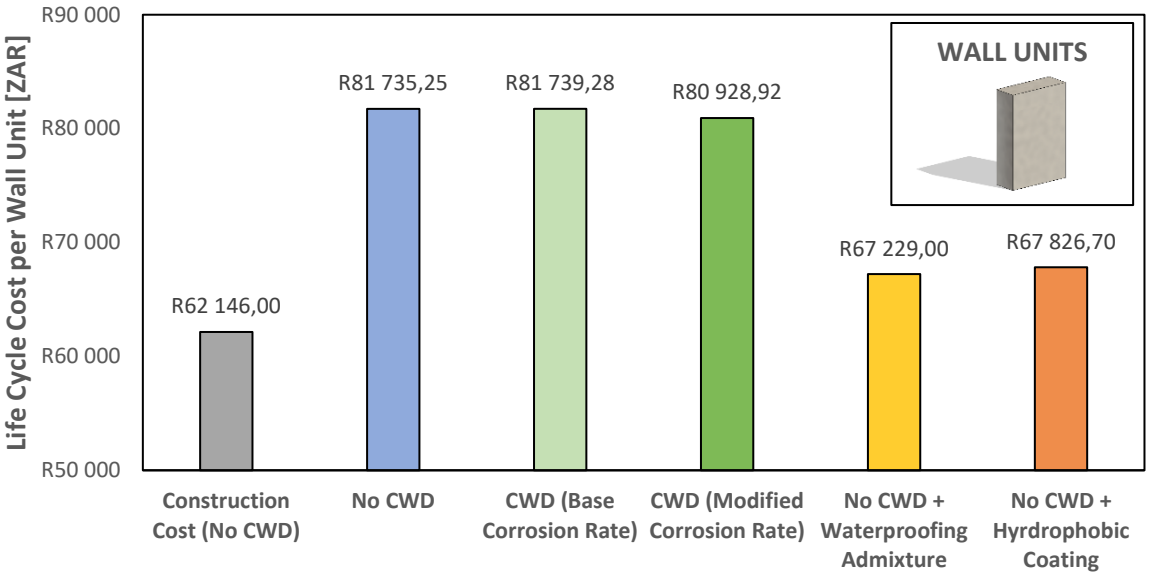

Figure 9-3: A summary of the LCCA results for the wall units.

Nevertheless, it is clear from the results that designing for the CWRs is not the most cost-effective strategy – it is significantly cheaper to make use of a crack-sealing and waterproofing admixture or hydrophobic coating. This is primarily as these alternate methods of providing durability avoid the need for repairs, which become costly over the 100-year design life of the wall units.

9.2.3 The Effect of Reapplication Time on the Life Cycle Cost of Hydrophobic Coatings

The results of the LCCAs presented above are highly sensitive to the reapplication times for the hydrophobic coatings used in Strategy D. Figure 9-4 and Figure 9-5 show how, for the beams and wall units respectively, reducing the time between reapplications of the hydrophobic coatings, which increases the maintenance costs, may significantly increase the overall LCC for Strategy D. However, based on the evidence presented in Section 7.2, namely the long-term studies conducted by Selander (2010) and Christodoulou et al. (2013), the 25-year reapplication time used in this study appears reasonable and realistic.

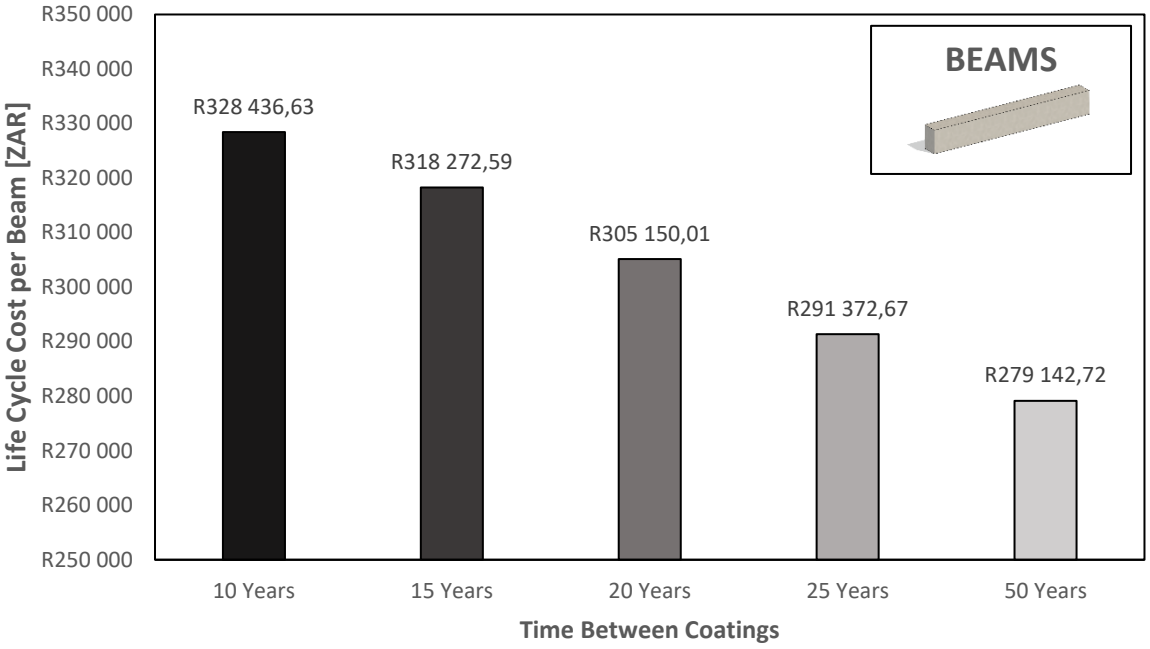

Figure 9-4: A bar graph showing the effect of varying the hydrophobic coating reapplication time on the LCC of the beams for Strategy D.

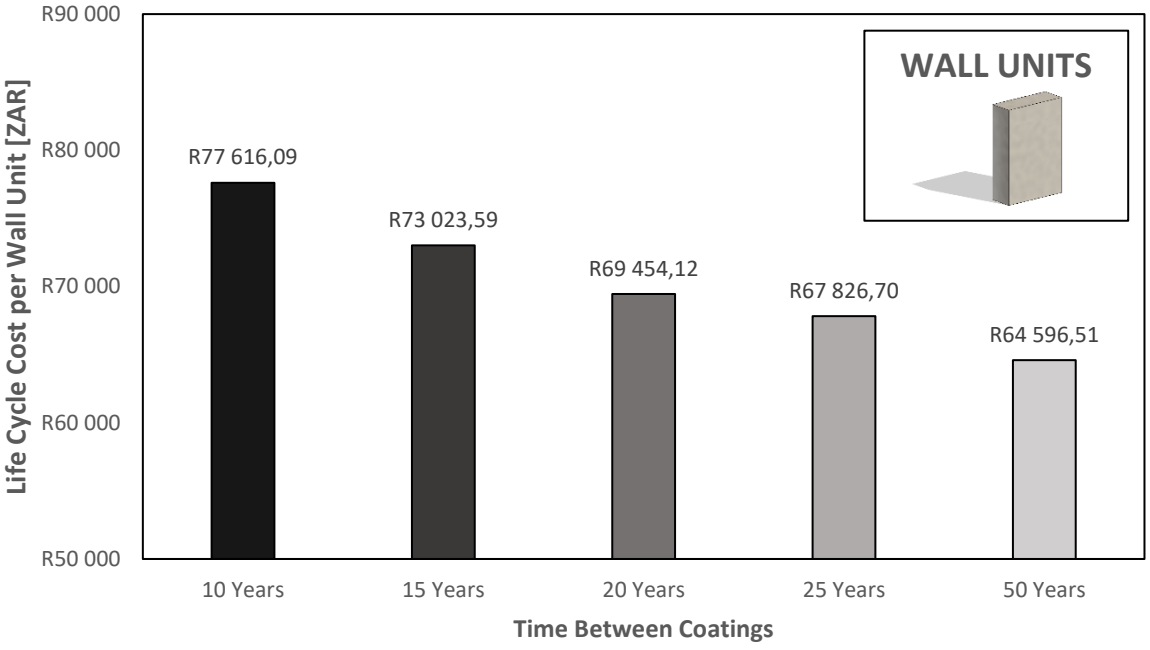

Figure 9-5: A bar graph showing the effect of varying the hydrophobic coating reapplication time on the LCC of the wall units for Strategy D.

9.2.4 The Cost-Effectiveness of the Crack Width Requirements

The results of the LCCA carried out in this study suggest that, although the costs of using the CWRs are not always significantly more than those of not using them, the use of the CWRs is never the most cost-effective option. In the case of the beams, it would be much cheaper to simply not design for the CWRs, or still somewhat cheaper to not design for the CWRs but use waterproofing admixtures or hydrophobic coatings. Likewise, for the wall units, it would be most cost-effective to make use of waterproofing

admixtures or hydrophobic coatings, instead of the CWRs. This is illustrated graphically in Figure 9-6, which shows how, for the beams, all other design strategies resulted in increases in LCC when compared to the members designed without the CWRs, with the biggest increases resulting from the use of the CWRs. In contrast to this, for the wall units, the use of the CWRs resulted in negligible changes in LCC, whereas the use of waterproofing admixtures and hydrophobic coatings resulted in significant reductions in LCC.

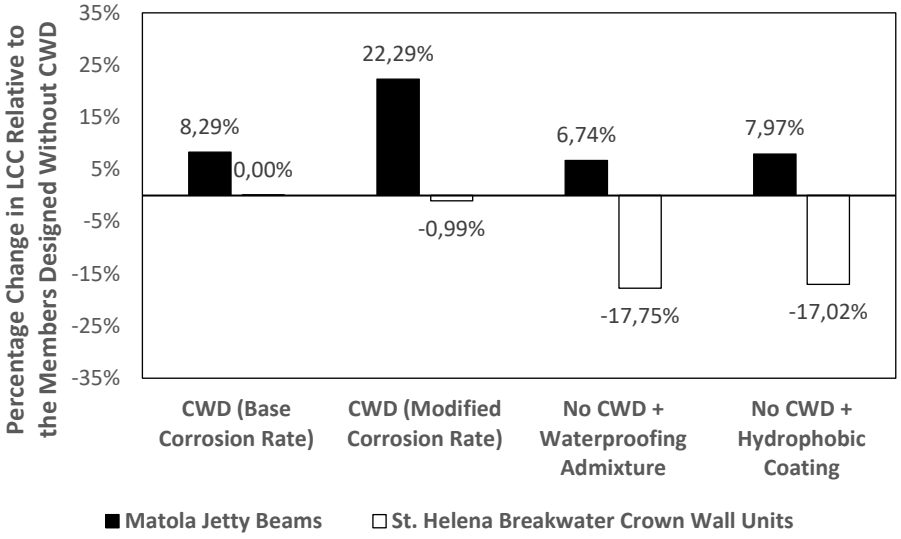

Figure 9-6: A bar graph showing the percentage change in LCC, relative to the members designed without the CWRs, for all the other design strategies.

Table 9-1 shows how, when viewed over the entire structure, considering that there are 72 beams which would need to be designed for crack width in the Matola jetty, and approximately 225 crown wall units in the St. Helena Island breakwater, the savings made by not using the CWRs could be significant. For example, using no CWD for the beams could result in a saving of about R 1.6 million considering the base corrosion rate, or about R 4.3 million if the modified corrosion rate is used. For the wall units, the use of a waterproofing admixture or hydrophobic coating, instead of the CWRs, could result in a total saving of about R 3.0 million.

Table 9-1: Increases in total project LCC for each of the design strategies, relative to the cheapest option (full calculations shown in Appendix F.4).

	Matola Jetty Beams (72 No.)	**St. Helena Crown Wall Units (225 No.)**
No CWD[a]	Cheapest Option	R 3 263 906.25
CWD[a] (Base Corrosion Rate)	R 1 611 702.00	R 3 264 813.00
CWD[a] (Modified Corrosion Rate)	R 4 331 356.56	R 3 082 482.00
No CWD[a] + Waterproofing Admixture	R 1 309 068.00	Cheapest Option
No CWD[a] + Hydrophobic Coating	R 1 548 570.24	Cheapest Option

a. Note that "CWD" refers to crack width design.

9.3 The Effect of the Crack Width Requirements on Environmental Sustainability

The effects of using the CWRs on the environmental sustainability of the members designed in this study were quantified by the determining the A1-A3 (product stage) embodied carbon ("EC") values for each of the members, designed with and without the CWRs. These values, summed over the entire Matola jetty and St. Helena Island breakwater – by considering that there are 72 beams and 225 wall units which need to be designed for the CWRs – are shown in Figure 9-7. Also shown in Figure 9-7, in the inset graph, are A1-A3 EC values estimated for the entire Matola jetty and for typical breakwaters of equivalent length to the St. Helena Island breakwater.

From the A1-A3 EC values shown in Figure 9-7, it can be seen that there is a noticeable (about 14%) increase in the A1-A3 EC values of the beams due to the use of the CWRs. This is caused by the relatively large (28%) increase in reinforcement volume needed to meet the CWRs for the beams. In contrast to this, the effect of the CWRs on the A1-A3 EC values of the wall units is negligible (producing an increase of about 1%), as very little additional reinforcing steel was needed to meet the CWRs for the wall units.

It should also be noted that the results do not consider the effects of repairs due to the worse durability of the members designed with the CWRs. However, the effect of this omission is expected to be relatively minor, as it is known that repairs do not generally result in significant increases in EC (The Institution of Structural Engineers, 2020:23).

When compared with the A1-A3 EC values of entire structures, the increase in EC due to the CWRs is still significant for the beams and makes up about 4% of the total A1-A3 EC of the Matola jetty. This is quite a large percentage for a single design requirement, for only one of the many types of members used in the Matola jetty. For the wall units, however, the increase in A1-A3 EC due to the CWRs is very minor and only accounts for about 0.02% of the total EC of typical breakwaters. It can thus be seen that the use of the CWRs may significantly increase the environmental impact of marine RC structures – although this is not always the case and depends on whether the use of the CWRs results in large increases in the required amount of reinforcement.

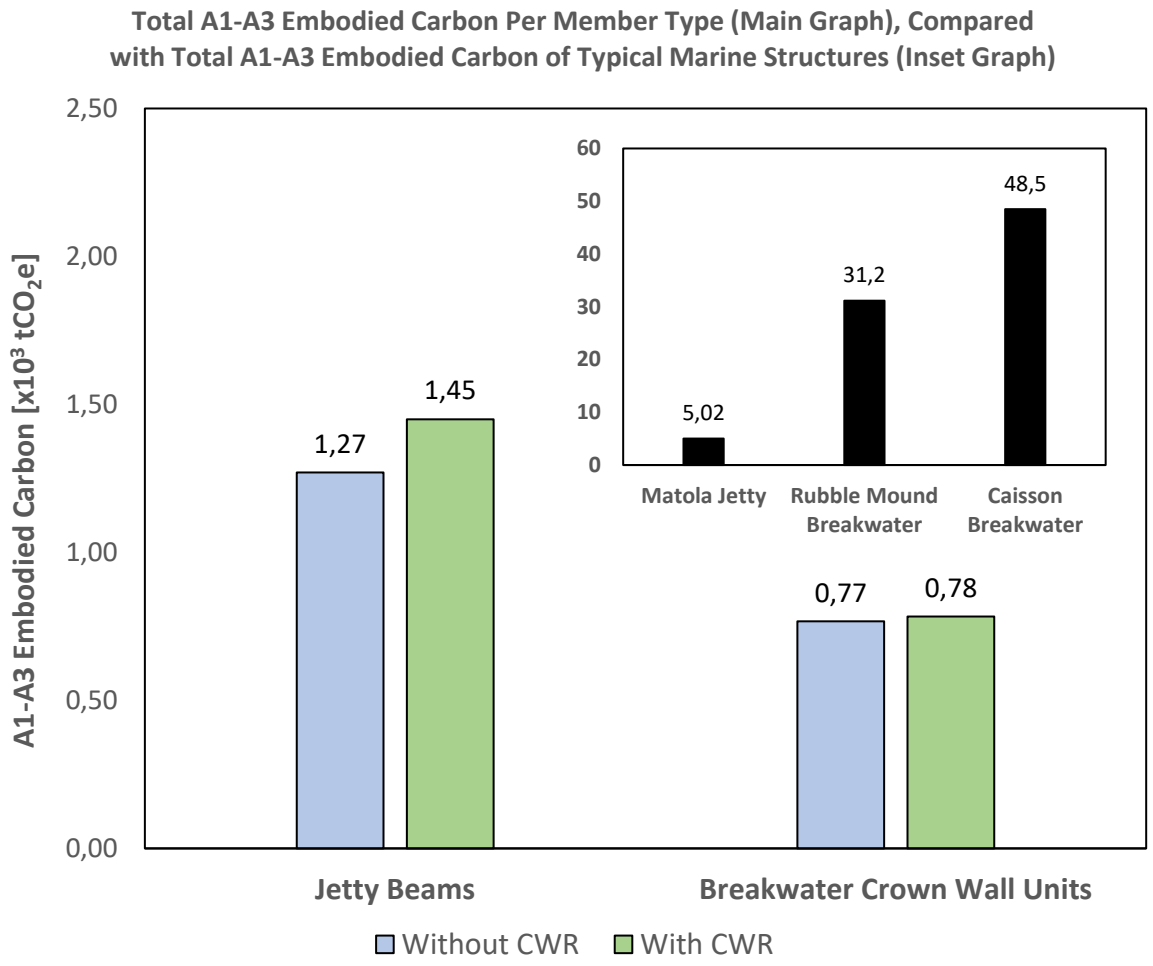

Figure 9-7: A summary of the A1-A3 EC values estimated for the members designed in this study.

9.4 Limitations of the Study

The results of the study, discussed in Sections 9.1 to 9.3, need to be placed in context by considering that there are significant limitations with the methodology used for the study, primarily relating to the service life modelling which was carried out. This is as the existing service life models ("SLMs"), especially those for cracked marine RC structures, do not account for uncertainties regarding:

- The determination and selection of representative corrosion rates
- The effect of reinforcement size and layout on corrosion rate, and the modification of corrosion rates to account for this effect
- The definition of the end of service life and the selection of an appropriate limit state
- The complexity of corrosion in real cracked marine RC structures, due to, for example, the effects of crack self-healing or sealing and crack frequency and orientation

It is worth noting that extensive research would be needed to address these issues, and owing to the complexity of cracking, it is unlikely that the fourth issue will ever by fully resolved, even with additional refinements of the existing SLMs.

The SLM results obtained in this study – and likely any SLM results obtained in future studies – therefore need to be viewed as engineering estimates and nothing more. As such, the results of this study cannot be viewed as definitive and instead should be seen as reasonable engineering estimates, based on sound logic and realistic assumptions.

9.5 Final Evaluation of the Effectiveness and Role of the Crack Width Requirements

Recall that, in Section 2, it was shown how, despite decades of research, there is no clear relationship between crack width and corrosion rate in the literature. Instead, there exist two opposing schools of thought – one which says that there is no relationship between crack width and corrosion rate, and one which argues that there is indeed such a relationship – with good evidence to support both schools of thought.

The findings of this study sidestep this issue, as they imply that, regardless of which school of thought is ultimately true, it does not make sense to design for the CWRs. The reasoning for this is shown diagrammatically in Figure 9-8 and may be understood as follows:

- If a relationship between crack width and corrosion rate does not exist, then it would appear to be unnecessary to design for the CWRs
- If a relationship between crack width and corrosion rate does exist, it may still make sense to design for the CWRs, depending on whether they improve durability or not
- However, according to the results of this study, the CWRs not only do not improve durability, but they may actually reduce it, by encouraging the use of more, smaller diameter reinforcement – which also results in potentially significant increases in cost and environmental impact
- It therefore does not make sense to design for the CWRs, regardless of which school of thought holds true

Ultimately, this suggests that the CWRs, in their current form, should not be included in the codes of practice used for the durability design of marine RC structures.

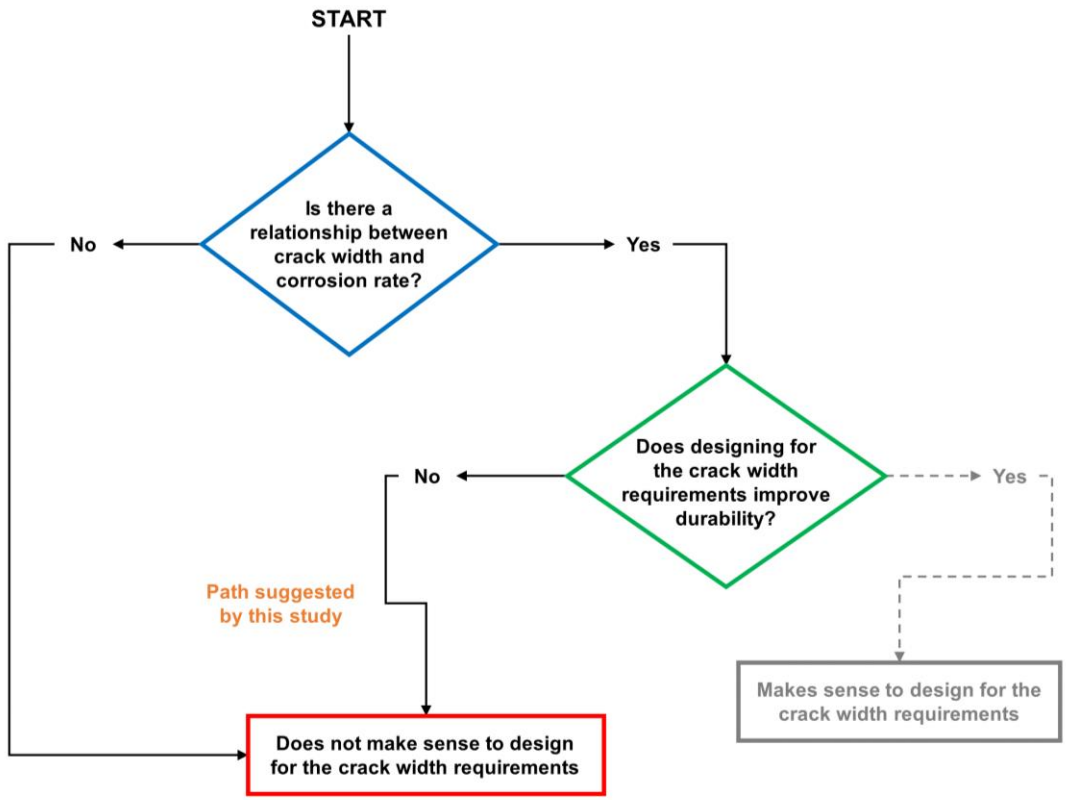

Figure 9-8: A flow chart showing how the results of this study suggest that it does not make sense to design for the CWRs.

9.6 The Way Forward

While it may not make sense to design for the CWRs in their current form, this does not mean that cracking is not an issue for marine RC structures. In some cases, such as when cracking is not controlled (i.e., when cracking causes yielding of the reinforcement) or if the cracks are very large, then these cracks may lead to significant durability problems. However, the member design carried out in this study suggests that the reinforcement used to meet the ULS (flexure) and SLS (minimum area of reinforcement) requirements of *EN 1992-1-1:2004* is generally enough to control cracking and limit crack widths to below about 0.5 mm, i.e., not large enough to result in significant increases in corrosion rate when compared to the *EN 1992-1-1:2004* crack width limit of 0.3 mm.

It can thus be seen that, for the range of crack widths typically occurring in practice, the current CWRs are not the most effective or efficient method to address the issue of cracking. Furthermore, as the crack width formula used in the *fib* Model Code 2010 is very similar to the formula in *EN 1992-1-1:2004* (Lapi, Orlando & Spinelli, 2018:1494), this is unlikely to change with future codes of practice. Instead, it would be better to still make sure that cracking is controlled (i.e., keep the check on the minimum area of reinforcement needed to ensure cracking is controlled), but remove and replace the existing crack width limitations with one (or multiple) of the following options:

- A limitation on steel stress, as recommended by Basteskår et al. (2019b:685-686), to indirectly limit cracking and its effects, as crack width is a function of steel stress. Such a limitation has already replaced the CWRs in the American Concrete Institute's *Building Code Requirements for Structural Concrete (ACI 318R-05)* (Yu et al., 2015:257) and is provided as an alternative to direct crack width design in the *fib* Model Code 2010 (Balázs et al., 2013:103)

- A more lenient crack width requirement, for example of 0.5 mm, rather than 0.3 mm, to account for the fact that the difference in corrosion rate between a 0.5 mm and 0.3 mm crack is likely to be relatively minor. It is expected that such a crack width requirement would prevent the development of excessively large cracks without requiring the large amounts of additional reinforcing steel associated with the current CWRs
- A performance-based crack width requirement, such as that suggested by Otieno, Beushausen and Alexander (2012), which accounts for the effect of exposure conditions and concrete quality and cover depth on corrosion in cracked RC
- A performance-based approach to durability design, in which crack width is calculated and serves as an input parameter for service life modelling but is not limited to a prescribed value. Such an approach is already utilised in the Japanese *Guidelines for Concrete No. 15*, although it is based on the corrosion initiation period only (Smith, 2016a:91)
- Give engineers the choice to use alternate methods of providing durability, such as the use of crack-sealing and waterproofing admixtures, or hydrophobic coatings, instead of limiting crack width

Prior to the implementation of any of the methods described above, the results of this study – which, due to the limitations discussed in Section 9.4, can only be viewed as engineering estimates – need to be confirmed. Owing to the inherent problems with service life modelling discussed in Section 9.4, and the problems with accelerated laboratory corrosion highlighted by authors such as Käthler et al. (2020a), it seems that the only way to do this would be an extensive evaluation of the durability performance of real marine RC structures which were designed for the current CWRs. Such an evaluation, which should focus on the range of crack widths which were actually achieved in practice, and the effect of this range on the extent of any corrosion damage which may have occurred, would be the only way that the debate over the CWRs could be resolved with any degree of certainty.

10. Conclusion

This study evaluated the effects of designing for the current crack width requirements (CWRs) on the durability, cost, and environmental sustainability of marine RC structures. RC may crack for a variety of reasons, including shrinkage, thermal movements, or applied loads. To mitigate any potential durability issues which may arise from these cracks, the durability design of marine RC structures tends to include designing to meet CWRs, which aim to limit cracks to certain maximum prescribed values. In the South African coastal engineering industry, the CWR of 0.3 mm specified in *EN 1992-1-1:2004* is typically used, and the process of designing to meet this requirement (referred to as "crack width design") is generally carried out using the provisions of *EN 1992-1-1:2004* for cracking due to applied loads and *CIRIA C660* for thermal and shrinkage cracking.

However, it is well-known in both the literature and the coastal engineering industry that the current CWRs tend to dominate the entire design of marine RC structures, often controlling the layout of the reinforcement and resulting in significant increases in the total amount of reinforcement used. Yet, at the same time, the effectiveness of the CWRs at providing durability is uncertain, despite decades of research. This suggests that the current CWRs are neither the most effective, nor efficient, way of addressing the effects of cracking on the durability of marine RC structures, as the use of additional reinforcement to meet the requirements may significantly increase costs and environmental impacts. There was thus a great need to evaluate the effect of designing for the current CWRs on the durability, cost, and environmental sustainability of marine RC structures.

This evaluation was carried out by designing two separate sets of typical marine RC members – one with, and one without, the current CWRs – according to the provisions of *EN 1992-1-1:2004*, *CIRIA C660*, and *BS 6349*. Two typical marine RC members were designed. The first was a crane rail beam for a coal export jetty in Matola, Mozambique, while the second was a precast crown wall unit for an armoured quay in Rupert's Bay, St. Helena Island. The effects of the CWRs on the durability, cost, and environmental sustainability of the chosen members were then determined by carrying out service life modelling, a life cycle cost analysis, and calculations of embodied carbon, and comparing the results for the members designed with, and without, the current CWRs. The results, and the conclusions drawn from them, are presented in Sections 10.1 to 10.3, before a final, overall evaluation of use of the current CWRs is made in Section 10.4.

10.1 The Effect of the Crack Width Requirements on Durability

The durability of the members designed in this study was quantified by determining the expected service life of each member – defined as the sum of the corrosion initiation and propagation periods. However, most existing service life models were developed for uncracked concrete and only consider the length of the initiation period. As such, the existing models were not suitable for use in this study. Instead, a new method, which accounted for the effect of cracking on both the initiation and propagation of corrosion, was developed for this study.

In the new method, the length of the corrosion initiation period was calculated using an existing initiation period model, but instead of using the full cover depth of the concrete, only the portion of the cover depth for which the concrete had a crack width less than 0.1 mm was used – as it was assumed that cracks with widths less than 0.1 mm have a negligible effect on corrosion initiation. The length of the corrosion propagation period was then calculated as the time from when corrosion was initiated, until 15% of the reinforcement cross-section had been lost to corrosion. The corrosion rate for the reinforcement in each member was determined from the corrosion rate model for cracked marine RC

developed by Otieno (2014), with additional modifications to account for the effect on corrosion rate of using different amounts and layouts of reinforcement to meet the CWRs.

The length of the corrosion initiation period was found to be zero for all the members designed in the study, regardless of whether they were designed for the CWRs or not. This was attributed to the fact that, even for the members designed with the CWRs, the cracks were sufficiently wide that they were greater than 0.1 mm wide at the level of the reinforcement. These results are corroborated by the established view in the literature, namely, that the initiation of corrosion is instant in cracked RC (Miyagawa, 1985; Otieno, Alexander & Beushausen, 2010; Bhaskar et al., 2011). It can therefore be seen that the effect of the CWRs on the initiation of corrosion is negligible.

The same cannot be said of the effects of the CWRs on the propagation of corrosion. The use of the CWRs was found to, at best, result in the same or slightly shorter propagation periods. In the worst case, the use of the CWRs resulted in significant decreases in the length of the propagation period, of 32% for the jetty beams, and 29% for the crown wall units. As the length of the initiation period was found to be zero for all members, the service life of each member was thus given by the length of the propagation period only – meaning that the use of the CWRs ultimately had a negative effect on service life.

There are several explanations for this. The first is that, while the use of the CWRs does result in smaller crack widths, and hence in lower corrosion rates, the reductions in corrosion rate were found to be relatively small – at best, the use of the CWRs was found to result in an 18% reduction in corrosion rate. This is as, even without the CWRs, the ULS and SLS requirements of *EN 1992-1-1:2004* tend to limit crack widths to relatively small values. The relatively minor reductions in corrosion rate achieved using the CWRs were then counteracted by the fact that the CWRs encourage the use of smaller diameter reinforcement, which has the effect of increasing the corrosion rate (by increasing the surface area of the reinforcement in the cathodic region) and reducing the time taken for 15% of the reinforcement cross-section to be corroded away, as cross-sectional area is a function of the square of the reinforcement diameter.

It can thus be seen that designing for the CWRs does not result in improved durability, and in fact may even reduce durability, through the use of smaller diameter reinforcement. This is at least partially corroborated by the conclusions of Basteskår et al. (2019b), who found that the use of the CWRs made no difference to the service lives of Norwegian marine RC structures.

10.2 The Effect of the Crack Width Requirements on Life Cycle Cost

The effect of the CWRs on the costs of marine RC structures was established by conducting a life cycle cost analysis (LCCA) on the members designed with, and without, the CWRs, as well as for two alternate design strategies, in which the members were designed without the CWRs, but made use of either a waterproofing and crack-sealing admixture, or a hydrophobic coating. The LCCA considered three different kinds of costs – construction costs, maintenance costs, and repair costs. The construction cost associated with each member was determined with the help of Concrete Units, a local precast concrete manufacturer, while the maintenance and repair costs were estimated from figures in the literature.

The results of the LCCA show that the use of the CWRs may significantly increase the costs of marine RC structures. In the case of the beams, the use of the CWRs was found to increase the life cycle cost (LCC) of the beams by as much as 22%, whereas for the crown wall units, the difference in cost between the wall units designed with and without the CWRs was negligible. These results can be explained by

the fact that the use of the CWRs resulted in a large (28%) increase in reinforcement volume for the beams, but only in a minor (5.7%) increase in reinforcement volume for the wall units.

The use of the CWRs was also found to be more expensive than the use of the alternate methods of providing durability. For the beams, this effect was relatively minor, whereas for the crown wall units the use of either a waterproofing admixture or hydrophobic coatings resulted in an approximately 17% decrease in LCC when compared to the members designed with the CWRs. This was attributed to the relatively poor durability performance of the members designed with the CWRs, which resulted in large repair costs.

Ultimately, these results suggest that the CWRs are not the most cost-effective method of accounting for the effect of cracks on the durability of marine RC structures. For the beams, it would be cheapest to simply not design for the CWRs, whereas for the crown wall units, the most cost-effective option would be to make use of an alternative method of providing durability, such as a waterproofing admixture or hydrophobic coating. Furthermore, considering that there are approximately 72 beams in the Matola jetty which would need to be designed for the CWRs, and about 225 crown wall units in the St. Helena Island armoured quay, the savings resulting from not using the CWRs could be significant – up to R 4.3 million for the beams and about R 3.0 million for the crown wall units.

10.3 The Effect of the Crack Width Requirements on Environmental Sustainability

The effect of using the CWRs on the environmental sustainability of the members designed in this study was quantified by estimating A1-A3 (product stage) embodied carbon (EC) values for each of the members designed with and without the CWRs. This was done using the *How to Calculate Embodied Carbon* (2020) guide produced by the Institution of Structural Engineers (IStructE). In order to place the estimates for the members in context, an A1-A3 EC value was also estimated for the entire Matola jetty and A1-A3 EC estimates for typical breakwaters were found from the literature.

The resultant A1-A3 EC estimates show that the effect of designing for the CWRs on environmental sustainability can be significant – the use of the CWRs for the beams resulted in a 14% increase in A1-A3 EC, from 17 600 $kgCO_2e$ to 20 200 $kgCO_2e$ per beam. However, this is not always the case, as for the wall units the use of the CWRs only resulted in a negligible (approximately 1%) increase in A1-A3 EC, from 3 410 $kgCO_2e$ to 3 480 $kgCO_2e$ per wall unit. As was the case for the LCCA results, this difference can be explained by the fact that the use of the CWRs resulted in a large (28%) increase in reinforcement volume for the beams but only in a minor (5.7%) increase for the wall units.

It can thus be seen that the use of the CWRs may result in large increases in environmental impact, depending on the amount of additional reinforcement needed to meet the requirements. When viewed over entire structures, these increases may be significant – the increase in A1-A3 EC caused by the use of the CWRs for the beams in the Matola jetty makes up about 4% of the total A1-A3 EC for the entire Matola jetty – which is a large amount considering that the beams are only one of many different types of members in the Matola jetty.

10.4 Overall Evaluation of the Effectiveness and Role of the Crack Width Requirements

One of the biggest criticisms of the current CWRs in the literature is the fact that, despite decades of research on the effect of cracks on the durability of marine RC structures, no clear relationship between crack width and corrosion rate has ever been found. Instead, opinion is divided between two competing schools of thought – one which states that there is a relationship between crack width and corrosion rate,

and one which argues that no such relationship exists – with good evidence to support both. There is thus a great deal of uncertainty about the role of the CWRs in the durability design of marine RC structures – as if a relationship between crack width and corrosion rate does exist, then it may be beneficial to design for the CWRs, whereas if no such relationship exists, designing for the CWRs would be unnecessary.

The findings of this study go some way towards resolving this issue, as they suggest that, even if there is a relationship between crack width and corrosion rate, the current CWRs do not improve durability, and may even have a detrimental effect, whilst also causing potentially significant increases in the costs and environmental impacts of marine RC structures. This ultimately implies that, regardless of which school of thought is true, it does not make sense to design for the current CWRs, as they are neither the most effective nor efficient way of accounting for the effects of cracking on durability. It is therefore recommended that, to better consider the effects of cracking on durability, the current CWRs should be removed from design codes of practice and replaced with one or more of the following options:

- A general limit on steel stress, rather than a specific limit on crack width – as crack width is a function of steel stress, limiting steel stress will indirectly limit crack widths
- A more lenient crack width requirement, for example of 0.5 mm – to account for the fact that the difference in corrosion rate between a 0.3 mm crack (i.e., the current *EN 1992-1-1:2004* requirement) and a 0.5 mm crack is likely to be relatively minor. It is envisaged that a more lenient crack width requirement would prevent the formation of excessively large cracks whilst avoiding the use of large amounts of additional reinforcing steel associated with the current CWRs
- A performance-based crack width requirement, such as that suggested by Otieno, Beushausen and Alexander (2012), which accounts for the influence of exposure conditions, concrete quality, and cover depth on the corrosion process in cracked RC
- A performance-based approach to durability design, in which crack width is calculated and serves as an input parameter for service life modelling, but is not limited to a prescribed value
- Give engineers the choice to use alternate methods of providing durability, such as the use of crack-sealing and waterproofing admixtures, or hydrophobic coatings, instead of limiting crack width

11. Recommendations for Further Work

It should be noted that there are several limitations with the methodology employed in this study, primarily relating to the service life modelling of the members designed in the study. As such, further work needs to be carried out to confirm the results presented in this dissertation. It is therefore recommended that additional research should be carried out, focusing in the following areas:

I. **The determination of representative corrosion rates:**

The representative corrosion rates used for the members designed in this study were determined using the corrosion rate model developed by Otieno (2014). However, this model was developed using data for beam samples exposed to accelerated laboratory corrosion and natural corrosion in the tidal zone for a period of 2 years and 3 months. It is unlikely that the corrosion rates of real marine RC structures will stay constant in the long-term, and as such, more research is needed to be able to reliably select representative corrosion rates for real marine RC structures

II. **The effect of reinforcement size and layout on corrosion rates:**

The effect of changing the size and layout of the reinforcement to meet the crack width requirements on the corrosion rate of the members designed in this study was accounted for using the factors α and β. However, these factors were determined based on very limited research, and can therefore be seen as engineering estimates only. Further research on the effect of reinforcement size and layout on corrosion rate is thus needed to better quantify the development of corrosion in real marine RC structures

III. **The definition of the end of service life:**

For the purposes of this study, the end of a member's service life was defined as the point at which 15% of the reinforcement cross-section had been lost to corrosion, as the safety of the structure will be severely reduced beyond this figure. However, more research on the end-of-life condition of real marine RC structures is needed to confirm whether this is a realistic definition of the end of a member's service life

IV. **The effect of the complexity of cracking on the development of corrosion:**

The effect of cracking on the durability of real marine RC structures is highly complex, and depends on several crack properties, such as the orientation and frequency of the crack, and whether the crack is active or dormant. Yet, due to a lack of data, this complexity could not be accounted for in the service life modelling conducted in this study. Further research, focusing on the propagation of corrosion in real, cracked marine RC structures is therefore needed to facilitate the development of more realistic service life models in future

However, even with extensive research, it is unlikely that future service life models will ever be able to properly account for the complexity of cracking. It thus appears that service life modelling results will never be more than engineering estimates and will therefore never be able to definitively resolve the debate surrounding the role of the crack width requirements. Furthermore, owing to the limitations with accelerated laboratory corrosion discussed by authors such as Käthler et al. (2020a), it is also unlikely that experimental studies conducted in laboratory environments will ever be definitive in their outcomes. It is therefore recommended that future research on the role of crack width requirements in the durability design of marine RC structures should instead take the form of an extensive evaluation of the durability performance of existing marine RC structures – as doing so is likely the only way that the "real-life" effectiveness of the crack width requirements can be properly established.

Reference List

ACI Committee 224. 1993. *Causes, Evaluation and Repair of Cracks in Concrete Structures (ACI 224.1R-93)*. Farmington Hills, Michigan, United States of America: American Concrete Institute.

ACI Committee 224. 2001. *Control of Cracking in Concrete Structures*. Farmington Hills, Michigan, United States of America: American Concrete Institute.

ACI Committee 357. 1997. *Guide for the Design and Construction of Fixed Offshore Concrete Structures (ACI 357-R84)*. Farmington Hills, Michigan, United States of America: American Concrete Institute.

Alexander, M. & Beushausen, H. 2009. Deformation and volume change of hardened concrete. In *Fulton's Concrete Technology*. 9th ed. G. Owens, Ed. Midrand, South Africa: Cement & Concrete Institute. 111–154.

Alexander, M. & Beushausen, H. 2019. Durability, service life prediction, and modelling for reinforced concrete structures – review and critique. *Cement and Concrete Research*. 122(February):17–29. DOI: 10.1016/j.cemconres.2019.04.018.

Alexander, M. & Nganga, G. 2016. Introduction: importance of marine concrete structures and durability design. In *Marine Concrete Structures*. M. Alexander, Ed. Duxford, United Kingdom: Woodhead Publishing. 1–13.

Alexander, M., Bentur, A. & Mindess, S. 2017. *Durability of Concrete: Design and Construction*. CRC Press.

Alexander, M.G., Beushausen, H. & Otieno, M.B. 2012. *Research Monograph No.9: Corrosion of steel in reinforced concrete: Influence of binder type, water/binder ratio, cover and cracking*. Cape Town, South Africa: Concrete Materials and Structural Integrity Research Unit, Department of Civil Engineering, University of Cape Town.

Andrade, C. 2020. Linear propagation models of deterioration processes of concrete. *Corrosion Engineering, Science and Technology*. 55(4):283–288. DOI: 10.1080/1478422X.2020.1750161.

Andrade, C. & Izquierdo, D. 2020. Propagation period modeling and limit state of degradation. *Structural Concrete*. 21(5):1720–1731. DOI: 10.1002/suco.201900427.

Angelucci, M. 2018. Concrete hydration temperatures for the design of crack-width reinforcement in concrete water-retaining structures-design values versus in-situ values. *MATEC Web of Conferences*. 199. DOI: 10.1051/matecconf/201819911014.

ArcelorMittal. n.d. *Life Cycle Assessment of a quay wall: building sustainable ports*. Available: https://constructalia.arcelormittal.com/en/news_center/articles/lca-of-a-quay-wall-building-sustainable-ports [2022, July 06].

Arya, C. & Myrzakulova, T. 2019. Condition Assessment and Protection of Concrete Structures Against Corrosion: Do Cracks Matter? In *UKIERI Concrete Congress*. Jalandhar, Punjab, India.

Athibaranan, S., Karthikeyan, J. & Rawat, S. 2022. Investigation on service life prediction models of reinforced concrete structures exposed to chloride laden environment. *Journal of Building Pathology and Rehabilitation*. 7(1):1–15. DOI: 10.1007/s41024-021-00149-8.

Australasian Corrosion Consultants. 2014. *Concrete Investigation - Xypex Panel: Investigation Report*. Victoria, Australia.

Balázs, G.L., Bisch, P., Borosnyõi, A., Burdet, O., Burns, C., Ceroni, F., Cervenka, V., Chiorino, M.A., et al. 2013. Design for SLS according to fib Model Code 2010. *Structural Concrete*. 14(2):99–123. DOI: 10.1002/suco.201200060.

Ballim, Y., Alexander, M. & Beushausen, H. 2009. Durability of Concrete. In *Fulton's Concrete Technology*. 9th ed. G. Owens, Ed. Midrand, South Africa: Cement & Concrete Institute. 155–188.

Bamforth, P.. 2007. *CIRIA C660: Early-age thermal crack control in concrete*. London, United Kingdom: CIRIA.

Barre, F. 2016. Cracking of Beams and Walls Subject to Restrained Deformations at SLS. In *Control of Cracking in Reinforced Concrete Structures*. Hoboken, New Jersey, United States of America: John Wiley & Sons, Inc.

Basheer, M. 2009. Concrete: an introduction. In *ICE Manual of Construction Materials*. ICE Publishing. 57–60. DOI: 10.1680/mocm.35973.0057.

Basheer, P.A.M. & Barbhuiya, S. 2009. Durability of concrete. In *ICE Manual of Construction Materials*. ICE Publishing. 169–184. DOI: 10.1680/mocm.35973.0169.

Basteskår, M., Engen, M., Kanstad, T., Johansen, H. & Fosså, K.T. 2019a. Serviceability limit state design of large concrete structures: Impact on reinforcement amounts and consequences of design code ambiguity. *Engineering Structures*. 201(June). DOI: 10.1016/j.engstruct.2019.109816.

Basteskår, M., Engen, M., Kanstad, T. & Fosså, K.T. 2019b. A review of literature and code requirements for the crack width limitations for design of concrete structures in serviceability limit states. *Structural Concrete*. 20(2):678–688. DOI: 10.1002/suco.201800183.

Beeby, A.. 1978. Corrosion of Reinforcing Steel in Concrete and Its Relation To Cracking. *The Structural Engineer*. 56(3):77–81.

Beeby, A.. & Narayanan, R.. 2005. *Designers' Guide to Eurocode 2: Design of Concrete Structures*. H. Gulvanessian, Ed. London: Thomas Telford Publishing. Available: https://doi.org/10.1680/dgte2docs.31050.

Bezuidenhout, S.R. & van Zijl, G.P.A.G. 2019. Corrosion propagation in cracked reinforced concrete, toward determining residual service life. *Structural Concrete*. 20(6):2183–2193. DOI: 10.1002/suco.201800275.

Bhaskar, S., Gettu, R., Bharatkumar, B.H. & Neelamegam, M. 2011. Studies on chloride induced corrosion of reinforcement steel in cracked concrete. *SDHM Structural Durability and Health Monitoring*. 7(4):231–251. DOI: 10.3970/sdhm.2011.007.231.

Boshoff, W.P. & Combrinck, R. 2013. Modelling the severity of plastic shrinkage cracking in concrete. *Cement and Concrete Research*. 48 (2013): 34-39.

Bras, A. & Faustino, P. 2019. Impact of repairs on embodied carbon dioxide expenditure for a reinforced-concrete quay. *Proceedings of the Institution of Civil Engineers - Engineering Sustainability*. 172(2):87–97. DOI: 10.1680/jensu.17.00010.

Broekens, R., Escarameia, M., Cantelmo, C. & Woolhouse, G. 2012. Quantifying the carbon footprint of coastal construction - A new tool HRCAT. *Innovative Coastal Zone Management: Sustainable Engineering for a Dynamic Coast - 7th International Coastal Management Conference*. 253–262. DOI: 10.1680/iczm.57494.253.

Burcharth, H.F. & Hughes, S.A. 2006. Types and Functions of Coastal Structures. In *Coastal Engineering Manual*. U.S. Army Corps of Engineers.

Chen, E., Berrocal, C.G., Lofgren, I. & Lundgren, K. 2020. Correlation between concrete cracks and corrosion characteristics of steel reinforcement in pre-cracked plain and fibre-reinforced concrete beams. *Materials and Structures*. 53(33). DOI: 10.1617/s11527-020-01466-z.

Christodoulou, C., Goodier, C.I., Austin, S.A., Webb, J. & Glass, G.K. 2013. Long-term performance of surface impregnation of reinforced concrete structures with silane. *Construction and Building Materials*. 48:708–716. DOI: 10.1016/j.conbuildmat.2013.07.038.

Cuenca, E., Rigamonti, S., Gastaldo Brac, E. & Ferrara, L. 2021. Crystalline Admixture as Healing Promoter in Concrete Exposed to Chloride-Rich Environments: Experimental Study. *Journal of Materials in Civil Engineering*. 33(3):1–14. DOI: 10.1061/(asce)mt.1943-5533.0003604.

Cui, Z. & Alipour, A. 2018. Concrete cover cracking and service life prediction of reinforced concrete

structures in corrosive environments. *Construction and Building Materials*. 159:652–671. DOI: 10.1016/j.conbuildmat.2017.03.224.

Dalrymple Bay Coal Terminal. n.d. *The Latest at DBCT P/L*. Available: https://www.dbct.com.au/latest-news [2022, July 07].

Dao, V.T.N., Dux, P.F., Morris, P.H. & Carse, A.H. 2010. Performance of permeability-reducing admixtures in marine concrete structures. *ACI Materials Journal*. 107(3):291–296. DOI: 10.14359/51663758.

Day, R. & Clarke, J. 2003. Plastic and thermal cracking. In *Advanced Concrete Technology*. J. Newman & B.S. Choo, Eds. Elsevier Ltd.

De Gijt, J. & Vinks, R. 2011. Cost of quay walls including life cycle aspects. In *Proceedings of the International Maritime-Port Technology and Development Conference, MTEC2011*. Singapore: MTEC. 135–139. Available: https://repository.tudelft.nl/islandora/object/uuid%3Acbac3e3f-a9c3-486a-862f-cecf0ebc036e.

Du Preez, M. 2004. *The Discount Rate for Public Sector Conservation Projects in South Africa*. Oxford, United Kingdom.

Dwaikat, L.N. & Ali, K.N. 2018. Green buildings life cycle cost analysis and life cycle budget development: Practical applications. *Journal of Building Engineering*. 18:303–311. DOI: 10.1016/j.jobe.2018.03.015.

Ehlen, M., Thomas, M. & Bentz, E. 2009. Life-365 Service Life Prediction Model ™. *Concrete International*. (May):41–46.

El-Reedy, M.A. 2019. *Assessment, Evaluation, and Repair of Concrete, Steel, and Offshore Structures*. Taylor & Francis. DOI: 10.1201/9780429425455.

Emborg, M. & Bernander, S. 1994. Assessment of Risk of Thermal Cracking in Hardening Concrete. *Journal of Structural Engineering*. 120(10):2893–2912.

European Commission. n.d. *Probabilistic Performance Based Durability Design of Concrete Structures*. Available: https://cordis.europa.eu/project/id/BRPR950132 [2022, May 10].

European Committe for Standardisation (CEN). 2004. *Eurocode 2: Design of concrete structures - Part 1-1: General rules and rules for buildings*. Brussels: European Committee for Standardisation.

Francois, R. & Arliguie, G. 1999. Effect of micro-cracking and cracking on the development of corrosion in reinforced concrete members. *Magazine of Concrete Research*.

Fredericks, B. 2019. Examination of Flexural Crack Width Prediction in Concrete: Comparison of Analytical and Numerical Models. University of Cape Town.

Fregonara, E., Ferrando, D.G. & Pattono, S. 2018. Economic-environmental sustainability in building projects: Introducing risk and uncertainty in LCCE and LCCA. *Sustainability*. 10(6). DOI: 10.3390/su10061901.

Gaythwaite, J.W. 2016. *Design of Marine Facilities - Engineering for Port and Harbor Structures*. 3rd ed. American Society of Civil Engineers (ASCE).

Geiker, M., Danner, T., Michel, A., Belda Revert, A., Linderoth, O. & Hornbostel, K. 2021. 25 Years of Field Exposure of Pre-Cracked Concrete Beams; Combined Impact of Spacers and Cracks on Reinforcement Corrosion. *Construction and Building Materials*. 286:1–18. DOI: 10.1016/j.conbuildmat.2021.122801.

Ghasemzadeh, F. & Pour-Ghaz, M. 2015. Effect of Damage on Moisture Transport in Concrete. *Journal of Materials in Civil Engineering*. 27(9). DOI: 10.1061/(asce)mt.1943-5533.0001211.

Gojević, A., Ducman, V., Grubeša, I.N., Baričević, A. & Pečur, I.B. 2021. The effect of crystalline waterproofing admixtures on the self-healing and permeability of concrete. *Materials*. 14(8). DOI: 10.3390/ma14081860.

Gulikers, J. 2005. Numerical modelling of reinforcement corrosion in concrete. In *Corrosion in Reinforced Concrete Structures*. H. Bohni, Ed. Cambridge, England: Woodhead Publishing. 71–90. DOI: 10.1533/9781845690434.71.

Hart, J., D'Amico, B. & Pomponi, F. 2021. Whole-life embodied carbon in multistory buildings: Steel, concrete and timber structures. *Journal of Industrial Ecology*. 25(2):403–418. DOI: 10.1111/jiec.13139.

Holt, E. & Leivo, M. 2004. Cracking risks associated with early age shrinkage. *Cement and Concrete Composites*. 26(5):521–530. DOI: 10.1016/S0958-9465(03)00068-4.

Jamali, A., Angst, U., Adey, B. & Elsener, B. 2013. Modeling of corrosion-induced concrete cover cracking: A critical analysis. *Construction and Building Materials*. 42:225–237. DOI: 10.1016/j.conbuildmat.2013.01.019.

Japan Society of Civil Engineers (JSCE). 2010a. *Standard Specifications for Concrete Structures - 2007: Materials and Construction (JSCE Guidelines for Concrete No. 16)*. Tokyo, Japan: Japan Society of Civil Engineers.

Japan Society of Civil Engineers (JSCE). 2010b. *Standard Specifications for Concrete Structures-2007: Design (JSCE Guidelines for Concrete No. 15)*. Tokyo, Japan: Japan Society of Civil Engineers.

Jappie, L. 2019. Literature Review of the Use of Common Protective Coatings for Concrete Structures with Experiences in the South African Context. University of Cape Town.

Käthler, C.B., Angst, U.M., Hornbostel, K. & Elsener, B. 2020a. Critical analysis of experiments on reinforcing bar corrosion in cracked concrete. *ACI Materials Journal*. 117(3):145–154. DOI: 10.14359/51722408.

Käthler, C.B., Angst, U.M., Hornbostel, K. & Elsener, B. 2020b. Chloride-induced reinforcement corrosion in cracked concrete: the influence of time of wetness on corrosion propagation. *Corrosion Engineering Science and Technology*. 1–10. DOI: 10.1080/1478422X.2020.1789371.

Kheaw-on, T., Khomwan, N. & Sujjavanich, S. 2021. The Effect of Crystalline Waterproofing Materials on Accelerated Corrosion of Steel Reinforcement in Concrete. *International Journal of Civil Engineering*. 19(6):699–716. DOI: 10.1007/s40999-020-00593-6.

Knoeri, C., Sanyé-Mengual, E. & Althaus, H.J. 2013. Comparative LCA of recycled and conventional concrete for structural applications. *International Journal of Life Cycle Assessment*. 18(5):909–918. DOI: 10.1007/s11367-012-0544-2.

Kubba, S. 2010. *Green Construction Project Management and Cost Oversight*. 1st ed. Oxford, United Kingdom: Elsevier. DOI: 10.1016/b978-1-85617-676-7.00007-5.

Lai, J., Cai, J., Chen, Q.J., He, A. & Wei, M.Y. 2020. Influence of crack width on chloride penetration in concrete subjected to alternating wetting-drying cycles. *Materials*. 13(17). DOI: 10.3390/MA13173801.

Lapi, M., Orlando, M. & Spinelli, P. 2018. A review of literature and code formulations for cracking in R/C members. *Structural Concrete*. 19(5):1481–1503. DOI: 10.1002/suco.201700248.

Li, K. & Li, L. 2019. Crack-altered durability properties and performance of structural concretes. *Cement and Concrete Research*. 124(July):1–11. DOI: 10.1016/j.cemconres.2019.105811.

Li, Z. & Liang, W. 2011. *Advanced Concrete Technology*. Hoboken, New Jersey, United States of America: John Wiley & Sons, Inc.

Life-365. n.d. *The Life-365 Consortium*. Available: http://www.life-365.org/consortium.html [2022, May 09].

Lu, C., Liu, R.. & Jin, W.. 2010. Modeling of time to corrosion-induced cover cracking in reinforced concrete structures. In *Fracture Mechanics of Concrete and Concrete Structures - Assessment, Durability, Monitoring and Retrofitting of Concrete Structures*. Korea Concrete Institute. 967–975.

Lu, C.H., Li, H. & Liu, R.G. 2017. Chloride transport in cracked RC beams under dry-wet cycles.

Magazine of Concrete Research. 69(9):453–466. DOI: 10.1680/jmacr.16.00364.

Lun, P.Y., Zhang, X.G., Jiang, C., Ma, Y.F. & Fu, L. 2021. Modelling of corrosion-induced concrete cover cracking due to chloride attacking. *Materials*. 14(6). DOI: 10.3390/ma14061440.

Ma, L., Zhao, Y. & Gong, J. 2019. Effect of restrained shrinkage cracking on chloride penetration of high-performance concrete containing fly ash and ground-granulated blast-furnace slag. *Structural Concrete*. 20(5):1561–1571. DOI: 10.1002/suco.201900099.

El Maaddawy, T. & Soudki, K. 2007. A model for prediction of time from corrosion initiation to corrosion cracking. *Cement and Concrete Composites*. 29(3):168–175. DOI: 10.1016/j.cemconcomp.2006.11.004.

Mackechnie, J.R. & Alexander, M.G. 2001. *Research Monograph No.5: Repair principles for corrosion-damaged reinforced concrete structures*. Cape Town, South Africa.

McLeod, C.H. & Viljoen, C., 2019. Quantification of crack prediction models in reinforced concrete under flexural loading. *Structural Concrete*, 20(6): 2096-2108.

Mihashi, H. & Leite, J.P.D.B. 2004. State-of-the-art report on control of cracking in early age concrete. *Journal of Advanced Concrete Technology*. 2(2):141–154. DOI: 10.3151/jact.2.141.

Miyagawa, T. 1985. Early Chloride Corrosion of Reinforcing Steel in Concrete. Kyoto University.

Moelich, G.M., Kruger, J. & Combrinck, R. 2020. Plastic shrinkage cracking in 3D printed concrete. *Composites Part B*. 1-16.

Mosley, W.H., Bungey, J.H. & Hulse, R. 2007. *Reinforced Concrete Design to Eurocode 2*. 6th ed. Palgrave Macmillan. DOI: 10.1007/978-1-349-14911-7_6.

Müller, H.S., Haist, M. & Vogel, M. 2014. Assessment of the sustainability potential of concrete and concrete structures considering their environmental impact, performance and lifetime. *Construction and Building Materials*. 67:321–337. DOI: 10.1016/j.conbuildmat.2014.01.039.

Nilsson, L. 2003. Durability concept ; pore structure and transport processes. In *Advanced Concrete Technology*. J. Newman & B.S. Choo, Eds. Elsevier Ltd.

Nilsson, L.O. 2019. Corrosion of steel in concrete. In *Developments in the Formulation and Reinforcement of Concrete*. 2nd ed. S. Mindess, Ed. Woodhead Publishing. 115–129. DOI: 10.1016/B978-0-08-102616-8.00005-8.

Oslakovic, I., Bjegovic, D. & Mikulic, D. 2010. Evaluation of service life design models on concrete structures exposed to marine environment. *Materials and Structures/Materiaux et Constructions*. 43(10):1397–1412. DOI: 10.1617/s11527-010-9590-z.

Otieno, M.B. 2014. The Development of Empirical Chloride-induced Corrosion Rate Prediction Models for Cracked and Uncracked Steel Reinforced Concrete Structures in the Marine Tidal Zone. University of Cape Town.

Otieno, M., Beushausen, H. & Alexander, M. 2012. Towards incorporating the influence of cover cracking on steel corrosion in RC design codes: the concept of performance-based crack width limits. *Materials and Structures*. 45:1805–1816. DOI: 10.1617/s11527-012-9871-9.

Otieno, M., Beushausen, H. & Alexander, M. 2016. Chloride-induced corrosion of steel in cracked concrete - Part I: Experimental studies under accelerated and natural marine environments. *Cement and Concrete Research*. 79:373–385. DOI: 10.1016/j.cemconres.2015.08.009.

Otieno, M.B., Alexander, M.G. & Beushausen, H.D. 2010. Corrosion in cracked and uncracked concrete - influence of crack width, concrete quality and crack reopening. *Magazine of Concrete Research*. 62(6):393–404. DOI: 10.1680/macr.2010.62.6.393.

Otieno, M.B., Beushausen, H.D. & Alexander, M.G. 2011. Modelling corrosion propagation in reinforced concrete structures - A critical review. *Cement and Concrete Composites*. 33(2):240–245. DOI: 10.1016/j.cemconcomp.2010.11.002.

Owens, G. Ed. 2013. *Fundamentals of Concrete*. 3rd ed. Midrand, South Africa: The Concrete Institute.

Paul, D.R. & Zietman, J. 1999. Design of Counterfort Units for Quay in Saldanha Bay. In *PIANC-COPEDEC IV*. Cape Town, South Africa.

Pillai, R.G. & Annapareddy, A. 2013. Service life prediction models for chloride-laden concrete structures: A review and nomographs. *International Journal of 3 R's*. 4(2):563–580.

PRDW. n.d. *St Helena Island: Rupert's Bay permanent wharf*. Available: https://prdw.com/st-helena-island-ruperts-bay-permanent-wharf/ [2022, March 30].

Principallo, A. 2020. Study on permeability of cracked concrete. *ACI Materials Journal*. 117(6):151–164. DOI: 10.14359/51725997.

Rahimi, A., Gehlen, C., Reschke, T. & Westendarp, A. 2014. Approaches for modelling the residual service life of marine concrete structures. *International Journal of Corrosion*. 2014:1–11. DOI: 10.1155/2014/432472.

Ramezanianpour, A.A., Ghoreishian, S.A.H., Ahmadi, B., Balapour, M. & Ramezanianpour, A.M. 2018. Modeling of chloride ions penetration in cracked concrete structures exposed to marine environments. *Structural Concrete*. 19(5):1460–1471. DOI: 10.1002/suco.201700285.

Raupach, M. 1996. Chloride-induced macrocell corrosion of steel in concrete - Theoretical background and practical consequences. *Construction and Building Materials*. 10(5 SPEC. ISS.):329–338. DOI: 10.1016/0950-0618(95)00018-6.

Richardson, M.G. 2002. *Fundamentals of Durable Reinforced Concrete*. London, United Kingdom: Spon Press.

Safiuddin, M., Kaish, A.B.M.A., Woon, C.O. & Raman, S.N. 2018. Early-age cracking in concrete: Causes, consequences, remedialmeasures, and recommendations. *Applied Sciences*. 8(10). DOI: 10.3390/app8101730.

Santhanam, M. & Otieno, M. 2016. Deterioration of concrete in the marine environment. In *Marine Concrete Structures*. M. Alexander, Ed. Duxford, United Kingdom: Woodhead Publishing. 137–149.

Schiessl, P. & Lay, S. 2005. Influence of concrete composition. In *Corrosion in Reinforced Concrete Structures*. H. Bohni, Ed. Cambridge, England: Woodhead Publishing. 91–134. DOI: 10.1533/9781845690434.91.

Schießl, P. & Raupach, M. 1997. Laboratory Studies and Calculations on the Influence of Crack Width on Chloride-Induced Corrosion of Steel in Concrete. *ACI Materials Journal*. 94(1):56–61.

Scott, A. & Alexander, M.G. 2007. The influence of binder type, cracking and cover on corrosion rates of steel in chloride- contaminated concrete. *Magazine of Concrete Research*. 59(7):495–505. DOI: 10.1680/macr.2007.59.7.495.

Selander, A. 2010. *Hydrophobic Impregnation of Concrete Structures - Effects on Concrete Properties*. Stockholm, Sweden.

Shaikh, F.U.A. 2018. Effect of Cracking on Corrosion of Steel in Concrete. *International Journal of Concrete Structures and Materials*. 12(1). DOI: 10.1186/s40069-018-0234-y.

Sideris, K.K., Chatzopoulos, A., Tassos, C. & Manita, P. 2019. Durability of concretes prepared with crystalline admixtures. *MATEC Web of Conferences*. 289. DOI: 10.1051/matecconf/201928909003.

Smith, P.E. 2016a. Design and specification of marine concrete structures. In *Marine Concrete Structures*. M. Alexander, Ed. Duxford, United Kingdom: Woodhead Publishing. 65–114.

Smith, P.E. 2016b. Types of marine concrete structures. In *Marine Concrete Structures*. M. Alexander, Ed. Duxford, United Kingdom: Woodhead Publishing. 17–64.

Sohawon, H. 2018. Service life extension of reinforced concrete structures using hydrophobic impregnation. University of Cape Town.

Sousa-Coutinho, J. 2009. Properties of hardened concrete. In *ICE Manual of Construction Materials*. ICE Publishing. 153–167. DOI: 10.4324/9780203487754.ch3.

South African National Standards. 2010. *Basis of structural design and actions for buildings and industrial structures, Part 2: Self-weight and imposed loads. (SANS 10160-2)*. Pretoria: South African National Standards.

South African National Standards. 2014. *The structural use of concrete, Part 2 : Materials and execution of work (SANS 10100-2)*. Pretoria: South African National Standards.

Standards Australia. 2005. *Guidelines for the design of maritime structures (AS 4997)*. Sydney, Australia: Standards Australia.

Stevens, A.J. 1978. The Economics of Buildings: Life Cycle Costing. University of Cape Town.

Strohmeier, J.H. 1994. Deterioration of reinforced concrete in a marine environment: repair costs and maintenance strategies. University of Cape Town.

Tang, L., Utgenannt, P. & Boubitsas, D. 2015. Durability and Service Life Prediction of Reinforced Concrete Structures. *Journal of the Chinese Ceramic Society*. 43(10):1408–1419.

The British Standards Institution. 2010. *Maritime works – Part 2: Code of practice for the design of quay walls, jetties and dolphins*.

The British Standards Institution. 2013a. *Maritime works – Part 1-4 : General – Code of practice for materials (BS 6349-1-4:2013)*. BSI Standards Limited.

The British Standards Institution. 2013b. *Maritime works – Part 1-1 : General – Code of practice for planning and design for operations (BS 6349-1-1:2013)*. BSI Standards Limited.

The Concrete Society. 2015. *Relevance of Cracking in Concrete to Reinforcement Corrosion, Technical Report 44*. Hampshire, United Kingdom.

The Institution of Structural Engineers. 2020. *How to Calculate Embodied Carbon*. 1st ed. London, United Kingdom: The Institution of Structural Engineers.

Thomas, M. 2016. The durability of concrete for marine construction: materials and properties. In *Marine Concrete Structures*. M.G. Alexander, Ed. Duxford, United Kingdom: Woodhead Publishing.

Torrijos, M.C., Giaccio, G. & Zerbino, R. 2010. Internal cracking and transport properties in damaged concretes. *Materials and Structures*. 43(SUPPL. 1):109–121. DOI: 10.1617/s11527-010-9602-z.

Tuutti, K. 1982. Corrosion of steel in concrete. [Doctoral Thesis (monograph), Division of Building Materials]. Swedish Cement and Concrete Research Institute, Stockholm.

Val, D. V. & Stewart, M.G. 2003. Life-cycle cost analysis of reinforced concrete structures in marine environments. *Structural Safety*. 25(4):343–362. DOI: 10.1016/S0167-4730(03)00014-6.

Van Belleghem, B., Van den Heede, P., Van Tittelboom, K. & De Belie, N.D. 2017. Quantification of the service life extension and environmental benefit of Chloride Exposed Self-Healing Concrete. *Materials*. 10(1). DOI: 10.3390/ma10010005.

Van Cauteren, D., Ramon, D., Stroeckx, J., Allacker, K. & Schevenels, M. 2022. Design optimization of hybrid steel/timber structures for minimal environmental impact and financial cost: A case study. *Energy and Buildings*. 254. DOI: 10.1016/j.enbuild.2021.111600.

Van Hung, N., Hung, V.V. & Viet, T.B. 2018. The effect of crack width on the service life of reinforced concrete structures. *IOP Conference Series: Earth and Environmental Science*. 143(1). DOI: 10.1088/1755-1315/143/1/012044.

Voo, Y.L., Sittampalam, K., Peng, C.W. & Singh, S. 2014. Design of Ultra-High Performance Concrete Jetty in Marine Environment. *Proceedings of the 12th International Conference on Concrete Engineering & Technology*. (December):1–8.

Wang, K., Jansen, D.C., Shah, S.P. & Karr, A.F. Permeability study of cracked concrete. *Cement and*

Concrete Research. 27(3): 381-393.

Wang, X.Y. & Zhang, L.N. 2016. Simulation of Chloride Diffusion in Cracked Concrete with Different Crack Patterns. *Advances in Materials Science and Engineering*. 2016. DOI: 10.1155/2016/1075452.

Xi, X. & Yang, S. 2017. Time to surface cracking and crack width of reinforced concrete structures under corrosion of multiple rebars. *Construction and Building Materials*. 155:114–125. DOI: 10.1016/j.conbuildmat.2017.08.051.

Xypex. 2022. *ADMIX C-500/C-500 NF product data sheet*. Richmond, Canada: Xypex Chemical Corporation.

Yang, L., Li, K. & Pang, X. 2013. Design and optimization of maintenance strategies for a long life-span port project. *Materials and Structures*. 46:161–172. DOI: 10.1617/s11527-012-9891-5.

Younis, A., Ebead, U. & Judd, S. 2018. Life cycle cost analysis of structural concrete using seawater, recycled concrete aggregate, and GFRP reinforcement. *Construction and Building Materials*. 175:152–160. DOI: 10.1016/j.conbuildmat.2018.04.183.

Yu, L., François, R., Dang, V.H., L'Hostis, V. & Gagné, R. 2015. Development of chloride-induced corrosion in pre-cracked RC beams under sustained loading: Effect of load-induced cracks, concrete cover, and exposure conditions. *Cement and Concrete Research*. 67:246–258. DOI: 10.1016/j.cemconres.2014.10.007.

Zhang, W., François, R. & Yu, L. 2020. Influence of load-induced cracks coupled or not with top-casting-induced defects on the corrosion of the longitudinal tensile reinforcement of naturally corroded beams exposed to chloride environment under sustained loading. *Cement and Concrete Research*. 129(October 2019):1–20. DOI: 10.1016/j.cemconres.2020.105972.

Zhang, Y., Zhang, S., Wei, G., Wei, X., Jin, L. & Xu, K. 2019. Water Transport in Unsaturated Cracked Concrete under Pressure. *Advances in Civil Engineering*. 2019. DOI: 10.1155/2019/4504892.

Appendix A: Matola Jetty Beam Design Calculation Sheets

Please find the calculation sheets attached on the following page.

	LOADING CALCULATIONS	
	Member: Matola jetty crane rail beam (Beam B402)	

Project:	MSc.Eng. Structural Engineering – Research
Sheet Series:	A (Loading Calculations)
Calculations By:	Nicholas Elias
Date:	28/01/2022

Date	Check No.	Checked By	Review Level	Approved
29/03/2022	A-01	P.E.S	-	Yes

Check No.	Check Notes	Action	Status
A-01			

Overview of Member	
Structure Type:	Coal export jetty
Member Type:	Reinforced concrete crane rail beam
Member Loads:	Self-weight of structural components
	Vehicle loads
	Live (imposed) loads
	Shiploader loads

Reference	INTRODUCTION
	The aim of these calculations is to convert the general loading information for the Matola jetty structure, supplied by PRDW Consulting Port and Coastal Engineers, into point and distributed loads to be applied to a typical crane rail beam (Beam B402) in the analysis stage of the design. The following calculations are presented in this calculation sheet: 1. Self-weight 2. Vehicle Loads 3. Live Loads 4. ELB Shiploader 5. Sandvik Shiploader 6. Load Combinations: ULS 7. Load Combinations: SLS 8. Load Combinations: Crack Width Design The design of the Matola jetty crane rail beam continues with the member analysis in Series B (Member Analysis) of these calculation sheets.
	1. SELF-WEIGHT CALCULATIONS
	From the design information provided by PRDW, it can be seen that there are three structural components whose self-weight needs to be considered in the design of beam B402: i. The vehicle barrier on the seaside of the jetty deck ii. The jetty deck slabs iii. Beam B402 itself These components are shown in Figure 1 below, which has been adapted from the drawings provided from PRDW. In order to simplify the calculations, the cross-sectional areas of the three components are taken to be as for the shaded rectangular areas shown in Figure 1.

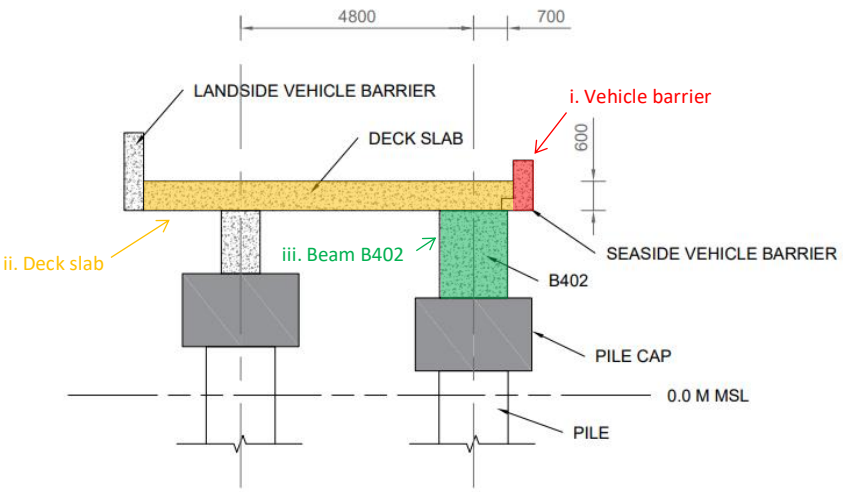

Figure 1: A simplified cross-section of a portion of the Matola jetty, adapted from the drawings provided by PRDW.

i. Vehicle Barrier Self-Weight

A value for the seaside vehicle barrier self-weight was provided in the loading calculations supplied by PRDW. However, as a portion of the vehicle barrier cross-section is included within the deck slab cross-section (see Figure 1), using the vehicle barrier self-weight provided by PRDW would result in an overestimation of the total self-weight acting on Beam B402.

The characteristic self-weight of the vehicle barrier, $w_{VB,c}$, is instead found using the following equation:

$$w_{VB,c} = \gamma_c \times A_{VB}$$

Where γ_C is the unit weight of reinforced concrete, and A_{VB} is the cross-sectional area of the vehicle barrier.

SANS 10160-2 Table A.1

γ_C = 24 kN/m^3 (assume nominal amount of reinforcement)

A_{VB} = 0.400 m x 1.030 m = 0.412 m^2, where the dimensions for the vehicle barrier are taken from the drawings provided by PRDW.

$$\therefore w_{VB,c} = 24\ \frac{kN}{m^3} \times 0.412\ m^2 = 9.89\ kN/m$$

Note that, as $w_{VB,c}$ acts at an eccentricity from the centreline of Beam B402, $w_{VB,c}$ will also exert a torsional moment on Beam B402. The magnitude of this moment, $T_{VB,c}$, can be calculated as follows:

$$T_{VB,c} = w_{VB,c} \times lever\ arm = 9.89\ kN/m \times\ 0.9\ m = \mathbf{8.90\ kN/m}$$

ii. Deck Slab Self-Weight

The characteristic self-weight of the deck slab, $w_{DS,c}$, which acts on Beam B402 can be found from the following equation:

$$w_{DS,c} = \gamma_c \times A_{DS}$$

Where γ_C = 24 kN/m^3, as before, and A_{DS} is the cross-sectional area of the portion of the deck slab supported by Beam B402.

Using the dimensions shown in Figure 1, A_{DS} = [0.7m + ½ (4.8m)] x 0.6 m = 1.86 m^2.

$$\therefore w_{DS,c} = 24\ \frac{kN}{m^3} \times 1.86\ m^2 = 44.64\ kN/m$$

iii. Beam B402 Self-Weight

The characteristic self-weight of Beam B402 can be found from the following equation:

$$w_{B402,c} = \gamma_c \times A_{B402}$$

Where γ_C = 24 kN/m^3, as before, and A_{B402} is the cross-sectional area of Beam B402.

Given that the dimensions of Beam B402 are 1400 mm x 1800 mm, A_{B402} = 1.4 m x 1.8 m = 2.52 m^2.

$$\therefore w_{B402,c} = 24\ \frac{kN}{m^3} \times 2.52\ m^2 = 60.48\ kN/m$$

iv. Summary

A summary of the self-weight calculations is shown in Table 1.

Table 1: Summary of the self-weight calculations.

Component	Self-Weight [kN/m]
Landside vehicle barrier	9.89
Deck slab	44.64
Beam B402	60.48
Σ	**115.0**

It can therefore be seen that the **total characteristic self-weight acting on Beam B402, $w_{S,c}$, is 115 kN/m**. The **total characteristic torsional moment acting on Beam B402 due to the self-weight of the vehicle barrier, $T_{VB,c}$, is 8.90 kNm/m.**

2. VEHICLE LOAD CALCULATIONS

In accordance with the loading calculations provided by PRDW, a vehicle load of 5.5 kN/m^2 was assumed to act over the entire deck. The characteristic vehicle load, $w_{V,c}$, acting on Beam B402 can therefore be calculated as follows:

$$w_{V,c} = 5.5\ \frac{kN}{m^2} \times tributary\ width\ of\ deck\ slab$$

The tributary width of the deck slab (i.e., the width of deck slab for which the applied vehicle load is supported by Beam B402) = 1/2 (4.8 m) + 0.7 m = 3.1 m.

$$\therefore w_{V,c} = 5.5\ \frac{kN}{m^2} \times 3.1\ m = 17.05\ kN/m$$

It can therefore be seen that the **total characteristic vehicle load acting on Beam B402, $w_{V,c}$, is 17.1 kN/m**.

3. LIVE LOAD CALCULATIONS

From the drawings provided by PRDW, it can be seen that Beam B402 supports the live loads which are applied to the access platforms on the seaward side of the jetty. It is assumed that the self-weight of the access platforms themselves is negligible.

In accordance with the loading calculations provided by PRDW, a characteristic live load of 3.0 kN/m^2 was applied to the access platforms. This resulted in a line load of 6.6 kN/m being applied to Beam B402. The access platforms, which are positioned at an eccentricity from Beam B402, will also result in a torsional moment of 7.3 kNm/m being applied to Beam B402.

It can therefore be seen that the **total characteristic live load acting on Beam B402, $w_{L,c}$, is 6.6 kN/m**, and that the **total characteristic torsional moment caused by this load, $T_{L,c}$, is 7.3 kNm/m**.

4. ELB SHIPLOADER CALCULATIONS

The following ELB shiploader dimensions were provided by PRDW:

- 0.82 m wheel spacing
- 1.82 m bogie spacing
- Four legs, two each on the seaside and landside
- Eight wheels for each seaside leg, and six wheels for each landside leg
- Seaside leg spacing: 12 m (centre to centre)
- Landside leg spacing: 13 m (centre to centre)

The B402 beams will support the seaside legs of the shiploader. It was assumed that each seaside leg has four bogies, each with two wheels.

For a typical B402 beam, there are two possible critical positions of the ELB shiploader:

- With the centre of one of the seaside legs placed at midspan of the beam, as shown in Figure 2.
- With the centre of the shiploader placed at midspan of the beam, as shown in Figure 3.

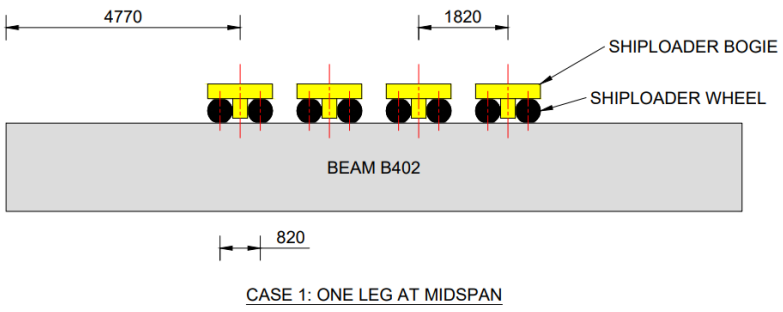

Figure 2: A sketch showing the wheels of a seaside leg of the ELB shiploader at midspan of Beam B402. Note that all dimensions are in mm.

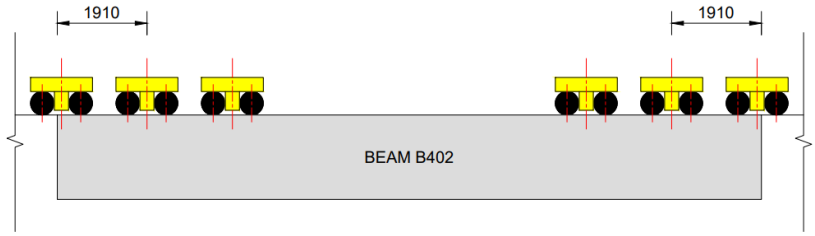

Figure 3: A sketch showing the wheels of the seaside legs of the ELB shiploader, with the shiploader at midspan of Beam B402. Note that all dimensions are in mm.

Loading information was provided by PRDW for both legs of the ELB shiploader. A summary of this loading information, for the seaside legs of the ELB shiploader, is shown in Table 2.

Both vertical (Z) and horizontal (X, perpendicular to the jetty) shiploader loads will be considered in the analysis of Beam B402. It is assumed that the horizontal components of the shiploader loads along the jetty (in the Y-direction) will not have a significant effect on the beams.

Table 2: A summary of the seaside leg loading information provided by PRDW.

Shiploader Situation	**Seaside Leg Load Per Wheel [kN]**		
	Z	X	Y
Parked	175	5	5.63
Operating (Extreme)	260	10	6.25

From Table 2, it can be seen that there are two possible shiploader situations to consider – parked and operating (extreme). The "**parked**" condition will be used in the **SLS analysis of the beam**, while the "**operating**" condition will be used in the **ULS analysis of the beam**. The resultant SLS and ULS wheel loads on Beam B402 are shown in Table 3.

Table 3: SLS and ULS ELB shiploader loads acting on Beam B402.

Analysis Type	Seaside ELB Shiploader Loads [kN]			
	Per Leg		Per Wheel	
	Z	X	Z	X
SLS	1400	40	175	5
ULS	2080	80	260	10

5. SANDVIK SHIPLOADER CALCULATIONS

The following Sandvik shiploader dimensions were provided by PRDW:

- 0.85 m wheel spacing
- 1.82 m bogie spacing
- Three legs, two on the seaside and one on the landside
- Ten wheels for each seaside leg, and twelve wheels for the landside leg
- Seaside leg spacing: 10 m (centre to centre)

The B402 beams will support the seaside legs of the shiploader. It was assumed that each seaside leg has five bogies, each with two wheels.

For a typical B402 beam, there are three possible critical positions of the Sandvik shiploader:

- With the centre of one of the seaside legs placed at midspan of the beam, as shown in Figure 4.
- With the centre of the shiploader placed at midspan of the beam, as shown in Figure 5.
- With one leg fully on the beam, and three bogies of the other leg on the beam, as shown in Figure 6.

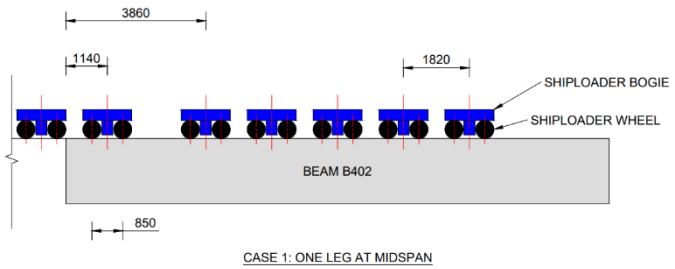

Figure 4: A sketch showing the wheels of a seaside leg of the Sandvik shiploader at midspan of Beam B402. Note that all dimensions are in mm.

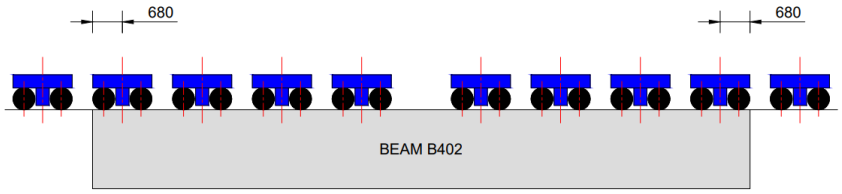

Figure 5: A sketch showing the wheels of the seaside legs of the Sandvik shiploader, with the shiploader at midspan of Beam B402. Note that all dimensions are in mm.

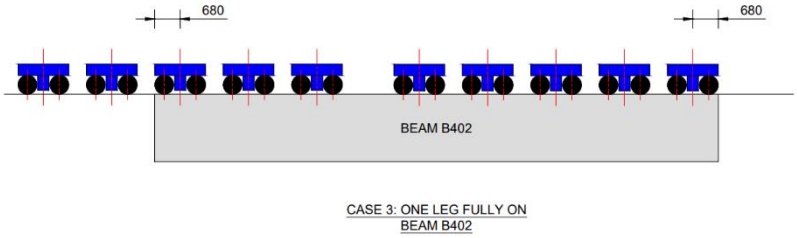

Figure 6: A sketch showing the wheels of the seaside legs of the Sandvik shiploader, with one leg fully on Beam B402.

Loading information was provided by PRDW for both legs of the Sandvik shiploader. A summary of this loading information, for the seaside legs of the Sandvik shiploader, is shown in Table 4.

Table 4: A summary of the seaside leg loading information provided by PRDW.

Shiploader Situation	**Seaside Leg Load Per Wheel [kN]**					
	East Leg			West Leg		
	Z	X	Y	Z	X	Y
Operating (Extreme)	175	26.25	26.25	211	31.65	31.65

It can thus be seen that there is only one case to consider for the Sandvik shiploader – the operating (extreme) case. This is as the Sandvik shiploader will only be used when the ELB shiploader is being serviced. As such, **the Sandvik shiploader loads shown in Table 4 above will only be used for the ULS analysis of the beam.**

6. LOAD COMBINATIONS: ULS

The load combinations which are to be considered for the ULS design of Beam B402 are shown in Table 5 below. The relevant partial and combination factors are shown in Table 6 and 7, respectively. The final factorted loads for the ULS analysis of Beam B402 are then shown in Tables 8 and 9.

Table 5: Load combinations to be used in the ULS design of Beam B402.

Load Combination	Combination Definition	Leading Load
U-A	D + L + V + E	E
U-B	D + L + V + S	S
U-C-1	D + L + V	L
U-C-2	D + L + V	V
Definition of Loads		
D	Self-weight of the beam and other structural components	
V	Vehicle load	
L	Live load	
E	ELB shiploader loads	
S	Sandvik shiploader loads	

BS 6349 Part 2
Table A.1 Set B

Table 6: ULS partial factors, taken from BS 6349.

Load	Partial Factor
Self-weight (D)	1.35
Vehicle load (V)	1.5
Live load (L)	1.35
Shiploader load (E or S)	1.35

BS 6349 Part 2
Table A.2

Table 7: ULS combination factors, taken from BS 6349.

Load	Combination Factor
Self-weight (D)	1.0
Vehicle load (V)	0.7
Live load (L)	0.75
Shiploader load (E or S)	0.75

Table 8: Factored vertical loads for the ULS analysis of Beam B402.

	ULS Factored Vertical Load				
Load Combination	D [kN/m]	V [kN/m]	L [kN/m]	E[a] [kN]	S[a] [kN]
U-A	155.3	18.0	6.7	351.0	-
U-B	155.3	18.0	6.7	-	236.3/284.9[b]
U-C-1	155.3	18.0	8.2	-	-
U-C-2	155.3	25.7	6.7	-	-

a. Shiploader loads given are loads per wheel.

b. East leg/West leg of the Sandvik shiploader.

Table 9: Factored torsional loads for the ULS analysis of Beam B402.

	ULS Factored Torsional Load			
Load Combination	D [kNm/m]	L [kNm/m]	E[a] [kNm]	S[a] [kNm]
U-A	12.0	7.4	12.15	-
U-B	12.0	7.4	-	31.9/38.5[b]
U-C-1	12.0	9.9	-	-
U-C-2	12.0	7.4	-	-

a. Shiploader loads given are loads per wheel, which have been converted from horizontal point loads by multiplying by the eccentricity (0.9 m) between the point of horizontal point load application and the centroid of Beam B402.

b. East leg/West leg of the Sandvik shiploader

7. LOAD COMBINATIONS: SLS

The load combinations which are to be considered for the SLS design of Beam B402 are shown in Table 10 on the following page.

In accordance with the original loading calculations for the Matola jetty provided by PRDW, partial and load combination factors of 1.0 were used for the SLS design of Beam B402. The resultant vertical and torsional loads to be used in the SLS analysis of Beam B402 are therefore shown in Tables 11 and 12 on the following page.

Table 10: Load combinations to be used in the SLS design of Beam B402

Load Combination	Combination Definition	Leading Load
S-A	D + L + V + E	-
S-B[a]	-	-
S-C	D + L + V	-
Definition of Loads		
D	Self-weight of the beam and other structural components	
V	Vehicle load	
L	Live load	
E	ELB shiploader loads	
S	Sandvik shiploader loads	

a. Load combination B not considered in the SLS case, as the Sandvik shiploader is only used when the ELB shiploader is being serviced.

Table 11: Factored vertical loads for the SLS design of Beam B402.

	SLS Factored Vertical Load				
Load Combination	D [kN/m]	V [kN/m]	L [kN/m]	E[a] [kN]	S[a] [kN]
S-A	115.0	17.1	6.6	175	-
S-B[b]	-	-	-	-	-
S-C	115.0	17.1	6.6	-	-

a. Shiploader loads given are loads per wheel.

b. Load combination B not considered for SLS case.

Table 12: Factored torsional loads for the SLS analysis of Beam B402.

	SLS Factored Torsional Load			
Load Combination	D [kNm/m]	L [kNm/m]	E[a] [kNm]	S[a] [kNm]
S-A	8.9	7.3	4.5	-
S-B[b]	-	-	-	-
S-C	8.9	7.3	-	-

a. Shiploader loads given are loads per wheel, which have been converted from horizontal point loads by multiplying by the eccentricity (0.9 m) between the point of horizontal point load application and the centroid of Beam B402.

b. Load combination B not considered for SLS case.

8. LOAD COMBINATIONS: CRACK WIDTH DESIGN

Crack width design is based upon sustained loads (i.e., loads which result in cracks remaining open for sufficiently long periods of time, such that the cracks may result in corrosion of the reinforcing steel). As such, the analysis required for crack width design must be based on a separate load combination to that used in the SLS analysis, based only on sustained loads.

In the case of Beam B402, this load combination should consider:

- Loads due to self-weight, which are always present
- Loads from the ELB shiploader, as when parked the ELB shiploader represents a significant sustained load

The crack width design factored loads for Beam B402 can therefore be seen in Table 13, where partial and combination factors of 1.0 were used (as for the SLS case), and only vertical loads (which will result in flexural cracking) were considered.

Table 13: Factored vertical loads for the crack width design of Beam B402.

	Crack Width Design (CWD) Factored Vertical Load				
Load Combination	D [kN/m]	V [kN/m]	L [kN/m]	E[a] [kN]	S[a] [kN]
CWD	115.0	-	-	175	-

a. Shiploader loads given are loads per wheel.

CONCLUSION

General loading information provided by PRDW for the Matola jetty has been converted into point and distributed loads to be applied to a typical crane rail beam (Beam B402) for the following cases:

- ULS
- SLS
- Crack Width Design

The resultant loads can be seen in Sections 6 to 8 of these calculation sheets, and were used in the analysis of the beam, as shown in Series B (Member Analysis) of these calculation sheets.

	ANALYSIS CALCULATIONS	
	Member: Matola jetty crane rail beam (Beam B402)	

Project:	MSc.Eng. Structural Engineering – Research
Sheet Series:	B (Analysis Calculations)
Calculations By:	Nicholas Elias
Date:	28/01/2022

Date	Check No.	Checked By	Review Level	Approved
01/03/2022	B-01	P.E.S	-	No
29/03/2022	B-02	P.E.S	-	Yes

Check No.	Check Notes	Action	Status
B-01	Only use continuous beam analysis for design	N.N.E	Complete

Overview of Member	
Structure Type:	Coal export jetty
Member Type:	Reinforced concrete crane rail beam
Member Loads:	Self-weight of structural components
	Vehicle loads
	Live (imposed) loads
	Shiploader loads
Limit States for Analysis:	Ultimate Limit State (ULS)
	Serviceability Limit State (SLS)
	Crack Width Design (CWD)

Reference	INTRODUCTION
	An explanation of the analysis process for Beam B402 of the Matola jetty is provided in these calculation sheets, along with the results of the analysis. The following calculations and results are presented in this calculation sheet: • 1. General Analysis Information • 2. Sample Analysis Outputs • 3. Analysis Results • 4. Analysis Verification: Load Combination U-C-1 • 5. Design Values for Moment, Shear, Torsion and Deflection The design of the Matola jetty crane rail beam continues with the design of the beam in Series C (ULS & SLS Design) of these calculation sheets.
	1. GENERAL ANALYSIS INFORMATION
	Analysis of Beam B402 was conducted using the analysis software *Prokon*, for the load combinations presented in the loading calculations (Series A of these calculation sheets). The beam was analysed with a 15 m span, for the following three support conditions: • Simply supported at both ends • Continuous beam, with the shiploaders placed on an interior span • Continuous beam, with the shiploaders placed on an end span The following specific information, relating to the analysis inputs, is also necessary to understand the results of the analysis: • For load combinations A and B, Beam B402 was analysed with the ELB and Sandvik shiploaders each in multiple possible critical positions. The numbers at the end of a particular shiploader load combination (e.g., U-A-1) refer to the position of the shiploader for that load combination (e.g., shiploader in the first position). For more information on the possible critical positions of the shiploaders, please see Series A (Loading Calculations) of these calculation sheets. • For the analysis of Beam B402 under torsional moments, the ends of the beam were fixed against torsion at both ends. For this reason, the results of the torsional analysis were the same for both the simply supported and continuous beams. • The continuous beams were modelled as having five spans, such that when the shiploaders were placed on the interior spans, no portion of the shiploaders were placed on the end spans.

2. SAMPLE ANALYSIS OUTPUTS

Sample analysis outputs are shown in Figures 1 to 8 below, for load case U-A-1 (ULS analysis, with the ELB shiploader as the leading load, in position 1 (i.e., with one leg at midspan)).

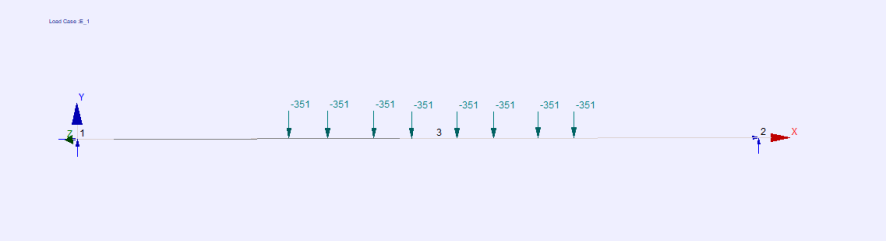

Figure 1: Position of the ELB shiploader loads on Beam B402.

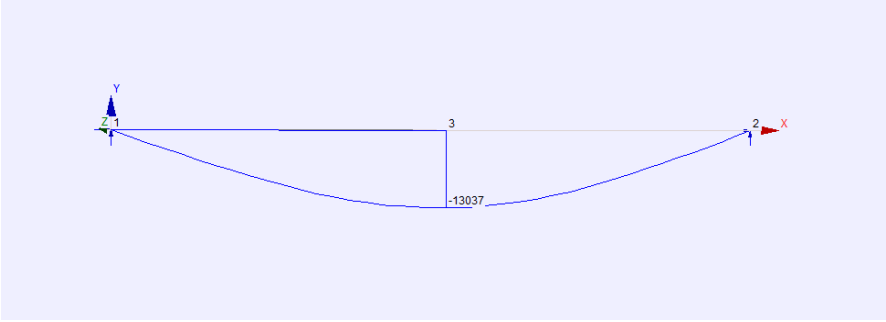

Figure 2: Bending moment diagram for load combination U-A-1, with ends simply supported.

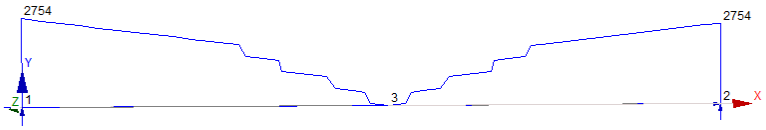

Figure 3: Shear force diagram for load combination U-A-1, with ends simply supported.

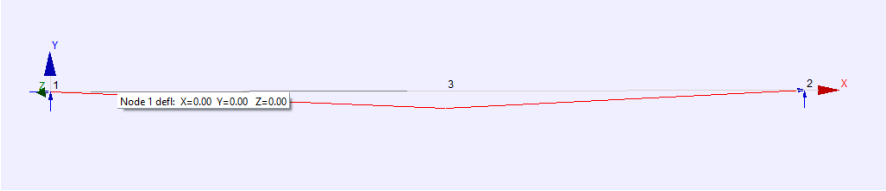

Figure 4: Deflection of Beam B402 for load combination U-A-1, with ends simply supported.

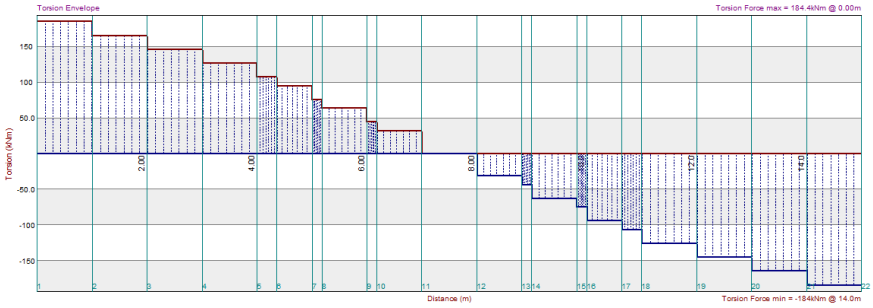

Figure 5: Torsional moment diagram for load combination U-A-1. Note that distributed torsional moments were applied as point moments at metre points.

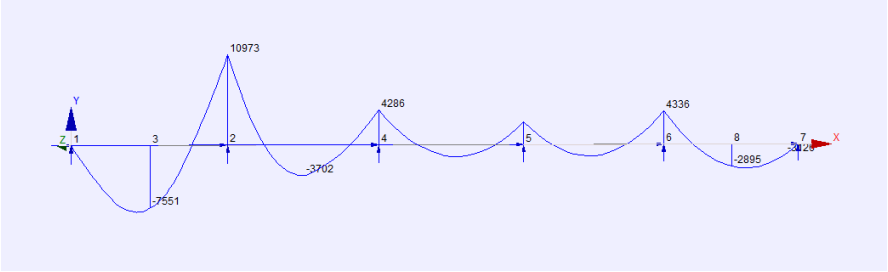

Figure 6: Bending moment diagram for load combination U-A-1, with the ELB shiploader placed on an end span of a continuous beam.

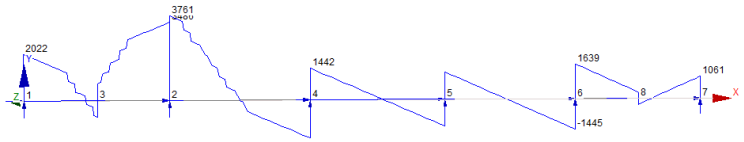

Figure 7: Shear force diagram for load combination U-A-1, with the ELB shiploader placed on an end span of a continuous beam.

Figure 8: Deflection of Beam B402 for load combination U-A-1, with the ELB shiploader placed on an end span of a continuous beam.

3. ANALYSIS RESULTS

Results of the analysis, for all end conditions and load combinations, are shown in Table 1 on pages 5 and 6 below.

Table 1: Results of the analysis – ultimate (maximum) bending moments, shear forces, torsional moments, and deflections for each load combination. ***Note that Table 1 is continued on the following page.***

	Load Combination	Mu [kNm]	Vu [kN]	Tu [kNm]	δ_{max} [mm]
	Simply Supported				
ULS	U-A-1	13037	2754	184.4	17.52
	U-A-2	9197	3105	196.6	13.47
	U-B-1	12783	3211	387.3	17.49
	U-B-2	12172	3541	431.8	17.13
	U-B-3	12726	3352	442.0	17.61
	U-C-1	5105	1361	153.3	7.08
	U-C-2	5279	1408	135.8	7.32
SLS	S-A-1	7877	1740	131.4	10.64
	S-A-2	5962	1915	135.9	8.63
	S-C	3901	1040	113.4	5.41
CWD	CWD-1	7210	1563	-	9.72
	CWD-2	5296	1738	-	7.70
	Continuous, Shiploader on Interior Span				
ULS	U-A-1	5753/-8696	3479	-	5.22
	U-A-2	3522/-5667	3092	-	4.03
	U-B-1	5854/-7448	3332	-	5.90
	U-B-2	5712/-6370	3516	-	6.35
	U-B-3	6057/-7022	3530	-	6.49
	U-C-1	3182/-4296	1648	-	3.50
	U-C-2	3289/-4442	1704	-	3.62
SLS	S-A-1	3368/-5515	2121	-	3.07
	S-A-2	2489/-3695	1915	-	2.8
	S-C	2431/-3283	1259	-	2.62
CWD	CWD-1	3125/-5094	1954	-	2.84
	CWD-2	2074/-3274	1737	-	2.34

*Positive bending moments indicate sagging; negative bending moments indicate hogging.

Table 1 (continued): Results of the analysis – ultimate (maximum) bending moments, shear forces, torsional moments, and deflections for each load combination.

		Continuous, Shiploader on End Span			
ULS	U-A-1	8022/-10973	3761	-	8.39
	U-A-2	6108/-7410	3599	-	7.31
	U-B-1	8231/-9905	3872	-	9.25
	U-B-2	8303/-8504	4108	-	10.05
	U-B-3	8815/-8936	3948	-	10.16
	U-C-1	3182/-4296	1648	-	3.50
	U-C-2	3289/-4442	1704	-	3.62
SLS	S-A-1	4878/-6626	2252	-	5.13
	S-A-2	3919/-4850	2239	-	4.59
	S-C	2431/-3283	1259	-	2.62
CWD	CWD-1	4463/-6065	2066	-	4.67
	CWD-2	3505/-4289	2023	-	4.13

*Positive bending moments indicate sagging; negative bending moments indicate hogging.

4. ANALYSIS VERIFICATION: LOAD COMBINATION U-C-1

The results of the analysis were verified by hand calculations of the ultimate bending moment, shear force and deflection for load combination U-C-1, for the simply supported case.

For load combination U-C-1, three line loads are applied to Beam B402:

- Self-weight, w_D = 155.3 kN/m
- Vehicle load, w_V = 18.0 kN/m
- Live load, w_L = 8.2 kN/m

The total line load acting on beam B402 is therefore 155.3 + 18.0 + 8.2 = 181.5 kN/m.

Redbook Table 5.19

For a simply supported beam subjected to uniform line loads, the ultimate bending moment, shear force and deflection can be calculated as follows:

$$M_u = \frac{wL^2}{8} = \frac{(181.5)(15)^2}{8} = 5104.69\ kNm$$

$$\therefore M_u \approx 5105\ kNm, as\ found\ from\ the\ Prokon\ analysis.$$

$$\therefore okay$$

$$V_u = \frac{wL}{2} = \frac{(181.5)(15)}{2} = 1361.25\ kN$$
$$\therefore V_u \approx 1361\ kN, as\ found\ from\ the\ Prokon\ analysis.$$
$$\therefore okay$$

$$\delta_{max} = \frac{5}{384}\frac{wL^4}{EI}$$

From the Prokon input values, E = 25 GPa = 25 x10^3 N/mm^2, I = 6.76 x10^{11} mm^4

$$\therefore \delta_{max} = \frac{5}{384}\frac{(181.5)(15\,000)^4}{(25 \times 10^3)(6.76 \times 10^{11})} = 7.079\ mm$$
$$\therefore \delta_{max} \approx 7.08\ mm, as\ found\ from\ the\ Prokon\ analysis.$$
$$\therefore okay$$

The hand calculation results therefore verify the analysis results.

5. DESIGN VALUES FOR MOMENT, SHEAR, TORSION AND DEFLECTION

A summary of the maximum moment, shear, torsion, and deflection values for each of the limit states (ULS, SLS, crack width design) is shown in Table 2 below. These are the values which were used in the design of Beam B402.

Note that, while the simply supported configuration produced the greatest bending moments in the beam, **it was decided to not consider these moments, and instead design the beam purely as a continuous beam**. This was done to avoid an overly conservative design, as the beam will only be simply supported during construction. In service (when the ultimate loads will be applied), the beam will be continuous, as in-situ concrete plugs will be used to connect the precast beam elements.

Table 2: A summary of the analysis results.

Limit State	M_u [kNm]	V_u [kN]	T_u [kNm]	δ_{max} [mm]
ULS	8815/-10973	4108	442.0	17.61
SLS	4878/-6626	2252	135.9	10.64
CWD	4463/-6065	2066	-	9.72

CONCLUSION

The results from the analysis of Beam B402 have been presented and verified. These results were used for the design of Beam B402, which can be seen in Series C (ULS and SLS Design) and D (Crack Width Design) of these calculation sheets.

	ULS & SLS DESIGN CALCULATIONS	
	Member: Matola jetty crane rail beam (Beam B402)	

Project:	MSc. Eng. Structural Engineering - Research
Sheet Series:	C (ULS & SLS Calculations)
Calculations By:	Nicholas Elias
Date:	16/03/2022

Date	Checked By	Check No.	Review Level	Approved
29/03/2022	P.E.S	C-01	-	Yes

Check No.	Action	Check Notes	Status
C-01	N.N.E		

Overview of Member	
Structure Type:	Coal export jetty
Member Type:	Reinforced concrete crane rail beam
Member Loads:	Self-weight of structural components
	Vehicle loads
	Live (imposed) loads
	Shiploader loads
Limit States for Analysis:	Ultimate Limit State (ULS)
	Serviceability Limit State (SLS)
	Crack Width Design (CWD)
ULS Design Checks:	Bending
	Shear
	Torsion (due to horizontal crane loads)
SLS Design Checks:	Deflection
	Minimum and maximum amount of steel
	Durability (i.e., cover depth and mix design selection)
CWD Design Checks:	See Calculation Sheet D (Crack Width Design)

I. DESIGN INPUT VALUES				
Input	Value	Unit	Reference	Explanation/Formula
Service life	50	years	BS 6349-1-1:2013 Table 1	The Matola jetty is a common commecial port structure.

II. SELECTION OF MEMBER PROPERTIES				
Property	Value	Unit	Reference	Explanation/Formula
Concrete Properties				
Nominal cover depth	60	mm	BS 6349-1-4: 2013 Table 2	Beam B402 in upper tidal/splash & spray zone (XS3). 60 mm nominal cover selected to avoid low w/b ratio (therefore reducing cost).
Design cover depth	75	mm	Marine Concrete Structures (Alexander, 2016) Table 3.7	A 15 mm reinforcement placing tolerance was added to the nominal cover to allow for errors in workmanship.
Concrete strength class	C35/45	MPa	BS 6349-1-4: 2013 Table 2	Recommended value for 60 mm nominal cover depth.
Maximum w/b ratio	0.4	-	BS 6349-1-4: 2013 Table 2	Recommended value for 60 mm nominal cover depth.
Minimum binder content	380	kg/m^3	BS 6349-1-4: 2013 Table 2	Recommended value for 60 mm nominal cover depth.
Binder type	IIIA	-	BS 6349-1-4: 2013 Table 2	With 46-65 % GGBS (Assume that sufficient GGBS is available).
Steel Properties				
Steel characteristic strength, f_{yk}	500	MPa	Mosley, Bungey & Hulse (2007) 1.6.2	Choose to use high yield steel bars.

III. BENDING STRENGTH CHECK - SAGGING				
Item	Value	Unit	Reference	Explanation/Formula
Information from Analysis				
Ultimate applied moment, M_u	8815	kNm	Calculation Sheet Series B	-
Section Properties				
Concrete characteristic cylinder strength, f_{ck}	35	MPa	-	-
Steel characteristic strength, f_{yk}	500	Mpa	-	-
Section width, b	1400	mm	-	-
Section height, h	1800	mm	-	-
Initial main reinforcement diameter	40	mm	-	Assume Y40 bars.
Initial shear link diameter	16	mm	-	Assume Y16 bars.
Determination of Effective Depth, d				
Design cover depth, C	75	mm	-	-
Effective depth, d	1689	mm	-	d = h - C - link diameter - (main reinforcement diameter/2)
Check K vs. K_{bal}				
K_{bal}	0.167	-	Mosley, Bungey & Hulse (2007) 7.2.1	-
K	0.0631	-	Mosley, Bungey & Hulse (2007) 7.2.1	$K = \frac{M}{bd^2 f_{ck}} \leq K_{bal} = 0.167$
K vs. K_{bal}	$K < K_{bal}$	-	Mosley, Bungey & Hulse (2007) 7.2.1	$K < K_{bal}$, therefore only tension steel required.
Lever Arm, z				
Lever arm, z	1589	mm	Mosley, Bungey & Hulse (2007) 7.2.1	$z = d\left[0.5 + \sqrt{(0.25 - K/1.134)}\right]$
0.95d	1605	mm	Mosley, Bungey & Hulse (2007) 7.2.1	z < 0.95d, therefore okay.

Amount of Tension Reinforcing Steel Required, As_{req}				
Amount of tension reinforcing steel required, As_{req}	12752	mm^2	Mosley, Bungey & Hulse (2007) 7.2.1	$A_s = \frac{M}{0.87 f_{yk} z}$
Selection of Tension Reinforcement				
Area of one Y40 bar	1257	mm^2	-	A = pi(diameter/2)^2
Number of Y40 bars required	10.1	-	-	-
Number of Y40 bars provided	11	-	-	-
Area of tension reinforcement provided, As_{prov}	13823	mm^2	-	$As_{prov} > As_{req}$, therefore okay.
Maximum Area of Steel Check				
As_{max}	100800	mm^2	Mosley, Bungey & Hulse (2007) 7.2.1	Formula rearranged to find As_{max}. $100\frac{A_{s,max}}{bh} \leq 4.0\%$
As_{prov} vs. As_{max}	$As_{prov} < As_{max}$	-	Mosley, Bungey & Hulse (2007) 7.2.1	$As_{prov} < As_{max}$, therefore okay.
Minimum Area of Steel Check				
Long-term tensile strength, f_{ctm}	3.21	MPa	CIRIA C660 Table 3.2	Value for C35/45 concrete class.
As_{min}	3947	mm^2	Mosley, Bungey & Hulse (2007) 7.2.1	Formula rearranged to find As_{min}. $100\frac{A_{s,min}}{bd} \geq 26\frac{f_{ctm}}{f_{yk}}\%$ and not less than 0.13%
As_{prov} vs. As_{min}	$As_{prov} > As_{min}$	-	Mosley, Bungey & Hulse (2007) 7.2.1	$As_{prov} > As_{min}$, therefore okay.
Reinforcement Fit Check				
Spacing between bars, S	77.80	mm	-	S = (b - 2 x cover - 2 x link diameter - n x bar diameter)/(n-1)
S_{min1}	40	mm	EN 1992-1-1: 8.2(2)	Tension reinforcement diameter.
S_{min2}	24	mm		Assume 19 mm aggregate.
S_{min3}	20	mm		-
S_{min}	40	mm	EN 1992-1-1: 8.2(2)	S_{min} given by the largest of S_{min1}, S_{min2} and S_{min3}.
S vs. S_{min}	$S > S_{min}$	-	-	$S > S_{min}$, therefore okay.
Therefore provide one layer of 11 Y40 bars.				

IV. BENDING STRENGTH CHECK - HOGGING				
Item	Value	Unit	Reference	Explanation/Formula
Information from Analysis				
Ultimate applied moment, M_u	10973	kNm	Calculation Sheet Series B	-
Section Properties				
Concrete characteristic cylinder strength, f_{ck}	35	MPa	-	-
Steel characteristic strength, f_{yk}	500	Mpa	-	-
Section width, b	1400	mm	-	-
Section height, h	1800	mm	-	-
Initial main reinforcement diameter	40	mm	-	Assume Y40 bars.
Initial shear link diameter	16	mm	-	Assume Y16 bars.
Determination of Effective Depth, d				
Design cover depth, C	75	mm	-	-
Effective depth, d	1689	mm	-	d = h - C - link diameter - (main reinforcement diameter/2)
Check K vs. K_{bal}				
K_{bal}	0.167	-	Mosley, Bungey & Hulse (2007) 7.2.1	-

K	0.0785	-	Mosley, Bungey & Hulse (2007) 7.2.1	$K = \frac{M}{bd^2 f_{ck}} \leq K_{bal} = 0.167$
K vs. K_{bal}	$K < K_{bal}$	-	Mosley, Bungey & Hulse (2007) 7.2.1	$K < K_{bal}$, therefore only tension steel required.
Lever Arm, z				
Lever arm, z	1563	mm	Mosley, Bungey & Hulse (2007) 7.2.1	$z = d\left[0.5 + \sqrt{(0.25 - K/1.134)}\right]$
0.95d	1605	mm	Mosley, Bungey & Hulse (2007) 7.2.1	z < 0.95d, therefore okay.
Amount of Tension Reinforcing Steel Required, As_{req}				
Amount of tension reinforcing steel required, As_{req}	16143	mm^2	Mosley, Bungey & Hulse (2007) 7.2.1	$A_s = \frac{M}{0.87 f_{yk} z}$
Selection of Tension Reinforcement				
Area of one Y40 bar	1257	mm^2	-	A = pi(diameter/2)^2
Number of Y40 bars required	12.8	-	-	-
Number of Y40 bars provided	13	-	-	-
Area of tension reinforcement provided, As_{prov}	16336	mm^2	-	$As_{prov} > As_{req}$, therefore okay.
Maximum Area of Steel Check				
As_{max}	100800	mm^2	Mosley, Bungey & Hulse (2007) 7.2.1	Formula rearranged to find As_{max}. $100\frac{A_{s,max}}{bh} \leq 4.0\%$
As_{prov} vs. As_{max}	$As_{prov} < As_{max}$	-	Mosley, Bungey & Hulse (2007) 7.2.1	$As_{prov} < As_{max}$, therefore okay.
Minimum Area of Steel Check				
As_{min}	3947	mm^2	Mosley, Bungey & Hulse (2007) 7.2.1	Formula rearranged to find As_{min}. $100\frac{A_{s,min}}{bd} \geq 26\frac{f_{ctm}}{f_{yk}}\%$ and not less than 0.13%
As_{prov} vs. As_{min}	$As_{prov} > As_{min}$	-	Mosley, Bungey & Hulse (2007) 7.2.1	$As_{prov} > As_{min}$, therefore okay.
Reinforcement Fit Check				
Spacing between bars, S	58.17	mm	-	S = (b - 2 x cover - 2 x link diameter - n x bar diameter)/(n-1)
S_{min1}	40	mm	EN 1992-1-1: 8.2(2)	Tension reinforcement diameter.
S_{min2}	24	mm		Assume 19 mm aggregate.
S_{min3}	20	mm		-
S_{min}	40	mm	EN 1992-1-1: 8.2(2)	S_{min} given by the largest of S_{min1}, S_{min2} and S_{min3}.
S vs. S_{min}	$S > S_{min}$	-	-	$S > S_{min}$, therefore okay.
Therefore provide one layer of 13 Y40 bars.				

V. SHEAR STRENGTH CHECK				
Item	Value	Unit	Reference	Explanation/Formula
Information from Analysis				
Ultimate design shear force, $V_u = V_{Ed}$	4108	kN	Calculation Sheet Series B	-
Section Properties				
Concrete characteristic cylinder strength, f_{ck}	35	MPa	-	-
Steel characteristic strength, f_{yk}	500	Mpa	-	-
Section width, $b = b_w$	1400	mm	-	-
Section height, h	1800	mm	-	-
Main reinforcement diameter	32	mm	-	-

Initial shear link diameter	16	mm	-	Assume Y16 bars.
Crushing Strength Check				
Average effective depth, d	1689	mm	-	-
Crushing strength, $V_{Rd,max}$	8826	kN	Mosley, Bungey & Hulse (2007) 7.6.1	$V_{Rd,max} = 0.124 b_w d(1 - f_{ck}/250) f_{ck}$
$V_{Rd,max}$ vs. V_{Ed}	$V_{Rd,max} > V_{Ed}$	-	Mosley, Bungey & Hulse (2007) 7.6.1	$V_{Rd,max} > V_{Ed}$, therefore okay.
Provision of Shear Links				
cotΘ	2.5	-	Mosley, Bungey & Hulse (2007) 7.6.1	cotΘ = 2.5, as $V_{Rd,max} > V_{Ed}$.
A_{sw}/s	2.495	-	Mosley, Bungey & Hulse (2007) 7.6.1	$\frac{A_{sw}}{s} = \frac{V_{Ed}}{0.78 d f_{yk} \cot\theta}$
Try Y16 shear links, at 150 mm c/c spacing.				
A_{sw}/s provided	2.680	-	Mosley, Bungey & Hulse (2007) Table A.4	-
Minimum Shear Link Requirements				
$A_{sw,min}/s$	1.325	-	Mosley, Bungey & Hulse (2007) 7.6.1	$\frac{A_{sw,min}}{s} = \frac{0.08 f_{ck}^{0.5} b_w}{f_{yk}}$
A_{sw}/s provided > $A_{sw,min}/s$, therefore okay. Choose to use Y16 shear links, at 150 mm c/c spacing, over entire length of beam, due to variability of SFD caused by moving shiploader loads - location of maximum shear force varies with shiploader position.				
Additional Longitudinal Tensile Force Caused by the Shear Force (Used in Curtailment Calculations)				
Additional longitudinal tensile force caused by the shear force, ΔF_{td}	5135	kN	Mosley, Bungey & Hulse (2007) 7.6.1	$\Delta F_{td} = 0.5 V_{Ed} \cot\theta$
Spacing Checks				
Minimum longitudinal spacing, $s_{min,l}$	80	mm	Mosley, Bungey & Hulse (2007) 7.6.1	s = 150 mm > $s_{min,l}$, therefore okay.
Maximum longitudinal spacing, $s_{max,l}$	1267	mm	Mosley, Bungey & Hulse (2007) 7.6.1	$S_{max,l}$ = 0.75d for vertical links. s = 150 mm < $s_{max,l}$, therefore okay.
Maximum transverse spacing, $s_{b,max}$	600	mm	Mosley, Bungey & Hulse (2007) 7.6.1	$S_{b,max}$ = 0.75d ≤ 600 mm. s_b = 1218 mm > $s_{b,max}$, therefore **not** okay.
Try provide 4 legs for each shear link, at an increased spacing of 300 mm c/c.				
A_{sw} with four legs for each shear link	804.2	mm^2	Mosley, Bungey & Hulse (2007) 7.6.1	A_{sw} = 4 x π x (link diameter/2)^2.
A_{sw}/s with four legs and 300 mm c/c spacing	2.681	mm	-	$A_{sw}/s > A_{sw,required}/s$, therefore okay.
S_b with four legs for each shear link	395	mm	-	S_b = 395 mm < $s_{b,max}$, therefore okay.
However, note that "the distance of a tension or compression bar from a vertical leg should not be greater than 150 mm" (IStructE Detailing Manual, 6.3.2). **Therefore, provide four links (with a total of eight legs) every 600 mm c/c.**				
A_{sw} with eight legs for each shear link	1608.5	mm^2	Mosley, Bungey & Hulse (2007) 7.6.1	A_{sw} = 8 x π x (link diameter/2)^2.
A_{sw}/s eight four legs and 600 mm c/c spacing	2.681	mm	-	$A_{sw}/s > A_{sw,required}/s$, therefore okay.
S_b with four legs for each shear link	160	mm	-	S_b = 160 mm < $s_{b,max}$, therefore okay.
This should allow the shear links to be arranged in such a way that the distance from any tension bar to a vertical leg should not be greater than 150 mm.				
Therefore provide Y16 shear links, with four links (i.e., eight legs in total) being provided every 600 mm c/c, over the entire length of each beam.				

VI. TORSION STRENGTH CHECK				
Item	Value	Unit	Reference	Explanation/Formula
Information from Analysis				
Ultimate design torsional moment, T_{Ed}	442	kNm	Calculation Sheet Series B	-

Section Properties				
Concrete characteristic cylinder strength, f_{ck}	35	MPa	-	-
Steel characteristic strength, f_{yk}	500	Mpa	-	-
Section width, b	1400	mm	-	-
Section height, h	1800	mm	-	-
Main reinforcement diameter	40	mm	-	-
Shear link diameter	16	mm	-	-
Conversion of Section to Equivalent Hollow Box Section				
Thickness of box section, t	393.75	mm	Mosley, Bungey & Hulse (2007) 7.10	$t = \frac{bh}{2(b+h)}$
Area within the centreline of the equivalent section, A_k	1415039	mm^2	Mosley, Bungey & Hulse (2007) 7.10	$A_k = (b-t)(h-t)$
Perimeter within the centreline of the equivalent section, u_k	4825	mm	Mosley, Bungey & Hulse (2007) 7.10	$u_k = 2(b+h-2t)$
Torsional Resistance of the Equivalent Hollow Box Section				
Θ	22	°	Mosley, Bungey & Hulse (2007) 7.6.1	$V_{Rd,max} > V_{Ed}$, therefore Θ = 22°.
cotΘ	2.475	-	-	-
tanΘ	0.404	-	-	-
v_1	0.516	-	Mosley, Bungey & Hulse (2007) 7.10	$v_1 = 0.6(1 - f_{ck}/250)$
Torsional resistance of the equivalent hollow box section, $T_{Rd,max}$	4648	kNm	Mosley, Bungey & Hulse (2007) 7.10	$T_{Rd,max} = \frac{1.33 v_1 f_{ck} t_{ef} A_k}{\cot\theta + \tan\theta}$
Combined Torsion and Shear Resistance Check				
V_{Ed}	4108	kN	-	See Section IV, "Shear Strength Check".
$V_{Rd,max}$	8826	kN		
Left-hand side of interaction equation	0.561	-	Mosley, Bungey & Hulse (2007) 7.10	$\frac{T_{Ed}}{T_{Rd,max}} + \frac{V_{Ed}}{V_{Rd,max}} \le 1.0$
Left-hand side of the equation < 1, therefore okay; the concrete within the section has adequate resistance. However, still need to provide additional reinforcement.				
Additional Link Reinforcement Requirements for Torsional Resistance				
$A_{sw,required}/s$, based on one link leg	0.1451	-	Mosley, Bungey & Hulse (2007) 7.10	$\frac{A_{sw}}{s} = \frac{T_{Ed}}{2A_k 0.87 f_{yk} \cot\theta}$
$A_{sw,required}/s$, based on eight link legs, for shear and torsion	3.655	-	Mosley, Bungey & Hulse (2007) Example 7.9	$A_{sw,total}/s = A_{sw,shear}/s + 8 \times 0.1451$
Try Y16 links, with eight legs per link, at 400 mm c/c spacing.				
A_{sw} with eight legs for each shear link	1608.5	mm^2	Mosley, Bungey & Hulse (2007) 7.6.1	$A_{sw} = 8 \times \pi \times$ (link diameter/2)^2.
A_{sw}/s with eight legs and 400 mm c/c spacing	4.021	mm	-	$A_{sw}/s > A_{sw,required}/s$, therefore okay.
Maximum longitudinal link spacing, $s_{max,l}$	603.1	mm	Mosley, Bungey & Hulse (2007) 7.10	$s < s_{max,l}$, therefore okay. The spacing s of the stirrups should not exceed the lesser of (a) $u_k/8$, (b) $0.75d$ or (c) the least dimension of the beam's cross-section. The stirrups should be of the closed type fully anchored by means of laps.
Therefore provide Y16 links, with eight legs per link, at 400 mm c/c spacing.				
Additional Longitudinal Reinforcement Requirements for Torsional Resistance				
Required longitudinal reinforcement, A_{sl}	4288	mm^2	Mosley, Bungey & Hulse (2007) 7.10	$A_{sl} = \frac{T_{Ed} u_k \cot\theta}{2A_k 0.87 f_{y1k}}$
Area of one Y32 bar	804	mm^2	-	A = pi(diameter/2)^2

Number of Y32 bars required	5.331	-	-	-
Number of Y32 bars provided	6	-	-	Place 4 bars in the corners of the cross-section, and 1 in each of the side faces, as shown in Example 7.9 of Mosley, Bungey & Hulse (2007).
Area of longitudinal reinforcement provided, $A_{sl,prov}$	4825	mm^2	-	$A_{sl,prov} > A_{sl,\ required}$, therefore okay.
Therefore provide six Y32 bars, with four bars placed in the corners of the cross-section, and one bar placed in each of the cross-section's side faces.				

VII. DEFLECTION CHECK				
Item	Value	Unit	Reference	Explanation/Formula
According to Mosley, Bungey & Hulse (2007), Chapter 7.11, it is not necessary to perform detailed deflection calculations - a simple check of the beam's span-to-depth ratio is sufficient.				
Beam span	15000	mm	-	-
Average effective depth, d	1689	mm	-	-
Span/d ratio	8.88	-	-	-
Reinforcement ratio, ρ	0.683	%	Mosley, Bungey & Hulse (2007) 6.2	ρ is given by $100A_{s,req}/bd$
Maximum span/d ratio	18	-	Mosley, Bungey & Hulse (2007) Table 6.10	Continuous beam. To be conservatice, use ρ = 1.5 %, as 0.5 % < ρ < 1.5 %.
Span/d ratio < maximum span/d ratio, therefore okay.				

SUMMARY OF REINFORCEMENT PROVIDED		
Type of reinforcement	Reinforcement Provided	Area of Reinforcement Provided
Sagging tension reinforcement	One layer of 11 Y40 bars	13823 mm^2
Hogging tension reinforcement	One layer of 13 Y40 bars	16336 mm^2
Shear and torsion links	Y16 links, with four links (eight legs) provided every 400 mm	4.021 mm^2/mm
Torsion longitudinal reinforcement	6 Y32 bars, with 4 placed in corners and 2 in side faces	4825 mm^2

VIII. DETAILING				
Item	Value	Unit	Reference	Explanation/Formula
The following detailing checks and calculations are carried out below: 1. Determination of anchorage lengths for the main reinforcement 2. Determination of lap lengths for the main reinforcement 3. Curtailment of the main reinforcement 4. Provision of $A_{s,min}$ in the side faces Note that side face reinforcement to control cracking was not provided, as this will be provided seperately, but only for the beams which are designed to meet the crack width requirements.				
1. Determination of Anchorage Lengths for the Main Reinforcement				
Main reinforcement diameter, ϕ	40	mm	-	-
Concrete strength, f_{ck}	35	MPa	-	-
Use straight bars for the sagging and hogging reinforcement.				
Bond conditions for sagging reinforcement	Good	-	Mosley, Bungey & Hulse (2007) Figure 5.8	Section deeper than 600 mm, and sagging reinforcement placed at a depth greater than 300 mm.
Straight bar anchorage coefficient, K_A, for f_{ck} = 35 MPa	32	-	Mosley, Bungey & Hulse (2007) Table A.6	-

Sagging reinforcement (straight bar) anchorage length, L	1280	mm	Mosley, Bungey & Hulse (2007) Table A.6	$L = K_A \times \phi$
Provided anchorage length, L_{prov}	1300	mm	-	Choose a multiple of 50 for practicality/convenience.
Minimum anchorage length, L_{min}	400	mm	Mosley, Bungey & Hulse (2007) 5.2	L_{min} = greater of 100 mm and 10 x ϕ. $L_{prov} > L_{min}$, therefore okay.
Therefore use an anchorage length of 1300 mm for the sagging (straight bar) reinforcement.				
Bond conditions for hogging reinforcement	Poor	-	Mosley, Bungey & Hulse (2007) Figure 5.8	Section deeper than 600 mm, but hogging reinforcement placed at a depth less than 300 mm.
Straight bar anchorage coefficient, K_A, for f_{ck} = 35 MPa	45.71	-	Mosley, Bungey & Hulse (2007) Table A.6	Divide by 0.7 due to poor bond conditions.
Hogging reinforcement (straight bar) anchorage length, L	1829	mm	Mosley, Bungey & Hulse (2007) Table A.6	$L = K_A \times \phi$
Provided anchorage length, L_{prov}	1850	mm	-	Choose a multiple of 50 for practicality/convenience.
Minimum anchorage length, L_{min}	400	mm	Mosley, Bungey & Hulse (2007) 5.2	L_{min} = greater of 100 mm and 10 x ϕ. $L_{prov} > L_{min}$, therefore okay.
Therefore use an anchorage length of 1850 mm for the hogging (straight bar) reinforcement.				
2. Determination of Lap Lengths for the Main Reinforcement				
Lap length coefficient for f_{ck} = 35 MPa	48	-	Mosley, Bungey & Hulse (2007) Table A.6	To be conservative, assume > 50 % of bars lapped at a section
Required lap length, L_{req}	1920	mm	-	L_{req} = lap length coefficient x ϕ
Provided lap length, L_{prov}	1950	mm	-	Choose a multiple of 50 for practicality/convenience.
Minimum lap length, L_{min}	600	mm	Mosley, Bungey & Hulse (2007) 5.3	L_{min} = greater of 100 mm and 15 x ϕ. $L_{prov} > L_{min}$, therefore okay.
Therefore provide lap lengths of 1950 mm.				
3. Curtailment of the Main Reinforcement (see BMDs used to determine curtailment lengths in sheet 2, "Curtailment BMDs")				
Sagging Reinforcement - 3 Segments of Different Amounts of Reinforcement, Based on the BMD of the Critical Continuous Beam				
1st Segment	11	bars	-	Provide 1 layer of 11 Y40 bars.
Length of 1st Segment	8.8	m	Mosley, Bungey & Hulse (2007) 7.9	"Extend each curtailed bar a full anchorage length beyond where it is no longer needed". Therefore segment length = (13 - 5.5) + 1.3
2nd Segment	9	bars	-	Provide 1 layer of 9 Y40 bars.
Length of 2nd Segment	13.3	m	Mosley, Bungey & Hulse (2007) 7.9	"Extend each curtailed bar a full anchorage length beyond where it is no longer needed". Therefore segment length = (15 - 3.0) + 1.3
3rd Segment	5	bars	-	Provide 1 layer of 5 Y40 bars.
Length of 3rd Segment	15	m	Mosley, Bungey & Hulse (2007) 7.9	"Extend each curtailed bar a full anchorage length beyond where it is no longer needed". Therefore segment length = (15 - 1.0) + 1.3 = 15.3, therefore no curtailment, provide 5 Y40 bars along full length of beam.
Hogging Reinforcement - 3 Segments of Different Amounts of Reinforcement, Based on the BMD of the Critical Continuous Beam				
1st Segment	13	bars	-	Provide 1 layer of 13 Y40 bars.
Length of 1st Segment	4.35	m	Mosley, Bungey & Hulse (2007) 7.9	"Extend each curtailed bar a full anchorage length beyond where it is no longer needed". Therefore segment length = 2.5 + 1.85
2nd Segment	11	bars	-	Provide 1 layer of 11 Y40 bars.
Length of 2nd Segment	5.35	m	Mosley, Bungey & Hulse (2007) 7.9	"Extend each curtailed bar a full anchorage length beyond where it is no longer needed". Therefore segment length = 3.5 + 1.85
3rd Segment	7	bars	-	Provide 1 layer of 7 Y40 bars.
Length of 3rd Segment	15	m	Mosley, Bungey & Hulse (2007) 7.9	Extend these bars the full length of the beam, in order to allow for joining of the shear links throughout the beam.

4. Provision of $A_{s,min}$ in the side faces				
Long-term tensile strength, f_{ctm}	3.21	MPa	CIRIA C660 Table 3.2	Value for C35/45 concrete class.
As_{min} for side faces	4206	mm^2	Mosley, Bungey & Hulse (2007) 7.2.1	Formula rearranged to find As_{min}. $100\frac{A_{s,min}}{bd} \geq 26\frac{f_{ctm}}{f_{yk}}\%$ and not less than 0.13%
As_{prov} for side faces	4926	mm^2	-	Two Y40 and three Y32 bars in each side face from tension/torsion reinforcement.
As_{prov} vs. As_{min}	$As_{prov} > As_{min}$	-	Mosley, Bungey & Hulse (2007) 7.2.1	$As_{prov} > As_{min}$, therefore okay.
Therefore no additional longitudinal reinforcement is required in the side faces.				

$$F_s = \frac{M_{Ed}}{0{,}87z} \qquad x_1 = x + a_1 \qquad F_r = As_{prov} \times f_y = As_{prov} \times 500\ N/mm^2 \qquad F_r = As_{prov} \times f_y = As_{prov} \times 500\ N/mm^2$$

Sagging - Based on Critical Continous Beam											
Position Along Beam, x [m]	Sagging Moment, M_{Ed} [kNm]	Acting Tensile Force, F_s [kN]	Shifted Position Along Beam, x_1 [m]	Shifted F_s [kN]	Minimum Number of Y40 Bars Required	Area of Steel Provided, As_{prov} [mm^2]	Minimum Resisting Tensile Force, $F_{r,min}$ [kN]	Actual Number of Y40 Bars Provided	Area of Steel Provided, As_{prov} [mm^2]	Actual Resisting Tensile Force, $F_{r,act}$ [kN]
0	0	0.0	2	0.0	0	0.0	0.0	0	0.0	0.0
0.5	0	0.0	2.5	0.0	0	0.0	0.0	0	0.0	0.0
1	0	0.0	3	542.5	1	1256.6	628.3	5	6283.2	3141.6
1.5	0	0.0	3.5	1425.8	3	3769.9	1885.0	5	6283.2	3141.6
2	0	0.0	4	2244.6	4	5026.5	2513.3	5	6283.2	3141.6
2.5	0	0.0	4.5	2964.3	5	6283.2	3141.6	5	6283.2	3141.6
3	750	542.5	5	3622.6	6	7539.8	3769.9	9	11309.7	5654.9
3.5	1971	1425.8	5.5	4204.9	7	8796.5	4398.2	9	11309.7	5654.9
4	3103	2244.6	6	4730.1	8	10053.1	5026.5	9	11309.7	5654.9
4.5	4098	2964.3	6.5	5245.8	9	11309.7	5654.9	9	11309.7	5654.9
5	5008	3622.6	7	5639.3	9	11309.7	5654.9	9	11309.7	5654.9
5.5	5813	4204.9	7.5	5975.0	10	12566.4	6283.2	11	13823.0	6911.5
6	6539	4730.1	8	6173.9	10	12566.4	6283.2	11	13823.0	6911.5
6.5	7252	5245.8	8.5	6334.5	11	13823.0	6911.5	11	13823.0	6911.5
7	7796	5639.3	9	6370.7	11	13823.0	6911.5	11	13823.0	6911.5
7.5	8260	5975.0	9	6370.7	11	13823.0	6911.5	11	13823.0	6911.5
8	8535	6173.9	9	6370.7	11	13823.0	6911.5	11	13823.0	6911.5
8.5	8757	6334.5	9	6370.7	11	13823.0	6911.5	11	13823.0	6911.5
9	8807	6370.7	9	6370.7	11	13823.0	6911.5	11	13823.0	6911.5
9.5	8752	6330.9	9	6370.7	11	13823.0	6911.5	11	13823.0	6911.5
10	8566	6196.3	9	6370.7	11	13823.0	6911.5	11	13823.0	6911.5
10.5	8269	5981.5	9	6370.7	11	13823.0	6911.5	11	13823.0	6911.5
11	7857	5683.5	9	6370.7	11	13823.0	6911.5	11	13823.0	6911.5
11.5	7271	5259.6	9.5	6330.9	11	13823.0	6911.5	11	13823.0	6911.5
12	6646	4807.5	10	6196.3	10	12566.4	6283.2	11	13823.0	6911.5
12.5	5793	4190.4	10.5	5981.5	10	12566.4	6283.2	11	13823.0	6911.5
13	4920	3559.0	11	5683.5	10	12566.4	6283.2	11	13823.0	6911.5
13.5	3860	2792.2	11.5	5259.6	9	11309.7	5654.9	9	11309.7	5654.9
14	2727	1972.6	12	4807.5	8	10053.1	5026.5	9	11309.7	5654.9
14.5	1400	1012.7	12.5	4190.4	7	8796.5	4398.2	9	11309.7	5654.9
15	0	0.0	13	3559.0	6	7539.8	3769.9	9	11309.7	5654.9

Lever Arm, z [m] 1.589
Additional Tension Shear Force, ΔF_{td} [kN] 5135
Distance to shift F_s diagram, a_1 [m] 1.906
*Round a_1 off to 2 m

$$a_1 = z(\cot\theta - \cot\alpha)/2$$

where cot(Θ) = 2.5, and cot(α) = 0
(Beeby & Narayanan, 2009:191)

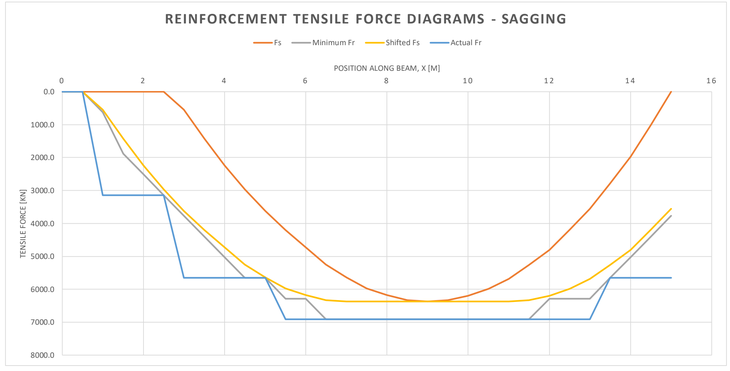

$$F_s = \frac{M_{Ed}}{0{,}87z} \qquad x_1 = x + a_1 \qquad F_r = As_{prov} \times f_y = As_{prov} \times 500\ N/mm^2 \qquad F_r = As_{prov} \times f_y = As_{prov} \times 500\ N/mm^2$$

Hogging - Based on Critical Continuous Beam											
Position Along Beam, x [m]	Hogging Moment, M_{Ed} [kNm]	Acting Tensile Force, F_s [kN]	Shifted Position Along Beam, x_1 [m]	Shifted F_s [kN]	Minimum Number of Y40 Bars Required	Area of Steel Provided, As_{prov} [mm^2]	Minimum Resisting Tensile Force, $F_{r,min}$ [kN]	Actual Number of Y40 Bars Provided	Area of Steel Provided, As_{prov} [mm^2]	Actual Resisting Tensile Force, $F_{r,act}$ [kN]
0	10973	8069.5	0	8069.5	13	16336.3	8168.1	13	16336.3	8168.1
0.5	9257	6807.6	0.5	8069.5	13	16336.3	8168.1	13	16336.3	8168.1
1	7553	5554.5	1	8069.5	13	16336.3	8168.1	13	16336.3	8168.1
1.5	5986	4402.1	1.5	8069.5	13	16336.3	8168.1	13	16336.3	8168.1
2	4372	3215.2	2	8069.5	13	16336.3	8168.1	13	16336.3	8168.1
2.5	2805	2062.8	2.5	6807.6	11	13823.0	6911.5	11	13823.0	6911.5
3	1368	1006.0	3	5554.5	9	11309.7	5654.9	11	13823.0	6911.5
3.5	0	0.0	3.5	4402.1	8	10053.1	5026.5	11	13823.0	6911.5
4	0	0.0	4	3215.2	6	7539.8	3769.9	7	8796.5	4398.2
4.5	0	0.0	4.5	2062.8	4	5026.5	2513.3	7	8796.5	4398.2
5	0	0.0	5	1006.0	2	2513.3	1256.6	7	8796.5	4398.2
5.5	0	0.0	5.5	0.0	0	0.0	0.0	0	0.0	0.0
6	0	0.0	6	0.0	0	0.0	0.0	0	0.0	0.0
6.5	0	0.0	6.5	0.0	0	0.0	0.0	0	0.0	0.0
7	0	0.0	7	0.0	0	0.0	0.0	0	0.0	0.0
7.5	0	0.0	7.5	0.0	0	0.0	0.0	0	0.0	0.0

*7 bars provided for practical reasons

Lever Arm, z [m] 1.563
Additional Tension Shear Force, ΔF_{td} [kN] 5135
Distance to shift F_s diagram, a_1 [m] 1.9425
*Round a_1 off to 2 m

$$a_1 = z(\cot\theta - \cot\alpha)/2$$

where cot(Θ) = 2.5, and cot(α) = 0
(Beeby & Narayanan, 2009:191)

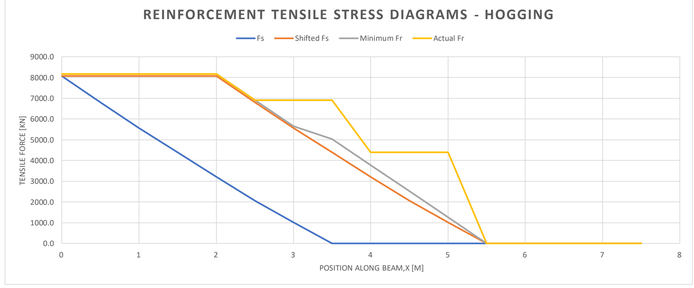

	CRACK WIDTH DESIGN CALCULATIONS	
	Member: Matola jetty crane rail beam (Beam B402)	

Project:	MSc. Eng. Structural Engineering - Research
Sheet Series:	D (Crack Width Design Calculations)
Calculations By:	Nicholas Elias
Date:	16/03/2022

Date	Checked By	Check No.	Review Level	Approved
29/03/2022	P.E.S	D-01	-	Yes

Check No.	Action	Check Notes	Status
D-01	N.N.E		

Overview of Member	
Structure Type:	Coal export jetty
Member Type:	Reinforced concrete crane rail beam
Member Loads:	Self-weight of structural components
	Vehicle loads
	Live (imposed) loads
	Shiploader loads
Limit States for Analysis:	Ultimate Limit State (ULS)
	Serviceability Limit State (SLS)
	Crack Width Design (CWD)
ULS Design Checks:	Bending
	Shear
	Torsion (due to horizontal crane loads)
SLS Design Checks:	Deflection
	Minimum and maximum amount of steel
	Durability (i.e., cover depth and mix design selection)
CWD Design Checks:	Flexural Cracking
	Thermal and Shrinkage Cracking

I. DESIGN INPUT VALUES				
Input	Value	Unit	Reference	Explanation/Formula
Service life	50	years	BS 6349-1-1:2013 Table 1	The Matola jetty is a common commecial port structure.

II. MEMBER PROPERTIES				
Property	Value	Unit	Reference	Explanation/Formula
Nominal cover depth	60	mm	BS 6349-1-4: 2013 Table 2	Beam B402 in upper tidal/splash & spray zone (XS3). 60 mm nominal cover selected to avoid low w/b ratio (therefore reducing cost).
Design cover depth	75	mm	Marine Concrete Structures (Alexander, 2016) Table 3.7	A 15 mm reinforcement placing tolerance was added to the nominal cover to allow for errors in workmanship.
Concrete strength class	C35/45	MPa	BS 6349-1-4: 2013 Table 2	Recommended value for 60 mm nominal cover depth.
Maximum w/b ratio	0.4	-	BS 6349-1-4: 2013 Table 2	Recommended value for 60 mm nominal cover depth.
Minimum binder content	380	kg/m^3	BS 6349-1-4: 2013 Table 2	Recommended value for 60 mm nominal cover depth.
Binder type	IIIA	-	BS 6349-1-4: 2013 Table 2	With 46-65 % GGBS (Assume that sufficient GGBS is available).
Steel characteristic strength, f_{yk}	500	MPa	Mosley, Bungey & Hulse (2007) 1.6.2	Choose to use high yield steel bars.
Member width, b	1400	mm	-	-
Member height, h	1800	mm	-	-

III. DESIGN FOR CRACK WIDTH: FLEXURAL CRACKING - SAGGING				
Item	Value	Unit	Reference	Explanation/Formula
Information from Analysis				
Sustained moment under service conditions, M_s	4463	kNm	Calculation Sheet Series B	-
Minimum Area of Reinforcing Steel Required to Control Cracking				
Maximum steel stress, $\sigma_{s,max}$	500	MPa	EN 1992-1-1:2004 7.3.2 (2)	σ_s may be taken as the yield strength of the steel, f_{yk}.
Stress distribution coefficient, k_c	0.4	-	Mosley, Bungey & Hulse (2007) 6.1.5	k_c = 0.4 for flexure.
Non-linear stress distribution coefficient, k	0.65	-	EN 1992-1-1:2004 7.3.2 (2)	k = 0.65 for webs > 800 mm deep.
Tensile strength at the time of cracking, $f_{ct,eff}$	3.00	MPa	Mosley, Bungey & Hulse (2007) 6.1.5	Suggested minimum value for $f_{ct,eff}$ = 3.00 MPa.
Area of tension steel provided in ULS, As_{prov}	13823	mm^2	-	-
Neutral axis depth, x	604.44	mm		Calculated by taking moments about the neutral axis - see sheet 2.
Area of concrete within the tensile zone, A_{ct}	1673784	mm^2	-	A_{ct} = b x (h-x)
Minimum area of reinforcing steel required to control cracking, As_{min}	2611	mm^2	EN 1992-1-1:2004 Equation 7.1	$A_{s,min}\sigma_s = k_c\ k\ f_{ct,eff}\ A_{ct}$
As_{prov} > As_{min}, therefore the area of steel provided to meet the ULS requirements is adequate to ensure cracking is controlled.				
Calculation of Crack Width				
Average effective depth, d	1689	mm	-	-
Stress in the tensile steel, σ_s	217.05	MPa	Mosley, Bungey & Hulse (2007) 6.4.3	$\sigma_s = M_s/[(d-x/3)As_{prov}]$
k_t	0.4	-	EN 1992-1-1:2004 7.3.4 (2)	Assume long-term loading.
$f_{ct,eff}$	3.00	MPa	Mosley, Bungey & Hulse (2007) 6.1.5	Suggested minimum value for $f_{ct,eff}$ = 3.00 MPa.
α_e	17.06	-	-	See sheet 2.
$A_{c,eff}$	388500	mm^2	EN 1992-1-1:2004 7.3.2 (2)	$A_{c,eff}$ = b x $h_{c,ef}$, where $h_{c,ef}$ = lesser of 2.5(h-d), (h-x)/3 and h/2.
$\rho_{p,eff}$	0.0355804	-	EN 1992-1-1:2004 7.3.4 (2)	$\rho_{p,eff} = As_{prov}/A_{c,eff}$
E_s	200	GPa	-	-

$\varepsilon_{sm} - \varepsilon_{cm}$	0.000814263	-	EN 1992-1-1:2004 7.3.4 (2)	$\varepsilon_{sm}-\varepsilon_{cm}=\frac{\sigma_s-k_t\frac{f_{ct,eff}}{\rho_{p,eff}}(1+\alpha_e\rho_{p,eff})}{E_s}\geq 0{,}6\frac{\sigma_s}{E_s}$
$0.6\sigma_s/E_s$	0.000651153	-	EN 1992-1-1:2004 7.3.4 (2)	$\varepsilon_{sm} - \varepsilon_{cm} > 0.6\sigma_s/E_s$, therefore okay.
Design cover, c	75	mm	-	-
Bar diameter, ϕ	40	mm	-	-
k_1	0.8	-	EN 1992-1-1:2004 7.3.4 (3)	k_1 = 0.8 for high bond bars.
k_2	0.5	-	EN 1992-1-1:2004 7.3.4 (3)	k_2 = 0.5 for bending.
k_3	3.4	-	EN 1992-1-1:2004 7.3.4 (3)	-
k_4	0.425	-	EN 1992-1-1:2004 7.3.4 (3)	-
$S_{r,max}$	446.12	mm	EN 1992-1-1:2004 7.3.4 (3)	$s_{r,max} = k_3c + k_1k_2k_4\phi/\rho_{p,eff}$
Crack width, w_k	0.3633	mm	EN 1992-1-1:2004 7.3.4 (1)	$w_k = s_{r,max}(\varepsilon_{sm} - \varepsilon_{cm})$
Maximum permissible crack width, w_{max}	0.3	mm	EN 1992-1-1:2004 Table 7.1N	Exposure class XS3. **$w_k > w_{max}$, therefore not okay**.
As $w_k > w_{max}$, try use 32 mm diameter bars at reduced spacing between bars, and recalculate w_k:				
Area of one Y32 bar	804.25	mm^2	-	A = pi(diameter/2)^2
As_{req} for ULS requirements	12752	mm^2	-	Ignore the slight reduction in Asreq caused by reducing the bar size.
Number of Y32 bars required	15.86	-	-	-
Number of Y32 bars provided	16	-	-	Provide two layers of 21 Y25 bars each, with a Y25 spacer bar.
Area of tension reinforcement provided, As_{prov}	12868	mm^2	-	-
Spacing between bars, S	47.07	mm	-	S = (b - 2 x cover - 2 x link diameter - n x bar diameter)/(n-1)
Minimum spacing, S_{min}	32	mm	EN 1992-1-1: 8.2(2)	S_{min} given by largest of reinforcement diameter, 20 mm or aggregate diameter (19 mm) + 5 mm. **$S > S_{min}$, therefore okay.**
Effective depth, d	1693	mm	-	Average d = h - C - link diameter - main reinforcement diameter/2
Neutral axis depth, x	588.52	mm	-	Calculated by taking moments about the neutral axis - see sheet 2.
Stress in the tensile steel, σ_s	231.71	MPa	Mosley, Bungey & Hulse (2007) 6.4.3	$\sigma_s = M_s/[(d-x/3)As_{prov}]$
k_t	0.4	-	EN 1992-1-1:2004 7.3.4 (2)	Assume long-term loading.
$f_{ct,eff}$	3.00	MPa	Mosley, Bungey & Hulse (2007) 6.1.5	Suggested minimum value for $f_{ct,eff}$ = 3.00 MPa.
α_e	17.06	-	-	See sheet 2.
$A_{c,eff}$	374500	mm^2	EN 1992-1-1:2004 7.3.2 (2)	$A_{c,eff}$ = b x $h_{c,ef}$, where $h_{c,ef}$ = lesser of 2.5(h-d), (h-x)/3 and h/2.
$\rho_{p,eff}$	0.0343604	-	EN 1992-1-1:2004 7.3.4 (2)	$\rho_{p,eff} = As_{prov}/A_{c,eff}$
E_s	200	GPa	-	-
$\varepsilon_{sm} - \varepsilon_{cm}$	0.000881572	-	EN 1992-1-1:2004 7.3.4 (2)	$\varepsilon_{sm}-\varepsilon_{cm}=\frac{\sigma_s-k_t\frac{f_{ct,eff}}{\rho_{p,eff}}(1+\alpha_e\rho_{p,eff})}{E_s}\geq 0{,}6\frac{\sigma_s}{E_s}$
$0.6\sigma_s/E_s$	0.000695131	-	EN 1992-1-1:2004 7.3.4 (2)	$\varepsilon_{sm} - \varepsilon_{cm} > 0.6\sigma_s/E_s$, therefore okay.
Design cover, c	75	mm	-	-
Bar diameter, ϕ	32	mm	-	-
k_1	0.8	-	EN 1992-1-1:2004 7.3.4 (3)	k_1 = 0.8 for high bond bars.
k_2	0.5	-	EN 1992-1-1:2004 7.3.4 (3)	k_2 = 0.5 for bending.

k_3	3.4	-	EN 1992-1-1:2004 7.3.4 (3)	-
k_4	0.425	-	EN 1992-1-1:2004 7.3.4 (3)	-
$S_{r,max}$	413.32	mm	EN 1992-1-1:2004 7.3.4 (3)	$s_{r,max} = k_3 c + k_1 k_2 k_4 \phi / \rho_{p,eff}$
Crack width, w_k	0.3644	mm	EN 1992-1-1:2004 7.3.4 (1)	$w_k = s_{r,max} (\varepsilon_{sm} - \varepsilon_{cm})$
Maximum permissible crack width, w_{max}	0.3	mm	EN 1992-1-1:2004 Table 7.1N	Exposure class XS3. **$w_k > w_{max}$, therefore not okay**.
As $w_k > w_{max}$, try use 25 mm diameter bars at reduced spacing between bars, and recalculate w_k:				
Area of one Y25 bar	490.87	mm^2	-	A = pi(diameter/2)^2
As_{req} for ULS requirements	12752	mm^2	-	Ignore the slight reduction in Asreq caused by reducing the bar size.
Number of Y25 bars required	25.98	-	-	-
Number of Y25 bars provided	26	-	-	Provide two layers of 33 Y20 bars each, with a Y20 spacer bar.
Area of tension reinforcement provided, As_{prov}	12763	mm^2	-	-
Spacing between bars, S	22.72	mm	-	S = (b - 2 x cover - 2 x link diameter - n x bar diameter)/(n-1)
Minimum spacing, S_{min}	25	mm	EN 1992-1-1: 8.2(2)	S_{min} given by least of reinforcement diameter, 20 mm or aggregate diameter (19 mm) + 5 mm. **S < S_{min}, therefore not okay.**
As S < S_{min}, Y25 bars cannot be used. Therefore try use Y32 bars, but iteratively increase the number of bars to decrease w_k until $w_k < w_{max}$, starting with 18 bars:				
Area of one Y32 bar	804.25	mm^2	-	A = pi(diameter/2)^2
As_{req} for ULS requirements	12752	mm^2	-	Ignore the slight reduction in Asreq caused by reducing the bar size.
Number of Y32 bars required	15.86	-	-	-
Number of Y32 bars provided	18	-	-	-
Area of tension reinforcement provided, As_{prov}	14476	mm^2	-	-
Spacing between bars, S	37.76	mm	-	S = (b - 2 x cover - 2 x link diameter - n x bar diameter)/(n-1)
Minimum spacing, S_{min}	32	mm	EN 1992-1-1: 8.2(2)	S_{min} given by least of reinforcement diameter, 20 mm or aggregate diameter (19 mm) + 5 mm. **S > S_{min}, therefore okay.**
Average effective depth, d	1693	mm	-	Average d = h - C - link diameter - main reinforcement diameter/2
Neutral axis depth, x	616.31	mm	-	Calculated by taking moments about the neutral axis - see sheet 2.
Stress in the tensile steel, σ_s	207.25	MPa	Mosley, Bungey & Hulse (2007) 6.4.3	$\sigma_s = M_s/[(d-x/3)As_{prov}]$
k_t	0.4	-	EN 1992-1-1:2004 7.3.4 (2)	Assume long-term loading.
$f_{ct,eff}$	3.00	MPa	Mosley, Bungey & Hulse (2007) 6.1.5	Suggested minimum value for $f_{ct,eff}$ = 3.00 MPa.
α_e	17.06	-	-	See sheet 2.
$A_{c,eff}$	374500	mm^2	EN 1992-1-1:2004 7.3.2 (2)	$A_{c,eff}$ = b x $h_{c,ef}$, where $h_{c,ef}$ = lesser of 2.5(h-d), (h-x)/3 and h/2.
$\rho_{p,eff}$	0.0386554	-	EN 1992-1-1:2004 7.3.4 (2)	$\rho_{p,eff} = As_{prov}/A_{c,eff}$
E_s	200	GPa	-	-
$\varepsilon_{sm} - \varepsilon_{cm}$	0.000778659	-	EN 1992-1-1:2004 7.3.4 (2)	$\varepsilon_{sm} - \varepsilon_{cm} = \frac{\sigma_s - k_t \frac{f_{ct,eff}}{\rho_{p,eff}}(1 + \alpha_e \rho_{p,eff})}{E_s} \geq 0{,}6 \frac{\sigma_s}{E_s}$
$0.6\sigma_s/E_s$	0.000621742	-	EN 1992-1-1:2004 7.3.4 (2)	$\varepsilon_{sm} - \varepsilon_{cm} > 0.6\sigma_s/E_s$, therefore okay.
Design cover, c	75	mm	-	-
Bar diameter, ϕ	32	mm	-	-

k_1	0.8	-	EN 1992-1-1:2004 7.3.4 (3)	k_1 = 0.8 for high bond bars.
k_2	0.5	-	EN 1992-1-1:2004 7.3.4 (3)	k_2 = 0.5 for bending.
k_3	3.4	-	EN 1992-1-1:2004 7.3.4 (3)	-
k_4	0.425	-	EN 1992-1-1:2004 7.3.4 (3)	-
$S_{r,max}$	395.73	mm	EN 1992-1-1:2004 7.3.4 (3)	$s_{r,max} = k_3 c + k_1 k_2 k_4 \phi / \rho_{p,eff}$
Crack width, w_k	0.3081	mm	EN 1992-1-1:2004 7.3.4 (1)	$w_k = s_{r,max} (\varepsilon_{sm} - \varepsilon_{cm})$
Maximum permissible crack width, w_{max}	0.3	mm	EN 1992-1-1:2004 Table 7.1N	Exposure class XS3. **$w_k > w_{max}$, therefore not okay**.
Try 19 Y32 bars:				
Area of one Y32 bar	804.25	mm^2	-	A = pi(diameter/2)^2
As_{req} for ULS requirements	12752	mm^2	-	Ignore the slight reduction in Asreq caused by reducing the bar size.
Number of Y32 bars required	15.86	-	-	-
Number of Y32 bars provided	19	-	-	-
Area of tension reinforcement provided, As_{prov}	15281	mm^2	-	-
Spacing between bars, S	33.89	mm	-	S = (b - 2 x cover - 2 x link diameter - n x bar diameter)/(n-1)
Minimum spacing, S_{min}	32	mm	EN 1992-1-1: 8.2(2)	S_{min} given by largest of reinforcement diameter, 20 mm or aggregate diameter (19 mm) + 5 mm. **$S > S_{min}$, therefore okay.**
Average effective depth, d	1693	mm	-	Average d = h - C - link diameter - main reinforcement diameter/2
Neutral axis depth, x	629.36	mm	-	Calculated by taking moments about the neutral axis - see sheet 2.
Stress in the tensile steel, σ_s	196.92	MPa	Mosley, Bungey & Hulse (2007) 6.4.3	$\sigma_s = M_s/[(d-x/3)As_{prov}]$
k_t	0.4	-	EN 1992-1-1:2004 7.3.4 (2)	Assume long-term loading.
$f_{ct,eff}$	3.00	MPa	Mosley, Bungey & Hulse (2007) 6.1.5	Suggested minimum value for $f_{ct,eff}$ = 3.00 MPa.
α_e	17.06	-	-	See sheet 2.
$A_{c,eff}$	374500	mm^2	EN 1992-1-1:2004 7.3.2 (2)	$A_{c,eff}$ = b x $h_{c,ef}$, where $h_{c,ef}$ = lesser of 2.5(h-d), (h-x)/3 and h/2.
$\rho_{p,eff}$	0.0408030	-	EN 1992-1-1:2004 7.3.4 (2)	$\rho_{p,eff} = As_{prov}/A_{c,eff}$
E_s	200	GPa	-	-
$\varepsilon_{sm} - \varepsilon_{cm}$	0.000735169	-	EN 1992-1-1:2004 7.3.4 (2)	$\varepsilon_{sm} - \varepsilon_{cm} = \frac{\sigma_s - k_t \frac{f_{ct,eff}}{\rho_{p,eff}}(1 + \alpha_e \rho_{p,eff})}{E_s} \geq 0{,}6 \frac{\sigma_s}{E_s}$
$0.6\sigma_s/E_s$	0.000590746	-	EN 1992-1-1:2004 7.3.4 (2)	$\varepsilon_{sm} - \varepsilon_{cm} > 0.6\sigma_s/E_s$, therefore okay.
Design cover, c	75	mm	-	-
Bar diameter, ϕ	32	mm	-	-
k_1	0.8	-	EN 1992-1-1:2004 7.3.4 (3)	k_1 = 0.8 for high bond bars.
k_2	0.5	-	EN 1992-1-1:2004 7.3.4 (3)	k_2 = 0.5 for bending.
k_3	3.4	-	EN 1992-1-1:2004 7.3.4 (3)	-
k_4	0.425	-	EN 1992-1-1:2004 7.3.4 (3)	-
$S_{r,max}$	388.32	mm	EN 1992-1-1:2004 7.3.4 (3)	$s_{r,max} = k_3 c + k_1 k_2 k_4 \phi / \rho_{p,eff}$
Crack width, w_k	0.2855	mm	EN 1992-1-1:2004 7.3.4 (1)	$w_k = s_{r,max} (\varepsilon_{sm} - \varepsilon_{cm})$

Maximum permissible crack width, w_{max}	0.3	mm	EN 1992-1-1:2004 Table 7.1N	Exposure class XS3. **$w_k < w_{max}$, therefore okay**.
Therefore provide 19 Y32 bars.				

IV. DESIGN FOR CRACK WIDTH: FLEXURAL CRACKING - HOGGING				
Item	Value	Unit	Reference	Explanation/Formula
Information from Analysis				
Sustained moment under service conditions, M_s	6065	kNm	Calculation Sheet Series B	-
Minimum Area of Reinforcing Steel Required to Control Cracking				
Maximum steel stress, $\sigma_{s,max}$	500	MPa	EN 1992-1-1:2004 7.3.2 (2)	σ_s may be taken as the yield strength of the steel, f_{yk}.
Stress distribution coefficient, k_c	0.4	-	Mosley, Bungey & Hulse (2007) 6.1.5	k_c = 0.4 for flexure.
Non-linear stress distribution coefficient, k	0.65	-	EN 1992-1-1:2004 7.3.2 (2)	k = 0.65 for webs > 800 mm deep.
Tensile strength at the time of cracking, $f_{ct,eff}$	3.00	MPa	Mosley, Bungey & Hulse (2007) 6.1.5	Suggested minimum value for $f_{ct,eff}$ = 3.00 MPa.
Area of tension steel provided in ULS, As_{prov}	16336	mm^2	-	-
Neutral axis depth, x	644.76	mm		Calculated by taking moments about the neutral axis - see sheet 2.
Area of concrete within the tensile zone, A_{ct}	1617336	mm^2	-	A_{ct} = b x (h-x)
Minimum area of reinforcing steel required to control cracking, As_{min}	2523	mm^2	EN 1992-1-1:2004 Equation 7.1	$A_{s,min}\sigma_s = k_c\, k\, f_{ct,eff}\, A_{ct}$
As_{prov} > As_{min}, therefore the area of steel provided to meet the ULS requirements is adequate to ensure cracking is controlled.				
Calculation of Crack Width				
Average effective depth, d	1689	mm	-	-
Stress in the tensile steel, σ_s	251.86	MPa	Mosley, Bungey & Hulse (2007) 6.4.3	$\sigma_s = M_s/[(d-x/3)As_{prov}]$
k_t	0.4	-	EN 1992-1-1:2004 7.3.4 (2)	Assume long-term loading.
$f_{ct,eff}$	3.00	MPa	Mosley, Bungey & Hulse (2007) 6.1.5	Suggested minimum value for $f_{ct,eff}$ = 3.00 MPa.
α_e	17.06	-	-	See sheet 2.
$A_{c,eff}$	388500	mm^2	EN 1992-1-1:2004 7.3.2 (2)	$A_{c,eff}$ = b x $h_{c,ef}$, where $h_{c,ef}$ = lesser of 2.5(h-d), (h-x)/3 and h/2.
$\rho_{p,eff}$	0.0420489	-	EN 1992-1-1:2004 7.3.4 (2)	$\rho_{p,eff} = As_{prov}/A_{c,eff}$
E_s	200	GPa	-	-
ε_{sm} - ε_{cm}	0.001014263	-	EN 1992-1-1:2004 7.3.4 (2)	$\varepsilon_{sm}-\varepsilon_{cm} = \frac{\sigma_s - k_t \frac{f_{ct,eff}}{\rho_{p,eff}}(1+\alpha_e\rho_{p,eff})}{E_s} \geq 0{,}6\frac{\sigma_s}{E_s}$
$0.6\sigma_s/E_s$	0.000755588	-	EN 1992-1-1:2004 7.3.4 (2)	ε_{sm} - ε_{cm} > $0.6\sigma_s/E_s$, therefore okay.
Design cover, c	75	mm	-	-
Bar diameter, ϕ	40	mm	-	-
k_1	0.8	-	EN 1992-1-1:2004 7.3.4 (3)	k_1 = 0.8 for high bond bars.
k_2	0.5	-	EN 1992-1-1:2004 7.3.4 (3)	k_2 = 0.5 for bending.
k_3	3.4	-	EN 1992-1-1:2004 7.3.4 (3)	-
k_4	0.425	-	EN 1992-1-1:2004 7.3.4 (3)	-
$S_{r,max}$	416.72	mm	EN 1992-1-1:2004 7.3.4 (3)	$s_{r,max} = k_3 c + k_1 k_2 k_4 \phi / \rho_{p,eff}$
Crack width, w_k	0.4227	mm	EN 1992-1-1:2004 7.3.4 (1)	$w_k = s_{r,max}(\varepsilon_{sm} - \varepsilon_{cm})$

Maximum permissible crack width, w_{max}	0.3	mm	EN 1992-1-1:2004 Table 7.1N	Exposure class XS3. **$w_k > w_{max}$, therefore not okay**.
As $w_k > w_{max}$, try use 32 mm diameter bars at reduced spacing between bars, and recalculate w_k:				
Area of one Y32 bar	804.25	mm^2	-	A = pi(diameter/2)^2
As_{req} for ULS requirements	16143	mm^2	-	Ignore the slight reduction in Asreq caused by reducing the bar size.
Number of Y32 bars required	20.07	-	-	-
Number of Y32 bars provided	21	-	-	-
Area of tension reinforcement provided, As_{prov}	16889	mm^2	-	-
Spacing between bars, S	27.30	mm	-	S = (b - 2 x cover - 2 x link diameter - n x bar diameter)/(n-1)
Minimum spacing, S_{min}	32	mm	EN 1992-1-1: 8.2(2)	S_{min} given by largest of reinforcement diameter, 20 mm or aggregate diameter (19 mm) + 5 mm. **$S < S_{min}$, therefore not okay.**
Try use 40 mm diameter bars, but iteratively increase the number of bars to decrease w_k until $w_k < w_{max}$:				
Area of one Y40 bar	1256.64	mm^2	-	A = pi(diameter/2)^2
As_{req} for ULS requirements	16143	mm^2	-	Ignore the slight reduction in Asreq caused by reducing the bar size.
Number of Y40 bars required	12.85	-	-	-
Number of Y40 bars provided	15	-	-	Provide two layers of 17 Y25 bars each, with a Y25 spacer bar.
Area of tension reinforcement provided, As_{prov}	18850	mm^2	-	-
Spacing between bars, S	44.14	mm	-	S = (b - 2 x cover - 2 x link diameter - n x bar diameter)/(n-1)
Minimum spacing, S_{min}	40	mm	EN 1992-1-1: 8.2(2)	S_{min} given by largest of reinforcement diameter, 20 mm or aggregate diameter (19 mm) + 5 mm. **$S > S_{min}$, therefore okay.**
Average effective depth, d	1689	mm	-	Average d = h - C - link diameter - main reinforcement diameter/2
Neutral axis depth, x	680.61	mm	-	Calculated by taking moments about the neutral axis - see sheet 2.
Stress in the tensile steel, σ_s	220.06	MPa	Mosley, Bungey & Hulse (2007) 6.4.3	$\sigma_s = M_s/[(d-x/3)As_{prov}]$
k_t	0.4	-	EN 1992-1-1:2004 7.3.4 (2)	Assume long-term loading.
$f_{ct,eff}$	3.00	MPa	Mosley, Bungey & Hulse (2007) 6.1.5	Suggested minimum value for $f_{ct,eff}$ = 3.00 MPa.
α_e	17.06	-	-	See sheet 2.
$A_{c,eff}$	388500	mm^2	EN 1992-1-1:2004 7.3.2 (2)	$A_{c,eff}$ = b x $h_{c,ef}$, where $h_{c,ef}$ = lesser of 2.5(h-d), (h-x)/3 and h/2.
$\rho_{p,eff}$	0.0485188	-	EN 1992-1-1:2004 7.3.4 (2)	$\rho_{p,eff} = As_{prov}/A_{c,eff}$
E_s	200	GPa	-	-
$\varepsilon_{sm} - \varepsilon_{cm}$	0.000874283	-	EN 1992-1-1:2004 7.3.4 (2)	$\varepsilon_{sm} - \varepsilon_{cm} = \frac{\sigma_s - k_t \frac{f_{ct,eff}}{\rho_{p,eff}}(1+\alpha_e\rho_{p,eff})}{E_s} \geq 0{,}6\frac{\sigma_s}{E_s}$
$0.6\sigma_s/E_s$	0.000660184	-	EN 1992-1-1:2004 7.3.4 (2)	$\varepsilon_{sm} - \varepsilon_{cm} > 0.6\sigma_s/E_s$, therefore okay.
Design cover, c	75	mm	-	-
Bar diameter, ϕ	25	mm	-	-
k_1	0.8	-	EN 1992-1-1:2004 7.3.4 (3)	k_1 = 0.8 for high bond bars.
k_2	0.5	-	EN 1992-1-1:2004 7.3.4 (3)	k_2 = 0.5 for bending.
k_3	3.4	-	EN 1992-1-1:2004 7.3.4 (3)	-
k_4	0.425	-	EN 1992-1-1:2004 7.3.4 (3)	-
$S_{r,max}$	342.59	mm	EN 1992-1-1:2004 7.3.4 (3)	$s_{r,max} = k_3c + k_1k_2k_4\phi/\rho_{p,eff}$

Crack width, w_k	0.2995	mm	EN 1992-1-1:2004 7.3.4 (1)	$w_k = s_{r,max}(\varepsilon_{sm} - \varepsilon_{cm})$
Maximum permissible crack width, w_{max}	0.3	mm	EN 1992-1-1:2004 Table 7.1N	Exposure class XS3. **$w_k < w_{max}$, therefore okay**.
Therefore provide 15 Y40 bars.				

V. DESIGN FOR CRACK WIDTH: THERMAL AND SHRINKAGE CRACKING - SIDE FACES				
Item	Value	Unit	Reference	Explanation/Formula
Typically, two different types of cracking need to be checked: early-age thermal cracking due to heat of hydration when the precast beams are cast, and long-term cracking due to shrinkage and variations in ambient temperature. However, in this case, long-term thermal and shrinkage movements of the beams won't be restrained, as the beams will sit on bearings which allow longitudinal movement of the beams. As such, only early-age thermal and shrinkage cracking needs to be checked.				
Early-Age Cracking				
Assume that when the beams are cast, the formwork provides an insignificant amount of exernal restraint, such that internal restraint is dominant.				
Cement content	395	kg/m^3	CIRIA C660 Table 4.2	50 % GGBS, value for C35/45 strength class.
Temperature drop, T_1	58.4	°C	CIRIA C660 Figure 4.6, Table 3.3	Assume plywood formwork to be conservative. Section thickness > 1000 mm, therefore cannot use Figure 4.6 to find T_1, and have to use Table 3.3. Note that Table 3.3 assumes CEM I cement, so this value of T_1 is conservative. Value for strength class C35/45 for depth = 1800 mm interpolated from values for depths of 1000 mm and 2000 mm. Assume summer casting.
Coefficient of thermal expansion, α_c	10	με/°C	CIRIA C660 4.5	No information about aggregates, so use value recommended by EN 1992-1-1.
Autogeneous shrinkage, ε_{ca}	0	με	CIRIA C660 5.3	Ignore autogenous shrinkage, as it will occur uniformly throughout the section, and therefore won't contribute to strain differentials.
Restraint, R	0.42	-	CIRIA C660 4.7.4	-
Creep coefficient, K_1	0.65	-	CIRIA C660 4.9.1	-
Early-age restrained strain, ε_r	159.4	με	CIRIA C660 3.2.1	$\varepsilon_r = K_1\{[\alpha_c T_1 + \varepsilon_{ca}]R$
Tensile strain capacity, ε_{ctu}	70	με	CIRIA C660 3.6.1	No information about aggregates, so use early-age value for simplified method.
Risk of early-age cracking?	Yes	-	CIRIA C660 1.4	$\varepsilon_r > \varepsilon_{ctu}$, so cracking will occur.
k_c	0.5	-	CIRIA C660 Table 3.1	To be conservatice, assume external restraint dominant.
k	1	-	CIRIA C660 Table 3.1	t > 800 mm.
A_{ct}	504000	mm^2	-	A_{ct} = area to depth 0.2h = 360 mm.
Early-age concrete tensile strength, $f_{ctm(3)}$	1.92	MPa	CIRIA C660 Table 3.2	-
f_{yk}	500	MPa	-	-

Minimum area of reinforcement per face, $A_{s,min}$	968	mm^2	CIRIA C660 3.3.1	$A_{s,prov} > A_{s,min}$, therefore okay - cracking is controlled. $A_{s,min} = k_c k A_{ct} \frac{f_{ctm}(t)}{f_{ky}}$
Design cover, C	75	mm	-	-
k_1	1.14	-	CIRIA C660 4.13	k_1 = 1.14 when calculating early-age thermal crack widths.
Reinforcement diameter, ϕ	40	mm	-	Reinforcement diameter varies, use largest for worst-case scenario.
$h_{e,ef}$	237.5	mm	CIRIA C660 5.2	$h_{e,eff} = 2.5 (C + \phi/2)$
$A_{c,eff}$	427500	mm^2	-	$A_{c,eff} = h_{e,eff}$ x 1800 for side faces (worst-case scenario)
As_{prov}	4299	mm^2/m	-	Use As_{prov} for the side faces (worst-case scenario)
$\rho_{p,eff}$	0.010056	-	CIRIA C660 3.4	$\rho_{p,eff} = As_{prov}/A_{c,eff}$
Crack spacing, $S_{r,max}$	2182	mm	CIRIA C660 3.4	$S_{r,max} = 3.4c + 0.425 \frac{k1\varphi}{\rho_{p,eff}}$
Crack-inducing strain, ε_{cr}	124.43	-	CIRIA C660 3.2.2	$\varepsilon_{cr} = \varepsilon_r - 0.5\varepsilon_{ctu}$
Crack width, w_k	0.272	mm	CIRIA C660 3.5.4	$w_k = S_{r,max}\varepsilon_{cr}$
Maximum permissible crack width, w_{max}	0.3	mm	EN 1992-1-1:2004 Table 7.1N	Exposure class XS3. **$w_k < w_{max}$, therefore okay**.
Therefore no additional reinforcement is required to control early-age cracking.				

VI. DETAILING				
Item	Value	Unit	Reference	Explanation/Formula
The following detailing checks and calculations are carried out below: 1. Determination of anchorage lengths for the main reinforcement 2. Determination of lap lengths for the main reinforcement 3. Maximum spacing of the main reinforcement 4. Provision of side face reinforcement to control cracking 5. Curtailment of the main reinforcement				
1. Determination of Anchorage Lengths for the Main Reinforcement				
Main reinforcement diameter, ϕ	32	mm	-	For 40 mm (hogging) bars, use anchorage lengths determined in ULS/SLS design.
Concrete strength, f_{ck}	35	MPa	-	-
Use straight bars for sagging reinforcement.				
Bond conditions for hogging reinforcement	Good	-	Mosley, Bungey & Hulse (2007) Figure 5.8	Section deeper than 600 mm, with sagging reinforcement placed at a depth greater than 300 mm.
Straight bar anchorage coefficient, K_A, for f_{ck} = 35 MPa	32.00	-	Mosley, Bungey & Hulse (2007) Table A.6	-
Sagging reinforcement (straight bar) anchorage length, L	1024	mm	Mosley, Bungey & Hulse (2007) Table A.6	$L = K_A$ x ϕ
Provided anchorage length, L_{prov}	1050	mm	-	Choose a multiple of 50 for practicality/convenience.
Minimum anchorage length, L_{min}	320	mm	Mosley, Bungey & Hulse (2007) 5.2	L_{min} = greater of 100 mm and 10 x ϕ. $L_{prov} > L_{min}$, therefore okay.
Therefore use an anchorage length of 1050 mm for the sagging (straight) reinforcement.				
2. Determination of Lap Lengths for the Main Reinforcement				

Lap length coefficient for f_{ck} = 35 MPa	48	-	Mosley, Bungey & Hulse (2007) Table A.6	To be conservative, assume > 50 % of bars lapped at a section
Required lap length, L_{req}	1536	mm	-	L_{req} = lap length coefficient x ϕ
Provided lap length, L_{prov}	1550	mm	-	Choose a multiple of 50 for practicality/convenience.
Minimum lap length, L_{min}	480	mm	Mosley, Bungey & Hulse (2007) 5.3	L_{min} = greater of 100 mm and 15 x ϕ. $L_{prov} > L_{min}$, therefore okay.
Therefore provide lap lengths of 1550 mm for the 32 mm diameter (sagging) reinforcement. Still provide lap lengths of 1950 mm for the 40 mm (hogging) reinforcement.				
3. Maximum Spacing of the Main Reinforcement				
Stress in the main reinforcement (sagging)	196.92	MPa	-	-
Stress in the main reinforcement (hogging)	220.06	MPa	-	-
Maximum stress in the main reinforcement	220.06	MPa	-	Maximum stress = hogging stress (220.06 MPa)
Maximum bar spacing, S_{max}	224.93	mm	Mosley, Bungey & Hulse (2007) Table 6.7	Value for 220.06 MPa interpolated between values for 200 and 240 MPa.
Spacing between bars, S (sagging)	33.89	mm	-	$S < S_{max}$, therefore okay.
Spacing between bars, S (hogging)	44.14	mm	-	$S < S_{max}$, therefore okay.
4. Provision of Side Face Reinforcement				
As the beam is deeper than 1 m, side face reinforcement should be provided to control flexural cracking in the side faces (Mosley, Bungey & Hulse, 2007:133). This reinforcement should be "evenly distributed between the main tension steel and the neutral axis" (Mosley, Bungey & Hulse, 2007: 133).				
Depth of neutral axis, x (sagging)	629.36	mm	-	-
Depth of neutral axis, x (hogging)	680.61	mm	-	-
Depth requiring side face reinforcement (sagging)	1064	mm	Mosley, Bungey & Hulse (2007) 6.1.8	Depth = d - x
Depth requiring side face reinforcement (hogging)	1008	mm	Mosley, Bungey & Hulse (2007) 6.1.8	Depth = d - x
Area of side face reinforcement required, $A_{s,min}$	4916.69	mm^2	Mosley, Bungey & Hulse (2007) 6.1.8	Use formula for $A_{s,min}$ to control cracking, but with k = 0.5 and k_c = 1.0.
Area of side face reinforcement provided, $A_{s,prov}$	5629.73	mm^2	-	Provide 7 Y32 bars in the side faces (NOTE: this includes the bars used for torsion reinforcement). Provide the sagging bars at a distance of 0.5 to 14.5 m along the beam, and the hogging bars up to a distance of 3 m from the ends of the beam.
Spacing of the side face reinforcement, S	130.67	mm	-	S = (1008 - 7 x 32)/6, where the 1008 mm is used for the worst-case scenario.
Maximum bar spacing, S_{max}	300	mm	Mosley, Bungey & Hulse (2007) 6.1.8, Table 6.7	Steel stress value = half of that for the main reinforcement, therefore < 160 MPa. $S < S_{max}$, therefore okay.
Therefore provide 7 Y32 bars in the side faces, along a length of 0.5 to 14.5 m for the sagging zone, and up to 3 m from the ends of the beam for the hogging zone.				
5. Curtailment of the Main Reinforcement				
Instead of recalculating the curtailment lengths of the reinforcement from the BMD, curtail the bars in the same proportions/percentages as the reinforcement in the ULS/SLS design.				
Sagging Reinforcement - 3 Segments of Different Amounts of Reinforcement, Based on the BMD of the Critical Continuous Beam				
1st Segment	19	bars	-	Provide 1 layer of 19 Y32 bars.
Length of 1st Segment	8.55	m	Mosley, Bungey & Hulse (2007) 7.9	"Extend each curtailed bar a full anchorage length beyond where it is no longer needed". Therefore segment length = (13 - 5.5) + 1.05
2nd Segment	17	bars	-	Provide 1 layer of 17 Y32 bars.
Length of 2nd Segment	13.05	m	Mosley, Bungey & Hulse (2007) 7.9	"Extend each curtailed bar a full anchorage length beyond where it is no longer needed". Therefore segment length = (15 - 3.0) + 1.05
3rd Segment	9	bars	-	Provide 1 layer of 9 Y40 bars.

Length of 3rd Segment	15	m	-	No curtailment of third segment.
Hogging Reinforcement - 3 Segments of Different Amounts of Reinforcement, Based on the BMD of the Critical Continuous Beam				
1st Segment	15	bars	-	Provide 1 layer of 15 Y40 bars.
Length of 1st Segment	4.35	m	Mosley, Bungey & Hulse (2007) 7.9	"Extend each curtailed bar a full anchorage length beyond where it is no longer needed". Therefore segment length = 2.5 + 1.85
2nd Segment	13	bars	-	Provide 1 layer of 13 Y40 bars.
Length of 2nd Segment	5.35	m	Mosley, Bungey & Hulse (2007) 7.9	"Extend each curtailed bar a full anchorage length beyond where it is no longer needed". Therefore segment length = 3.5 + 1.85
3rd Segment	7	bars	-	Provide 1 layer of 7 Y40 bars.
Length of 3rd Segment	15	m	Mosley, Bungey & Hulse (2007) 7.9	Provide these bars over the full length of the beam, to allow for fixing of shear reinforcement over the full length of the beam.

FOR ONE LAYER OF 11 Y40 BARS				
Item	**Value**	**Unit**	**Reference**	**Explanation/Formula**
b	1400	mm	-	-
Average effective depth, d	1689	mm	-	-
As_{prov}	13823	mm^2	-	-
E_{cm}	34	GPa	Mosley, Bungey & Hulse (2007) Table 6.11	Value for C35/45 strength class.
Creep coefficient, ϕ	1.9	-	Mosley, Bungey & Hulse (2007) Table 6.12	Assume loading at 28 days. Outdoor exposure, $2A_c/u = 2 \times [(1400 \times 1800)/2(1400 + 1800)] = 787.5$.
$E_{c,eff}$	11.72	GPa	Mosley, Bungey & Hulse (2007) Equation 6.8	Use effective concrete modulus to account for effects of creep - cracking must still be controlled, even in the long-term.
E_{steel}	200	GPa	-	-
α_e	17.06	-	Mosley, Bunger & Hulse 6.3.2	$\alpha_e = E_{steel}/E_{c,eff}$
Taking moments about the neutral axis, and manually equating the left- and right- hand sides of the equation by varying "x":				
Neutral axis depth, x	604.4402905	mm	-	-
Left-hand side, LHS:	255743645.3	-	Mosley, Bunger & Hulse 4.10.1	LHS = (b).(x).(x/2)
Right -hand side, RHS:	255743645.3	-	Mosley, Bunger & Hulse 4.10.1	RHS = $(a_e).(As_{prov}).(d-x)$
LHS-RHS	0.000788987	-	-	-
Therefore x = 604.44 mm (approximately)				

FOR ONE LAYER OF 16 Y32 BARS				
Item	**Value**	**Unit**	**Reference**	**Explanation/Formula**
b	1400	mm	-	-
Average effective depth, d	1693	mm	-	-
As_{prov}	12868	mm^2	-	-
E_{cm}	34	GPa	Mosley, Bungey & Hulse (2007) Table 6.11	Value for C35/45 strength class.
Creep coefficient, ϕ	1.9	-	Mosley, Bungey & Hulse (2007) Table 6.12	Assume loading at 28 days. Outdoor exposure, $2A_c/u = 2 \times [(1400 \times 1800)/2(1400 + 1800)] = 787.5$.
$E_{c,eff}$	11.72	GPa	Mosley, Bungey & Hulse (2007) Equation 6.8	Use effective concrete modulus to account for effects of creep - cracking must still be controlled, even in the long-term.
E_{steel}	200	GPa	-	-
α_e	17.06	-	Mosley, Bunger & Hulse 6.3.2	$\alpha_e = E_{steel}/E_{c,eff}$
Taking moments about the neutral axis, and manually equating the left- and right- hand sides of the equation by varying "x":				
Neutral axis depth, x	588.5186583	mm	-	-
Left-hand side, LHS:	242447947.8	-	Mosley, Bunger & Hulse 4.10.1	LHS = (b).(x).(x/2)
Right -hand side, RHS:	242447947.8	-	Mosley, Bunger & Hulse 4.10.1	RHS = $(a_e).(As_{prov}).(d-x)$
LHS-RHS	0.005092263	-	-	-
Therefore x = 588.52 mm (approximately)				

FOR ONE LAYER OF 18 Y32 BARS				
Item	**Value**	**Unit**	**Reference**	**Explanation/Formula**

b	1400	mm	-	-
Average effective depth, d	1693	mm	-	-
As_{prov}	14476	mm^2	-	-
E_{cm}	34	GPa	Mosley, Bungey & Hulse (2007) Table 6.11	Value for C35/45 strength class.
Creep coefficient, ϕ	1.9	-	Mosley, Bungey & Hulse (2007) Table 6.12	Assume loading at 28 days. Outdoor exposure, $2A_c/u = 2 \times [(1400 \times 1800)/2(1400 + 1800)] = 787.5$.
$E_{c,eff}$	11.72	GPa	Mosley, Bungey & Hulse (2007) Equation 6.8	Use effective concrete modulus to account for effects of creep - cracking must still be controlled, even in the long-term.
E_{steel}	200	GPa	-	-
α_e	17.06	-	Mosley, Bunger & Hulse 6.3.2	$\alpha_e = E_{steel}/E_{c,eff}$
Taking moments about the neutral axis, and manually equating the left- and right- hand sides of the equation by varying "x":				
Neutral axis depth, x	616.3055103	mm	-	-
Left-hand side, LHS:	265882737.4	-	Mosley, Bunger & Hulse 4.10.1	LHS = (b).(x).(x/2)
Right -hand side, RHS:	265882737.4	-	Mosley, Bunger & Hulse 4.10.1	RHS = $(a_e).(As_{prov}).(d-x)$
LHS-RHS	0.000290304	-	-	-
Therefore x = 616.31 mm (approximately)				

FOR ONE LAYER OF 19 Y32 BARS				
Item	**Value**	**Unit**	**Reference**	**Explanation/Formula**
b	1400	mm	-	-
Average effective depth, d	1693	mm	-	-
As_{prov}	15281	mm^2	-	-
E_{cm}	34	GPa	Mosley, Bungey & Hulse (2007) Table 6.11	Value for C35/45 strength class.
Creep coefficient, ϕ	1.9	-	Mosley, Bungey & Hulse (2007) Table 6.12	Assume loading at 28 days. Outdoor exposure, $2A_c/u = 2 \times [(1400 \times 1800)/2(1400 + 1800)] = 787.5$.
$E_{c,eff}$	11.72	GPa	Mosley, Bungey & Hulse (2007) Equation 6.8	Use effective concrete modulus to account for effects of creep - cracking must still be controlled, even in the long-term.
E_{steel}	200	GPa	-	-
α_e	17.06	-	Mosley, Bunger & Hulse 6.3.2	$\alpha_e = E_{steel}/E_{c,eff}$
Taking moments about the neutral axis, and manually equating the left- and right- hand sides of the equation by varying "x":				
Neutral axis depth, x	629.3595523	mm	-	-
Left-hand side, LHS:	277265412.2	-	Mosley, Bunger & Hulse 4.10.1	LHS = (b).(x).(x/2)
Right -hand side, RHS:	277265412.2	-	Mosley, Bunger & Hulse 4.10.1	RHS = $(a_e).(As_{prov}).(d-x)$
LHS-RHS	0.000584126	-	-	-
Therefore x = 629.36 mm (approximately)				

FOR ONE LAYER OF 13 Y40 BARS				
Item	**Value**	**Unit**	**Reference**	**Explanation/Formula**
b	1400	mm	-	-
Average effective depth, d	1689	mm	-	-
As_{prov}	16336	mm^2	-	-

E_{cm}	34	GPa	Mosley, Bungey & Hulse (2007) Table 6.11	Value for C35/45 strength class.
Creep coefficient, ϕ	1.9	-	Mosley, Bungey & Hulse (2007) Table 6.12	Assume loading at 28 days. Outdoor exposure, $2A_c/u = 2 \times [(1400 \times 1800)/2(1400 + 1800)] = 787.5$.
$E_{c,eff}$	11.72	GPa	Mosley, Bungey & Hulse (2007) Equation 6.8	Use effective concrete modulus to account for effects of creep - cracking must still be controlled, even in the long-term.
E_{steel}	200	GPa	-	-
α_e	17.06	-	Mosley, Bunger & Hulse 6.3.2	$\alpha_e = E_{steel}/E_{c,eff}$
Taking moments about the neutral axis, and manually equating the left- and right- hand sides of the equation by varying "x":				
Neutral axis depth, x	644.7605179	mm	-	-
Left-hand side, LHS:	291001287.8	-	Mosley, Bunger & Hulse 4.10.1	LHS = (b).(x).(x/2)
Right -hand side, RHS:	291001287.8	-	Mosley, Bunger & Hulse 4.10.1	RHS = $(a_e).(As_{prov}).(d-x)$
LHS-RHS	0.005031765	-	-	-
Therefore x = 644.76 mm (approximately)				

FOR ONE LAYER OF 15 Y40 BARS				
Item	**Value**	**Unit**	**Reference**	**Explanation/Formula**
b	1400	mm	-	-
Average effective depth, d	1689	mm	-	-
As_{prov}	18850	mm^2	-	-
E_{cm}	34	GPa	Mosley, Bungey & Hulse (2007) Table 6.11	Value for C35/45 strength class.
Creep coefficient, ϕ	1.9	-	Mosley, Bungey & Hulse (2007) Table 6.12	Assume loading at 28 days. Outdoor exposure, $2A_c/u = 2 \times [(1400 \times 1800)/2(1400 + 1800)] = 787.5$.
$E_{c,eff}$	11.72	GPa	Mosley, Bungey & Hulse (2007) Equation 6.8	Use effective concrete modulus to account for effects of creep - cracking must still be controlled, even in the long-term.
E_{steel}	200	GPa	-	-
α_e	17.06	-	Mosley, Bunger & Hulse 6.3.2	$\alpha_e = E_{steel}/E_{c,eff}$
Taking moments about the neutral axis, and manually equating the left- and right- hand sides of the equation by varying "x":				
Neutral axis depth, x	680.6066428	mm	-	-
Left-hand side, LHS:	324257781.6	-	Mosley, Bunger & Hulse 4.10.1	LHS = (b).(x).(x/2)
Right -hand side, RHS:	324257781.6	-	Mosley, Bunger & Hulse 4.10.1	RHS = $(a_e).(As_{prov}).(d-x)$
LHS-RHS	0.001115978	-	-	-
Therefore x = 680.61 mm (approximately)				

Appendix B: St. Helena Breakwater Crown Wall Design Calculation Sheets

Please find the calculation sheets attached on the following page.

	LOADING CALCULATIONS	
	Member: St. Helena Crown Wall (Precast Unit F01)	

Project:	MSc.Eng. Structural Engineering – Research
Sheet Series:	A (Loading Calculations)
Calculations By:	Nicholas Elias
Date:	02/03/2022

Date	Check No.	Checked By	Review Level	Approved
01/03/2022	A-01	P.E.S	-	No
29/03/2022	A-02	P.E.S	-	Yes

Check No.	Check Notes	Action	Status
A-01	Add wave loading for crack width design.	N.N.E	Complete

Overview of Member	
Structure Type:	Horizontal composite harbour breakwater
Member Type:	Reinforced concrete wall
Member Loads:	Wave Loading

Reference	INTRODUCTION
	The aim of these calculations is to convert the wave loading information for the St. Helena Breakwater crown wall, supplied by PRDW Consulting Port and Coastal Engineers, into distributed loads to be applied to a typical precast crown wall unit (Precast Unit F01) in the analysis stage of the design. The following calculations are presented in this calculation sheet: 1. Wave Loads 2. Load Combinations: ULS 3. Load Combinations: Crack Width Design The design of the St. Helena Bay crown wall continues with the member analysis in Series B (Member Analysis) of these calculation sheets.
	1. WAVE LOAD CALCULATIONS
	From the wave loading information provided by PRDW, the wave loading pressures exerted on the crown wall may be broken up into two components, as shown in Figure 1. 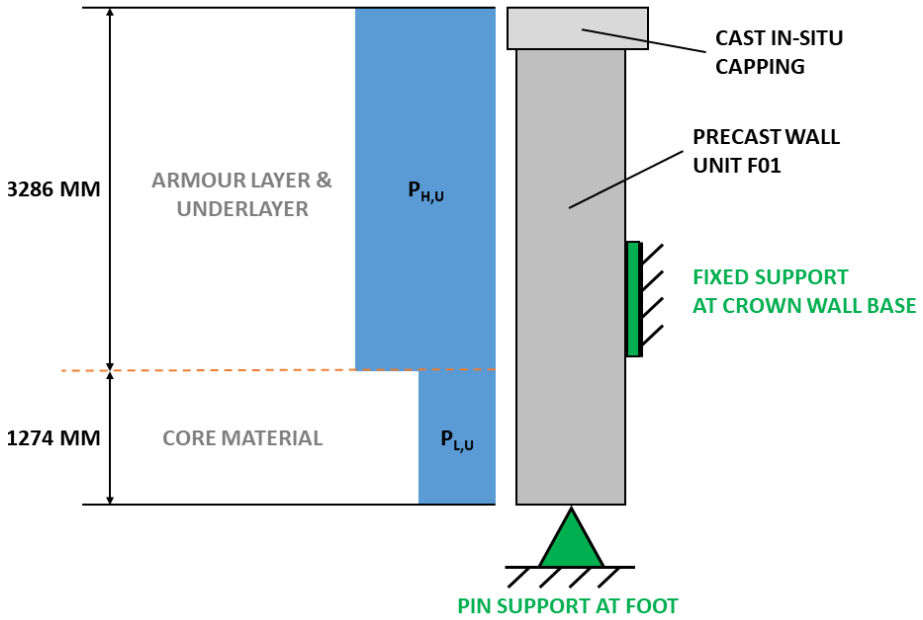 *Figure 1: An illustration of the distribution of wave loading pressures on the St. Helena Crown Wall, adapted from the wave loading information provided by PRDW.* Values for the upper and lower wave pressure components ($P_{H,U}$ and $P_{H,L}$, respectively) were calculated by PRDW and are shown in Table 1.

Table 1: A summary of the wave loading pressure values provided by PRDW.

Wave Return Period [Years]	Wave Loading Pressure [kPa]			
	Peak Wave Period of 13 Seconds		Peak Wave Period of 19 Seconds	
	$P_{H,U}$	$P_{H,L}$	$P_{H,U}$	$P_{H,L}$
1	28.3	14.1	41.3	20.7
10	39.9	19.9	58.3	29.2
100	51.5	25.8	75.3	37.6
1000	63.1	31.6	92.3	46.1

Of the wave pressures shown in Table 1, the most significant are the 1:100 and 1:1000 year pressures, which represent the maximum pressures for normal and extreme operating conditions, respectively. As such, only the 1:100 and 1:1000 year pressures will be used in the ULS analysis of the crown wall. The 1:1 year pressures, which may be used (conservatively) to represent the service wave loads on the crown wall, will be used for crack width design.

As the 19 second period wave loads are greater in magnitude than the 13 second period loads, and thus represent the "worst-case" scenario, only the 19 second period loads will be used in the analysis of the crown wall.

2. LOAD COMBINATIONS: ULS

The ULS load factors to be used in the ULS analysis of the crown wall are shown in Table 2.

BS 6349 Part 2 Table A.1 Set B

Beeby & Narayanan (2009) Table 2.3

Table 2: Load factors to be used in the analysis of the crown wall, taken from BS 6349. Note that the 1:1000 year (extreme) case is taken as an "accidental" load due to its low probability of occurrence.

Wave Return Period [Years]	Load Factor
100 (Operating Case)	1.4
1000 (Extreme Case)	1.0

As the crown wall will be analysed under the action of wave loading only, load combination factors are not required. The wave loads to be used in the analysis of the crown wall are therefore shown in Table 3. Note that, as the crown wall will be analysed and designed as a beam with unit width, the wave pressures shown in Table 1 have been multiplied by 1 metre to convert them to line loads.

Table 3: ULS factored wave loads to be used in the analysis of the crown wall.

Wave Return Period [Years]	Factored Wave Load [kN/m]	
	$w_{H,U}$	$w_{H,L}$
100	105.4	52.6
1000	92.3	46.1

3. LOAD COMBINATIONS: CRACK WIDTH DESIGN

A load factor of 1.0 is to be used in the analysis of the crown wall for crack width design. Resultant wave loads are therefore shown in Table 4.

Table 4: Factored wave loads to be used in the analysis of the crown wall for crack width design.

Wave Return Period [Years]	Factored Wave Load [kN/m]	
	$w_{H,U}$	$w_{H,L}$
1	41.3	20.7

CONCLUSION

The wave loading information provided by PRDW for the St. Helena Bay breakwater crown wall has been factored and converted into distributed (line) loads for use in the ULS and crack width design analysis of the crown wall. The resultant loads can be seen in **Tables 3 and 4**.

The design of the St. Helena Bay crown wall continues with the member analysis in Series B (Member Analysis) of these calculation sheets.

	ANALYSIS CALCULATIONS	PRDW Consulting Port and Coastal Engineers
	Member: St. Helena Crown Wall (Precast Unit F01)	

Project:	MSc.Eng. Structural Engineering – Research
Sheet Series:	B (Analysis Calculations)
Calculations By:	Nicholas Elias
Date:	22/02/2022

Date	Check No.	Checked By	Review Level	Approved
01/03/2022	B-01	P.E.S	-	No
29/03/2022	B-02	P.E.S	-	Yes

Check No.	Check Notes	Action	Status
B-01	Add wave loading for crack width design	N.N.E	Complete

Overview of Member	
Structure Type:	Horizontal composite harbour breakwater
Member Type:	Reinforced concrete wall
Member Loads:	Wave Loading
Limit States for Analysis:	Ultimate Limit State (ULS) and Crack Width Design (CWD)

Reference	INTRODUCTION
	An explanation of the analysis process for the St. Helena breakwater crown wall (Precast Unit F01) is provided in these calculation sheets, along with the results of the analysis. The following calculations and results are presented in this calculation sheet: 1. Analysis Model 2. Analysis Results (ULS) 3. Design Values for Moment and Shear (ULS) 4. Analysis Results (CWD) The design of the St. Helena Bay crown wall continues with the member design in Series C (ULS & SLS Design) of these calculation sheets.
	1. ANALYSIS MODEL
	The crown wall was analysed as a beam with unit width, as shown in Figure 1. For the purposes of the analysis, the precast crown wall unit, F01, and the cast in-situ capping were treated as one rigid member (i.e., one beam). 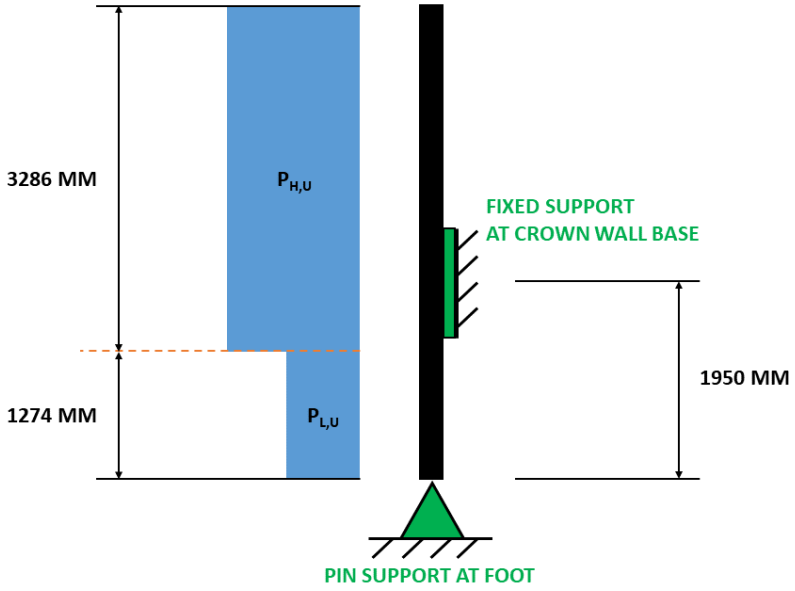 *Figure 1: A diagram of the analysis model for the St. Helena crown wall.* Analysis of the crown wall was carried out using the analysis software *Prokon*, for the 1:100 and 1:1000 year wave loads determined in the loading calculations (Series A of these calculation sheets).

2. ANALYSIS RESULTS (ULS)

Results of the analysis are shown in Table 1. Bending moment and shear force diagrams for the critical load case (the 1:100 year wave loading case) are shown in Figures 2 and 3, respectively.

Table 1: A summary of the Prokon analysis results.

Wave Return Period [Years]	Maximum Sagging Moment [kNm]	Maximum Hogging Moment [kNm]	Maximum Shear Force [kN]
100	15.53	359.0	275.1
1000	13.61	314.4	240.9

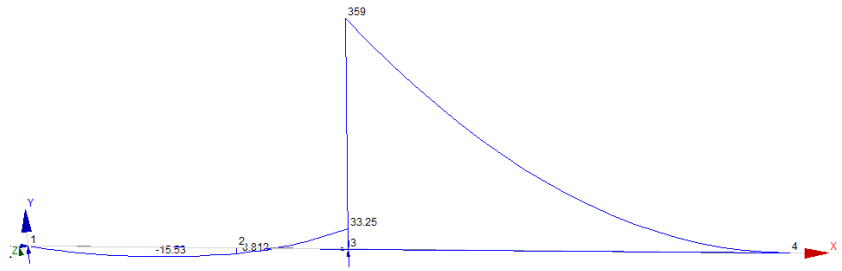

Figure 2: Bending moment diagram for the critical (1:100 year) wave loading case.

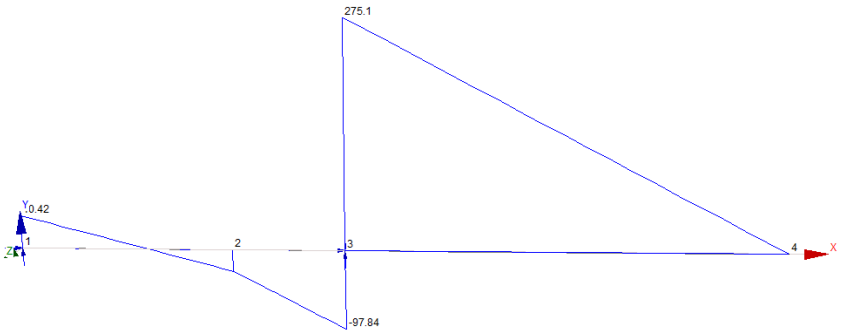

Figure 3: Shear force diagram for the critical (1:100 year) wave loading case.

3. DESIGN VALUES FOR MOMENT AND SHEAR (ULS)

Values for the maximum sagging and hogging moments, and shear forces, to be used in the design of the crown wall, are shown in Table 2.

Table 2: Design values for bending moment and shear forces.

Type of Force	Design Value
Bending (Sagging)	15.53 kNm
Bending (Hogging)	359.0 kNm
Shear	275.1 kN

4. ANALYSIS RESULTS (CWD)

Results of the analysis are shown in Table 3. The bending moment diagram for the 1:1 year wave loading case is shown in Figure 4.

Table 3: A summary of the Prokon analysis results.

Wave Return Period [Years]	Maximum Sagging Moment [kNm]	Maximum Hogging Moment [kNm]	Maximum Shear Force [kN]
1	6.107	140.7	107.8

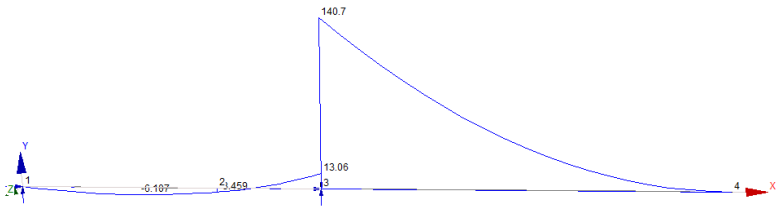

Figure 4: Bending moment diagram for the 1:1 year wave loading case.

CONCLUSION

The results of the analysis of the St. Helena breakwater crown wall were presented in this calculation sheet. These results were used in the design of Precast Unit F01 of the crown wall, as shown in Series C (ULS and SLS Design) and D (Crack Width Design) of these calculation sheets.

	ULS & SLS DESIGN CALCULATIONS	
	Member: St. Helena Breakwater Crown Wall (Precast Unit F01)	

Project:	MSc. Eng. Structural Engineering - Research
Sheet Series:	C (ULS & SLS Design Calculations)
Calculations By:	Nicholas Elias
Date:	16/03/2022

Date	Checked By	Check No.	Review Level	Approved
29/03/2022	P.E.S	C-01	-	Yes

Check No.	Action	Check Notes	Status
C-01	N.N.E		

Overview of Member	
Structure Type:	Horizontal composite harbour breakwater
Member Type:	Reinforced concrete wall
Member Loads:	Wave loading
Limit States for Analysis:	Ultimate Limit State (ULS)
	Serviceability Limit State (SLS)
	Crack Width Design (CWD)
ULS Design Checks:	Bending
	Shear
SLS Design Checks:	Minimum and maximum amount of steel
	Durability (i.e., cover depth and mix design selection)
CWD Design Checks:	See Calculation Sheet D (Crack Width Design)

I. DESIGN INPUT VALUES				
Input	Value	Unit	Reference	Explanation/Formula
Service life	100	years	BS 6349-1-1:2013 Table 1	The St. Helena breakwater is a port structure of national significance.

II. SELECTION OF MEMBER PROPERTIES				
Property	Value	Unit	Reference	Explanation/Formula
Concrete Properties				
Nominal cover depth	60	mm	BS 6349-1-4: 2013 Table 3	Crown wall in upper tidal/splash & spray zone (XS3). 60 mm nominal cover selected to avoid low w/b ratio (therefore reducing cost).
Design cover depth	75	mm	Marine Concrete Structures (Alexander, 2016) Table 3.7	A 15 mm reinforcement placing tolerance was added to the nominal cover to allow for errors in workmanship.
Concrete strength class	C35/45	MPa	BS 6349-1-4: 2013 Table 2	Recommended value for 60 mm nominal cover depth.
Maximum w/b ratio	0.4	-	BS 6349-1-4: 2013 Table 2	Recommended value for 60 mm nominal cover depth.
Minimum binder content	380	kg/m^3	BS 6349-1-4: 2013 Table 2	Recommended value for 60 mm nominal cover depth.
Binder type	IIIA	-	BS 6349-1-4: 2013 Table 2	With 50 % GGBS (Assume that sufficient GGBS is available).
Steel Properties				
Steel characteristic strength, f_{yk}	500	MPa	Mosley, Bungey & Hulse (2007) 1.6.2	Choose to use high yield steel bars.

III. BENDING STRENGTH CHECK - SAGGING				
Item	Value	Unit	Reference	Explanation/Formula
Information from Analysis				
Ultimate applied moment, M_u	15.53	kNm	Calculation Sheet Series B	-
Section Properties				
Concrete characteristic cylinder strength, f_{ck}	35	MPa	-	-
Steel characteristic strength, f_{yk}	500	Mpa	-	-
Section width, b	1000	mm	-	-
Section height, h	1000	mm	-	-
Initial main reinforcement diameter	20	mm	-	Assume Y20 bars.
Initial shear link diameter	8	mm	-	Assume Y8 bars.
Determination of Effective Depth, d				
Design cover depth, C	75	mm	-	-
Effective depth, d	907	mm	-	d = h - C - link diameter - (main reinforcement diameter/2)
Check K vs. K_{bal}				
K_{bal}	0.167	-	Mosley, Bungey & Hulse (2007) 7.2.1	-
K	0.000539	-	Mosley, Bungey & Hulse (2007) 7.2.1	$K = \frac{M}{bd^2 f_{ck}} \leq K_{bal} = 0.167$
K vs. K_{bal}	$K < K_{bal}$	-	Mosley, Bungey & Hulse (2007) 7.2.1	$K < K_{bal}$, therefore only tension steel required.
Lever Arm, z				
Lever arm, z	907	mm	Mosley, Bungey & Hulse (2007) 7.2.1	$z = d\left[0.5 + \sqrt{(0.25 - K/1.134)}\right]$
0.95d	862	mm	-	-
Lever arm, z	862	mm	Mosley, Bungey & Hulse (2007) 7.2.1	z > 0.95d, therefore use z = 0.95d.

Amount of Tension Reinforcing Steel Required, As_{req}				
Amount of tension reinforcing steel required, As_{req}	41	mm^2/m	Mosley, Bungey & Hulse (2007) 7.2.1	$A_s = \frac{M}{0.87 f_{yk} z}$
Selection of Tension Reinforcement				
Area of one Y20 bar	314	mm^2	-	A = pi(diameter/2)^2
Number of Y20 bars required	0.1	-	-	-
Number of Y20 bars provided	1	-	-	-
Area of tension reinforcement provided, As_{prov}	314	mm^2/m	-	$As_{prov} > As_{req}$, therefore okay.
Maximum Area of Steel Check				
As_{max}	40000	mm^2	Mosley, Bungey & Hulse (2007) 7.2.1	Formula rearranged to find As_{max}. $100\frac{A_{s,max}}{bh} \leq 4.0\%$
As_{prov} vs. As_{max}	$As_{prov} < As_{max}$	-	Mosley, Bungey & Hulse (2007) 7.2.1	$As_{prov} < As_{max}$, therefore okay.
Minimum Area of Steel Check				
Mean concrete tensile strength, f_{ctm}	3.2	MPa	Beeby & Narayanan (2009) Table 4.1	Value for C35/45 concrete strength class.
As_{min}	1509	mm^2/m	Mosley, Bungey & Hulse (2007) 7.2.1	Formula rearranged to find As_{min}. $100\frac{A_{s,min}}{bd} \geq 26\frac{f_{ctm}}{f_{yk}}\%$ and not less than 0.13%
As_{prov} vs. As_{min}	$As_{prov} < As_{min}$	-	Mosley, Bungey & Hulse (2007) 7.2.1	$As_{prov} < As_{min}$, therefore not okay.
As_{prov}	1571	mm^2/m	-	Provide 5 Y20 bars per metre. $As_{prov} > As_{min}$, therefore okay.
Reinforcement Fit Check				
Spacing between bars, S	183.50	mm	-	S = (b - 2 x cover - 2 x link diameter - n x bar diameter)/(n-1)
S_{min1}	20	mm	EN 1992-1-1: 8.2(2)	Tension reinforcement diameter.
S_{min2}	24	mm		Assume 19 mm aggregate.
S_{min3}	20	mm		-
S_{min}	24	mm	EN 1992-1-1: 8.2(2)	S_{min} given by the largest of S_{min1}, S_{min2} and S_{min3}.
S vs. S_{min}	$S > S_{min}$	-	-	$S > S_{min}$, therefore okay.
Therefore provide 5 Y20 bars per metre of crown wall.				

IV. BENDING STRENGTH CHECK - HOGGING				
Item	Value	Unit	Reference	Explanation/Formula
Information from Analysis				
Ultimate applied moment, M_u	359.0	kNm	Calculation Sheet Series B	-
Section Properties				
Concrete characteristic cylinder strength, f_{ck}	35	MPa	-	-
Steel characteristic strength, f_{yk}	500	Mpa	-	-
Section width, b	1000	mm	-	-
Section height, h	1000	mm	-	-
Initial main reinforcement diameter	20	mm	-	Assume Y20 bars.
Initial shear link diameter	8	mm	-	Assume Y8 bars.
Determination of Effective Depth, d				
Design cover depth, C	75	mm	-	-
Effective depth, d	907	mm	-	d = h - C - link diameter - (main reinforcement diameter/2)
Check K vs. K_{bal}				

K_{bal}	0.167	-	Mosley, Bungey & Hulse (2007) 7.2.1	-
K	0.012468	-	Mosley, Bungey & Hulse (2007) 7.2.1	$K = \frac{M}{bd^2 f_{ck}} \leq K_{bal} = 0.167$
K vs. K_{bal}	K < K_{bal}	-	Mosley, Bungey & Hulse (2007) 7.2.1	K< K_{bal}, therefore only tension steel required.
Lever Arm, z				
Lever arm, z	897	mm	Mosley, Bungey & Hulse (2007) 7.2.1	$z = d\left[0.5 + \sqrt{(0.25 - K/1.134)}\right]$
0.95d	862	mm	-	-
Lever arm, z	862	mm	Mosley, Bungey & Hulse (2007) 7.2.1	z > 0.95d, therefore use z = 0.95d.
Amount of Tension Reinforcing Steel Required, As $_{req}$				
Amount of tension reinforcing steel required, As_{req}	958	mm^2/m	Mosley, Bungey & Hulse (2007) 7.2.1	$A_s = \frac{M}{0.87 f_{yk} z}$
Selection of Tension Reinforcement				
Area of one Y20 bar	314	mm^2	-	A = pi(diameter/2)^2
Number of Y20 bars required	3.05	-	-	-
Number of Y20 bars provided	4	-	-	-
Area of tension reinforcement provided, As_{prov}	1257	mm^2/m	-	As_{prov} > As_{req}, therefore okay.
Maximum Area of Steel Check				
As_{max}	40000	mm^2	Mosley, Bungey & Hulse (2007) 7.2.1	Formula rearranged to find As_{max}. $100\frac{A_{s,max}}{bh} \leq 4.0\%$
As_{prov} vs. As_{max}	As_{prov} < As_{max}	-	Mosley, Bungey & Hulse (2007) 7.2.1	As_{prov} < As_{max}, therefore okay.
Minimum Area of Steel Check				
Mean concrete tensile strength, f_{ctm}	3.2	MPa	Beeby & Narayanan (2009) Table 4.1	Value for C35/45 concrete strength class.
As_{min}	1509	mm^2/m	Mosley, Bungey & Hulse (2007) 7.2.1	Formula rearranged to find As_{min}. $100\frac{A_{s,min}}{bd} \geq 26\frac{f_{ctm}}{f_{yk}}\%$ and not less than 0.13%
As_{prov} vs. As_{min}	As_{prov} < As_{min}	-	Mosley, Bungey & Hulse (2007) 7.2.1	As_{prov} < As_{min}, therefore not okay.
As_{prov}	1571	mm^2/m	-	Provide 5 Y20 bars per metre. As_{prov} > As_{min}, therefore okay.
Reinforcement Fit Check				
Spacing between bars, S	183.50	mm	-	S = (b - 2 x cover - 2 x link diameter - n x bar diameter)/(n-1)
S_{min1}	20	mm	EN 1992-1-1: 8.2(2)	Tension reinforcement diameter.
S_{min2}	24	mm		Assume 19 mm aggregate.
S_{min3}	20	mm		-
S_{min}	24	mm	EN 1992-1-1: 8.2(2)	S_{min} given by the largest of S_{min1}, S_{min2} and S_{min3}.
S vs. S_{min}	S > S_{min}	-	-	S > S_{min}, therefore okay.
Therefore provide 5 Y20 bars per metre of crown wall.				

V. MINIMUM HORIZONTAL STEEL REQUIREMENTS				
Item	Value	Unit	Reference	Explanation/Formula
Provide minimum reinforcement in both directions, vertical and horizontal				
As_{min}	1509	mm^2/m	Mosley, Bungey & Hulse (2007) 7.2.1	Formula rearranged to find As_{min}. $100\frac{A_{s,min}}{bd} \geq 26\frac{f_{ctm}}{f_{yk}}\%$ and not less than 0.13%

As_{prov}	1571	mm^2/m	-	Provide 5 Y20 bars per metre. $As_{prov} > As_{min}$, therefore okay.
Therefore provide 5 horizontal Y20 bars per metre of crown wall.				

VI. SHEAR STRENGTH CHECK				
Item	Value	Unit	Reference	Explanation/Formula
Information from Analysis				
Ultimate design shear force, $V_u = V_{Ed}$	275.1	kN/m	Calculation Sheet Series B	-
Section Properties				
Concrete characteristic cylinder strength, f_{ck}	35	MPa	-	-
Steel characteristic strength, f_{yk}	500	Mpa	-	-
Section width, $b = b_w$	1000	mm	-	-
Section height, h	1000	mm	-	-
Main reinforcement diameter	20	mm	-	-
Initial shear link diameter	8	mm	-	Assume Y8 bars.
Crushing Strength Check				
Effective depth, d	907	mm	-	-
Crushing strength, $V_{Rd,max}$	3385	kN/m	Mosley, Bungey & Hulse (2007) 7.6.1	$V_{Rd,max} = 0.124 b_w d(1 - f_{ck}/250) f_{ck}$
$V_{Rd,max}$ vs. V_{Ed}	$V_{Rd,max} > V_{Ed}$	-	Mosley, Bungey & Hulse (2007) 7.6.1	$V_{Rd,max} > V_{Ed}$, therefore okay.
Concrete Shear Resistance Check				
k	1.470	-	Mosley, Bungey & Hulse (2007) 5.1.1	$k = \left(1 + \sqrt{\frac{200}{d}}\right) \leq 2.0$ with d expressed in mm
ρ_1	0.00173	-	Mosley, Bungey & Hulse (2007) 5.1.1	$\rho_1 = \frac{A_{s1}}{b_w d} \leq 0.02$
Shear resistance of the concrete, $V_{Rd,c}$	291.637	kN/m	Mosley, Bungey & Hulse (2007) 5.1.1	$V_{Rd,c} = \left[0.12k(100\rho_1 f_{ck})^{1/3}\right] b_w d$
Minimum $V_{Rd,c}$ check	334.580	kN/m	Mosley, Bungey & Hulse (2007) 5.1.1	$V_{Rd,c} < V_{Rd,c,min}$, therefore $V_{Rd,c} = V_{Rd,c,min}$. $V_{Rd,c} = \left[0.035k^{3/2} f_{ck}^{1/2}\right] b_w d$
$V_{Rd,c} > V_{Ed}$. Therefore shear reinforcement is not required for the wall. It is not necessary to provide nominal/minimum shear reinforcement in this case, as doing so will result in excessive use of reinforcement. Instead, Shape Code 85 support bars will be used to hold the reinforcement cage together.				

VII. DETAILING				
Item	Value	Unit	Reference	Explanation/Formula
The following detailing checks and calculations are carried out below: 1. Determination of anchorage lengths for the main reinforcement 2. Determination of lap lengths for the main reinforcement 3. Spacing of clips for the main reinforcement As the provision of reinforcement was governed by the minimum requirements, for both the longitudinal and shear reinforcement, no curtailment of the reinforcement is possible. Note that side face reinforcement to control cracking was not provided, as this wil be provided seperately, but only for the wall units which are designed to meet the crack width requirements.				
1. Determination of Anchorage Lengths for the Main Reinforcement				

Main reinforcement diameter, ϕ	20	mm	-	-
Concrete strength, f_{ck}	35	MPa	-	-
Use bent bars for both sagging and hogging reinforcement, to aid in the construction of the reinforcement cages.				
Bond conditions for main reinforcement	Poor	-	Mosley, Bungey & Hulse (2007) Figure 5.8	Section deeper than 600 mm, but hogging reinforcement placed at a depth less than 300 mm.
Bent bar anchorage coefficient, K_A, for f_{ck} = 35 MPa	31.43	-	Mosley, Bungey & Hulse (2007) Table A.6	Divide by 0.7 due to poor bond conditions.
Hogging reinforcement (bent bar) anchorage length, L	629	mm	Mosley, Bungey & Hulse (2007) Table A.6	$L = K_A \times \phi$
Provided anchorage length, L_{prov}	650	mm	-	Choose a multiple of 50 for practicality/convenience.
Minimum anchorage length, L_{min}	200	mm	Mosley, Bungey & Hulse (2007) 5.2	L_{min} = greater of 100 mm and 10 x ϕ. $L_{prov} > L_{min}$, therefore okay.
Minimum bend diameter	140	mm	Mosley, Bungey & Hulse (2007) 5.2	ϕ > 16 mm, therefore minimum bend diameter = 7 x ϕ
Minimum bend radius	70	mm	-	Minimum bend radius = minimum bend diameter/2
Provided bend radius	70	mm	-	Choose a multiple of 10 for practicality/convenience.
Minimum bend length	100	mm	Mosley, Bungey & Hulse (2007) 5.2	Minimum bend length = 5 x ϕ
Provided bend length	700	mm	-	Provide bend lengths such that the reinforcement forms a closed cage.
Therefore use an anchorage length of 650 mm for the longitudinal (bent bar) reinforcement, with a bend radius of 70 mm and a bend length of 500 mm.				
2. Determination of Lap Lengths for the Main Reinforcement				
Lap length coefficient for f_{ck} = 35 MPa	48	-	Mosley, Bungey & Hulse (2007) Table A.6	> 50 % of bars will be lapped at a section.
Required lap length, L_{req}	960	mm	-	L_{req} = lap length coefficient x ϕ
Provided lap length, L_{prov}	1000	mm	-	Choose a multiple of 50 for practicality/convenience.
Minimum lap length, L_{min}	300	mm	Mosley, Bungey & Hulse (2007) 5.3	L_{min} = greater of 100 mm and 15 x ϕ. $L_{prov} > L_{min}$, therefore okay.
Therefore provide lap lengths of 1000 mm.				
3. Spacing of Clips for the Main Reinforcement				
Maximum clip spacing (centre-to-centre)	1000	mm	SANS 10144 10.7, 10.10, Figure 65	This maximum spacing is in both the vertical and horizontal directions. The clips are to be used to connect the two inner (horizontal) layers of steel, and should be alternatively reversed, as Shape Code 85 bars will be used (SANS 10144 Figure 65).
Clip diameter	12	mm	-	-
Minimum bend radius	24	mm	IStructE Detailing Manual Table B.1	For Y12 clips.
Provided bend radius	25	mm	-	Choose a multiple of 5 for practicality/convenience.
Minimum bend length/end projection	125	mm	IStructE Detailing Manual Table B.1	For Y12 clips.
Provided bend length	125	mm	-	Choose a multiple of 5 for practicality/convenience.
Therefore provide Y12, Shape Code 85 clips, at a maximum vertical and horizontal spacing of 1000 mm c/c.				

	CRACK WIDTH DESIGN CALCULATIONS	
	Member: St. Helena Breakwater Crown Wall (Precast Unit F01)	

Project:	MSc. Eng. Structural Engineering - Research
Sheet Series:	D (Crack Width Design Calculations)
Calculations By:	Nicholas Elias
Date:	16/03/2022

Date	Checked By	Check No.	Review Level	Approved
29/03/2022	P.E.S	D-01	-	Yes

Check No.	Action	Check Notes	Status
D-01	N.N.E		

Overview of Member	
Structure Type:	Horizontal composite harbour breakwater
Member Type:	Reinforced concrete wall
Member Loads:	Wave loading
Limit States for Analysis:	Ultimate Limit State (ULS)
	Serviceability Limit State (SLS)
	Crack Width Design (CWD)
ULS Design Checks:	Bending
	Shear
SLS Design Checks:	Minimum and maximum amount of steel
	Durability (i.e., cover depth and mix design selection)
CWD Design Checks:	Flexural Cracking
	Thermal and Shrinkage Cracking

I. DESIGN INPUT VALUES				
Input	Value	Unit	Reference	Explanation/Formula
Service life	100	years	BS 6349-1-1:2013 Table 1	The St. Helena breakwater is a port structure of national significance.

II. MEMBER PROPERTIES				
Property	Value	Unit	Reference	Explanation/Formula
Nominal cover depth	60	mm	BS 6349-1-4: 2013 Table 3	Crown wall in upper tidal/splash & spray zone (XS3). 60 mm nominal cover selected to avoid low w/b ratio (therefore reducing cost).
Design cover depth	75	mm	Marine Concrete Structures (Alexander, 2016) Table 3.7	A 15 mm reinforcement placing tolerance was added to the nominal cover to allow for errors in workmanship.
Concrete strength class	C35/45	MPa	BS 6349-1-4: 2013 Table 2	Recommended value for 60 mm nominal cover depth.
Maximum w/b ratio	0.4	-	BS 6349-1-4: 2013 Table 2	Recommended value for 60 mm nominal cover depth.
Minimum binder content	380	kg/m^3	BS 6349-1-4: 2013 Table 2	Recommended value for 60 mm nominal cover depth.
Binder type	IIIA	-	BS 6349-1-4: 2013 Table 2	With 46-65 % GGBS (Assume that sufficient GGBS is available).
Steel characteristic strength, f_{yk}	500	MPa	Mosley, Bungey & Hulse (2007) 1.6.2	Choose to use high yield steel bars.
Member width, b	2680	mm	-	-
Member height, h	3900	mm	-	-
Member thickness, t	1000	mm	-	-

III. DESIGN FOR CRACK WIDTH: FLEXURAL CRACKING - VERTICAL STEEL IN FRONT AND BACK FACES				
Item	Value	Unit	Reference	Explanation/Formula
As it is assumed that the crown wall is on an active/stormy coast, and is regularly subjected to wave loads, the crown wall will be designed for flexural cracking. It is assumed that wave loading is frequent enough that cracks opened as a result of wave loading will pose a threat to durability.				
Information from Analysis				
Sustained moment under service conditions, M_s	140.7	kNm	Calculation Sheet Series B	-
Minimum Area of Reinforcing Steel Required to Control Cracking				
Maximum steel stress, $\sigma_{s,max}$	500	MPa	EN 1992-1-1:2004 7.3.2 (2)	σ_s may be taken as the yield strength of the steel, f_{yk}.
Stress distribution coefficient, k_c	0.4	-	Mosley, Bungey & Hulse (2007) 6.1.5	k_c = 0.4 for flexure.
Non-linear stress distribution coefficient, k	0.65	-	EN 1992-1-1:2004 7.3.2 (2)	k = 0.65 for webs > 800 mm deep.
Tensile strength at the time of cracking, $f_{ct,eff}$	3.00	MPa	Mosley, Bungey & Hulse (2007) 6.1.5	Suggested minimum value for $f_{ct,eff}$ = 3.00 MPa.
Area of tension steel provided in ULS, As_{prov}	1571	mm^2/m	-	-
Neutral axis depth, x	272.78	mm		Calculated by taking moments about the neutral axis - see sheet 3.
Area of concrete within the tensile zone, A_{ct}	727220	mm^2/m	-	A_{ct} = b x (h-x)
Minimum area of reinforcing steel required to control cracking, As_{min}	1134	mm^2/m	EN 1992-1-1:2004 Equation 7.1	$A_{s,min}\sigma_s = k_c\, k\, f_{ct,eff}\, A_{ct}$
As_{prov} > As_{min}, therefore the area of steel provided to meet the ULS requirements is adequate to ensure cracking is controlled.				
Calculation of Crack Width				
Average effective depth, d	915	mm	-	-
Stress in the tensile steel, σ_s	108.68	MPa	Mosley, Bungey & Hulse (2007) 6.4.3	$\sigma_s = M_s/[(d-x/3)As_{prov}]$
k_t	0.4	-	EN 1992-1-1:2004 7.3.4 (2)	Assume long-term loading.

$f_{ct,eff}$	3.00	MPa	Mosley, Bungey & Hulse (2007) 6.1.5	Suggested minimum value for $f_{ct,eff}$ = 3.00 MPa.
α_e	17.06	-	-	See sheet 3.
$A_{c,eff}$	242406.6667	mm^2	EN 1992-1-1:2004 7.3.2 (2)	$A_{c,eff}$ = b x $h_{c,ef}$, where $h_{c,ef}$ = lesser of 2.5(h-d), (h-x)/3 and h/2.
$\rho_{p,eff}$	0.0064808	-	EN 1992-1-1:2004 7.3.4 (2)	$\rho_{p,eff} = As_{prov}/A_{c,eff}$
E_s	200	GPa	-	-
ε_{sm} - ε_{cm}	-0.00048476	-	EN 1992-1-1:2004 7.3.4 (2)	$\varepsilon_{sm}-\varepsilon_{cm}=\frac{\sigma_s-k_t\frac{f_{ct,eff}}{\rho_{p,eff}}(1+\alpha_e\rho_{p,eff})}{E_s}\geq 0{,}6\frac{\sigma_s}{E_s}$
$0.6\sigma_s/E_s$	0.000326042	-	EN 1992-1-1:2004 7.3.4 (2)	ε_{sm} - ε_{cm} < $0.6\sigma_s/E_s$, therefore use $0.6\sigma_s/E_s$.
Design cover, c	75	mm	-	-
Bar diameter, ϕ	20	mm	-	-
k_1	0.8	-	EN 1992-1-1:2004 7.3.4 (3)	k_1 = 0.8 for high bond bars.
k_2	0.5	-	EN 1992-1-1:2004 7.3.4 (3)	k_2 = 0.5 for bending.
k_3	3.4	-	EN 1992-1-1:2004 7.3.4 (3)	-
k_4	0.425	-	EN 1992-1-1:2004 7.3.4 (3)	-
$S_{r,max}$	779.62	mm	EN 1992-1-1:2004 7.3.4 (3)	$s_{r,max} = k_3c + k_1k_2k_4\phi/\rho_{p,eff}$
Crack width, w_k	0.2542	mm	EN 1992-1-1:2004 7.3.4 (1)	$w_k = s_{r,max}(\varepsilon_{sm}-\varepsilon_{cm})$
Maximum permissible crack width, w_{max}	0.3	mm	EN 1992-1-1:2004 Table 7.1N	Exposure class XS3. **$w_k < w_{max}$, therefore okay**.
Therefore provide minimum reinforcement (5 Y20 bars per metre) in the vertical direction; this will be adequate to control flexural cracking.				

IV. DESIGN FOR CRACK WIDTH: THERMAL & SHRINKAGE CRACKING - HORIZONTAL AND VERTICAL STEEL IN FRONT AND BACK FACES				
Item	Value	Unit	Reference	Explanation/Formula
Two different types of cracking need to be checked: early-age thermal cracking due to heat of hydration when the wall elements are cast, and long-term cracking due to shrinkage and variations in ambient temperature. Early-age cracking may result in both vertical and horizontal cracks, whereas long-term cracking, caused by restraint along the base of the wall, will only result in vertical cracking.				
Early-Age Cracking				
When the wall units are cast, assume that the formwork provides an insignificant amount of exernal restraint, such that internal restraint is dominant.				
Cement content	455	kg/m^3	CIRIA C660 Table 4.2	46 - 65 % GGBS, therefore "worst-case" value for strength class C35/45 interpolated from values for 60 and 70 % GGBS, assuming 65 % GGBS.
Temperature drop, T_1	51.5	°C	CIRIA C660 Figure 4.6, Table 3.3	Assume plywood formwork to be conservative. Section thickness = 1000 mm, therefore Figure 4.6 can be used to find T_1. To be conservative, assume 50 % GGBS.
Coefficient of thermal expansion, α_c	10	με/°C	CIRIA C660 4.5	No information about aggregates, so use value recommended by EN 1992-1-1.
Autogeneous shrinkage, ε_{ca}	0	με	CIRIA C660 5.3	Ignore autogenous shrinkage, as it will occur uniformly throughout the section, and therefore won't contribute to strain differentials.
Restraint, R	0.42	-	CIRIA C660 4.7.4	-
Creep coefficient, K_1	0.65	-	CIRIA C660 4.9.1	-

Early-age restrained strain, ε_r	140.6	με	CIRIA C660 3.2.1	$\varepsilon_r = K_1[[\alpha_c T_1 + \varepsilon_{ca}]R$
Tensile strain capacity, ε_{ctu}	70	με	CIRIA C660 3.6.1	No information about aggregates, so use early-age value for simplified method.
Risk of early-age cracking?	Yes	-	CIRIA C660 1.4	$\varepsilon_r > \varepsilon_{ctu}$, so cracking will occur.
k_c	0.5	-	CIRIA C660 Table 3.1	To be conservatice, assume external restraint dominant.
k	1	-	CIRIA C660 Table 3.1	t > 800 mm.
A_{ct}	200000	mm^2/m	-	A_{ct} = area to depth 0.2t = 200mm. Use b = 1000 m to find A_{ct} per metre width.
Early-age concrete tensile strength, $f_{ctm(3)}$	1.92	MPa	CIRIA C660 Table 3.2	-
f_{yk}	500	MPa	-	-
Minimum area of reinforcement per metre per face, $A_{s,min}$	384	mm^2/m	CIRIA C660 3.3.1	As,prov > As,min, therefore okay - cracking is controlled. $A_{s,min} = k_c k A_{ct} \frac{f_{ctm}(t)}{f_{ty}}$
Design cover, C	75	mm	-	-
k_1	1.14	-	CIRIA C660 4.13	k_1 = 1.14 when calculating early-age thermal crack widths.
Reinforcement diameter, ϕ	20	mm	-	-
$h_{e,ef}$	212.5	mm	CIRIA C660 5.2	$h_{e,eff} = 2.5 (C + \phi/2)$
$A_{c,eff}$	212500	mm^2/m	-	$A_{c,eff} = h_{e,eff}$ x 1000 for reinforcement per metre.
As_{prov}	1571	mm^2/m	-	5 Y20 bars per metre.
$\rho_{p,eff}$	0.007393	-	CIRIA C660 3.4	$\rho_{p,eff} = As_{prov}/A_{c,eff}$
Crack spacing, $S_{r,max}$	1566	mm	CIRIA C660 3.4	$S_{r,max} = 3.4c + 0.425 \frac{k1\varphi}{\rho_{p,eff}}$
Crack-inducing strain, ε_{cr}	105.60	-	CIRIA C660 3.2.2	$\varepsilon_{cr} = \varepsilon_r - 0.5\varepsilon_{ctu}$
Crack width, w_k	0.165	mm	CIRIA C660 3.5.4	$w_k = S_{r,max}\varepsilon_{cr}$
Maximum permissible crack width, w_{max}	0.3	mm	EN 1992-1-1:2004 Table 7.1N	Exposure class XS3. **$w_k < w_{max}$, therefore okay**.
Long-Term Cracking				
In the long-term, restraint to volume changes due to shrinkage and temperature changes will be provided by the crown wall base, which is rigidly connected to the crown wall. Reinforcement to control long-term cracking will only be provided in the top portion of the wall, above and at the level of the base - the lower portion, which is buried in fill material, is not expected to be subjected to long-term temperature changes and drying shrinkage, and will therefore only be provided with nominal/minimum reinforcement.				
Long-term temperature change, T_2	20	°C	CIRIA C660 4.3	Assume summer casting.
Autogeneous shrinkage, ε_{ca}	41	με	CIRIA C660 4.6.1; Table 4.5; 5.1	Use 28-day value for long-term cracking. Class C35/45 concrete.
Drying shrinkage, ε_{cd}	113.5	με	CIRIA C660 4.6.2; Table 4.9	External exposure. Value for 1000 mm thick wall extrapolated from values for 300 mm and 500 mm thick walls.
Tensile strain capacity, ε_{ctu}	100	με	CIRIA C660 3.6.1	No information about aggregates, so use long-term value for simplified method.
Creep coefficient, K_1	0.65	-	CIRIA C660 4.9.1	-
Early thermal restraint, R_1	0.42	-	CIRIA C660 4.7.4	-
Long-term restraint, R_2 & R_3, at base of wall	0.6	-	CIRIA C660 Table 4.10	As the cast in-situ crown wall base is rigidly-connected to the midpoint of the crown wall.

Coefficient of thermal expansion, α_c	10	με/°C	CIRIA C660 4.5	No information about aggregates, so use value recommended by EN 1992-1-1.
Crack-inducing strain, ε_{cr}	224.1	με	CIRIA C660 3.2.1	$\varepsilon_{cr} = K1\{[\alpha_c T1 + \varepsilon_{ca}]R1 + \alpha_c T2\ R2 + \varepsilon_{cd}\ R3\} - 0.5\varepsilon_{ctu}$
k_1	1.14	-	CIRIA C660 4.13	k_1 = 1.14 when calculating early-age thermal crack widths; assume that long-term cracking results in the widening of existing early-age cracks (CIRIA C660 5.1).
Reinforcement diameter, ϕ	20	mm	-	-
$h_{e,ef}$	212.5	mm	CIRIA C660 5.2	$h_{e,eff}$ = 2.5 (C + ϕ/2)
$A_{c,eff}$	212500	mm^2/m	-	$A_{c,eff}$ = $h_{e,eff}$ x 1000 for reinforcement per metre.
As_{prov}	1571	mm^2/m	-	5 Y20 bars per metre.
$\rho_{p,eff}$	0.007392	-	CIRIA C660 3.4	$\rho_{p,eff} = As_{prov}/A_{c,eff}$
Crack spacing, $S_{r,max}$	1566	mm	CIRIA C660 3.4	$S_{r,max} = 3.4c + 0.425\frac{k1\varphi}{\rho_{p,eff}}$
Crack width, w_k	0.351	mm	CIRIA C660 3.5.4	$w_k = S_{r,max}\varepsilon_{cr}$
Maximum permissible crack width, w_{max}	0.3	mm	EN 1992-1-1:2004 Table 7.1N	Exposure class XS3. **$w_k > w_{max}$, therefore not okay**.
Try provide 8 Y16 bars per metre in each of the faces, and recalculate crack widths:				
Reinforcement diameter, ϕ	16	mm	-	-
As_{prov}	1608	mm^2/m	-	8 Y16 bars per metre.
$\rho_{p,eff}$	0.007569	-	CIRIA C660 3.4	$\rho_{p,eff} = As_{prov}/A_{c,eff}$
Crack spacing, $S_{r,max}$	1279	mm	CIRIA C660 3.4	$S_{r,max} = 3.4c + 0.425\frac{k1\varphi}{\rho_{p,eff}}$
Crack width, w_k	0.287	mm	CIRIA C660 3.5.4	$w_k = S_{r,max}\varepsilon_{cr}$
Maximum permissible crack width, w_{max}	0.3	mm	EN 1992-1-1:2004 Table 7.1N	Exposure class XS3. **$w_k < w_{max}$, therefore okay**.
Therefore provide 8 Y16 bars per metre in the horizontal direction, in the top portion of each of the front and back faces. However, this reinforcement does not need to be provided over the entire height of the wall - as the distance from the base increases, the restraint to the wall decreases. Therefore, check the crack width at a height of 0.5 m above the base, without crack width reinforcement:				
Reinforcement diameter, ϕ	20	mm	-	-
As_{prov}	1571	mm^2/m	-	5 Y20 bars per metre.
Crack spacing, $S_{r,max}$	1566	mm	CIRIA C660 3.4	$S_{r,max} = 3.4c + 0.425\frac{k1\varphi}{\rho_{p,eff}}$
Long-term restraint, R_2 & R_3, at base of wall	0.37778	-	CIRIA C660 Table 4.10	Assume restraint decreases linearly from 0.6 at the base of the wall (height of 0 m) to 0 at the top of the wall (height of 1.35 m) and interpolate to find restrain at a height of 1 m.
Crack-inducing strain, ε_{cr}	178.8	με	CIRIA C660 3.2.1	$\varepsilon_{cr} = K1\{[\alpha_c T1 + \varepsilon_{ca}]R1 + \alpha_c T2\ R2 + \varepsilon_{cd}\ R3\} - 0.5\varepsilon_{ctu}$
Crack width, w_k	0.280	mm	CIRIA C660 3.5.4	$w_k = S_{r,max}\varepsilon_{cr}$
Maximum permissible crack width, w_{max}	0.3	mm	EN 1992-1-1:2004 Table 7.1N	Exposure class XS3. **$w_k < w_{max}$, therefore okay**.
Therefore only provide crack width reinforcement (8 Y16 bars per metre) at the level of the crown all base, and to a height of 0.5 m above the base. Provide the minimum amount of reinforcement (5 Y20 bars per metre) in all other areas.				

V. DETAILING				
Item	Value	Unit	Reference	Explanation/Formula
The following detailing checks and calculations are carried out below: 1. Determination of anchorage lengths for the crack width reinforcement 2. Determination of lap lengths for the crack width reinforcement Curtailment of the main reinforcement is not possible, as the reinforcement was provided based on thermal and shrinkage crack width requirements, and not due to bending moments. Maximum bar spacing requirements are also irrelevant, as they are based upon flexural cracking, which was deemed to not be a significant issue for the crown wall.				
1. Determination of Anchorage Lengths for the Crack Width Reinforcement				
Cracking reinforcement diameter, ϕ	16	mm	-	-
Concrete strength, f_{ck}	35	MPa	-	-
Use bent bars for both sagging and hogging reinforcement, to aid in the construction of the reinforcement cages and ensure adequate reinforcement for crack control in the top and bottom faces.				
Bond conditions for reinforcement	Poor	-	Mosley, Bungey & Hulse (2007) Figure 5.8	Section deeper than 600 mm, but reinforcement placed at a depth less than 300 mm.
Bent bar anchorage coefficient, K_A, for f_{ck} = 35 MPa	31.43	-	Mosley, Bungey & Hulse (2007) Table A.6	Divide by 0.7 due to poor bond conditions.
Hogging reinforcement (bent bar) anchorage length, L	503	mm	Mosley, Bungey & Hulse (2007) Table A.6	$L = K_A \times \phi$
Provided anchorage length, L_{prov}	550	mm	-	Choose a multiple of 50 for practicality/convenience.
Minimum anchorage length, L_{min}	160	mm	Mosley, Bungey & Hulse (2007) 5.2	L_{min} = greater of 100 mm and 10 x ϕ. $L_{prov} > L_{min}$, therefore okay.
Minimum bend diameter	112	mm	Mosley, Bungey & Hulse (2007) 5.2	ϕ > 16 mm, therefore minimum bend diameter = 7 x ϕ
Minimum bend radius	56	mm	-	Minimum bend radius = minimum bend diameter/2
Provided bend radius	60	mm	-	Choose a multiple of 10 for practicality/convenience.
Minimum bend length	80	mm	Mosley, Bungey & Hulse (2007) 5.2	Minimum bend length = 5 x ϕ
Provided bend length	500	mm	-	Provide bend lengths such that the reinforcement forms a closed cage.
Therefore use an anchorage length of 550 mm for the longitudinal (bent bar) reinforcement, with a bend radius of 60 mm and a bend length of 500 mm.				
2. Determination of Lap Lengths for the Crack Width Reinforcement				
Lap length coefficient for f_{ck} = 35 MPa	48	-	Mosley, Bungey & Hulse (2007) Table A.6	To be conservative, assume > 50 % of bars lapped at a section
Required lap length, L_{req}	768	mm	-	L_{req} = lap length coefficient x ϕ
Provided lap length, L_{prov}	800	mm	-	Choose a multiple of 50 for practicality/convenience.
Minimum lap length, L_{min}	240	mm	Mosley, Bungey & Hulse (2007) 5.3	L_{min} = greater of 100 mm and 15 x ϕ. $L_{prov} > L_{min}$, therefore okay.
Therefore provide lap lengths of 800 mm.				

Early-age (3 day) Elastic Modulus, $E_{cm(3)}$				
Item	**Value**	**Unit**	**Reference**	**Explanation/Formula**
Concrete characteristic strength, f_{ck}	35	MPa	-	Characteristic value.
Concrete strength, f_{cm}, at 28 days	43	MPa	EN 1992-1-1:2004 Table 3.1	$f_{cm} = f_{ck} + 8$
Age of concrete, t	3	days	EN 1992-1-1:2004 3.1.2	-
s	0.20	-	EN 1992-1-1:2004 3.1.2	Assume Class R cement.
$\beta_{cc(3)}$	0.6630	-	EN 1992-1-1:2004 3.1.2	$\beta_{cc}(t) = \exp\left\{s\left[1-\left(\frac{28}{t}\right)^{1/2}\right]\right\}$
Concrete strength, f_{cm}, at 3 days	28.51	MPa	EN 1992-1-1:2004 3.1.2	$f_{cm}(t) = \beta_{cc}(t)\, f_{cm}$
Equivalent f_{ck} at 3 days	20.51	MPa	EN 1992-1-1:2004 Table 3.1	$f_{cm} = f_{ck} + 8$
Early-age (3 day) Elastic Modulus, $E_{cm(3)}$	30	MPa	Mosley, Bungey & Hulse (2007) 1.2.1, Table 1.1	$E_{cm(3)}$ estimated using f_{ck} = 20 Mpa (approx. = to 20.51 MPa).

FOR ONE LAYER OF 5 Y20 BARS PER METER				
Item	**Value**	**Unit**	**Reference**	**Explanation/Formula**
b	1000	mm	-	-
Average effective depth, d	1661	mm	-	-
As_{prov}	1571	mm^2/m	-	-
E_{cm}	34	GPa	Mosley, Bungey & Hulse (2007) Table 6.11	Value for C35/45 strength class.
Creep coefficient, ϕ	1.9	-	Mosley, Bungey & Hulse (2007) Table 6.12	Assume loading at 28 days. Outdoor exposure, $2A_c/u$ = 2 x [(1000 x 1000)/2(1000 + 1000)] = 500.
$E_{c,eff}$	11.72	GPa	Mosley, Bungey & Hulse (2007) Equation 6.8	Use effective concrete modulus to account for effects of creep - cracking must still be controlled, even in the long-
E_{steel}	200	GPa	-	-
α_e	17.06	-	Mosley, Bunger & Hulse 6.3.2	$\alpha_e = E_{steel}/E_{c,eff}$
Taking moments about the neutral axis, and manually equating the left- and right- hand sides of the equation by varying "x":				
Neutral axis depth, x	272.776713	mm	-	-
Left-hand side, LHS:	37203567.58	-	Mosley, Bunger & Hulse 4.10.1	LHS = (b).(x).(x/2)
Right -hand side, RHS:	37203567.49	-	Mosley, Bunger & Hulse 4.10.1	RHS = $(a_e).(As_{prov}).(d-x)$
LHS-RHS	0.087875709	-	-	-
Therefore x = 272.78 mm (approximately)				

Appendix C: Matola Jetty Beam Drawings

Please find the drawings – one for the beams designed without the crack width requirements, and one for the beams designed with the requirements – attached on the following page.

Rebar Schedule													
Schedule Mark	Bar Diameter	Bar Length	A	B	C	D	E	F	G	Quantity	Total Bar Length	Reinforcement Volume	Image
S1	16 mm	5980	140	1650	1250	1650	1250	0	140	39	233220	46891663 mm³	
B1	40 mm	14850	0	14850	0	0	0	0	0	2	29700	37322121 mm³	
B2	40 mm	14850	0	14850	0	0	0	0	0	2	29700	37322121 mm³	
B3	40 mm	14850	0	14850	0	0	0	0	0	1	14850	18661060 mm³	
B4	40 mm	13300	0	13300	0	0	0	0	0	2	26600	33426546 mm³	
B5	40 mm	13300	0	13300	0	0	0	0	0	2	26600	33426546 mm³	
B6	40 mm	8800	0	8800	0	0	0	0	0	2	17600	22116812 mm³	
T1	40 mm	14850	0	14850	0	0	0	0	0	7	103950	130627423 mm³	
T2	40 mm	5350	0	5350	0	0	0	0	0	4	21400	26892033 mm³	
T3	40 mm	4350	0	4350	0	0	0	0	0	2	8700	10932742 mm³	

Rebar Schedule													
Schedule Mark	Bar Diameter	Bar Length	A	B	C	D	E	F	G	Quantity	Total Bar Length	Reinforcement Volume	Image
T4	40 mm	5350	0	5350	0	0	0	0	0	4	21400	26892033 mm³	
T5	40 mm	4350	0	4350	0	0	0	0	0	2	8700	10932742 mm³	
S2	16 mm	4110	140	320	1650	320	1650	0	140	39	160290	32228217 mm³	
S3	16 mm	4110	140	320	1650	320	1650	0	140	39	160290	32228217 mm³	
S4	16 mm	4140	140	330	1650	330	1650	0	140	39	161460	32463459 mm³	
X1	32 mm	14850	0	14850	0	0	0	0	0	2	29700	23886157 mm³	
X2	32 mm	14850	0	14850	0	0	0	0	0	2	29700	23886157 mm³	
X3	32 mm	14850	0	14850	0	0	0	0	0	2	29700	23886157 mm³	

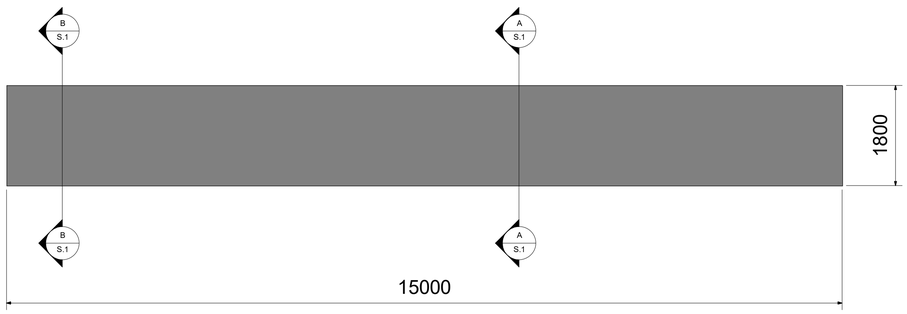

SIDE ELEVATION

SCALE 1:50

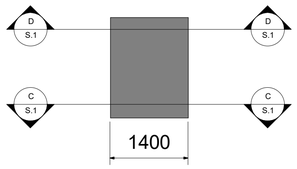

FRONT ELEVATION

SCALE 1:50

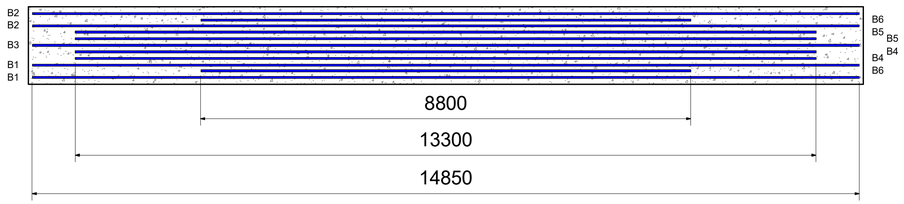

SECTION C-C (MAIN REINFORCEMENT ONLY)

SCALE 1:50

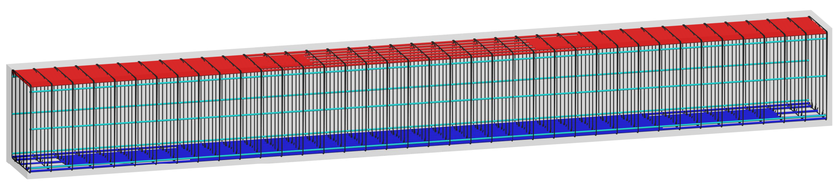

3D VIEW OF REINFORCEMENT

SCALE 1:50

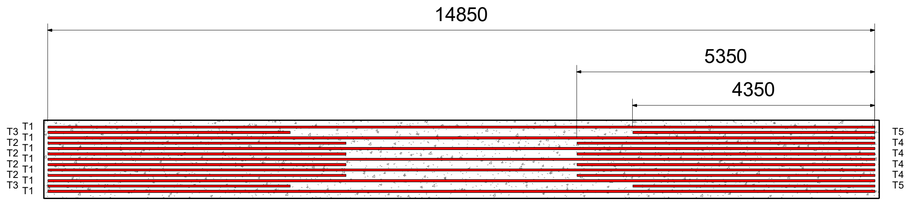

SECTION D-D (MAIN REINFORCEMENT ONLY)

SCALE 1:50

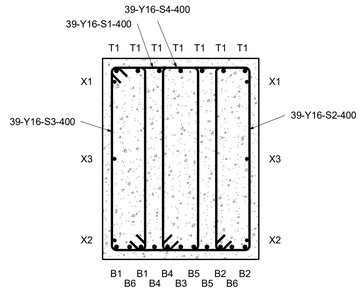

SECTION A-A

SCALE 1:25

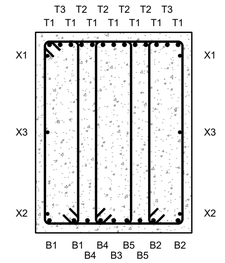

SECTION B-B

SCALE 1:25

PRECAST BEAM B402

NOTE THAT, WHILE NOT SHOWN HERE, THE FLEXURAL REINFORCEMENT WILL BE EXTENDED TO ALLOW FOR IN-SITU RIGID CONNECTIONS BETWEEN THE PRECAST BEAMS.

NOTES

GENERAL

1. ALL DIMENSIONS ARE IN MM.

CONCRETE

1. CONCRETE CLASS: C35/45
2. MIX DESIGN:
   a) MAXIMUM W/B RATIO: 0.4
   b) MINIMUM BINDER CONTENT: 380 kg/m³, INCLUDING 50 % GGBS
3. MINIMUM COVER: 75 MM

REINFORCEMENT

1. MINIMUM REINFORCEMENT TENSILE STRENGTH: 500 MPa

No.	Description	Date
01	FIRST DRAFT	16/02/2022
02	REVISED	14/03/2022

UNIVERSITY OF CAPE TOWN

MSc.ENG RESEARCH

BEAM B402 REBAR SCHEDULE - WITH REINFORCEMENT DESIGNED TO MEET ULS & SLS REQUIREMENTS ONLY

Project number	0-01A
Date	14/03/2022
Drawn by	N.N.E
Checked by	P.E.S
	S.1
Scale	As indicated

2022/03/30 14:16:27

Rebar Schedule													
Schedule Mark	Bar Diameter	Bar Length	A	B	C	D	E	F	G	Quantity	Total Bar Length	Reinforcement Volume	Image
S1	16 mm	5980	140	1650	1250	1650	1250	0	140	39	233220	46891663 mm³	
X1	32 mm	14850	0	14850	0	0	0	0	0	2	29700	23886157 mm³	
X2	32 mm	14850	0	14850	0	0	0	0	0	2	29700	23886157 mm³	
T1	40 mm	14850	0	14850	0	0	0	0	0	2	29700	37322121 mm³	
T2	40 mm	14850	0	14850	0	0	0	0	0	5	74250	93305302 mm³	
T3	40 mm	5350	0	5350	0	0	0	0	0	6	32100	40338050 mm³	
T4	40 mm	4350	0	4350	0	0	0	0	0	2	8700	10932742 mm³	
T5	40 mm	5350	0	5350	0	0	0	0	0	6	32100	40338050 mm³	
T6	40 mm	4350	0	4350	0	0	0	0	0	2	8700	10932742 mm³	
B1	32 mm	14850	0	14850	0	0	0	0	0	2	29700	23886157 mm³	
B2	32 mm	14850	0	14850	0	0	0	0	0	5	74250	59715393 mm³	
B3	32 mm	13050	0	13050	0	0	0	0	0	6	78300	62972596 mm³	

Rebar Schedule													
Schedule Mark	Bar Diameter	Bar Length	A	B	C	D	E	F	G	Quantity	Total Bar Length	Reinforcement Volume	Image
B4	32 mm	8550	0	8550	0	0	0	0	0	2	17100	13752636 mm³	
S2	16 mm	4180	140	350	1650	350	1650	0	140	39	163020	32777116 mm³	
S3	16 mm	4160	140	340	1650	340	1650	0	140	39	162240	32620287 mm³	
S4	16 mm	4190	140	350	1650	350	1650	0	140	39	163410	32855530 mm³	
C1	32 mm	14850	0	14850	0	0	0	0	0	5	74250	59715393 mm³	
C2	32 mm	14850	0	14850	0	0	0	0	0	5	74250	59715393 mm³	
C3	32 mm	3000	0	3000	0	0	0	0	0	2	6000	4825486 mm³	
C4	32 mm	3000	0	3000	0	0	0	0	0	2	6000	4825486 mm³	
C5	32 mm	3000	0	3000	0	0	0	0	0	2	6000	4825486 mm³	
C6	32 mm	3000	0	3000	0	0	0	0	0	2	6000	4825486 mm³	
B5	32 mm	14850	0	14850	0	0	0	0	0	2	29700	23886157 mm³	
B6	32 mm	14850	0	14850	0	0	0	0	0	2	29700	23886157 mm³	

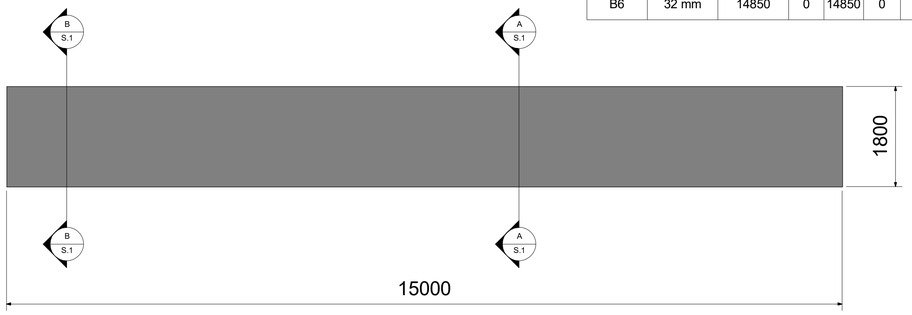

SIDE ELEVATION

SCALE 1:50

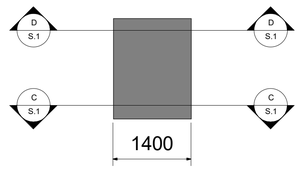

FRONT ELEVATION

SCALE 1:50

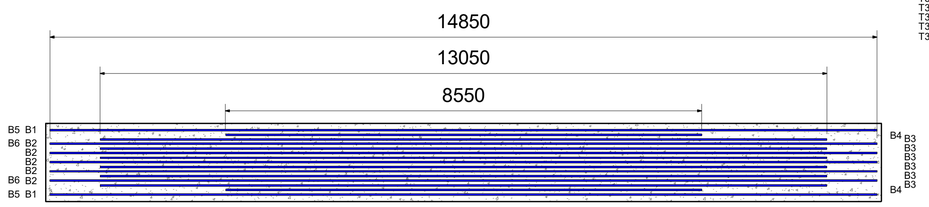

SECTION C-C (MAIN REINFORCEMENT ONLY)

SCALE 1:50

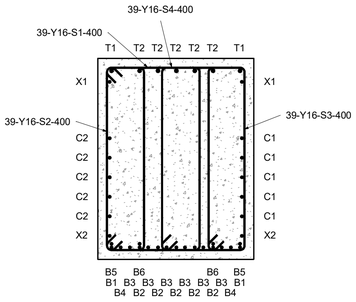

SECTION A-A

SCALE 1:25

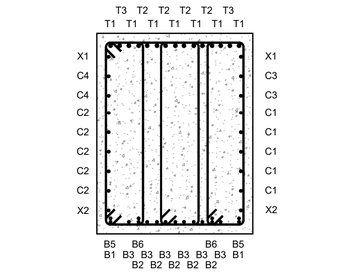

SECTION B-B

SCALE 1:25

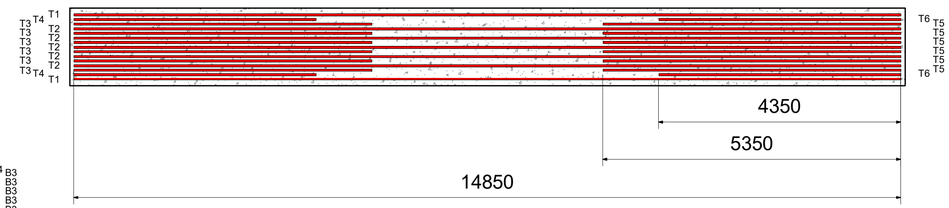

SECTION D-D (MAIN REINFORCEMENT ONLY)

SCALE 1:50

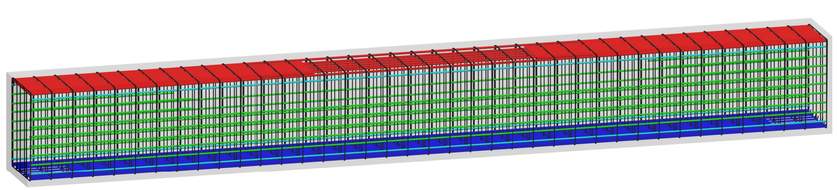

3D VIEW OF REINFORCEMENT

SCALE 1:50

PRECAST BEAM B402

NOTE THAT, WHILE NOT SHOWN HERE, THE FLEXURAL REINFORCEMENT WILL BE EXTENDED TO ALLOW FOR IN-SITU RIGID CONNECTIONS BETWEEN THE PRECAST BEAMS.

NOTES

GENERAL

1. ALL DIMENSIONS ARE IN MM.

CONCRETE

1. CONCRETE CLASS: C35/45
2. MIX DESIGN:
   a) MAXIMUM W/B RATIO: 0.4
   b) MINIMUM BINDER CONTENT: 380 kg/m³, INCLUDING 50 % GGBS
3. MINIMUM COVER: 75 MM

REINFORCEMENT

1. MINIMUM REINFORCEMENT TENSILE STRENGTH: 500 MPa

No.	Description	Date
01	FIRST DRAFT	16/02/2022
02	REVISED	14/03/2022

UNIVERSITY OF CAPE TOWN

MSc.ENG RESEARCH

BEAM B402 REBAR SCHEDULE - WITH REINFORCEMENT DESIGNED TO MEET CRACK WIDTH REQUIREMENTS

Project number	0-01B
Date	14/03/2022
Drawn by	N.N.E
Checked by	P.E.S
	S.1
Scale	As indicated

2022/03/30 14:20:46

Appendix D: St. Helena Breakwater Crown Wall Drawings

Please find the drawings – one for the wall units designed without the crack width requirements, and one for the wall units designed with the requirements – attached on the following page.

Rebar Schedule													
Schedule Mark	Bar Diameter	Bar Length	A	B	C	D	E	F	G	Quantity	Total Bar Length	Reinforcement Volume	Image
V1	20	3050	0	700	2400	0	0	0	0	12	36600	11498229 mm³	
V2	20	3050	0	2400	700	0	0	0	0	12	36600	11498229 mm³	
V3	20	3050	0	700	2400	0	0	0	0	12	36600	11498229 mm³	
V4	20	3050	0	2400	700	0	0	0	0	12	36600	11498229 mm³	
H1	20	2530	0	2530	0	0	0	0	0	5	12650	3974115 mm³	
H2	20	2530	0	2530	0	0	0	0	0	10	25300	7948229 mm³	
H3	20	2530	0	2530	0	0	0	0	0	10	25300	7948229 mm³	
H4	20	2530	0	2530	0	0	0	0	0	5	12650	3974115 mm³	

Rebar Schedule													
Schedule Mark	Bar Diameter	Bar Length	A	B	C	D	E	F	G	Quantity	Total Bar Length	Reinforcement Volume	Image
S1	12	1080	150	830	0	0	0	0	130	4	4320	488580 mm³	
S2	12	1080	150	830	0	0	0	0	130	4	4320	488580 mm³	
S3	12	1060	150	810	0	0	0	0	130	4	4240	479533 mm³	
S4	12	1080	150	830	0	0	0	0	130	4	4320	488580 mm³	
S5	12	1080	150	830	0	0	0	0	130	4	4320	488580 mm³	

PRECAST CROWN WALL UNIT F01 (TYPICAL)

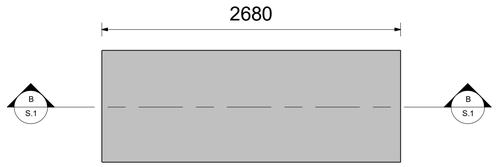

PLAN VIEW

SCALE 1:25

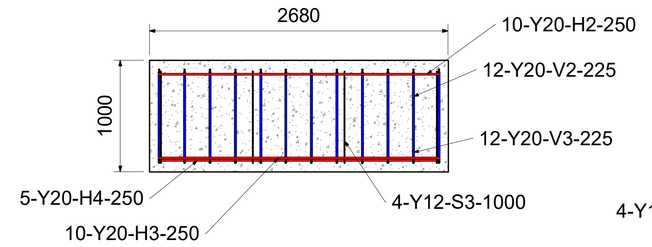

SECTION A-A

SCALE 1:25

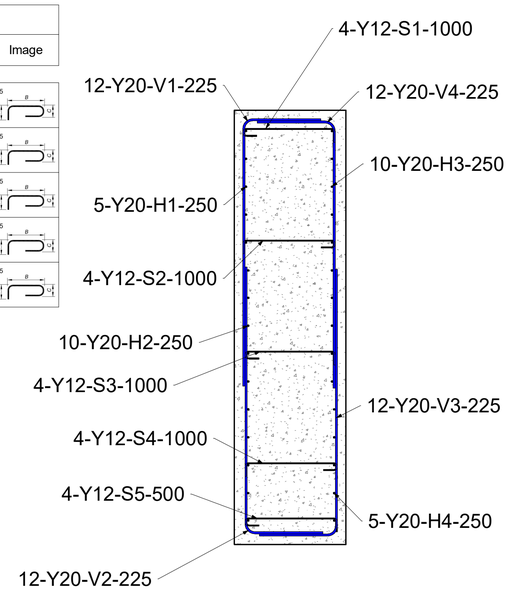

SECTION C-C

SCALE 1:25

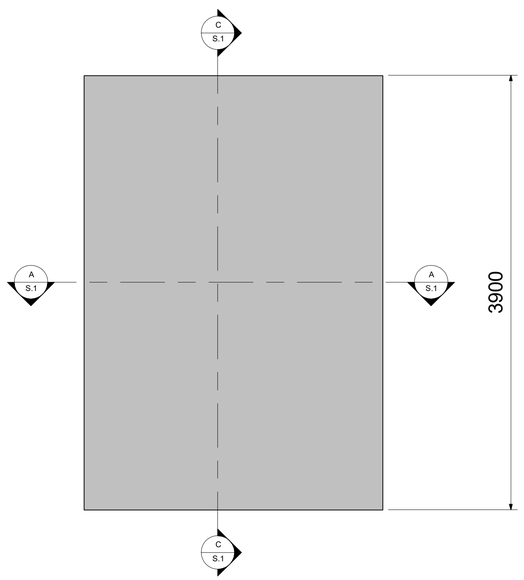

ELEVATION

SCALE 1:25

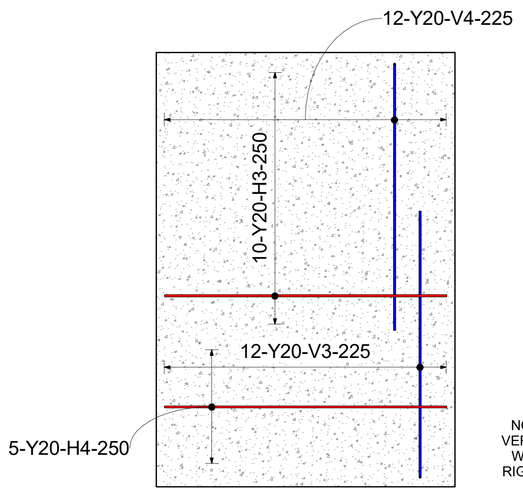

SECTION B-B - LAYOUT OF MAIN REINFORCEMENT

SCALE 1:25

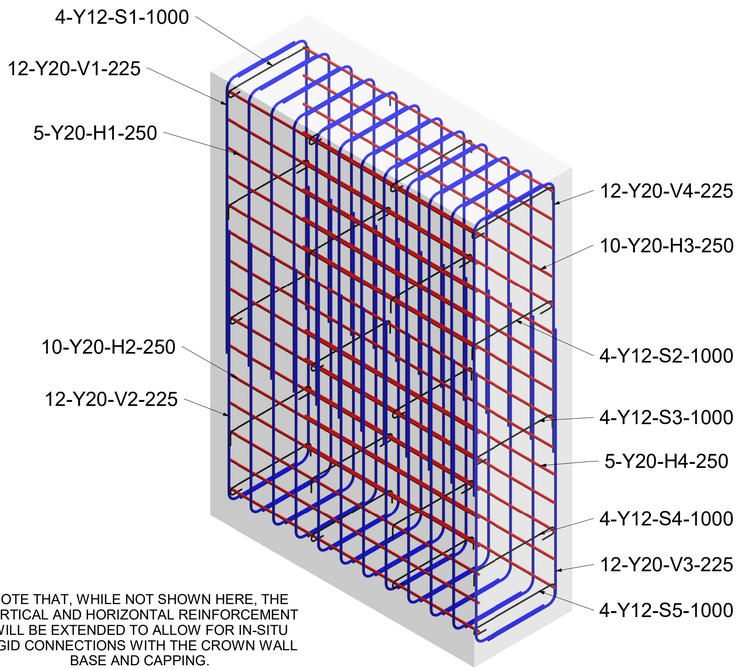

NOTE THAT, WHILE NOT SHOWN HERE, THE VERTICAL AND HORIZONTAL REINFORCEMENT WILL BE EXTENDED TO ALLOW FOR IN-SITU RIGID CONNECTIONS WITH THE CROWN WALL BASE AND CAPPING.

3D VIEW OF REINFORCEMENT

SCALE 1:20

NOTES

GENERAL

1. ALL DIMENSIONS ARE IN MM.

CONCRETE

1. CONCRETE CLASS: C35/45
2. MIX DESIGN:
   a) MAXIMUM W/B RATIO: 0.4
   b) MINIMUM BINDER CONTENT: 380 kg/m³, INCLUDING 50 % GGBS
3. MINIMUM COVER: 75 MM

REINFORCEMENT

1. MINIMUM REINFORCEMENT TENSILE STRENGTH: 500 MPa

No.	Description	Date
01	FIRST DRAFT	28/02/2022
02	REVISED DRAFT	05/03/2022

UNIVERSITY OF CAPE TOWN

MSc. ENG RESEARCH

ST. HELENA CROWN WALL (PRECAST WALL UNIT F01) REINFORCEMENT SCHEDULE - WITH REINFORCEMENT DESIGNED TO MEET ULS & SLS REQUIREMENTS ONLY

Project number	0-02A
Date	05/03/2022
Drawn by	N.N.E
Checked by	P.E.S
	S.1
Scale	AS SHOWN

2022/03/30 14:05:20

Rebar Schedule													
Schedule Mark	Bar Diameter	Bar Length	A	B	C	D	E	F	G	Quantity	Total Bar Length	Reinforcement Volume	Image
V1	20	3050	0	700	2400	0	0	0	0	12	36600	11498229 mm³	
V2	20	3050	0	2400	700	0	0	0	0	12	36600	11498229 mm³	
V3	20	3050	0	700	2400	0	0	0	0	12	36600	11498229 mm³	
V4	20	3050	0	2400	700	0	0	0	0	12	36600	11498229 mm³	
H1	20	2530	0	2530	0	0	0	0	0	3	7590	2384469 mm³	
H2	20	2530	0	2530	0	0	0	0	0	5	12650	3974115 mm³	
H3	20	2530	0	2530	0	0	0	0	0	3	7590	2384469 mm³	
H4	20	2530	0	2530	0	0	0	0	0	5	12650	3974115 mm³	
S1	12	1080	150	830	0	0	0	0	130	4	4320	488580 mm³	

Rebar Schedule													
Schedule Mark	Bar Diameter	Bar Length	A	B	C	D	E	F	G	Quantity	Total Bar Length	Reinforcement Volume	Image
S2	12	1080	150	830	0	0	0	0	130	4	4320	488580 mm³	
S3	12	1060	150	810	0	0	0	0	130	4	4240	479533 mm³	
S4	12	1080	150	830	0	0	0	0	130	4	4320	488580 mm³	
S5	12	1080	150	830	0	0	0	0	130	4	4320	488580 mm³	
C1	16	2530	0	2530	0	0	0	0	0	10	25300	5086867 mm³	
C2	16	2530	0	2530	0	0	0	0	0	5	12650	2543433 mm³	
C3	16	2530	0	2530	0	0	0	0	0	14	35420	7121614 mm³	
C4	16	2530	0	2530	0	0	0	0	0	1	2530	508687 mm³	

PRECAST CROWN WALL UNIT F01 (TYPICAL)

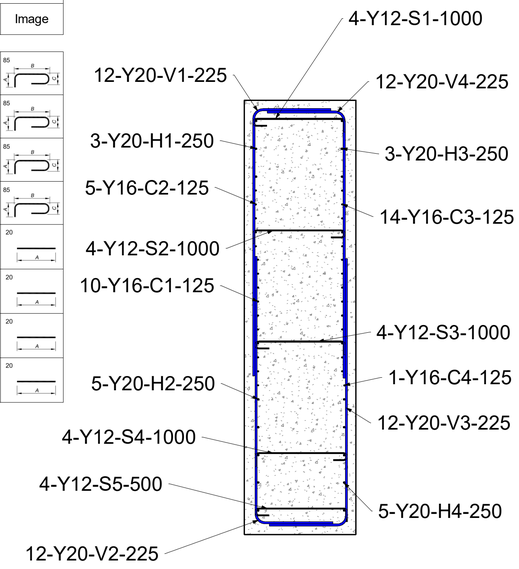

SECTION C-C

SCALE 1:25

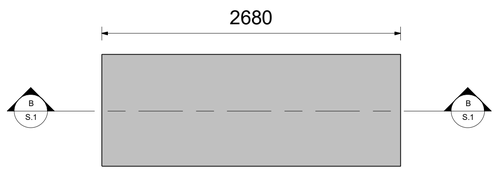

PLAN VIEW

SCALE 1:25

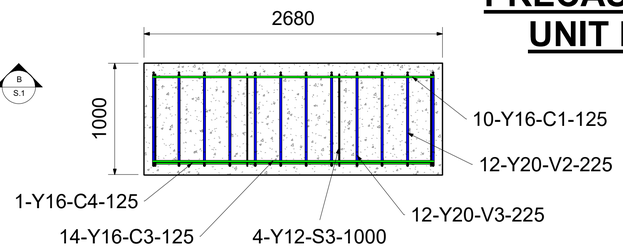

SECTION A-A

SCALE 1:25

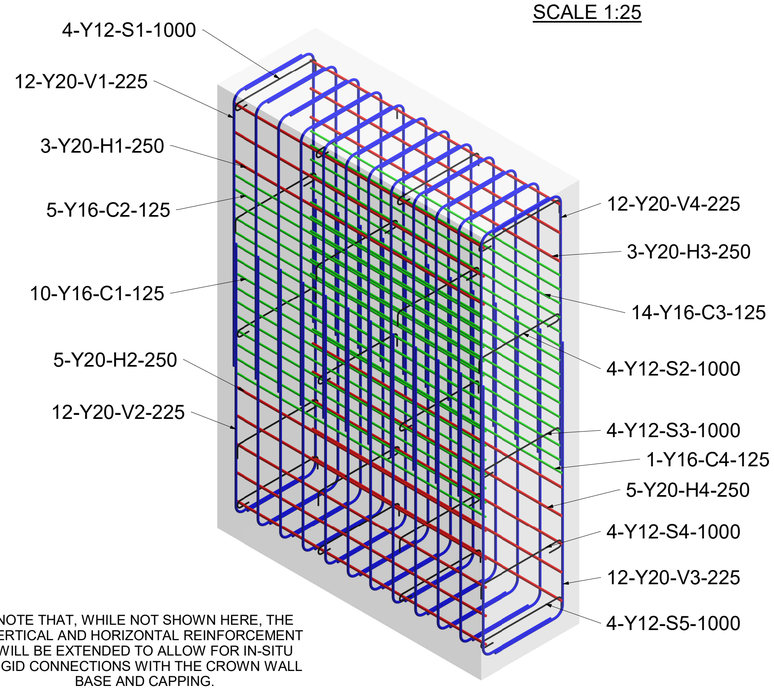

NOTE THAT, WHILE NOT SHOWN HERE, THE VERTICAL AND HORIZONTAL REINFORCEMENT WILL BE EXTENDED TO ALLOW FOR IN-SITU RIGID CONNECTIONS WITH THE CROWN WALL BASE AND CAPPING.

3D VIEW OF REINFORCEMENT

SCALE 1:20

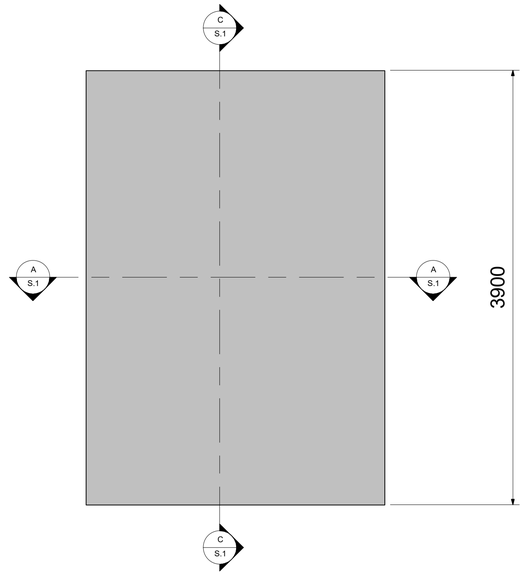

ELEVATION

SCALE 1:25

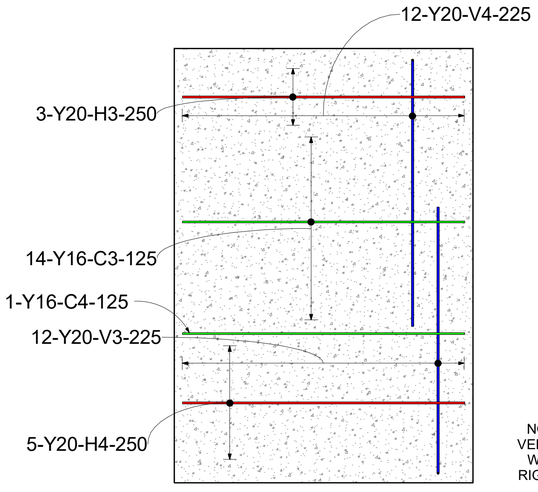

SECTION B-B - LAYOUT OF MAIN REINFORCEMENT

SCALE 1:25

NOTES

GENERAL

1. ALL DIMENSIONS ARE IN MM.

CONCRETE

1. CONCRETE CLASS: C35/45
2. MIX DESIGN:
   a) MAXIMUM W/B RATIO: 0.4
   b) MINIMUM BINDER CONTENT: 380 kg/m³, INCLUDING 50 % GGBS
3. MINIMUM COVER: 75 MM

REINFORCEMENT

1. MINIMUM REINFORCEMENT TENSILE STRENGTH: 500 MPa

No.	Description	Date
01	FIRST DRAFT	28/02/2022
02	REVISED DRAFT	06/03/2022

UNIVERSITY OF CAPE TOWN

MSc. ENG RESEARCH

ST. HELENA CROWN WALL (PRECAST WALL UNIT F01) REINFORCEMENT SCHEDULE - WITH REINFORCEMENT DESIGNED TO MEET CRACK WIDTH REQUIREMENTS

Project number	0-02B
Date	06/03/2022
Drawn by	N.N.E
Checked by	P.E.S
	S.1
Scale	AS SHOWN

2022/03/30 14:07:52

Appendix E: Service Life Modelling Calculations

Please find the service life calculation sheet attached on the following page.

	SERVICE LIFE MODELLING CALCULATIONS	

Project:	MSc. Eng. Structural Engineering - Research
Calculations By:	Nicholas Elias
Date:	25/05/2022

Reference	**Introduction**

The aim of these calculations is to determine the service lives of the RC members designed in this study. The following calculations are presented in this calculation sheet:

1. Determination of Effective Cover Depth
2. Calculation of the Corrosion Initiation Period
3. Determination of Representative Corrosion Rates
4. Calculation of the Corrosion Propagation Period
5. Calculation of the Total Service Life

The following general input parameters were used in the service life modelling calculations for all members:

Table 1: General input parameters.

Input Parameter	Value
Concrete Class	C35/45
Binder Type	50 % PC, 50 % GGBS
Water/Binder Ratio, *w/b*	0.40
In-Situ Cover Depth, *C*	60 mm

The following specific input parameters were used for each member:

Table 2: Specific input parameters for each member.

Member	Design Type[a]	Reinforcement Diameter, *D* [mm]	Maximum Crack Width, w_{cr} [mm]
Matola Jetty Beams	Without CWR	40	0.45
	With CWR	32	0.30
St. Helena Breakwater Crown Wall Units	Without CWR	20	0.35
	With CWR	16	0.30

a. Note that “CWR” stands for “crack width requirements”

1. Determination of Effective Cover Depth, C_{eff}

The effective cover depth, C_{eff}, is shown graphically in Figure 1, assuming a triangular-shaped crack.

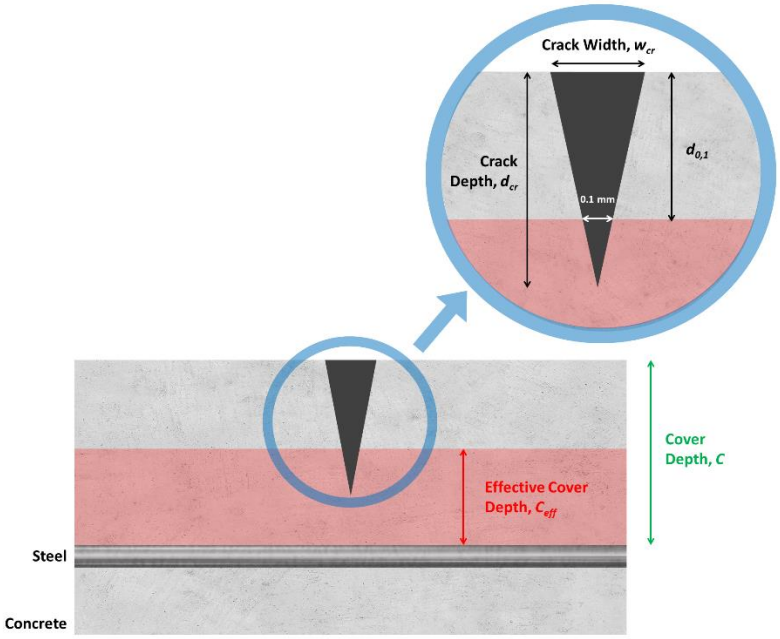

Figure 1: A diagrammatic representation of a typical triangular-shaped crack.

Based on Figure 1, C_{eff} can be determined by the following equation:

$$C_{eff} = C - d_{0.1} \quad (1)$$

Where the depth to a crack width of 0.1 mm, $d_{0.1}$, can be determined using the properties of similar triangles:

$$\frac{d_{cr} - d_{0.1}}{0.1} = \frac{d_{cr}}{w_{cr}}$$

$$d_{cr} - d_{0.1} = 0.1\left(\frac{d_{cr}}{w_{cr}}\right)$$

$$\therefore d_{0.1} = d_{cr} - 0.1\left(\frac{d_{cr}}{w_{cr}}\right) \quad (2)$$

Ramezanianpour et al. (2018)	Equation (2) can thus be substituted into Equation (1), such that C_{eff} is a function of w_{cr} and d_{cr} only: $$C_{eff} = C - d_{cr} + 0.1\left(\frac{d_{cr}}{w_{cr}}\right) \quad (3)$$ The crack depth, d_{cr}, can be determined using the equations developed by Ramezanianpour et al. (2018): $$For\ plain\ PC\ concrete: d_{cr} = 1.67 + \sqrt{(416 \times w_{cr}) - 0.63}\ [cm] \quad (4)$$ $$For\ concrete\ with\ 7.5\ \%\ SF: d_{cr} = 0.2 + \sqrt{(375 \times w_{cr}) - 4.53}\ [cm] \quad (5)$$ Ramezanianpour et al. (2018: 1467) noted that the concrete with 7.5 % SF replacement had a finer microstructure, resulting in reduced crack depth in the 7.5 % SF samples, such that Equation (5) will predict lower crack depth values than Equation (4). As the members in this study used 50 % GGBS replacement, which will also result in a finer concrete microstructure (Li & Liang, 2011:158), **it was decided to use Equation (5) to calculate crack depth in this study**. To demonstrate the process of finding d_{cr}, $d_{0.1}$, and thus C_{eff}, a sample calculation is carried out below for the Matola jetty beam, designed without crack width requirements: d_{cr} is found using Equation (5), with the maximum in-service crack width, w_{cr}, equal to 0.45 mm: $$d_{cr} = 0.2 + \sqrt{(375 \times 0.45) - 4.53} = 13.01\ cm = 130.1\ mm$$ $d_{0.1}$ is then found using Equation (2), and compared to C: $$d_{0.1} = 130.1 - 0.1\left(\frac{130.1}{0.45}\right) = 101.2\ mm$$ The depth at which the crack is 0.1 mm wide, $d_{0.1}$, is thus greater than the cover depth of the reinforcement, C – meaning that the effective cover depth, C_{eff}, is zero, as the crack is wider than 0.1 mm at the level of the reinforcement.

The method applied in the sample calculation above was applied to all the members designed for the study. The resultant crack depths and effective cover depths for the four members designed in this study are thus shown in Table 3.

Table 3: A summary of the effective cover depth calculations for the study.

	Matola Jetty Beams		St. Helena Breakwater Crown Wall Units	
	Without CWR	**With CWR**	**Without CWR**	**With CWR**
Cover Depth, C [mm]	60	60	60	60
Crack Width, w_{cr} [mm]	0.45	0.30	0.35	0.30
Crack Depth, d_{cr} [mm]	130.1	105.9	114.6	105.9
Depth at Which the Crack is 0.1 mm Wide, $d_{0.1}$ [mm]	101.2	70.6	81.9	70.6
Is $d_{0.1} > C$?	Yes	Yes	Yes	Yes
Effective Cover Depth, C_{eff} [mm]	0	0	0	0

The effective cover depth, C_{eff}, is therefore zero for all four members designed in this study.

2. Calculation of the Corrosion Initiation Period, t_i

As the effective cover depth is zero for all the members designed in this study, corrosion will be initiated instantly in all members. As such, the length of the corrosion initiation period is zero for all four members designed in this study, and no further initiation period calculations are required.

3. Determination of Representative Corrosion Rates, i_{corr}

The representative corrosion rate for each member, i_{corr}, was determined for each member as follows:

$$i_{corr} = \alpha \times \beta \times i_{base} \quad (6)$$

Where: α is a factor that accounts for the differences in reinforcement diameter between the members designed with and without the crack width requirements

: β is a factor that accounts for the differences in the number of reinforcement bars used in the members designed with and without the crack width requirements

: i_{base} is the base corrosion rate of each member, determined as a function of cover depth, concrete quality, and crack width, using the model developed by Otieno (2014)

It can thus be seen that there are three steps in the determination of i_{corr}:

I. Determination of α
II. Determination of β
III. Calculation of i_{base}

I. Determination of α

Raupach (1996:335) found that corrosion rate, *i*, increases with decreases in bar diameter, *D*, assuming the same total area of steel is used. This effect is accounted for in this study by introducing the factor α, defined as follows:

$$\alpha = \frac{i_{smaller\ D}}{i_{larger\ D}} \quad (7)$$

Schießl and Raupach (1997:61) found that, in general, the value of α ranges from about 1 to 3. However, they did not provide a general method to calculate α, and only calculated corrosion rates as a function of bar diameter for 8- and 20-mm diameter bars, as shown in Table 4 below:

Table 4: Corrosion rates calculated by Schießl and Raupach (1997).

Reinforcement Diameter, *D* [mm]	Corrosion rate, *i* [µA/cm^2]
8	5.60
20	3.11

As an example, based on Schießl and Raupach's (1997) results, α could be calculated as follows:

$$\alpha = \frac{i_{D=8\ mm}}{i_{D=20mm}} = \frac{5.60}{3.11} = 1.8$$

To calculate α for the members designed in this study, corrosion rate values for 16-, 32- and 40-mm diameter bars needed to be estimated. This was done by plotting the results from Table 4, and fitting an exponential relationship to them, as shown in the graph below.

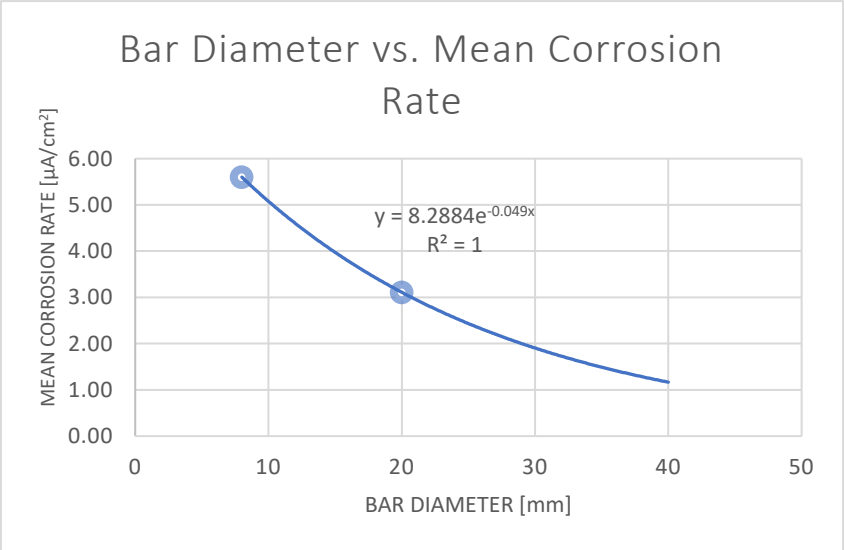

The equation for the exponential relationship, shown in Equation 8 below, was then used to estimate corrosion rate values for the various diameter bars. The results are shown in Table 5.

$$i = 8.2884 \times e^{-0.049D} \quad (8)$$

An exponential relationship was chosen to account for the fact that the decrease in corrosion rate with increasing bar diameter will not continue infinitely, until negative corrosion rates are reached, and will instead be asymptotic. A logarithmic relationship could also have been used and would have given very similar results. The exponential relationship shown in the graph is unlikely to be accurate, given that it was generated using only two data points, but it is sufficient for providing rough engineering estimates of α.

Table 5: Corrosion rates calculated as a function of bar diameter, using Equation 8.

Reinforcement Diameter, *D* [mm]	Corrosion rate, *i* [µA/cm^2]
8	5.60
10	5.08
12	4.60
16	3.78
20	3.11
25	2.43
32	1.73
40	1.17

α values were thus calculated for each of the members in this study, using Equation 7 and the corrosion rate values shown in Table 5. The results are shown in Table 6. It should be noted that the α values were calculated relative to the members designed without the crack width requirements, as these members had the larger reinforcement diameters.

Table 6: α values for each of the members in the study.

	Matola Jetty Beams		St. Helena Breakwater Crown Wall Units	
	Without CWR	**With CWR**	**Without CWR**	**With CWR**
Change in Bar Diameter due to CWR	-	Y40 to Y32	-	Y20 to Y16
α [-]	**1.00**	**1.48**	**1.00**	**1.22**

The resultant α values, which range between 1.00 and 1.48, are therefore in good agreement with the range of 1 to 3 reported by Schießl and Raupach (1997:61).

II. Determination of β

Bezuidenhout and van Zijl (2019:2189) found that corrosion rate decreases as the number of bars (i.e., area of steel provided, As_{prov}) increases. Their results, for members with single cracks (such as those used by Otieno (2014) to develop his corrosion rate model) are shown in Table 7 below:

Table 7: A summary of Bezuidenhout and van Zijl's (2019) results.

Number of Y10 Bars [-]	As_{prov} [mm^2]	Corrosion rate, i^a [µA/cm^2]	Increase in $As_{prov}{}^b$ [%]	Decrease in Corrosion Rate, $\Delta_i{}^b$ [%]
1	78.5	2.75	0	0
2	157	2.15	100	27.9
3	236	1.70	200	61.8

a. Corrosion rate results estimated by reading off bar graph (Bezuidenhout & van Zijl, 2019:2189)

b. Relative to the values for 1 Y10 bar

The decrease in corrosion rate (Δ_i) values can be used to calculate a factor expressing the corrosion rate (for any number of bars) relative to the corrosion rate for 1 Y10 bar – such that multiplying the corrosion rate for 1 Y10 bar (2.75 µA/cm^2) by this factor would give the corrosion rate for the number of bars associated with that factor. This factor is then β:

$$\beta = \frac{1}{1+\left(\frac{\Delta_i}{100}\right)} \quad (9)$$

Resultant values of β, for each number of bars, are shown in Table 8.

Table 8: Resultant β values.

Number of Y10 Bars [-]	Increase in As_{prov} [%]	Decrease in Corrosion Rate, Δ_i [%]	β [-]
1	0	0	1.00
2	100	27.9	0.78
3	200	61.8	0.62

The values shown in Table 8 can be used to plot a graph of "Increase in As_{prov}" vs. "β":

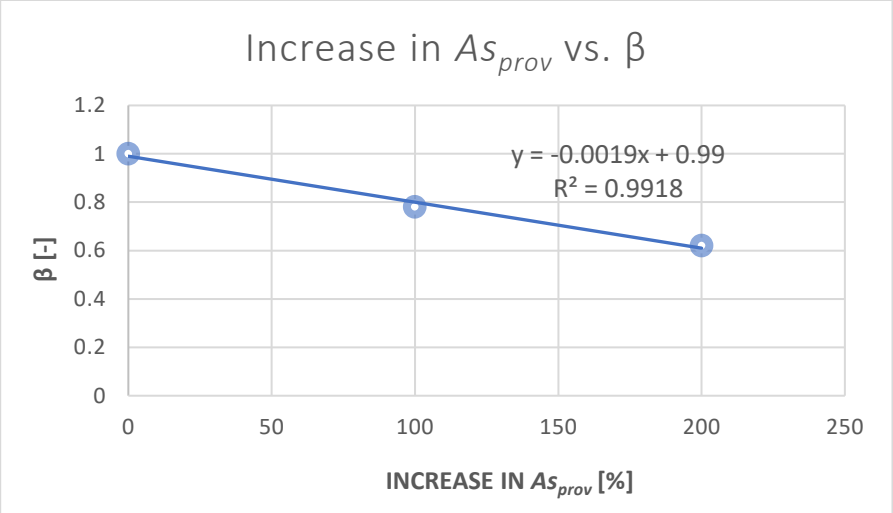

From this graph, the relationship between "Increase in As_{prov}" and "β" can be effectively approximated by a linear relationship, with the following equation for β:

$$\beta = -0.0019 \times (\%\ Increase\ in\ As_{prov}) + 0.99 \quad (10)$$

Equation 10 was then used to estimate β for each of the members, with the % increase in As_{prov} being calculated relative to the members designed without the crack width requirements. The results are shown in Table 9:

Table 9: β values for the members designed in the study.

	Matola Jetty Beams		St. Helena Breakwater Crown Wall Units	
	Without CWR	**With CWR**	**Without CWR**	**With CWR**
Maximum As_{prov} [mm²]	16336	18850	1571 (/m)	1608 (/m)
Increase in As_{prov} [%]	0	15.4	0	2.36
β [-]	**1.00**	**0.96**	**1.00**	**0.99**

It can thus be seen that, for the increases in reinforcement area experienced by typical marine RC members, the influence of this increase on corrosion rate is relatively minor, with β values close to 1.00.

III. Calculation of i_{base}

The base corrosion rate, i_{base}, was calculated for each member using the corrosion rate model developed by Otieno (2014). Otieno (2014) developed two formulas for corrosion rate in cracked RC, based on samples exposed to either laboratory or field conditions:

Otieno (2014:170)

$$i_{base} = 5.18 \times e^{0.01(D_{90} \times 10^{10})} \times \left(\frac{C}{w_{cr}}\right)^{-a} for\ laboratory\ conditions \quad (11)$$

Otieno (2014:171)

$$i_{base} = 0.64 \times e^{0.06 \times (D_{90} \times 10^{10})} \times \left(\frac{C}{w_{cr}}\right)^{-b} for\ field\ conditions \quad (12)$$

Where: D_{90} is the 90-day chloride diffusion coefficient

: C is the in-situ cover depth

: w_{cr} is the crack width

: $a = 0.96 \times (D_{90} \times 10^{10})^{-0.35}$

: $b = 0.21 \times e^{0.02(D_{90} \times 10^{10})}$

However, Otieno (2014:192) recommends using the model for laboratory conditions, as the data for field conditions was too variable at the end of the 2.25-year study period, such that no stable corrosion rate could be determined without further, long-term, research. **The model for laboratory conditions (Equation 11) was thus chosen for use in this study**. This is a somewhat conservative approach, as the model for laboratory conditions was found to result in significantly higher corrosion rates than the model for field conditions (Otieno, 2014:172).

The variables C and w_{cr} are already known, as input parameters for each of the members (see Tables 1 and 2). However, the variable D_{90} still needs to be determined for the members. An empirical relationship between the chloride conductivity index (CCI) and D_{90} was presented by Otieno (2014:239), in a two-step procedure. In the first step, the apparent diffusion coefficient, D_i, is calculated according to Equation 13:

Otieno (2014:239)

$$D_i = (1.1072 \times 10^{-3}) e^{0.8999 \times CCI} \ (for\ 50/50\ PC/GGBS\ concrete) \quad (13)$$

D_i is then used to calculate D_{90}, according to Equation 14:

$$D_{90} = \frac{D_i}{(t_{age})^{\alpha}} \quad (14)$$

Otieno (2014:214)

Where t_{age} is the expected service life of the structure, expressed in seconds, and α is a factor equal to 0.68 for 50/50 PC/GGBS concrete (Otieno, 2014:240). Otieno (2014:240) recommends using 50 as a typical value for t_{age}.

From the test specimens he produced, Otieno (2014:214) found that the average 90-day *CCI* value for 50/50 PC/GGBS concrete, with a w/b ratio of 0.40 (the same as the concrete used in this study) was 0.15 mS/cm, with a range of 0.12 to 0.18 mS/cm. **A *CCI* value of 0.15 mS/cm will thus be used for all concrete in this study**, allowing for the calculation of D_{90} for all members as follows:

$$D_i = (1.1072 \times 10^{-3}) e^{0.8999(0.15)} = 1.267 \times 10^{-3} cm^2/s$$

$$D_{90} = \frac{1.267 \times 10^{-3}}{(50 \times 365 \times 24 \times 60 \times 60)^{0.68}} = 7.05 \times 10^{-10} cm^2/s$$

$$\therefore \boldsymbol{D_{90} = 7.05 \times 10^{-10} cm^2/s}$$

i_{base} was thus calculated for all the members, using Equation 11. The results are shown in Table 10:

Table 10: Input parameters and final i_{base} values for each of the members in the study.

	Matola Jetty Beams		St. Helena Breakwater Crown Wall Units	
	Without CWR	**With CWR**	**Without CWR**	**With CWR**
C [mm]	60	60	60	60
w_{cr} [mm]	0.45	0.30	0.35	0.30
D_{90} [x10^{-10} cm^2/s]	7.05	7.05	7.05	7.05
a [-]	0.485	0.485	0.485	0.485
i_{base} [µA/cm^2]	**0.518**	**0.426**	**0.459**	**0.426**

Determination of i_{corr}

With the values of α, β and i_{base} all being known, i_{corr} was determined for each member using Equation 6 ($i_{corr} = \alpha \times \beta \times i_{base}$). **The resultant representative corrosion rates for the members in this study are thus shown in Table 11.**

Table 11: A summary of the representative corrosion rates for the members in this study.

	Matola Jetty Beams		St. Helena Breakwater Crown Wall Units	
	Without CWR	With CWR	Without CWR	With CWR
α [-]	1.00	1.48	1.00	1.22
β [-]	1.00	0.96	1.00	0.99
i_{base} [µA/cm^2]	0.518	0.426	0.459	0.426
i_{corr} [µA/cm^2]	**0.518**	**0.605**	**0.459**	**0.515**

4. Calculation of the Corrosion Propagation Period, t_p

Bezuidenhout & van Zijl (2019:2191)

The length of the corrosion propagation period, t_p, was calculated for each member using the model proposed by Bezuidenhout and van Zijl (2019), in which the end of service life is said to be reached when a certain percentage of the steel cross-section has been lost to corrosion. t_p was thus calculated for each member according to Equation 15:

$$t_p = \frac{LS}{100 - \left[\left(D - \left(0.0116 \times i_{corr} \times \alpha_{pit}\right)\right)^2 \times \frac{1}{D^2}\right] \times 100} \quad (15)$$

Where: LS is the limit state, i.e., the percentage loss in steel cross-section which defines the end of service life

: D is the initial reinforcement diameter

: i_{corr} is the representative corrosion rate for the member

: α_{pit} is the pitting factor, used to account for the fact that the corrosion rate at a macrocell "pit" will be higher than the representative corrosion rate, which was determined for the entire steel bar

Based on the literature, the following values were used for *LS* and α_{pit}:

- A *LS* value of 15 % was chosen; this is the median of the 5 – 25 % range for loss in cross-section which can safely be accommodated by design safety factors, before failure of the member occurs (Otieno, 2014:188)
- An α_{pit} value of 10 was selected, as there is general agreement in the literature that highly localised macrocell corrosion, as would typically occur at the locations of cracks in marine RC members, is best represented by a pitting factor of 10 (Andrade, 2020:285; Chen et al., 2020:32; Bezuidenhout & van Zijl, 2019:2192)

t_p values were thus calculated for each member using Equation 15; the results are shown in Table 12. Note that t_p values were calculated using both the base and representative corrosion rates, such that there are two different t_p values for each member.

Table 12: A summary of the t_p results for the members in the study.

	Matola Jetty Beams		St. Helena Breakwater Crown Wall Units	
	Without CWR	**With CWR**	**Without CWR**	**With CWR**
D [mm]	40	32	20	16
i_{base} [µA/cm^2]	0.518	0.426	0.459	0.426
i_{corr} [µA/cm^2]	0.518	0.605	0.459	0.515
t_p, using i_{base} [years]	**50**	**49**	**28**	**24**
t_p, using i_{corr} [years]	**50**	**34**	**28**	**20**

5. Calculation of Total Service Life, t_s

The total service life, t_s, of each member is defined as the sum of the initiation and propagation periods (t_i and t_p, respectively). However, as t_i was found to be zero for all members in the study, t_s is simply equal to t_p. The total service life for each member in the study is thus shown in Table 13.

Table 13: Final total service life values for the members in the study.

	TOTAL SERVICE LIFE, t_s [years]			
	Matola Jetty Beams		St. Helena Breakwater Crown Wall Units	
	Without CWR	With CWR	Without CWR	With CWR
Using base corrosion rate, i_{base}	50	49	28	24
Using representative corrosion rate, i_{corr}	50	34	28	20

Appendix F: Life Cycle Cost Analysis Calculations

F.1 Construction Costs: Concrete Units Quotation

CONCRETE UNITS

Specialists in the Manufacture of Precast Concrete (PTY) LTD

Reg no. 87/000031/07 VAT Reg no. 4480126301

CAPE TOWN
Montreal Drive
Airport Industria 7490
P.O. Box 6074
Roggebaai 8012
Tel ++27 21 386 1923
Fax ++27 21 386 2514
Email:
precast@concreteunits.co.za
Website:
www.concreteunits.co.za

CLIENT:

ATTENTION: NICK ELIAS

TENDER: EX YARD QUOTATION DATE: 26/07/2022

CONTRACT No.: UNKNOWN QUOTATION REF: C 3186 Pg 1 of 2

CONSULTANT: UNKNOWN CLOSING DATE: UNKNOWN

THANK YOU FOR THE OPPORTUNITY TO PRICE THE ABOVE CONTRACT.

ITEM 1: OUR EX YARD **BUDGET** PRICE, EXCLUDING VAT FOR THE SUPPLY OF PRECAST WALLS AND BEAMS, IS:
(WITH REINFORCEMENT DESIGNED TO MEET ULS &SLS REQUIREMENTS)

225 No.	**OPTION 1**	**2680 x 1000 x 3,900 mm LONG CROWN WALL**	**R 54,040.00 EACH PLUS VAT**
72 No.	**OPTION 1**	**1400 x 1800 x 15,000 mm LONG BEAM**	**R 234,665.00 EACH PLUS VAT**

ITEM 2: OUR EX YARD **BUDGET** PRICE, EXCLUDING VAT FOR THE SUPPLY OF PRECAST WALLS AND BEAMS, IS:
(WITH REINFORCEMENT DESIGNED TO MEET CRACK WIDTH REQUIREMENTS)

225 No.	**OPTION 2**	**2680 x 1000 x 3,900 mm LONG CROWN WALL**	**R 54,780.00 EACH PLUS VAT**
72 No.	**OPTION 2**	**1400 x 1800 x 15,000 mm LONG BEAM**	**R 254,130.00 EACH PLUS VAT**

ITEM 3: OUR **EXTRA OVER BUDGET PRICE**, EXCLUDING VAT FOR ADMIXTURE IN OUR CONCRETE MIX, IS:

xxx m³	SIKA WT200 3,2 KG/m³	**R 280.00 PER m³ PLUS VAT**
xxx m³	PENETRON 3 KG/m³	**R 440.00 PER m³ PLUS VAT**
xxx m³	XYPEX 5 KG/m³ (AGGRESSIVE CHEMICAL ENVIRONMENT)	**R 715.00 PER m³ PLUS VAT**
xxx m³	XYPEX 3 KG/m³ (GENERAL)	**R 425.00 PER m³ PLUS VAT**

OUR PRICE IS BASED ON THE FOLLOWING:

PLEASE SEE PAGE 2.

CONDITIONS OF SALE:

Rates exclude VAT.	
Rates are nett and valid for 30 days.	
We trade as suppliers and not as sub-contractors.	
Rates are subject to escalation by means of the Consumer Price Index base month	**MAY 22**
Rates are subject to change depending on Rise and Fall of the reinforcing steel price, base rate	**R15.86/kg**
Rates are subject to change depending on Rise and Fall of the Diesel price, base rate	**R21.56/LITRE (MAY '22)**
Payment terms strictly 30 days from date of statement.(on granting of credit facilities)	
We require to be paid 80% of the full value of units cast and stored in our yard.	
Ownership of goods sold remains vested in Concrete Units until all monies owing have been paid in full.	
We will not accept the with holding of any retention money, nor will we accept any penalty clauses or claims for damages of whatsoever nature how so ever arising.	

Directors: W.R. Robinson M.A. (Cantab)* G.P. Blackburn (Pr. Eng)**
*British **Australian

ISO 14001 ISO 45001 DEKRA DEKRA

SABS ISO 9001

CONCRETE UNITS

Specialists in the Manufacture of Precast Concrete (PTY) LTD
Reg no. 87/000031/07 VAT Reg no. 4480126301

CAPE TOWN
Montreal Drive
Airport Industria 7490
P.O. Box 6074
Roggebaai 8012
Tel ++27 21 386 1923
Fax ++27 21 386 2514
Email:
precast@concreteunits.co.za
Website:
www.concreteunits.co.za

CLIENT:

ATTENTION: NICK ELIAS

TENDER: EX YARD QUOTATION DATE: 26/07/2022

CONTRACT No.: UNKNOWN QUOTATION REF: C 3186 Pg 2 of 2

CONSULTANT: UNKNOWN CLOSING DATE: UNKNOWN

OUR PRICE IS BASED ON THE FOLLOWING:

* ITEM 1 & 2: ABOVE PRICE IS EX YARD.
* ITEM 1 & 2: WE REQUIRE 8 - 10 WEEKS FOR SET UP BEFORE WE CAN COMMENCE WITH CASTING.
* WE HAVE ALLOWED TO CAST 20 No. PRECAST WALL AND 5 No. PRECAST BEAM PER WEEK.
* ACCELERATED PRODUCTION RATES CAN BE ARRANGED ON REQUEST.
* ITEM 1 & 2: WE HAVE ALLOWED FOR THE WALL UNITS TO BE CASTED FLAT AND LOADED FLAT ON THE TRUCK SUPPLIED BY THE CLIENT.
* ITEM 1 & 2: INVESTMENT FOR NEW GANTRY CRANES IN OUR CAPE TOWN FACTORY ARE EXCLUDED IN OUR BUDGET PRICING. WE CAN CURRENTLY HANDLE A MAX OF 60 TON BEAMS.
* ITEM 1 : WE HAVE ALLOWED REINFORCING 568 KG (54 KG/m³) PER PRECAST WALL AND 4741 KG (125 KG/m³) PER PRECAST BEAM .
* ITEM 2 : WE HAVE ALLOWED REINFORCING 600 KG (57 KG/m³) PER PRECAST WALL AND 5597 KG (148 KG/m³) PER PRECAST BEAM .
* CONDITIONS AS SET OUT BELOW, APPLY.

REGARDS,

CHARL COETZEE (084 513 6699) PRECILLIAN NGANDU (081 563 9737)

CONDITIONS OF SALE:

Rates exclude VAT.
Rates are nett and valid for 30 days.
We trade as suppliers and not as sub-contractors.
Rates are subject to escalation by means of the Consumer Price Index base month MAY 22
Rates are subject to change depending on Rise and Fall of the reinforcing steel price, base rate R15.86/kg
Rates are subject to change depending on Rise and Fall of the Diesel price, base rate R21.56/LITRE (MAY '22)
Payment terms strictly 30 days from date of statement.(on granting of credit facilities)
We require to be paid 80% of the full value of units cast and stored in our yard.
Ownership of goods sold remains vested in Concrete Units until all monies owing have been paid in full.
We will not accept the with holding of any retention money, nor will we accept any penalty clauses or claims for damages of whatsoever nature how so ever arising.

Directors: W.R. Robinson M.A. (Cantab)* G.P. Blackburn (Pr. Eng)**
*British **Australian

ISO 14001 ISO 45001 DEKRA DEKRA SABS ISO 9001

F.2 Construction Cost Calculations

Table F-1: Costing Calculations for Member Cost Estimates

Item	Cost per Item [ZAR, excl. VAT]		Explanation
	Beams	*Wall Units*	
Cost per Unit Designed without CWR[a] (A)	234 665.00	54 040.00	-
Cost per Unit Designed with CWR[a] (B)	254 130.00	54 780.00	-
Cost Difference per Unit due to CWR[a] (C)	19 465.00	740.00	B - A
Price of Steel (D)	15.86/kg		-
Quantity of Steel per Unit Designed without CWR[a] (E)	4 741 kg	568 kg	-
Quantity of Steel per Unit Designed with CWR[a] (F)	5 597 kg	600 kg	-
Steel Material Cost per Unit Designed without CWR[a] (G)	75 192.26	9 008.48	D x E
Steel Material Cost per Unit Designed with CWR[a] (H)	88 768.42	9516.00	D x F
Difference in Steel Material Cost per Unit due to CWR[a] (I)	13 576.16	507.52	H - G
Difference in Steel Fixing Cost per Unit due to CWR[a] (J)	5 888.84	232.48	C – I[b]

a. Note that “CWR” refers to the crack width requirements

b. It is assumed that all the concrete costs (material, formwork, casting labour) are the same, regardless of whether a member was designed with or without CWR – such that the cost difference per unit due to CWR (Item C) is only due to differences in the steel material and fixing costs

Table F-2: Costing calculations for admixture cost estimates.

Item	Item Value		Explanation
	Beams	*Wall Units*	
Concrete Quantity [m^3] (A)	37.2	10.4	-
Sika WT-200 P (Waterproofing & Crack-sealing Admixture)			
Price per m^3 [ZAR, excl. VAT] (B)	280.00		-
Cost per Unit [ZAR, excl. VAT] (C)	10 416.00	2 912.00	A x B
PENETRON Admix (Waterproofing & Crack-sealing Admixture)			
Price per m^3 [ZAR, excl. VAT] (D)	440.00		-
Cost per Unit [ZAR, excl. VAT] (E)	16 368.00	4 576.00	A x D
XYPEX ADMIX C-Series (Waterproofing & Crack-sealing Admixture)			
Price per m^3 [ZAR, excl. VAT] (F)	425.00[a]		-
Cost per Unit [ZAR, excl. VAT] (G)	15 810.00	4 420.00	A x F

a. Xypex prices were quoted for dosages for both general exposure (3.0 kg/m^3) and exposure to aggressive chemical environments (5.0 kg/m^3). The price for general exposure (R 425.00/m^3) was chosen for use in this study, as the marine environment, while severe, is not an aggressive chemical environment

F.3 Full Life Cycle Cost Calculations

F.3.1 Matola Jetty Beams

General Info	
Escalation Rate (% p.a)	9.2
Discount Rate (% p.a)	8.0

Calculated from June 2021 to June 2022 using CPAP for precast concrete

Escalation Formula:

$$A = P(1 + \frac{r}{n})^{nt}$$

Present Value Formula:

$$PV = FV\frac{1}{(1+r)^n}$$

Strategy A (No CWD + Patch Repairs)		
Item	*Value*	*Explanation*
Construction Cost (C_C)		
2022 Construction Cost (excl. VAT)	R234 665.00	-
VAT (%)	15.00	-
2022 Construction Cost (incl. VAT)	R269 864.75	-
Repair Cost (C_R)		
Vulnerable Surface Area [m^2]	75	Assume repairs needed on soffit and side faces of beams only
Surface Area to be Repaired [m^2]	15	Assume 20 % of surface area needs repair (based on range of 15-30 % from Mackechnie and Alexander (2001))
2001 Cost of Repairs [R/m^2]	280	Assume extensive, good quality repairs. Rate from Mackechnie and Alexander (2001)
2001 Cost per Repair	R4 200.00	-
Predicted Service Life (Base Corrosion Rate) [years]	50	-
Predicted Service Life (Modified Corrosion Rate) [years]	50	-
Design Life [years]	50	-
Repairs Required?	No	Service life = design life
2022 Cost of Repairs	R0.00	-
Total Life Cycle Cost (LCC)		
2022 LCC	**R269 864.75**	$LCC = C_C + C_R$

Strategy B (CWD + Patch Repairs)		
Item	*Value*	*Explanation*
Construction Cost (C_C)		
2022 Construction Cost (excl. VAT)	R254 130.00	-
VAT (%)	15.00	-
2022 Construction Cost (incl. VAT)	R292 249.50	-
Repair Cost (C_R)		
Vulnerable Surface Area [m^2]	75	Assume repairs needed on soffit and side faces of beams only
Surface Area to be Patch Repaired [m^2]	9.375	Assume 12.5 % of surface area needs patch repairing. Based on discussion with supervisor (Professor Hans Beushausen)
Surface Area Requiring Hydrophobic Coating [m^2]	75	Coat entire vulnerable surface area, to avoid continuing corrosion adjacent to patch repairs
2001 Cost of Patch Repairs [R/m^2]	280	Assume extensive, good quality repairs. Rate from Mackechnie and Alexander (2001)
2001 Cost per Patch Repair	R2 625.00	-
2019 Cost of Hydrophobic Coating Repair	R7 125.00	Sikagard-706 Thixo silane cream, price of R 95/m^2 from Jappie (2019)
Predicted Service Life (Base Corrosion Rate) [years]	49	-
Predicted Service Life (Modified Corrosion Rate) [years]	34	-
Design Life [years]	50	-
Repairs Required?	Yes	For modified corrosion rate only
Repair Service Life [years]	20	Based on discussion with supervisor (Professor Hans Beushasen). Therefore repair at 34 years (2056) only
2056 Cost of Patch Repair	R332 180.72	Escalated at 9.2 % p.a. for 55 years (from 2001 to 2056)
2056 Cost of Hydrophobic Coating Repair	R184 936.44	Escalated at 9.2 % p.a. for 37 years (from 2019 to 2056)
Total 2056 Cost of Repair	R517 117.15	2056 Cost of Patch Repair + 2056 Cost of Hydrophobic Coating Repair
Discounted 2056 Cost of Repair	R37 772.98	Discounted at 8.0 % p.a. over 34 years (from 2056 to 2022)
Total Discounted (2022) Cost of Repairs	R37 772.98	Sum of all repairs
2022 Cost of Repairs (Base Corrosion Rate)	R0.00	-
2022 Cost of Repairs (Modified Corrosion Rate)	R37 772.98	-
Total Life Cycle Cost (LCC)		
2022 LCC (Base Corrosion Rate)	**R292 249.50**	$LCC = C_C + C_R$
2022 LCC (Modified Corrosion Rate)	**R330 022.48**	$LCC = C_C + C_R$

Strategy C (No CWD + XYPEX ADMIX C-Series)		
Item	*Value*	*Explanation*
Construction Cost (C_C)		
2022 Construction Cost (excl. VAT)	R234 665.00	-
2022 Admixture Cost (excl. VAT)	R15 810.00	-
Total 2022 Construction Cost (excl. VAT)	R250 475.00	-
VAT (%)	15.00	-
2022 Construction Cost (incl. VAT)	R288 046.25	-
Total Life Cycle Cost (LCC)		
2022 LCC	**R288 046.25**	$LCC = C_C + C_R$

Strategy D (No CWD + Hydrophobic Coating)		
Item	*Value*	*Explanation*
Construction Cost (C_C)		
2022 Construction Cost (excl. VAT)	R234 665.00	-
VAT (%)	15.00	-
2022 Construction Cost (incl. VAT)	R269 864.75	-
Maintenance Cost (C_M)		
Surface Area to be Coated [m^2]	75	Assume coating applied on soffit and side faces of beams only
2019 Coating Cost [R/m^2]	R95.00	Sikagard-706 Thixo silane cream, price from Jappie (2019)
2019 Total Coating Cost	R7 125.00	-
2022 Coating Cost	R9 277.97	Escalated at 9.2 % p.a. for 3 years (from 2019 to 2022)
2047 Coating Cost	R83 756.54	Escalated at 9.2 % p.a. for 28 years (from 2019 to 2047)
Discounted 2047 Coating Cost	R12 229.95	Discounted at 8.0 % p.a. over 25 years (from 2047 to 2022)
Total Discounted (2022)Maintenance Cost	R21 507.92	Sum of the 2022 and 2047 discounted coating costs
Total Life Cycle Cost (LCC)		
2022 LCC	**R291 372.67**	$LCC = C_C + C_M$

F.3.2 St. Helena Breakwater Crown Wall Units

General Info	
Escalation Rate (% p.a)	9.2
Discount Rate (% p.a)	8.0

Calculated from June 2021 to June 2022 using CPAP for precast concrete

Escalation Formula:

$$A = P(1 + \frac{r}{n})^{nt}$$

Present Value Formula:

$$PV = FV\frac{1}{(1+r)^n}$$

Strategy A (No CWD + Patch Repairs)		
Item	*Value*	*Explanation*
Construction Cost (C_C)		
2022 Construction Cost (excl. VAT)	R54 040.00	-
VAT (%)	15.00	-
2022 Construction Cost (incl. VAT)	R62 146.00	-
Repair Cost (C_R)		
Vulnerable Surface Area [m^2]	7.236	Assume repairs needed on both sides of walls, but only on exposed (i.e., above-base) portions
Surface Area to be Patch Repaired [m^2]	0.905	Assume 12.5 % of surface area needs patch repairing. Based on discussion with supervisor (Professor Hans Beushausen)
Surface Area Requiring Hydrophobic Coating [m^2]	7.236	Coat entire vulnerable surface area, to avoid continuing corrosion adjacent to patch repairs
2001 Cost of Patch Repairs [R/m^2]	280	Assume extensive, good quality repairs. Rate from Mackechnie and Alexander (2001)
2001 Cost per Patch Repair	R253.26	-
2019 Cost of Hydrophobic Coating Repair	R687.42	Sikagard-706 Thixo silane cream, price of R 95/m^2 from Jappie (2019)
Predicted Service Life (Base Corrosion Rate) [years]	28	-
Predicted Service Life (Modified Corrosion Rate) [years]	28	-
Design Life [years]	100	-
Repairs Required?	Yes	Service life < design life
Repair Service Life [years]	20	Based on discussion with supervisor (Professor Hans Beushasen). Therefore repair at 28 years (2050), 48 years (2070), 68 years (2090) and 88 years (2110)
2050 Cost of Patch Repair	R18 900.61	Escalated at 9.2 % p.a. for 49 years (from 2001 to 2050)
2050 Cost of Coating Repair	R10 522.62	Escalated at 9.2 % p.a. for 31 years (from 2019 to 2050)
2070 Cost of Patch Repair	R109 882.53	Escalated at 9.2 % p.a. for 69 years (from 2001 to 2070)
2070 Cost of Coating Repair	R61 175.39	Escalated at 9.2 % p.a. for 51 years (from 2019 to 2070)
2090 Cost of Patch Repair	R638 824.28	Escalated at 9.2 % p.a. for 89 years (from 2001 to 2090)
2090 Cost of Coating Repair	R355 655.47	Escalated at 9.2 % p.a. for 71 years (from 2019 to 2090)
2110 Cost of Patch Repair	R3 713 934.03	Escalated at 9.2 % p.a. for 109 years (from 2001 to 2110)
2110 Cost of Coating Repair	R2 067 674.90	Escalated at 9.2 % p.a. for 91 years (from 2019 to 2110)
Total 2050 Cost of Repair	R29 423.23	Sum of patch and coating repairs
Total 2070 Cost of Repair	R171 057.92	Sum of patch and coating repairs
Total 2090 Cost of Repair	R994 479.75	Sum of patch and coating repairs
Total 2110 Cost of Repair	R5 781 608.92	Sum of patch and coating repairs
Discounted 2050 Cost of Repair	R3 410.56	Discounted at 8.0 % p.a. over 28 years (from 2050 to 2022)
Discounted 2070 Cost of Repair	R4 254.05	Discounted at 8.0 % p.a. over 48 years (from 2070 to 2022)
Discounted 2090 Cost of Repair	R5 306.16	Discounted at 8.0 % p.a. over 68 years (from 2090 to 2022)
Discounted 2110 Cost of Repair	R6 618.48	Discounted at 8.0 % p.a. over 88 years (from 2110 to 2022)
Total Discounted (2022) Cost of Repairs	R19 589.25	Sum of all repairs
2022 Cost of Repairs	R19 589.25	-
Total Life Cycle Cost (LCC)		
2022 LCC	**R81 735.25**	$LCC = C_C + C_R$

Strategy B (CWD + Patch Repairs)		
Item	*Value*	*Explanation*
Construction Cost (C_C)		
2022 Construction Cost (excl. VAT)	R54 780.00	-
VAT (%)	15.00	-
2022 Construction Cost (incl. VAT)	R62 997.00	-
Repair Cost (C_R)		
Vulnerable Surface Area [m^2]	7.236	Assume repairs needed on both sides of walls, but only on exposed (i.e., above-base) portions
Surface Area to be Patch Repaired [m^2]	0.905	Assume 12.5 % of surface area needs patch repairing. Based on discussion with supervisor (Professor Hans Beushausen)
Surface Area Requiring Hydrophobic Coating [m^2]	7.236	Coat entire vulnerable surface area, to avoid continuing corrosion adjacent to patch repairs
2001 Cost of Patch Repairs [R/m^2]	280	Assume extensive, good quality repairs. Rate from Mackechnie and Alexander (2001)
2001 Cost per Patch Repair	R253.26	-
2019 Cost of Hydrophobic Coating Repair	R687.42	Sikagard-706 Thixo silane cream, price of R 95/m^2 from Jappie (2019)
Predicted Service Life (Base Corrosion Rate) [years]	24	-
Predicted Service Life (Modified Corrosion Rate) [years]	20	-
Design Life [years]	100	-
Repairs Required?	Yes	Service life < design life
Base Corrosion Rate		
Repair Service Life [years]	20	Based on discussion with supervisor (Professor Hans Beushasen). Therefore repair at 24 years (2046), 44 years (2066), 64 years (2086) and 84 years (2106)
2046 Cost of Patch Repair	R13 291.85	Escalated at 9.2 % p.a. for 45 years (from 2001 to 2046)
2046 Cost of Coating Repair	R7 400.03	Escalated at 9.2 % p.a. for 27 years (from 2019 to 2046)
2066 Cost of Patch Repair	R77 274.84	Escalated at 9.2 % p.a. for 65 years (from 2001 to 2066)
2066 Cost of Coating Repair	R43 021.56	Escalated at 9.2 % p.a. for 47 years (from 2019 to 2066)
2086 Cost of Patch Repair	R449 252.87	Escalated at 9.2 % p.a. for 85 years (from 2001 to 2086)
2086 Cost of Coating Repair	R250 114.54	Escalated at 9.2 % p.a. for 67 years (from 2019 to 2086)
2106 Cost of Patch Repair	R2 611 822.33	Escalated at 9.2 % p.a. for 105 years (from 2001 to 2106)
2106 Cost of Coating Repair	R1 454 091.39	Escalated at 9.2 % p.a. for 87 years (from 2019 to 2106)
Total 2046 Cost of Repair	R20 691.88	Sum of patch and coating repairs
Total 2066 Cost of Repair	R120 296.40	Sum of patch and coating repairs
Total 2086 Cost of Repair	R699 367.41	Sum of patch and coating repairs
Total 2106 Cost of Repair	R4 065 913.72	Sum of patch and coating repairs
Discounted 2046 Cost of Repair	R3 263.10	Discounted at 8.0 % p.a. over 24 years (from 2046 to 2022)
Discounted 2066 Cost of Repair	R4 070.12	Discounted at 8.0 % p.a. over 44 years (from 2066 to 2022)
Discounted 2086 Cost of Repair	R5 076.74	Discounted at 8.0 % p.a. over 64 years (from 2086 to 2022)
Discounted 2106 Cost of Repair	R6 332.32	Discounted at 8.0 % p.a. over 84 years (from 2106 to 2022)
Total Discounted (2022) Cost of Repairs	R18 742.28	Sum of all repairs
2022 Cost of Repairs (Base Corrosion Rate)	R18 742.28	-
Modified Corrosion Rate		
Repair Service Life [years]	20	Based on discussion with supervisor (Professor Hans Beushasen). Therefore repair at 20 years (2042), 40 years (2062), 60 years (2082) and 80 years (2102)
2042 Cost of Patch Repair	R9 347.48	Escalated at 9.2 % p.a. for 41 years (from 2001 to 2042)
2042 Cost of Coating Repair	R5 204.07	Escalated at 9.2 % p.a. for 23 years (from 2019 to 2042)
2062 Cost of Patch Repair	R54 343.49	Escalated at 9.2 % p.a. for 61 years (from 2001 to 2062)
2062 Cost of Coating Repair	R30 254.89	Escalated at 9.2 % p.a. for 43 years (from 2019 to 2062)
2082 Cost of Patch Repair	R315 936.87	Escalated at 9.2 % p.a. for 81 years (from 2001 to 2082)
2082 Cost of Coating Repair	R175 892.93	Escalated at 9.2 % p.a. for 63 years (from 2019 to 2082)
2102 Cost of Patch Repair	R1 836 762.81	Escalated at 9.2 % p.a. for 101 years (from 2001 to 2102)
2102 Cost of Coating Repair	R1 022 589.07	Escalated at 9.2 % p.a. for 83 years (from 2019 to 2102)
Total 2042 Cost of Repair	R14 551.55	Sum of patch and coating repairs
Total 2062 Cost of Repair	R84 598.38	Sum of patch and coating repairs
Total 2082 Cost of Repair	R491 829.80	Sum of patch and coating repairs
Total 2102 Cost of Repair	R2 859 351.89	Sum of patch and coating repairs
Discounted 2042 Cost of Repair	R3 122.01	Discounted at 8.0 % p.a. over 20 years (from 2042 to 2022)
Discounted 2062 Cost of Repair	R3 894.14	Discounted at 8.0 % p.a. over 40 years (from 2062 to 2022)
Discounted 2082 Cost of Repair	R4 857.24	Discounted at 8.0 % p.a. over 60 years (from 2082 to 2022)
Discounted 2102 Cost of Repair	R6 058.53	Discounted at 8.0 % p.a. over 80 years (from 2102 to 2022)
Total Discounted (2022) Cost of Repairs	R17 931.92	Sum of all repairs
2022 Cost of Repairs (Modified Corrosion Rate)	R17 931.92	-
2022 LCC (Base Corrosion Rate)	**R81 739.28**	$LCC = C_C + C_R$
2022 LCC (Modified Corrosion Rate)	**R80 928.92**	$LCC = C_C + C_R$

Strategy C (No CWD + XYPEX ADMIX C-Series)		
Item	*Value*	*Explanation*
Construction Cost (C_C)		
2022 Construction Cost (excl. VAT)	R54 040.00	-
2022 Admixture Cost (excl. VAT)	R4 420.00	-
Total 2022 Construction Cost (excl. VAT)	R58 460.00	-
VAT (%)	15.00	-
2022 Construction Cost (incl. VAT)	R67 229.00	-
Total Life Cycle Cost (LCC)		
2022 LCC	**R67 229.00**	$LCC = C_C + C_R$

Strategy D (No CWD + Hydrophobic Coating)		
Item	*Value*	*Explanation*
Construction Cost (C_C)		
2022 Construction Cost (excl. VAT)	R54 040.00	-
VAT (%)	15.00	-
2022 Construction Cost (incl. VAT)	R62 146.00	-
Maintenance Cost (C_M)		
Surface Area to be Coated [m^2]	7.236	Assume coating applied on exposed areas only, but on both sides
2019 Coating Cost [R/m^2]	R95.00	Sikagard-706 Thixo silane cream, price from Jappie (2019)
2019 Total Coating Cost	R687.42	-
2022 Coating Cost	R895.14	Escalated at 9.2 % p.a. for 3 years (from 2019 to 2022)
2047 Coating Cost	R8 080.83	Escalated at 9.2 % p.a. for 28 years (from 2019 to 2047)
2072 Coating Cost	R72 949.45	Escalated at 9.2 % p.a. for 53 years (from 2019 to 2072)
2097 Coating Cost	R658 548.79	Escalated at 9.2 % p.a. for 78 years (from 2019 to 2097)
Discounted 2047 Coating Cost	R1 179.95	Discounted at 8.0 % p.a. over 25 years (from 2047 to 2022)
Discounted 2072 Coating Cost	R1 555.37	Discounted at 8.0 % p.a. over 50 years (from 2072 to 2022)
Discounted 2097 Coating Cost	R2 050.25	Discounted at 8.0 % p.a. over 75 years (from 2097 to 2022)
Total Discounted (2022)Maintenance Cost	R5 680.70	Sum of the 2022, 2047, 2072 and 2097 discounted coating costs
Total Life Cycle Cost (LCC)		
2022 LCC	**R67 826.70**	$LCC = C_C + C_M$

F.3.3 Coating Time Sensitivity Analysis

F.3.3.1 Matola Jetty Beams

BEAMS		
Reapplication Every 10 Years		
Item	*Value*	*Explanation*
Construction Cost (C_C)		
2022 Construction Cost (excl. VAT)	R234 665.00	-
VAT (%)	15.00	-
2022 Construction Cost (incl. VAT)	R269 864.75	-
Maintenance Cost (C_M)		
Surface Area to be Coated [m^2]	75	Assume coating applied on soffit and side faces of beams only
2019 Coating Cost [R/m^2]	R95.00	Sikagard-706 Thixo silane cream, price from Jappie (2019)
2019 Total Coating Cost	R7 125.00	-
2022 Coating Cost	R9 277.97	Escalated at 9.2 % p.a. for 3 years (from 2019 to 2022)
2032 Coating Cost	R22 370.68	Escalated at 9.2 % p.a. for 13 years (from 2019 to 2032)
2042 Coating Cost	R53 939.33	Escalated at 9.2 % p.a. for 23 years (from 2019 to 2042)
2052 Coating Cost	R130 056.46	Escalated at 9.2 % p.a. for 33 years (from 2019 to 2052)
2062 Coating Cost	R313 587.19	Escalated at 9.2 % p.a. for 43 years (from 2019 to 2062)
Discounted 2032 Coating Cost	R10 361.95	Discounted at 8.0 % p.a. over 10 years (from 2032 to 2022)
Discounted 2042 Coating Cost	R11 572.59	Discounted at 8.0 % p.a. over 20 years (from 2042 to 2022)
Discounted 2052 Coating Cost	R12 924.66	Discounted at 8.0 % p.a. over 30 years (from 2052 to 2022)
Discounted 2062 Coating Cost	R14 434.71	Discounted at 8.0 % p.a. over 40 years (from 2062 to 2022)
Total Discounted (2022)Maintenance Cost	R58 571.88	Sum of the 2022, 2032, 2042, 2052 and 2062 discounted coating costs
Total Life Cycle Cost (LCC)		
2022 LCC	**R328 436.63**	$LCC = C_C + C_M$
Reapplication Every 15 Years		
Item	*Value*	*Explanation*
Construction Cost (C_C)		
2022 Construction Cost (excl. VAT)	R234 665.00	-
VAT (%)	15.00	-
2022 Construction Cost (incl. VAT)	R269 864.75	-
Maintenance Cost (C_M)		
Surface Area to be Coated [m^2]	75	Assume coating applied on soffit and side faces of beams only
2019 Coating Cost [R/m^2]	R95.00	Sikagard-706 Thixo silane cream, price from Jappie (2019)
2019 Total Coating Cost	R7 125.00	-
2022 Coating Cost	R9 277.97	Escalated at 9.2 % p.a. for 3 years (from 2019 to 2022)
2037 Coating Cost	R34 737.00	Escalated at 9.2 % p.a. for 18 years (from 2019 to 2037)
2052 Coating Cost	R130 056.46	Escalated at 9.2 % p.a. for 33 years (from 2019 to 2052)
2067 Coating Cost	R486 935.58	Escalated at 9.2 % p.a. for 48 years (from 2019 to 2067)
Discounted 2037 Coating Cost	R10 950.55	Discounted at 8.0 % p.a. over 15 years (from 2037 to 2022)
Discounted 2052 Coating Cost	R12 924.66	Discounted at 8.0 % p.a. over 30 years (from 2052 to 2022)
Discounted 2067 Coating Cost	R15 254.66	Discounted at 8.0 % p.a. over 45 years (from 2067 to 2022)
Total Discounted (2022)Maintenance Cost	R48 407.84	Sum of the 2022, 2037, 2052and 2067 discounted coating costs
Total Life Cycle Cost (LCC)		
2022 LCC	**R318 272.59**	$LCC = C_C + C_M$

Reapplication Every 20 Years		
Item	*Value*	*Explanation*
Construction Cost (C_C)		
2022 Construction Cost (excl. VAT)	R234 665.00	-
VAT (%)	15.00	-
2022 Construction Cost (incl. VAT)	R269 864.75	-
Maintenance Cost (C_M)		
Surface Area to be Coated [m^2]	75	Assume coating applied on soffit and side faces of beams only
2019 Coating Cost [R/m^2]	R95.00	Sikagard-706 Thixo silane cream, price from Jappie (2019)
2019 Total Coating Cost	R7 125.00	-
2022 Coating Cost	R9 277.97	Escalated at 9.2 % p.a. for 3 years (from 2019 to 2022)
2042 Coating Cost	R53 939.33	Escalated at 9.2 % p.a. for 23 years (from 2019 to 2042)
2062 Coating Cost	R313 587.19	Escalated at 9.2 % p.a. for 43 years (from 2019 to 2062)
Discounted 2042 Coating Cost	R11 572.59	Discounted at 8.0 % p.a. over 20 years (from 2042 to 2022)
Discounted 2062 Coating Cost	R14 434.71	Discounted at 8.0 % p.a. over 40 years (from 2062 to 2022)
Total Discounted (2022)Maintenance Cost	R35 285.26	Sum of the 2022, 2042 and 2062 discounted coating costs
Total Life Cycle Cost (LCC)		
2022 LCC	**R305 150.01**	$LCC = C_C + C_M$
Reapplication Every 25 Years		
Item	*Value*	*Explanation*
Construction Cost (C_C)		
2022 Construction Cost (excl. VAT)	R234 665.00	-
VAT (%)	15.00	-
2022 Construction Cost (incl. VAT)	R269 864.75	-
Maintenance Cost (C_M)		
Surface Area to be Coated [m^2]	75	Assume coating applied on soffit and side faces of beams only
2019 Coating Cost [R/m^2]	R95.00	Sikagard-706 Thixo silane cream, price from Jappie (2019)
2019 Total Coating Cost	R7 125.00	-
2022 Coating Cost	R9 277.97	Escalated at 9.2 % p.a. for 3 years (from 2019 to 2022)
2047 Coating Cost	R83 756.54	Escalated at 9.2 % p.a. for 28 years (from 2019 to 2047)
Discounted 2047 Coating Cost	R12 229.95	Discounted at 8.0 % p.a. over 25 years (from 2047 to 2022)
Total Discounted (2022)Maintenance Cost	R21 507.92	Sum of the 2022 and 2047 discounted coating costs
Total Life Cycle Cost (LCC)		
2022 LCC	**R291 372.67**	$LCC = C_C + C_M$
Reapplication Every 50 Years		
Item	*Value*	*Explanation*
Construction Cost (C_C)		
2022 Construction Cost (excl. VAT)	R234 665.00	-
VAT (%)	15.00	-
2022 Construction Cost (incl. VAT)	R269 864.75	-
Maintenance Cost (C_M)		
Surface Area to be Coated [m^2]	75	Assume coating applied on soffit and side faces of beams only
2019 Coating Cost [R/m^2]	R95.00	Sikagard-706 Thixo silane cream, price from Jappie (2019)
2019 Total Coating Cost	R7 125.00	-
2022 Coating Cost	R9 277.97	Escalated at 9.2 % p.a. for 3 years (from 2019 to 2022)
Total Discounted (2022)Maintenance Cost	R9 277.97	Cost at time of construction (2022) only
Total Life Cycle Cost (LCC)		
2022 LCC	**R279 142.72**	$LCC = C_C + C_M$

F3.3.2 St. Helena Breakwater Crown Wall Units

WALL UNITS		
Reapplication Every 10 Years		
Item	*Value*	*Explanation*
Construction Cost (C_C)		
2022 Construction Cost (excl. VAT)	R54 040.00	-
VAT (%)	15.00	-
2022 Construction Cost (incl. VAT)	R62 146.00	-
Maintenance Cost (C_M)		
Coated [m^2]	7.236	Assume coating applied on exposed areas only, but on both sides
Cost [R/m^2]	R95.00	Sikagard-706 Thixo silane cream, price from Jappie (2019)
2019 Total Coating Cost	R687.42	-
2022 Coating Cost	R895.14	Escalated at 9.2 % p.a. for 3 years (from 2019 to 2022)
2032 Coating Cost	R2 158.32	Escalated at 9.2 % p.a. for 13 years (from 2019 to 2032)
2042 Coating Cost	R5 204.07	Escalated at 9.2 % p.a. for 23 years (from 2019 to 2042)
2052 Coating Cost	R12 547.85	Escalated at 9.2 % p.a. for 33 years (from 2019 to 2052)
2062 Coating Cost	R30 254.89	Escalated at 9.2 % p.a. for 43 years (from 2019 to 2062)
2072 Coating Cost	R72 949.45	Escalated at 9.2 % p.a. for 53 years (from 2019 to 2072)
2082 Coating Cost	R175 892.93	Escalated at 9.2 % p.a. for 63 years (from 2019 to 2082)
2092 Coating Cost	R424 106.34	Escalated at 9.2 % p.a. for 73 years (from 2019 to 2092)
2102 Coating Cost	R1 022 589.07	Escalated at 9.2 % p.a. for 83 years (from 2019 to 2102)
2112 Coating Cost	R2 465 627.88	Escalated at 9.2 % p.a. for 93 years (from 2019 to 2112)
Discounted 2032 Coating Cost	R999.72	Discounted at 8.0 % p.a. over 10 years (from 2032 to 2022)
Discounted 2042 Coating Cost	R1 116.52	Discounted at 8.0 % p.a. over 20 years (from 2042 to 2022)
Discounted 2052 Coating Cost	R1 246.97	Discounted at 8.0 % p.a. over 30 years (from 2052 to 2022)
Discounted 2062 Coating Cost	R1 392.66	Discounted at 8.0 % p.a. over 40 years (from 2062 to 2022)
Discounted 2072 Coating Cost	R1 555.37	Discounted at 8.0 % p.a. over 50 years (from 2062 to 2022)
Discounted 2082 Coating Cost	R1 737.09	Discounted at 8.0 % p.a. over 60 years (from 2062 to 2022)
Discounted 2092 Coating Cost	R1 940.05	Discounted at 8.0 % p.a. over 70 years (from 2062 to 2022)
Discounted 2102 Coating Cost	R2 166.71	Discounted at 8.0 % p.a. over 80 years (from 2062 to 2022)
Discounted 2112 Coating Cost	R2 419.86	Discounted at 8.0 % p.a. over 90 years (from 2062 to 2022)
Total Discounted (2022)Maintenance Cost	R15 470.09	Sum of the discounted coating costs
Total Life Cycle Cost (LCC)		
2022 LCC	**R77 616.09**	$LCC = C_C + C_M$
Reapplication Every 15 Years		
Item	*Value*	*Explanation*
Construction Cost (C_C)		
2022 Construction Cost (excl. VAT)	R54 040.00	-
VAT (%)	15.00	-
2022 Construction Cost (incl. VAT)	R62 146.00	-
Maintenance Cost (C_M)		
Coated [m^2]	7.236	Assume coating applied on exposed areas only, but on both sides
Cost [R/m^2]	R95.00	Sikagard-706 Thixo silane cream, price from Jappie (2019)
2019 Total Coating Cost	R687.42	-
2022 Coating Cost	R895.14	Escalated at 9.2 % p.a. for 3 years (from 2019 to 2022)
2037 Coating Cost	R3 351.43	Escalated at 9.2 % p.a. for 18 years (from 2019 to 2037)
2052 Coating Cost	R12 547.85	Escalated at 9.2 % p.a. for 33 years (from 2019 to 2052)
2067 Coating Cost	R46 979.54	Escalated at 9.2 % p.a. for 48 years (from 2019 to 2067)
2082 Coating Cost	R175 892.93	Escalated at 9.2 % p.a. for 63 years (from 2019 to 2082)
2097 Coating Cost	R658 548.79	Escalated at 9.2 % p.a. for 78 years (from 2019 to 2097)
2112 Coating Cost	R2 465 627.88	Escalated at 9.2 % p.a. for 93 years (from 2019 to 2112)
Discounted 2037 Coating Cost	R1 056.51	Discounted at 8.0 % p.a. over 15 years (from 2037 to 2022)
Discounted 2052 Coating Cost	R1 246.97	Discounted at 8.0 % p.a. over 30 years (from 2052 to 2022)
Discounted 2067 Coating Cost	R1 471.77	Discounted at 8.0 % p.a. over 45 years (from 2067 to 2022)
Discounted 2082 Coating Cost	R1 737.09	Discounted at 8.0 % p.a. over 60 years (from 2082 to 2022)
Discounted 2097 Coating Cost	R2 050.25	Discounted at 8.0 % p.a. over 75 years (from 2097 to 2022)
Discounted 2112 Coating Cost	R2 419.86	Discounted at 8.0 % p.a. over 90 years (from 2112 to 2022)
Total Discounted (2022)Maintenance Cost	R10 877.59	Sum of the discounted coating costs
Total Life Cycle Cost (LCC)		
2022 LCC	**R73 023.59**	$LCC = C_C + C_M$

Reapplication Every 20 Years		
Item	*Value*	*Explanation*
Construction Cost (C_C)		
2022 Construction Cost (excl. VAT)	R54 040.00	-
VAT (%)	15.00	-
2022 Construction Cost (incl. VAT)	R62 146.00	-
Maintenance Cost (C_M)		
Coated [m^2]	7.236	Assume coating applied on exposed areas only, but on both sides
Cost [R/m^2]	R95.00	Sikagard-706 Thixo silane cream, price from Jappie (2019)
2019 Total Coating Cost	R687.42	-
2022 Coating Cost	R895.14	Escalated at 9.2 % p.a. for 3 years (from 2019 to 2022)
2042 Coating Cost	R5 204.07	Escalated at 9.2 % p.a. for 23 years (from 2019 to 2042)
2062 Coating Cost	R30 254.89	Escalated at 9.2 % p.a. for 43 years (from 2019 to 2062)
2082 Coating Cost	R175 892.93	Escalated at 9.2 % p.a. for 63 years (from 2019 to 2082)
2102 Coating Cost	R1 022 589.07	Escalated at 9.2 % p.a. for 83 years (from 2019 to 2102)
Discounted 2042 Coating Cost	R1 116.52	Discounted at 8.0 % p.a. over 20 years (from 2042 to 2022)
Discounted 2062 Coating Cost	R1 392.66	Discounted at 8.0 % p.a. over 40 years (from 2062 to 2022)
Discounted 2082 Coating Cost	R1 737.09	Discounted at 8.0 % p.a. over 60 years (from 2082 to 2022)
Discounted 2102 Coating Cost	R2 166.71	Discounted at 8.0 % p.a. over 80 years (from 2102 to 2022)
Total Discounted (2022)Maintenance Cost	R7 308.12	Sum of the discounted coating costs
Total Life Cycle Cost (LCC)		
2022 LCC	**R69 454.12**	$LCC = C_C + C_M$

Reapplication Every 25 Years		
Item	*Value*	*Explanation*
Construction Cost (C_C)		
2022 Construction Cost (excl. VAT)	R54 040.00	-
VAT (%)	15.00	-
2022 Construction Cost (incl. VAT)	R62 146.00	-
Maintenance Cost (C_M)		
Coated [m^2]	7.236	Assume coating applied on exposed areas only, but on both sides
Cost [R/m^2]	R95.00	Sikagard-706 Thixo silane cream, price from Jappie (2019)
2019 Total Coating Cost	R687.42	-
2022 Coating Cost	R895.14	Escalated at 9.2 % p.a. for 3 years (from 2019 to 2022)
2047 Coating Cost	R8 080.83	Escalated at 9.2 % p.a. for 28 years (from 2019 to 2047)
2072 Coating Cost	R72 949.45	Escalated at 9.2 % p.a. for 53 years (from 2019 to 2072)
2097 Coating Cost	R658 548.79	Escalated at 9.2 % p.a. for 78 years (from 2019 to 2097)
Discounted 2047 Coating Cost	R1 179.95	Discounted at 8.0 % p.a. over 25 years (from 2047 to 2022)
Discounted 2072 Coating Cost	R1 555.37	Discounted at 8.0 % p.a. over 50 years (from 2072 to 2022)
Discounted 2097 Coating Cost	R2 050.25	Discounted at 8.0 % p.a. over 75 years (from 2097 to 2022)
Total Discounted (2022)Maintenance Cost	R5 680.70	Sum of the discounted coating costs
Total Life Cycle Cost (LCC)		
2022 LCC	**R67 826.70**	$LCC = C_C + C_M$

Reapplication Every 50 Years		
Item	*Value*	*Explanation*
Construction Cost (C_C)		
2022 Construction Cost (excl. VAT)	R54 040.00	-
VAT (%)	15.00	-
2022 Construction Cost (incl. VAT)	R62 146.00	-
Maintenance Cost (C_M)		
Coated [m^2]	7.236	Assume coating applied on exposed areas only, but on both sides
Cost [R/m^2]	R95.00	Sikagard-706 Thixo silane cream, price from Jappie (2019)
2019 Total Coating Cost	R687.42	-
2022 Coating Cost	R895.14	Escalated at 9.2 % p.a. for 3 years (from 2019 to 2022)
2072 Coating Cost	R72 949.45	Escalated at 9.2 % p.a. for 53 years (from 2019 to 2072)
Discounted 2072 Coating Cost	R1 555.37	Discounted at 8.0 % p.a. over 50 years (from 2072 to 2022)
Total Discounted (2022)Maintenance Cost	R2 450.51	Sum of the discounted coating costs
Total Life Cycle Cost (LCC)		
2022 LCC	**R64 596.51**	$LCC = C_C + C_M$

F.4 Calculation of Increases in LCC

F.4.1 Matola Jetty Beams

Table F-3: Calculation of LCC increases for the Matola jetty beams.

	Strategy A	**Strategy B** (Base Corrosion Rate)	**Strategy B** (Modified Corrosion Rate)	**Strategy C**	**Strategy D**
LCC [ZAR/beam]	R 269 864.75	R 292 249.50	R 330 022.48	R 288 046.25	R 291 372.67
Difference in LCC Compared to Cheapest Option [ZAR/beam]	Cheapest Option	R 22 384.75	R 60 157.73	R 18 181.50	R 21 507.92
Total No. of Beams Designed for CWRs	72	72	72	72	72
Total Difference in LCC Compared to Cheapest Option [ZAR]	**Cheapest Option**	**R 22 384.75 x 72 = R 1 611 702.00**	**R 60 157.73 x 72 = R 4 331 356.56**	**R 18 181.50 x 72 = R 1 309 068.00**	**R 21 507.92 x 72 = R 1 548 570.24**

F.4.2 St. Helena Island Crown Wall Units

Table F-4: Calculation of LCC increases for the St. Helena Island crown wall units.

	Strategy A	**Strategy B** (Base Corrosion Rate)	**Strategy B** (Modified Corrosion Rate)	**Strategy C**	**Strategy D**
LCC [ZAR/unit]	R 81 735.25	R 81 739.28	R 80 928.92	R 67 229.00	R 67 826.70
Difference in LCC Compared to Cheapest Option [ZAR/unit]	R 14 506.25	R 14 510.28	R 13 699.92	Cheapest Option	Cheapest Option
Total No. of Wall Units Designed for CWRs	225	225	225	225	225
Total Difference in LCC Compared to Cheapest Option [ZAR]	**R 14 506.25 x 225 = R 3 263 906.25**	**R 14 510.28 x 225 = R 3 264 813.00**	**R 13 699.92 x 225 = R 3 082 482.00**	**Cheapest Option**	**Cheapest Option**

Appendix G: Embodied Carbon Estimates

Please find the embodied carbon estimate calculation sheet attached on the following page.

	EMBODIED CARBON CALCULATIONS	

Project:	MSc. Eng. Structural Engineering - Research
Calculations By:	Nicholas Elias
Date:	01/07/2022

Reference	**Introduction**
	The aim of these calculations is to estimate embodied carbon (EC) values for each of the members designed in this study, and to contextualise them by finding total EC values, considering the entire number of members across the structure they belong to. Typical EC values for marine RC structures were also found in the literature, or determined by calculations, to evaluate the significance of the results. The following calculations are therefore presented in this calculation sheet: 1. Estimation of Member EC Values 2. Estimation of Total EC Values 3. EC Values for Typical Marine Structures
	1. Estimation of Member EC Values
IStructE (2020:4)	Member EC values were estimated using the approach given in the Institution of Civil Engineer's (IStructE's) *How to Calculate Embodied Carbon* (2020) guide. The EC value for each material in the members was estimated according to the following formula: $$EC = Q \times ECF \quad (1)$$ Where: Q is the quantity of the material, measured in kilograms : *ECF* is the Embodied Carbon Factor for that material, determined from the data provided in the IStructE guide, for the relevant stage of the material's lifecycle
SANS 10160-2 Tables A.1 and A.5	From the "Quantification of Material Amounts" section of this study, the volume of material used in each of the members is known and is shown in Table 1. These volumes were converted to masses using the mass density of steel and unreinforced concrete (7800 and 2300 kg/m^3, respectively). The resultant material quantities are shown in Table 2.

As the members designed in the study will not actually be produced, data about their installation on site, use, and end-of-life treatment was not available. **EC values were therefore only determined for the production stage (referred to as "A1-A3 emissions")**, which are likely to account for the majority of emissions produced by the members (IStructE, 2020:9).

Table 1: Material volumes, per member, for each member.

Member Type	**Matola Jetty Beams**		**St. Helena Breakwater Crown Wall Units**	
Design Type	Without CWR[a]	With CWR[a]	Without CWR[a]	With CWR[a]
Concrete Volume [m^3]	37.2	37.0	10.4	10.4
Reinforcement Volume [m^3]	0.604	0.773	0.072	0.076

a. Where "CWR" refers to "crack width requirements"

Table 2: Material quantities, per member, for each member.

Member Type	**Matola Jetty Beams**		**St. Helena Breakwater Crown Wall Units**	
Design Type	Without CWR	With CWR	Without CWR	With CWR
Concrete Quantity [kg]	85 560	85 100	23 920	23 920
Reinforcement Quantity [kg]	4 711	6 029	561.6	592.8

IStructE (2020) Table 2.3

The final EC values, calculated according to Equation 1, are shown in Table 3. Production stage (A1-A3) ECF values were chosen as follows:

- The concrete ECF value was chosen for concrete with 50 % GGBS replacement, as was used in the mix design for the members.

IStructE (2020) Table 2.3

- Due to a lack of data for precast members, the concrete ECF value was chosen for cast-in-situ concrete
- The IStructE (2020) guide only provides ECF values for Class C32/40 and C40/50 concrete. ECF values for Class C35/45 concrete, as was used in the mix design for the members, were therefore interpolated.
- The Reinforcement ECF value was selected using the worldwide data in Table 2.3 of the IStructE (2020) guide, as the members were not designed for structures located in the UK and would therefore not use UK reinforcement.

The concrete ECF value for each member was thus found to be 0.096 $kgCO_2e/kg$, while the reinforcement ECF value was found to be 1.99 $kgCO_2e/kg$.

Table 3: Final production stage (A1-A3) EC values for each of the members in the study.

Member Type	**Matola Jetty Beams**		**St. Helena Breakwater Crown Wall Units**	
Design Type	Without CWR	With CWR	Without CWR	With CWR
Concrete EC [$kgCO_2e$]	8 214	8 170	2 296	2 296
Reinforcement EC [$kgCO_2e$]	9 375	11 998	1 118	1 180
Total A1-A3 EC [$kgCO_2e$]	**17 600**	**20 200**	**3 410**	**3 480**

2. Estimation of Total EC Values

Total EC values, considering the total number of members in each structure (the Matola jetty or St. Helena Island breakwater) were calculated according to the following assumptions:

- From the original drawings of the Matola jetty provided by PRDW, there were found to be approximately 144 beams in the jetty. However, only about half of the beams had the same dimensions and loading conditions as the B401 beams designed in this study

- The total number of B401-like beams (i.e., beams for which crack width design is critical) in the Matola jetty was thus estimated to be 72
- From the original drawings of the St. Helena Island breakwater provided by PRDW, the breakwater crown wall is about 600 m long
- As each F01 precast crown wall unit is 2.7 m wide, there are approximately 225 F01 wall units in the breakwater

The total production stage (A1-A3) EC values, considering the total number of designed members in each structure, are therefore shown in Table 4.

Table 4: Total production stage (A1-A3) EC values, considering the total number of members in the entire structure.

Member Type	**Matola Jetty Beams**		**St. Helena Breakwater Crown Wall Units**	
Design Type	Without CWR	With CWR	Without CWR	With CWR
Total No. of Members [-]	72	72	225	225
A1-A3 EC per Member [$kgCO_2e$]	17 600	20 200	3 410	3 480
Total A1-A3 EC Over Entire Structure [$kgCO_2e$]	**1 270 000**	**1 450 000**	**767 000**	**783 000**

3. EC Values for Typical Marine Structures

To evaluate the significance of the EC results determined above, it is helpful to place them in context by comparing them to typical EC values of marine structures. The following EC values were therefore found in the literature:

- Broekens et al. (2012) found that a 1.4 km long rubble mound breakwater, with an average seabed depth of 14 m below sea level, would have a total EC value of 212 000 000 $kgCO_2e$ and an A1-A3 EC value of 62 300 000 $kgCO_2e$.

- For the same conditions (1.4 km long breakwater, with an average seabed depth of 14 m below sea level), Broekens et al. (2012) found that a caisson breakwater would have a total EC value of 188 000 000 $kgCO_2e$, of which 97 000 000 $kgCO_2e$ were associated with A1-A3 emissions
- For a 200 m long quay wall, ArcelorMittal (n.d.) found that a steel sheet pile wall would have a total EC value of 1 266 000 $kgCO_2e$, of which 919 000 $kgCO_2e$ were associated with A1-A3 emissions
- For a 200 m long quay wall, constructed using a reinforced concrete diaphragm wall, ArcelorMittal (n.d.) found a total EC value of 1 825 000 $kgCO_2e$, and an A1-A3 EC value of 1 698 000 $kgCO_2e$

Unfortunately, no EC values were found in the literature for jetty structures. An A1-A3 EC value was therefore estimated for the Matola jetty, using the same process as was used for the individual members above, and the following approximations of the members used in the jetty:

- 120 piles, with an average length of 22 m and an average diameter of 1.35 m
- 120 pile caps, with average dimensions of 2.5 x 2.5 x 1.5 m
- 144 beams, with average dimensions of 1.4 x 1.5 x 12 m
- 216 slabs, with average dimensions of 2.8 x 0.25 x 6.1 m

Each of the RC members were assumed to have 2 % reinforcement by volume of concrete; this is a typical value for heavily loaded/reinforced members (see SANS 10160-2, Table A.1) and is in line with the reinforcement percentage of the B401 beams which were designed in this study.

The Matola jetty was therefore found to have an A1-A3 EC of approximately 5 020 000 $kgCO_2e$, noting of course that this is a rough estimate. However, for a 350 m long, heavily reinforced jetty, this estimate seems reasonable and roughly in line with the values found in the literature (as the jetty uses more material than the quay walls, but significantly less than the breakwaters).

Appendix H: Signed Ethics Approval

Application for Approval of Ethics in Research (EiR) Projects
Faculty of Engineering and the Built Environment, University of Cape Town

ETHICS APPLICATION FORM

Please Note:
Any person planning to undertake research in the Faculty of Engineering and the Built Environment (EBE) at the University of Cape Town is required to complete this form **before** collecting or analysing data. The objective of submitting this application *prior* to embarking on research is to ensure that the highest ethical standards in research, conducted under the auspices of the EBE Faculty, are met. Please ensure that you have read, and understood the **EBE Ethics in Research Handbook** (available from the UCT EBE, Research Ethics website) prior to completing this application form: http://www.ebe.uct.ac.za/ebe/research/ethics1

APPLICANT'S DETAILS		
Name of principal researcher, student or external applicant		NICHOLAS ELIAS
Department		CIVIL ENGINEERING
Preferred email address of applicant:		ELSNIC007@myuct.ac.za
If Student	Your Degree: e.g., MSc, PhD, etc.	MSc.Eng. STRUCTURAL ENGINEERING
	Credit Value of Research: e.g., 60/120/180/360 etc.	120
	Name of Supervisor (if supervised):	PROFESSOR HANS BEUSHAUSEN
If this is a researchcontract, indicate the source of funding/sponsorship		N/A
Project Title		CRITICAL EVALUATION OF THE USE OF CRACK WIDTH REQUIREMENTS FOR THE DURABILITY DESIGN OF REINFORCED CONCRETE MARINE STRUCTURES

I hereby undertake to carry out my research in such a way that:

- there is no apparent legal objection to the nature or the method of research; and
- the research will not compromise staff or students or the other responsibilities of the University;
- the stated objective will be achieved, and the findings will have a high degree of validity;
- limitations and alternative interpretations will be considered;
- the findings could be subject to peer review and publicly available; and
- I will comply with the conventions of copyright and avoid any practice that would constitute plagiarism.

APPLICATION BY	Full name	Signature	Date
Principal Researcher/ Student/External applicant	NICHOLAS NORMAN ELIAS		14/05/2021
SUPPORTED BY	Full name	Signature	Date
Supervisor (where applicable)	Hans Beushausen		

APPROVED BY	Full name	Signature	Date
HOD (or delegated nominee) Final authority for all applicants who have answered NO to all questions in Section 1; and for all Undergraduate research (Including Honours).	Prof. Alphose Zingoni		31/05/2021
Chair: Faculty EIR Committee For applicants other than undergraduate students who have answered YES to any of the questions in Section 1.			